ASEAN
Journal of Scientific and Technological Reports
Online ISSN:2773-8752

Vol. 27 No. 3, May-June 2024

ISSN 2773-8752 (online)
https://ph02.tci-thaijo.org/index.php/tsujournal/issue/view/17078

ASEAN
Journal of Scientific and Technological Reports
Online ISSN:2773-8752

ASEAN Journal of Scientific and Technological Reports (AJSTR)

Contact Us Institute of Research and Innovation, Thaksin University
222 M. 2 Ban-Prao sub-district, Pa-Pra-Yom district, Phatthalung province, Thailand
Tel. 0 7460 9600 # 7242 , E-mail: aseanjstr@tsu.ac.th

List of Contents

ASEAN
Journal of Scientific and Technological Reports
Online ISSN:2773-8752

ASEAN
Journal of Scientific and Technological Reports
Online ISSN:2773-8752

Research article

Fabrication, 'Optimisation,' Characterization, and *In Vivo* Pharmacokinetic Evaluation of Testosterone Undecanoate Loaded Proniosome Capsule for Enhanced Oral Bioavailability

Ajay Singh[1], Abhishek Soni[2*], and Chinu Kumari[3]

[1] Research Scholar, School of Pharmacy, Abhilashi University, Chail-Chowk, Mandi (H.P.) – 175028, India; saikiamed1@gmail.com
[2] School of Pharmacy, Abhilashi University, Chail-Chowk, Mandi (H.P.) – 175028, India; asoniphd2023@gmail.com
[3] School of Pharmacy, Abhilashi University, Chail-Chowk, Mandi (H.P.) – 175028, India; btpharma2011@gmail.com
* Correspondence: asoniphd2023@gmail.com; (Dr. A. Soni)

Citation:
Singh, A.; Soni, A., Kumari, C. Fabrication-Optimisation, Characterization, and *In Vivo* Pharmacokinetic Evaluation of Proniosome Capsule Loaded with Testosterone Undecanoate for Enhanced Oral Bioavailability. *ASEAN J. Sci. Tech. Report.* **2024**, *27*(3), e250993. https://doi.org/10.55164/ajstr.v27i3.250993

Article history:
Received: September 21, 2023
Revised: March 23, 2024
Accepted: March 27, 2024
Available online: April 20, 2024

Abstract: This study focuses on creating and evaluating proniosome capsules as a potential drug delivery method to increase the oral bioavailability of testosterone undecanoate. The three main stages of the study are proniosome capsule fabrication optimization, characterization, and *in vivo* pharmacokinetic evaluation. The most prominent response surface approach (CCD – Central Composite Design) was used in the fabrication-optimization phase to determine the appropriate ratios of the factors that have the greatest effects on the particle size, PDI, and percentage of drug entrapment of testosterone undecanoate proniosomes. Creating testosterone undecanoate-loaded proniosomal formulations was possible using various ratios of span 60 and cholesterol. The physical and chemical characteristics of proniosome capsules, such as size, shape, surface charge, and drug-release kinetics, such as percentage drug entrapment, Vesicle size (nm), and PDI, must be thoroughly analyzed. Animal models were used to determine how the proniosome capsules affect the bioavailability of testosterone undecanoate after oral administration. Factors like absorption, distribution, metabolism, and excretion are carefully evaluated to determine whether the capsules successfully enhance drug delivery. The reduced particle size, polydispersity index (PDI, 282.33 ± 1.52 nm and 0.181 ± 0.003), and the highest entrapment efficiency (98.12 ± 1.03%) made the optimized formulation the ideal formulation. The Higuchi model provided the most comprehensive justification for releasing the testosterone undecanoate from proniosome compositions. Up to six months of storage, no changes of any type, even those to the proniosomes' color, were seen. There was no drug leakage during the stability study, according to the percentage of drug entrapment data. Positive findings from the *in vivo* pharmacokinetic investigation also suggested that testosterone undecanoate proniosome formulations may last significantly longer than a pure drug in *vivo*.

Keywords: Testosterone undecanoate; proniosome; testosterone insufficiency; vesicular drug delivery; formulation optimization

1. Introduction

To achieve targeted and controlled drug delivery, new drug delivery systems have emerged that incorporate multiple administration routes. One such system that contributes to extending the duration of a drug in systemic circulation and reducing toxicity through selective uptake is drug encapsulation in vesicles. This method has led to the developing of several vesicular drug delivery systems, including liposomes, niosomes, and provesicular systems like proliposomes and proniosomes [1]. Even though the oral route of drug administration has advantages, researchers are constantly looking for newer approaches because they are aware of the major roles that poor drug solubility and absorption, rapid metabolism, high fluctuations in drug plasma, and variability due to food effect play in disappointing *in vivo* results that ultimately cause the conventional delivery system to fail [2, 3].

Due to many new chemical entities (NCEs) and poor water solubility, which impairs therapeutic absorption, effective drug administration is essential [1, 3, 5]. Low solubility, enzyme breakdown, and acidic stomach conditions are among the difficulties associated with oral delivery [2, 3]. Colloidal lipid carriers have been used as treatment, improving drug solubility and gastrointestinal barrier permeability [4-6]. Designing proniosome-like vesicular drug delivery devices shows potential [1, 2]. Due to its limited solubility and promise for increased oral administration, extended-release, and improved patient compliance, testosterone undecanoate was chosen for proniosome manufacture. However, extensive study, formulation improvement, and strict evaluation methods are required to guarantee success.

Age-related increases in testosterone insufficiency prevalence are well-documented, but declining testosterone levels in aging individuals can be partly attributed to illness or senility [7-11]. Symptoms associated with aging and hypogonadism overlap, suggesting a potential link between age-related symptoms and androgen deficiency. However, diagnosing hypogonadism in older males is challenging due to symptom similarities [10, 12, 13]. The conventional testosterone formulation has low oral bioavailability (3-10%) due to hepatic metabolism and poor solubility. Enhancing tablet bioavailability can be achieved through vesicular systems and proniosomes, with potential benefits for oral delivery [12].

Therefore, this current study aimed to determine whether the proniosome could improve the oral bioavailability of testosterone undecanoate despite its poor water solubility and bioavailability. Proniosomes have been established to deliver a wide variety of drugs through the oral route and have been well-known for improving the oral bioavailability of several pharmaceuticals with poor bioavailability. Along with increasing their bioavailability, decreasing first-pass metabolism, lowering their dosage, preventing off-target distribution, preventing an undesired plasma peak, increasing the duration of action, modulating and controlling drug release, and improving the benefit-to-risk ratio, the current study also sought to explore the potential of testosterone undecanoate loaded proniosomes.

2. Materials and Methods

2.1 Material

Testosterone undecanoate and Span 60 were purchased from Sisco Research Laboratories Pvt. Ltd., Mumbai, India. Tween 80 and Span 40 were procured from Thomas Baker (Chemicals) Pvt. Ltd., Mumbai, India. Tween 20 and Cholesterol were purchased from Qualikems Lifesciences Pvt. Ltd., Sadar Bazaar, Delhi, India. Methanol, Potassium Dihydrogen orthophosphate, Sodium hydroxide, and other excipients were procured from Finar, Ahmedabad, Gujarat, India. All other reagents, chemicals, and excipients were of standard pharmaceutical & analytical grade.

2.2 Methods

2.2.1 Drug and excipients compatibility study

The drug and excipients compatibility study is essential to assess chemical and physical interactions between the drug and excipients, ensuring safety and stability and further optimizing the formulation for enhanced efficacy, shelf life, and patient compliance [14, 15].

2.2.1.1 FTIR spectroscopy

FTIR analyses of testosterone undecanoate, Span 60, cholesterol, a physical mixture of testosterone undecanoate, Span 60, cholesterol, mannitol, and optimized proniosome powder were conducted using this method [15, 16].

2.2.1.2 Differential scanning calorimetry (DSC)

The physicochemical composition of the drug in the optimized proniosome formulation was evaluated using DSC analysis. All samples were subjected to a 30 ml/min nitrogen purge while being scanned at 20°C/min from 30 to 350°C [17, 18].

2.2.2 Preparation of the testosterone undecanoate loaded proniosomes (TU-PNs)

Proniosomes loaded with testosterone undecanoate were created using testosterone undecanoate (40 mg) and Span 60/cholesterol at various molar ratios. A slurry technique was used to dissolve the drug and lipid mixtures in 20 ml of a solvent mixture that contained a 2:1 mixture of chloroform and methanol. The resulting mixture was then put into a 100 ml round-bottomed flask with a determined amount of solid carrier and vortexes for 5–10 minutes to create a slurry. The flask was equipped with a rotary evaporator, which was used to evaporate the chloroform and methanol solution for 15-20 minutes at 60°C under decreased pressure. After that, a mortar was used to ground the solid film into powder, and a 100-mesh screen was used to sift it. The obtained proniosome power was vacuum-sealed and kept at room temperature away from light for further evaluation [15, 17, 18].

2.2.3 Screening of the process parameters for preparation of TU-PNs using the slurry method

A variety of process and formulation characteristics were examined to find the optimal conditions for preparing the TU-PNs with the intended outcomes. Effect of different types of surfactant, type of solid carrier, surfactant: cholesterol molar ratio, various amounts of the total lipid, and other amounts of the solid carrier on the appearance, yield, drug entrapment, particle size, PDI, and micrometric properties was evaluated previously in our lab to select the best possible combinations for the fabrication of proniosomes.

2.2.4 Optimization of the TU-PNs using the central composite design

To optimize testosterone undecanoate proniosomes, the study used Central Composite Design (CCD) as the main response surface methodology. The best model among the linear, two-factor interaction and quadratic models was selected using the ANOVA F-value, allowing the development of a second-order polynomial equation to forecast responses [19]. The primary composite design specifications and formulation details were presented in the supplemental material. Design-Expert software made statistical analysis and graph plotting easier. The influence of independent factors on the responses was estimated using Fisher's test and ANOVA. A *P*-value of 0.05 or less was considered statistically significant [19, 20].

2.2.5 In-vitro characterization

2.2.5.1 Percentage yield

Using the following calculation the percent yield of all manufactured TU-PNs was calculated using the below formula [21]:

$$\text{Percentage yield} = \frac{\text{Practical yield}}{\text{Theoretical yield}} \times 100 \quad (1)$$

2.2.5.2 Percentage drug entrapment and Percentage drug loading

Through centrifuging the amount of unentrapped drug (a drug not contained in TU-loaded proniosomes), the encapsulation efficiency (EE) of TU-loaded Proniosomes was measured. Proniosome powder was hydrated with 10 ml of water and vortexed for 5 minutes to create the noisome solution. Around 2 ml of a diluted suspension in an Eppendorf tube was spun at 15000 rpm for 15 minutes at 5oC in a cooling centrifuge to separate the non-encapsulated drug from the suspension. Methanol was used to dilute the supernatant after it had been appropriately removed. By using UV spectroscopy, the amount of free drug was calculated. When calculating the amount of drug that was entrapped, the total amount of drug in the suspension was subtracted from the amount of drug that was not trapped. The following equation calculated the entrapment efficiency and drug loading [22, 23].

$$\text{Entrapment efficiency } (\%) = \frac{\text{Amount of drug present in proniosomes}}{\text{Initial amount of drug added}} \times 100 \quad (2)$$

$$\text{Drug loading } (\%) = \frac{\text{Amount of drug present in proniosomes}}{\text{Amount of drug}-\text{loaded proniosomes}} \times 100 \quad (3)$$

Three different batches of each sample were utilized. Before analysis, TU-PN samples were adequately diluted in a 1:50 ratio with HPLC-grade water. The average of three observations was used to determine the particle size.

2.2.5.3 Micromeritic property

The prepared proniosome formulation's flow properties were measured using various factors like the angle of repose, bulk density, tapped density, Carr's Index, and Hausner's ratio. These were measured by using standard procedures [24].

2.2.5.4 Transmission electron microscopy

Testosterone undecanoate-loaded optimized proniosome formulation morphology and shape were investigated using transmission electron microscopy (TEM, JEM CX 100) [25, 26].

2.2.5.5 In-vitro dissolution

Studies on drug dissolution were performed using pure drugs free of cholesterol and span 60, as well as optimized testosterone undecanoate proniosome formulation. The tests were conducted at 37.0±0.5°C with 900 ml of dissolution medium (pH 1.2 HCl or 6.8 phosphate buffer saline). The apparatus received the equivalent of 40mg of testosterone undecanoate. At set intervals (5, 10, 20, 30, 60, 120, 240, and 300 minutes), samples were removed, replaced with an equivalent new medium, and filtered through a 0.45 membrane. UV spectrophotometers were used at 242 nm [2, 18] to assess the concentrations.

2.2.5.6 In-vitro drug release study

Using the dialysis bag method in sink settings, the release behavior of reconstituted niosome suspension from various formulations and testosterone undecanoate suspension was examined. For 24 hours before usage, the dialysis bags with a cut-off of 8000–14000 kDa were submerged in the 1% ethanolic solution. The proniosome and pure drug equivalent to 40 mg of testosterone undecanoate was accurately measured and poured into the appropriate medium before being poured into the dialysis bag with the two ends snugly sealed and bound on the shaft. Next, 900 ml of release medium (pH 1.2 HCl and pH 6.8 phosphate buffer saline) held at a constant 37.0±0.5°C were added to the dialysis bag. At a rate of 100 revolutions per minute, the paddles were turning. 5ml aliquots were removed and replaced with an equivalent dissolving medium at predetermined time intervals of 0.25 hr, 0.5 hr, 1 hr, 2 hr, 4 hr, 6 hr, 8 hr, 10 hr, 12 hr, 16 hr, and 24 hr. To measure the content of testosterone undecanoate, the withdrawal samples were filtered through a 0.45 membrane filter (0.45 μm Pore Size) and charged into UV spectrophotometers (242 nm) [2, 18].

2.2.5.7 In vitro drug release kinetic study

The release kinetics were analyzed using various kinetic models, including zero-order plots, first-order plots, Higuchi plots, and Korsmeyer Peppas plots [27].

2.2.5.8 Stability analysis

The chosen testosterone undecanoate-loaded proniosome formulation was stored for six months at five °C, 30°C/65%RH, and 40°C/75%RH, respectively, in transparent glass vials. Entrapment effectiveness and drug loading efficiency of proniosome formulations were evaluated every 1, 3, and 6 months compared to newly formed proniosomal [2, 18]. The phase separation and aggregation of all created formulations were visually assessed. Furthermore, significant changes were observed for 6 months. Finally, the estimation of change in physical appearance, percentage of drug entrapment, and percentage of drug loading were evaluated [28].

2.2.6 In vivo pharmacokinetic study

Male Wistar rats weighing 250–300 g were obtained from SBSPM B Pharmacy College, Ambejogai, Beed, India. All animals used in the experiments received care in compliance with the guidelines of The Committee for Control and Supervision of Experiments on Animals. The Institutional Ethical Committee approved the experimental protocol, SBSPM B Pharmacy College, Ambejogai, Beed, India (approval no. CPCSEA – SBSPM/22-23/871). The rats were randomly divided into three groups (n = 3), where group 1 was receiving water *ad libitum* and normal pellet diet only (Control), group 2 was receiving plain pure drug suspension, and group 3 was receiving optimized testosterone undecanoate loaded proniosome formulation, respectively. For the current study, a dose of 10 mg/kg of testosterone undecanoate was employed based on earlier research. Animals were given testosterone proniosomes (100 mg, equivalent to 10 mg of testosterone undecanoate) and a pure drug suspension (10 mg/kg dose) [7, 8, 12]. In compliance with USFDA rules [29], blood samples were taken at predetermined intervals (30 min, 1 hr, 2 hr, 4 hr, 6 hr, 8 hr, 10 hr, 12 hr, and 24 hr), given the drug's 2-hour half-life. Serum was collected by centrifuging blood samples at 3000 rpm for 12

minutes, which was then kept at -20°C for later HPLC analysis [7, 8, 12]. The accurate assessment of the pharmacokinetics of testosterone undecanoate was made possible by this stringent approach. The pharmacokinetic parameters such as mean residence time (MRT), elimination rate constant (k_e), maximum plasma concentration (Cmax), and time to achieve the maximum plasma concentration (T_{max}) were obtained from the plasma concentration versus time curve. The area under the plasma concentration-time curve from time zero to the final concentration time point (AUC0-t) and the area under the plasma concentration-time curve from time zero to infinity (AUC0–∞) was also calculated using the measured drug plasma concentrations. The acquired information was presented as mean standard deviation [30].

2.2.7 Statistical analysis

All the results are the mean ± SD of three independent experiments. The significance of differences ($P < 0.05$) between experimental variables was determined by the use of a two-tailed Student's test as well as by one-way ANOVA (Analysis of Variance) followed by *post hoc* Turkey's test (GraphPad Software Package, Version 8). The statistical significance was indicated by $P < 0.05$.

3. Results and Discussion

3.1 Determination of absorption maxima of testosterone undecanoate

The drug's maximum absorption was determined by using a UV spectrophotometer to scan a 12µg/ml solution of testosterone undecanoate in methanol between 200 and 400 nm. The 242 nm UV absorption maxima were discovered to be relatively near to the absorption maxima reported in the literature [7, 9].

3.2 Drug and excipients compatibility study

The retention of significant peaks, indicating compatibility, was confirmed by the FTIR analysis of testosterone undecanoate, span 60, cholesterol, and mannitol separately and in a physical mixture (figure 1). The absence of any incompatibility ensured stability. A crystal structure with melting peaks at 61.30°C was visible in Span 60. The optimized proniosome formulation showed testosterone undecanoate's endothermic peak at 64.35°C, indicating effective encapsulation inside the proniosomes. This analysis demonstrated the stable integration of drugs and excipients, crucial for the formulation's effectiveness and safety.

3.3 Preparation of the Testosterone undecanoate loaded proniosomes (TU-PNs)

Proniosomes, loaded with testosterone undecanoate and nonionic surfactant span 60, were created using a literature-described technique [15, 18, 30]. Despite the advantages, traditional noisome dispersions face issues like aggregation and drug leakage. The proniosome technique resolves these problems, ensuring stable aqueous niosomes. Tactics like adding cholesterol are employed to enhance vesicle stability in stomach juices. Nonionic surfactant and cholesterol concentrations determine niosome stability; any change leads to drug leakage. Interestingly, the creation of niosomes from proniosome powder occurred spontaneously, forming vesicular structures on the carrier's surface, transforming into spherical multilamellar vesicles with gentle agitation, aligning with existing literature studies [15, 18, 30].

3.4 Optimization of testosterone-loaded proniosome using the central composite design

The central composite design is one of the response surface models used in experiment design to hit the mark, eliminate variability, and maximize or minimize reactions that increase product production or decrease waste. Utilizing the central composite response surface methodology, the ratio of the amounts of span 60 and cholesterol were two of the three significant variables chosen based on the initial Screening results. These variables were used to reduce the particle size and increase the loading efficiency of the testosterone undecanoate proniosome (Table 3).

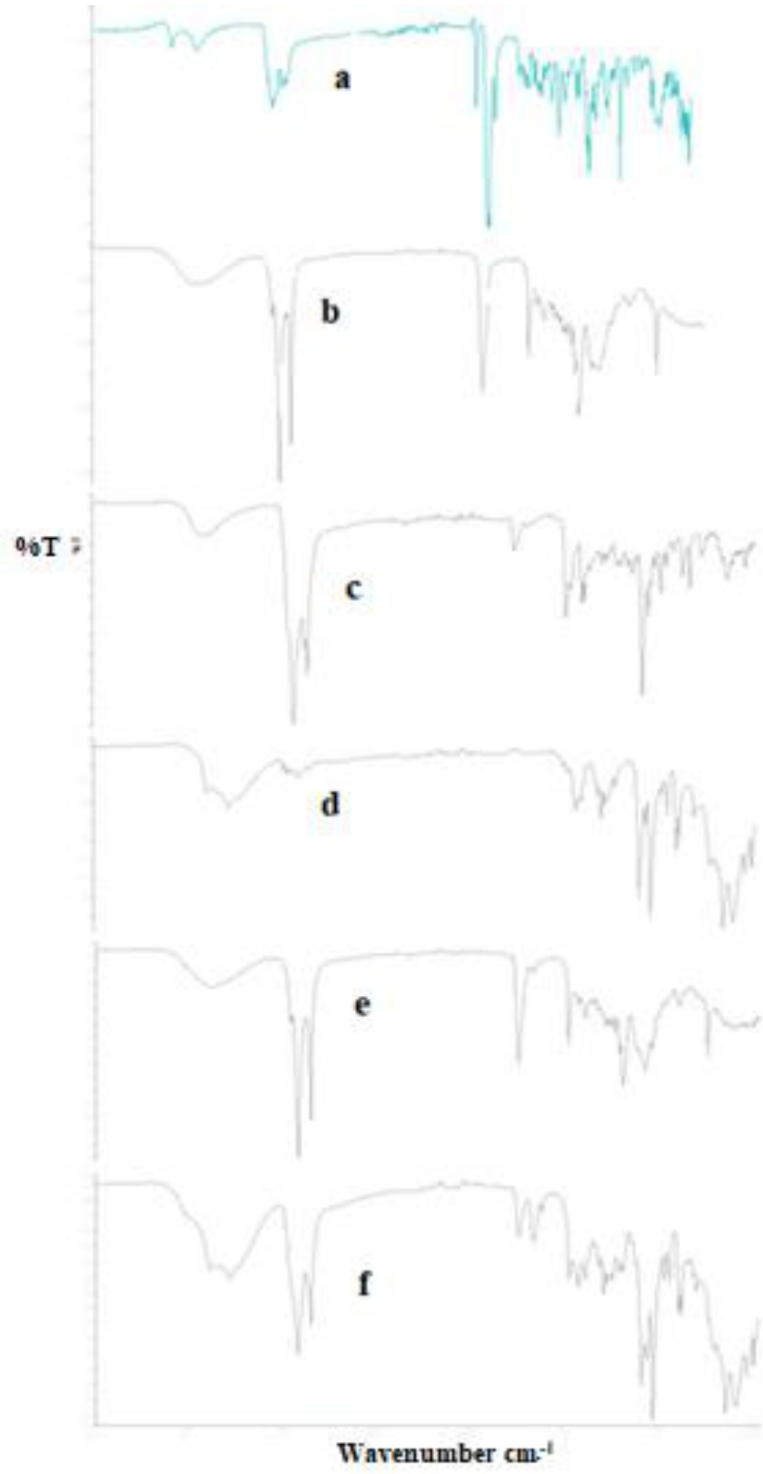

Figure 1. FTIR spectra of the testosterone undecanoate (a), span 60 (b), cholesterol (c), mannitol (d), a physical mixture consisting of testosterone undecanoate, span 60, cholesterol and mannitol (e) and optimized formulation (f, DTU-PNs14)

Table 3. Composition of the testosterone undecanoate proniosome with response

Formulation code	Factor 1 X1: Amount of SPAN 60 (μM)	Factor 2 X2: Amount of cholesterol (μM)	Response Y1 Percentage drug entrapment (%)	Response Y2 Vesicle size (nm)	Response Y3 PDI
DTU-PNs1	160.3553391	125	99.61	335.05	0.238
DTU-PNs2	100	100	80.00	279.14	0.220
DTU-PNs3	125	89.64466094	84.68	258.29	0.214
DTU-PNs4	125	125	97.84	283.00	0.181
DTU-PNs5	125	160.3553391	90.69	281.02	0.218
DTU-PNs6	89.64466094	125	85.69	300.08	0.235
DTU-PNs7	125	125	98.85	284.15	0.178
DTU-PNs8	125	125	98.71	286.27	0.180
DTU-PNs9	100	150	90.17	284.32	0.230
DTU-PNs10	125	125	98.54	285.18	0.179
DTU-PNs11	150	150	94.17	319.20	0.226
DTU-PNs12	150	100	95.78	293.12	0.228
DTU-PNs13	125	125	97.91	285.08	0.177

All the formulations' results were evaluated to determine the best study design. Software called Design Expert 7.0 was used to create contour plots and a desirability plot. A quadratic model was proposed regarding particle size, PDI, and entrapment effectiveness. ANOVA was used to determine the factors that significantly impacted the replies (Analysis of variance). The findings showed that the chosen independent variables had a significant impact on the chosen answers because the ranges for particle size (nm), PDI, and entrapment efficiency (%) were, respectively, 281-335 nm, 0.178-0.238, and 80.00-99.61%.

3.4.1 Percentage drug entrapment (Y1)

The impact of span 60 and the amount of cholesterol on percentage drug entrapment on particle size was studied, and the responses obtained were given in Tables 4 and 5.

Table 4. Model Summary Statistics

Model	Std. Dev.	R-Squared	Adjusted R-Squared	Predicted R-Squared	PRESS	
Linear	5.2034	0.4605	0.3526	0.0777	462.8394	
2FI	5.1214	0.5296	0.3728	-0.0542	529.0455	
Quadratic	0.3599	0.9982	0.9969	0.9967	1.6353	Suggested
Cubic	0.4255	0.9982	0.9957	0.9925	3.7753	Aliased

The model's significance, denoted by the large Model F-value of 773.38 (occurring due to noise only 0.01% of the time), highlights the significance of terms X1, X2, X1X2, $X1^2$, and $X2^2$ ('Prob > F' < 0.0500). Model reduction, excluding unnecessary terms (except for hierarchy maintenance), could enhance the model's accuracy. The 'Lack of Fit F-value' of 0.06 indicates insignificance compared to pure error, with a 97.80% probability of being caused by noise. A non-significant lack of fit is desirable for a well-fitting model. The experimental model displayed minimal deviations, evident in high R^2 (0.9981), adjusted R^2 (0.9969), and predicted R^2 (0.9967) values. Predictions for particle size, based on specific element amounts, were made using a polynomial equation in terms of coded factors, ensuring accurate estimations. The equation is as follows:

Percentage drug entrapment (Y1) = 98.37+ 4.933231599 X1+ 2.132427939X2 -2.945 X1X2- 2.894375$X1^2$- 5.376875$X2^2$ (4)

The entrapment efficiency (EE) of testosterone undecanoate was enhanced by elevated cholesterol and span 60 levels. The molecule was more easily accommodated by the higher lipophilic environment produced by lipophilic surfactants with substantial hydrophobic components. These surfactants produced well-closed, uniformly packed bilayer structures. They ordered gel states due to their high transition temperatures (Tc) and low HLB values (4-6), which enabled the highly lipophilic material to be intercalated effectively. Increased entrapment was caused by the surfactant's solid state, hydrophobicity, and high phase transition temperature. However, for other formulae, a rise in TU content resulted in a drop in EE, except for one where a higher surfactant concentration inhibited drug entrapment because excessive surfactant had destabilized lipid bilayers. The 3D response plot shows that this instability caused quick drug diffusion and a decrease in percent EE, possibly leading to the formation of pores.

Cholesterol addition makes the formulation dense, indicating a stiffer bilayer membrane. Furthermore, highly organized surfactant and cholesterol systems allow easier drug partitioning. The structure of the surfactant phase affected the lamellar surfactant phase's capacity to accommodate drugs. The higher stability and bilayer hydrophobicity for niosomes might cause a rise in testosterone undecanoate entrapment efficiency with increased cholesterol content.

Table 5. Entrapment efficiency ANOVA Response for Quadratic Model.

Source	Sum of Squares	df	Mean Square	F Value	p-value Prob > F	
Model	500.9188	5	100.1838	773.3816	< 0.0001	significant
X1-Amount of SPAN 60 (A)	194.6942	1	194.6942	1502.967	< 0.0001	
X2-Amount of cholesterol (B)	36.37799	1	36.37799	280.8247	< 0.0001	
X1X2	34.6921	1	34.6921	267.8102	< 0.0001	
$X1^2$	58.27761	1	58.27761	449.8816	< 0.0001	
$X2^2$	201.1185	1	201.1185	1552.561	< 0.0001	
Residual	0.906779	7	0.12954			
Lack of Fit	0.039379	3	0.013126	0.060532	0.9780	not significant
Pure Error	0.8674	4	0.21685			
Cor Total	501.8256	12				
R-Squared	0.9982					
Adj R-Squared	0.9969					
Pred R-Squared	0.9967					
Adeq Precision	79.626					

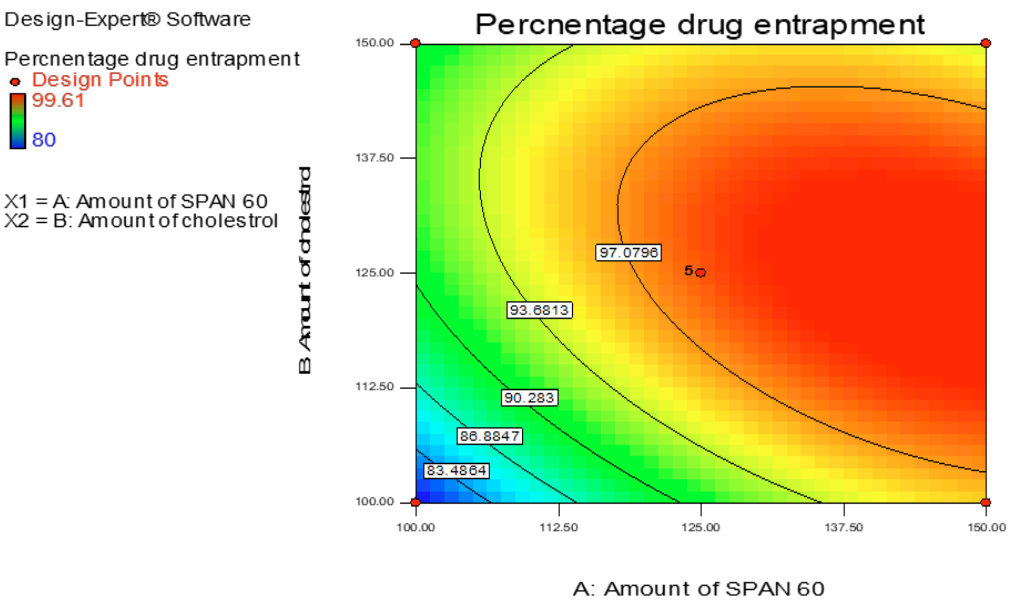

Figure 2. The counterplot of the response

The link between the dependent and independent variables was clarified by creating contour plots. Figure 2 displays the impacts of X1 and X2 together with their interaction on the percentage of drug entrapment. Up to 93% PDE, the graphs were found to be linear, but above this point, the plots were found to be nonlinear, indicating a nonlinear relationship between X1 and X2.

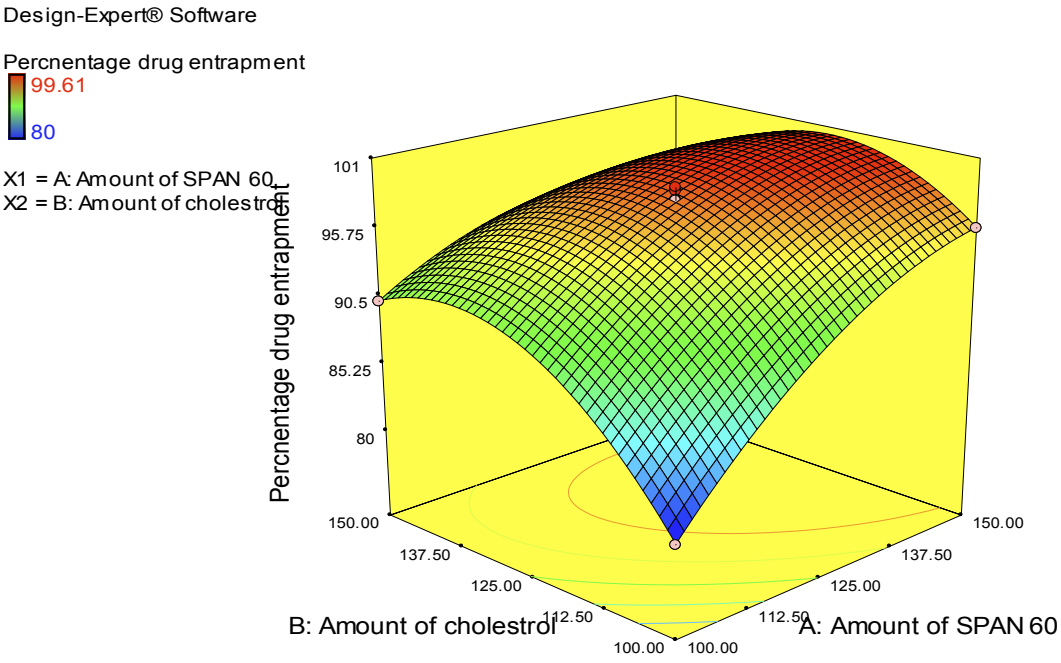

Figure 3. 3D response graph

The effects of independent variables on EE were depicted using 3D response surface plots. It was discovered that all DTU-PNs had EE percentages ranging from 80 to 99.61%. As the concentration of span 60, cholesterol (CHO), and drug increases, so does the EE (%) of testosterone undecanoate. By strengthening the lipid bilayer and reducing drug leakage, cholesterol improved the EE. Additionally, Span 60 concentration

increased the EE of testosterone undecanoate in proniosomes, which increased the maximal phase transition temperature. It was also discovered that all formulae displayed a different degree of EE decrease with an increase in TU content, except for one formulation where a higher concentration of the surfactant reduced the percentage of drug entrapment because a higher concentration of the surfactant might cause the destabilization of lipid bilayers. The following elements may play a role in why entrapment efficiency declines as cholesterol proportions rise above a certain point in time:

(1) The diameter of the bilayer shrank due to the increase in cholesterol, resulting in a smaller interspace;

(2) the increased cholesterol might fight with testosterone undecanoate for packing space within the bilayer. Additionally, the elevated cholesterol might have harmed the bilayer's normal linear shape, leading to the leakage of the entrapped drug, as shown in the 3D response plot (Figure 3).

3.4.2 Vesicle size

According to Table 6, the proniosome formulae's vesicles ranged in size from 279.14 nm to 335.04 nm. Smaller vesicles resulted from the homogeneous thin film of the surfactant mixture being hydrated more effectively with low surfactant amounts than more significant surfactant amounts. The high cholesterol content in the formulation may be the cause of the large size of the cysts. It was claimed that cholesterol made the lipid bilayers wider. Additionally, by lowering the peak temperature at which the vesicle phase transition occurs, it is in charge of increasing the rigidity and strength of the bilayer membrane of the vesicles and decreasing their fluidity [15, 18, 30].

Analysis of variance (ANOVA) was implemented to recognize the significant terms of the quadratic model on vesicle size. Multiple regressions were done to vesicle size values at various levels of the two factors (X1 and X2) to give up a regression equation determination coefficient (R^2) of 0.99.

Table 6. Model Summary Statistics and ANOVA

Model Summary Statistics						
Source	**Std. Dev.**	**R-Squared**	**Adjusted R-Squared**	**Predicted R-Squared**	**PRESS**	
Linear	16.31716	0.391186	0.269423	-0.30585	5710.814	
2FI	16.84338	0.416157	0.221542	-0.29185	5649.603	
Quadratic	0.955611	0.998538	0.997494	0.997251	12.02233	Suggested
Cubic	1.118049	0.998571	0.99657	0.994562	23.77999	Aliased
ANOVA						
Source	**Sum of Squares**	**df**	**Mean Square**	**F Value**	**p-value Prob > F**	
Model	4366.862	5	873.3723	956.3942	< 0.0001	significant
A-Amount of SPAN 60	1208.231	1	1208.231	1323.084	< 0.0001	
B-Amount of cholesterol	502.5254	1	502.5254	550.295	< 0.0001	
AB	109.2025	1	109.2025	119.5832	< 0.0001	
A^2	1893.511	1	1893.511	2073.507	< 0.0001	
B^2	386.8043	1	386.8043	423.5735	< 0.0001	
Residual	6.39235	7	0.913193			
Lack of Fit	0.36663	3	0.12221	0.081126	0.9668	not significant
Pure Error	6.02572	4	1.50643			
Cor Total	4373.254	12				
R-Squared	0.998538308					
Adj R-Squared	0.997494242					
Pred R-Squared	0.997250941					
Adeq Precision	117.8329807					

The model's significance, indicated by the Model F-value of 956.39 (occurring in noise only 0.01% of the time), led to the significance of terms X1, X2, X1X2, $X1^2$, and $X2^2$ ('Prob > F' < 0.0500). Model reduction excluding unnecessary terms maintains hierarchy. The 'Lack of Fit F-value' of 0.11, not significant compared to pure error, suggests good model fit, with R^2 (0.9985), adjusted R^2 (0.9975), and predicted R^2 (0.9973) showing minimal experimental differences. A polynomial equation, derived from coded factors, predicted particle size for specific element amounts:

$$\text{Vesicle size (Y2)} = 284.74 + 12.29\,X1 + 7.93X2 + 5.23\,X1X2 + 16.50X1^2 - 7.46X2^2 \quad (5)$$

Span 60 and cholesterol levels affected the size of testosterone undecanoate vesicles, demonstrating the surfactant's hydrophobicity. Adding Span 60 resulted in more giant vesicles, whereas low surfactant concentrations produced smaller, hydrated vesicles. Cholesterol initially decreased vesicle size and shrank after that [4, 11, 13]. Higher cholesterol was connected with more giant vesicles (>100 nm). However, increased cholesterol levels thickened the bilayer and decreased fluidity, as shown in the 3D response graph. Underscoring the complexity of their interactions, the complicated interplay between surfactant and cholesterol had a major impact on vesicle properties.

The link between the dependent and independent variables was clarified by creating contour plots. The effects of X1 and X2 with their interaction on vesicle size are shown in Figures 4 and 5. The plots were found to be nonlinear, indicating a nonlinear relationship between X1 and X2

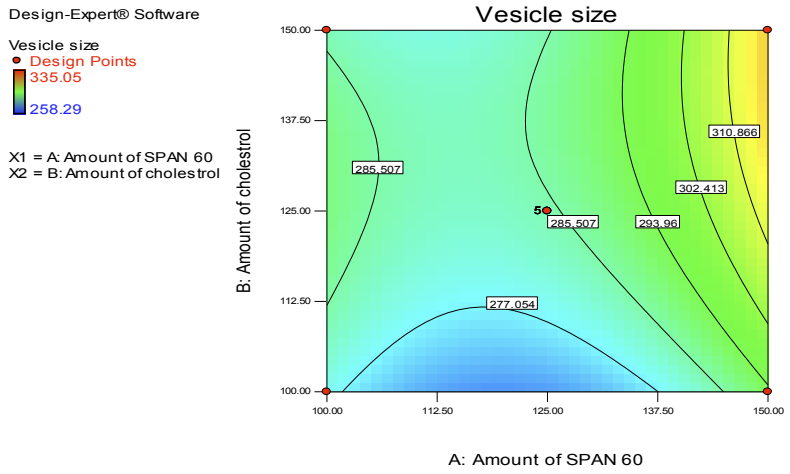

Figure 4. Counter plot

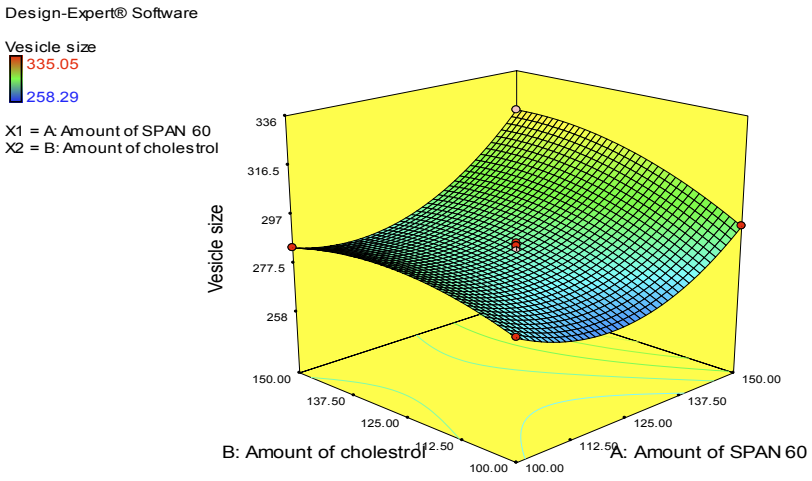

Figure 5. 3D response graph

3.4.3 Polydispersity index (PDI)

The PDI of the proniosome formulae ranged from 0.177 -0.238, as shown in Table 7. Analysis of variance (ANOVA) was implemented to recognize the significant terms of the quadratic model on PDI. Multiple regressions were done to vesicle size values at various levels of the two factors (X1 and X2) to give up a regression equation (Eq. the determination coefficient (R^2) of 0.99.

Table 7. Model Summary Statistics and ANOVA

Model Summary Statistics						
Source	**Std. Dev.**	**R-Squared**	**Adjusted R-Squared**	**Predicted R-Squared**	**PRESS**	
Linear	0.027019	0.004338	-0.19479	-0.6035	0.011757	
2FI	0.02841	0.009248	-0.321	-1.19017	0.016058	
Quadratic	0.001243	0.998524	0.997471	0.997075	2.14E-05	Suggested
Cubic	0.001423	0.998619	0.996686	0.996778	2.36E-05	Aliased
ANOVA						
Source	**Sum of Squares**	**df**	**Mean Square**	**F Value**	**p-value Prob > F**	
Model	0.007321	5	0.001464	947.4059	< 0.0001	significant
A-Amount of SPAN 60	8.49E-06	1	8.49E-06	5.495	0.0515	
B-Amount of cholesterol	2.33E-05	1	2.33E-05	15.08469	0.0060	
AB	3.6E-0	1	3.6E-05	23.29311	0.0019	
A^2	0.005725	1	0.005725	3704.269	< 0.0001	
B^2	0.002365	1	0.002365	1530.105	< 0.0001	
Residual	1.08E-05	7	1.55E-06			
Lack of Fit	8.19E-07	3	2.73E-07	0.109153	0.9503	not significant
Pure Error	0.00001	4	2.5E-06			
Cor Total	0.007332	12				
R-Squared	0.9985					
Adj R-Squared	0.9975					
Pred R-Squared	0.9971					

The model's significance, indicated by the large Model F-value of 947.4059 (occurring due to noise only 0.01% of the time), highlights the significance of terms X1, X2, X1X2, $X1^2$, and $X2^2$ ('Prob > F' < 0.0500). Model reduction, excluding unnecessary terms except for hierarchy-maintaining ones, could enhance the model's accuracy. The 'Lack of Fit F-value' of 0.11 indicates minor significance compared to pure error, primarily caused by noise (95.03%). A minimal lack of fit is desirable for a well-fitting model. The experimental model displayed minimal fluctuations, evident in high R^2 (0.9985), adjusted R^2 (0.9975), and predicted R^2 (0.9971) values. Predictions for particle size, based on specific factor levels, were made using a polynomial equation in coded factors, ensuring accurate estimations. The equation is as follows:

$$PDI\ (Y3) = 0.18 + 1.03\ X1 + 1.07X2 - 3.00\ X1X2 + 0.029X1^2 - 0.018X2^2 \quad (6)$$

The positive coefficients of X1 show that span 60 increases with a rise in vesicles PDI. Here, the surfactant (span 60, X1) has a favorable impact on PDI, increasing PDI for PNs as the concentration of span60 is raised. Cholesterol has a biphasic impact on PDI. The effect of cholesterol and amount of span 60 on the PDI of PNs was shown in the 3D response graph.

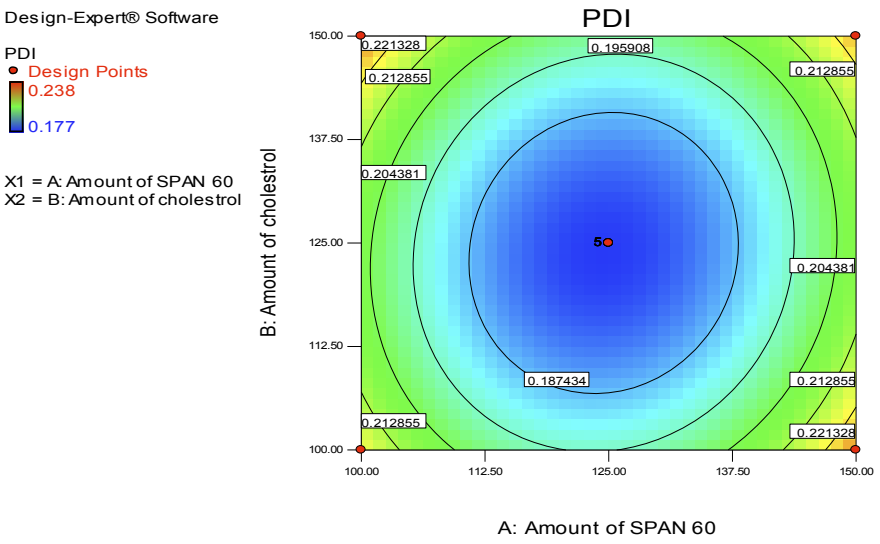

Figure 6. Counter plot

The relationship between the dependent and independent variables was further elucidated by constructing contour plots. The effects of X1 and X2 with their interaction on PDI are shown in Figure 7. The plots were nonlinear, indicating a nonlinear relationship between X1 and X2.

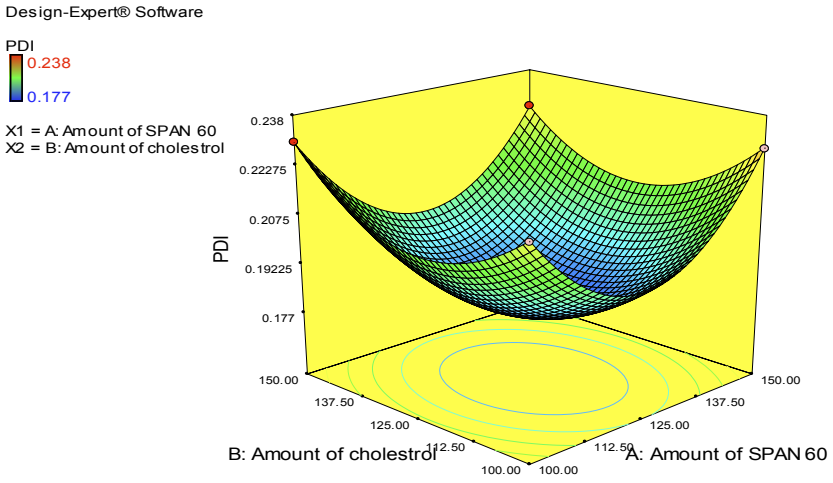

Figure 7. 3D response graph.

3.4.4 Checkpoint analysis

Expected mean vesicle diameter (MVD) and percentage drug entrapment (PDE) values were validated during the fabrication and evaluation of a checkpoint batch, validating the predictive accuracy of the derived coefficients and contour plots. In terms of drug entrapment, vesicle size, and PDI, standard deviation comparisons between actual and predicted values did not find any appreciable variations. The best formulation, DTU-PNs14, was chosen due to the study's determination of the coefficients' accuracy in predicting the values of independent variables. This formulation ensures small vesicle size, low PDI, and maximum entrapment efficiency. Therefore, formulation DTU-PNs14 was deemed to be the most optimal formulation since it had the lowest particle size and PDI (282.33 ± 1.52 nm and 0.181 ± 0.003) and the highest entrapment efficiency (98.12 ± 1.03%).

Table 8. Composition of the optimized formulation with the predicted and actual value of the percentage drug entrapment, vesicle size, and PDI

Predicted						
Formulation code	**Amount of SPAN 60 (μM)**	**Amount of cholesterol (μM)**	**Percentage drug entrapment (%)**	**Vesicle size (nm)**	**PDI**	**Desirability**
DTU-PNs14	125.36	123.09	98.249	284.261	0.179	0.841
Actual						
Formulation code	**Percentage drug entrapment (%)**		**Vesicle size (nm)**		**PDI**	
DTU-PNs14	98.12 ± 1.03		282.33 ± 1.52		0.181 ± 0.003	

3.5 *In vitro* characterization parameters

3.5.1 Percentage yield, Percentage drug entrapment, Percentage drug loading, Vesicle size and PDI

The percentage yield of all prepared formulations is shown in Table 9. The percentage yield of all prepared formulations was determined to be between 98.24 ± 0.65% to 99.64 ± 0.53%. The optimized formulation DTU- PNs14's percentage yield was discovered to be 99.41 ± 0.20%. The range of the testosterone undecanoate drug entrapment percentage in the entire formulation was determined to be between 80.00 ± 0.10% and 99.61 ± 0.03%. Whereas the percentage of drug entrapment of the optimized formulation DTU-PNs14 was 98.12 ± 0.03%. It was discovered that the percentage drug loading of all produced formulations ranged from 8.16 ± 0.01 to 10.16 ± 0.06. While the optimized formulation DTU-PNs14 drug loading was discovered to be 10.06 ± 0.01%. Vesicle size and PDI of all created formulations were determined to be between 258.29 ± 1.63nm to 335.05 ± 1.01 and 0.177 ± 0.004 to 0.238 ± 0.002, respectively. While the optimized formulation DTU-particle PNs14's size and PDI were discovered to be 282.33 ± 1.52nm and 0.181 ± 0.003, respectively.

Table 9. Percentage yield, Percentage drug entrapment, Percentage drug loading, Vesicle size, and PDI of all prepared formulations.

Formulation code	**Percentage yield (%)**	**% Drug entrapment**	**Percentage drug loading**	**Vesicle size (nm)**	**PDI**
DTU-PNs1	98.88 ± 0.66	99.61 ± 0.03	10.16 ± 0.06	335.05 ± 1.01	0.238 ± 0.002
DTU-PNs2	98.24 ± 0.65	80.00 ± 0.10	8.16 ± 0.01	279.14 ± 0.99	0.220 ± 0.003
DTU-PNs3	99.42 ± 0.48	84.68 ± 0.26	8.64 ± 0.04	258.29 ± 1.63	0.214 ± 0.004
DTU-PNs4	98.33 ± 0.39	97.84 ± 0.05	9.98 ± 0.01	283.00 ± 1.00	0.181 ± 0.002
DTU-PNs5	99.06 ± 0.54	90.69 ± 0.30	9.26 ± 0.03	281.02 ± 1.42	0.218 ± 0.004
DTU-PNs6	99.18 ± 0.55	85.69 ± 0.02	8.74 ± 0.02	300.08 ± 1.05	0.235 ± 0.003
DTU-PNs7	99.44 ± 0.27	98.85 ± 0.05	10.09 ± 0.04	284.15 ± 1.82	0.178 ± 0.003
DTU-PNs8	99.22 ± 0.52	98.71 ± 0.08	10.07 ± 0.02	286.27 ± 0.84	0.180 ± 0.006
DTU-PNs9	99.52 ± 0.51	90.17 ± 0.30	9.13 ± 0.05	284.32 ± 0.94	0.230 ± 0.004
DTU-PNs10	99.39 ± 0.63	98.54 ± 0.04	10.00 ± 0.03	285.18 ± 1.20	0.179 ± 0.003
DTU-PNs11	99.01 ± 0.67	94.17 ± 0.67	9.59 ± 0.07	319.20 ± 1.98	0.226 ± 0.005
DTU-PNs12	99.64 ± 0.53	95.78 ± 0.69	9.77 ± 0.02	293.12 ± 0.94	0.228 ± 0.008
DTU-PNs13	99.03 ± 0.42	97.91 ± 0.11	10.04 ± 0.01	285.08 ± 1.80	0.177 ± 0.004
DTU-PNs14	99.41 ± 0.20	98.12 ± 0.03	10.06 ± 0.01	282.33 ± 1.52	0.181 ± 0.003

3.5.2 Micromeritic properties

Micromeritic properties of all prepared testosterone undecanoate-loaded proniosome formulations are shown in Table 10. All prepared formulations' Micromeritic parameters, such as the bulk density, tapped density, Carr's index, and Hausner ratio, were found to fall within the following ranges: 0.157 ± 0.002 to 0.218 ± 0.001, 0.167 ± 0.001 to 0.226 ± 0.001, 1.538 ± 0.377 -9.221 ± 1.742%, 1.016 ± .0004-1.102 ± 0.021. The values of the bulk

density tapped density, Carr's index, and Hausner ratio for the optimized formulations were determined to be 0.218 ± 0.001g/cm^3, 0.226 ± 0.001 g/cm^3, 3.583 ± 0.426%, and1.037 ± 0.005, respectively.

Table 10. Micromeritic properties of all prepared testosterone undecanoate proniosome formulations, including the optimized formulation

Formulation code	Bulk density (gm/cm^3)	Tapped density (gm/cm^3)	Carr's index (%)	Hausner ratio
DTU-PNs1	0.160 ± 0.002	0.167 ± 0.001	3.912 ± 1.302	1.041 ± 0.014
DTU-PNs2	0.164 ± 0.001	0.174 ± 0.001	5.826 ± 0.804	1.062 ± 0.009
DTU-PNs3	0.186 ± 0.002	0.200 ± 0.001	7.016 ± 1.220	1.076 ± 0.014
DTU-PNs4	0.212 ± 0.002	0.222 ± 0.001	4.236 ± 1.369	1.044 ± 0.015
DTU-PNs5	0.157 ± 0.002	0.173 ± 0.022	9.221 ± 1.742	1.102 ± 0.021
DTU-PNs6	0.171 ± 0.001	0.181 ± 0.002	5.693 ± 1.920	1.061 ± 0.022
DTU-PNs7	0.208 ± 0.003	0.216 ± 0.003	3.699 ± 1.433	1.039 ± 0.015
DTU-PNs8	0.200 ± 0.002	0.213 ± 0.002	5.774 ± 1.837	1.062 ± 0.021
DTU-PNs9	0.188 ± 0.001	0.197 ± 0.002	4.785 ± 1.265	1.050 ± 0.014
DTU-PNs10	0.198 ± 0.002	0.201 ± 0.001	1.538 ± 0.377	1.016 ±. 0004
DTU-PNs11	0.165 ± 0.002	0.177 ± 0.003	6.948 ± 1.703	1.075 ± 0.019
DTU-PNs12	0.192 ± 0.001	0.203 ± 0.003	5.541 ± 1.309	1.059 ± 0.015
DTU-PNs13	0.201 ± 0.002	0.215 ± 0.002	6.466 ± 1.504	1.069 ± 0.007
DTU-PNs14	0.218 ± 0.001	0.226 ± 0.001	3.583 ± 0.426	1.037 ± 0.005

3.5.3 Transmission electron microscopy

Vesicle formation on further dilution of the optimized formulation proniosome powder with water was further confirmed by TEM, as shown in Figure 8.

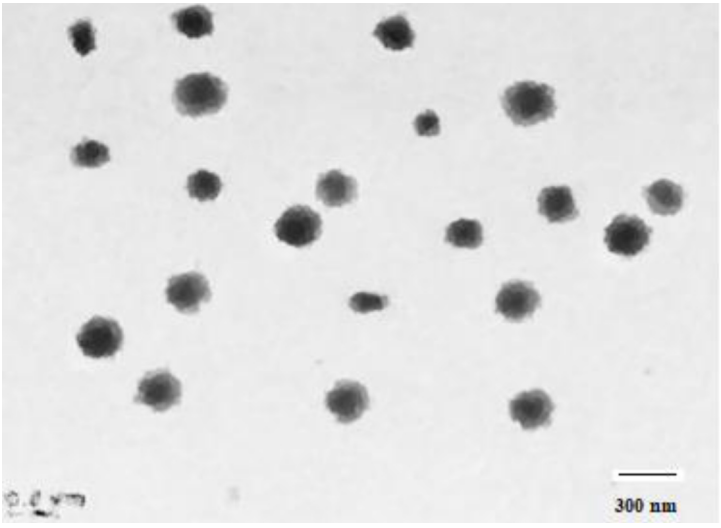

Figure 8. TEM image of the optimized formulation of the DTU-PNs14 Upon dilution of the proniosome powder with the water

The niosome was an easily recognized, nearly perfect sphere with an internal aqueous space, as shown in Figure 8. Additionally, the outermost bilayer could be seen. Additionally, the proniosome vesicle had a spherical shape, and no signs of drug crystal or aggregation were found. It could be quickly redistributed in water.

3.5.4 In vitro dissolution study

The dissolution profile of pure drug and TU-loaded proniosome powder in HCl (pH 1.2) and phosphate buffer solution (pH 6.8) is shown in Figure 9.

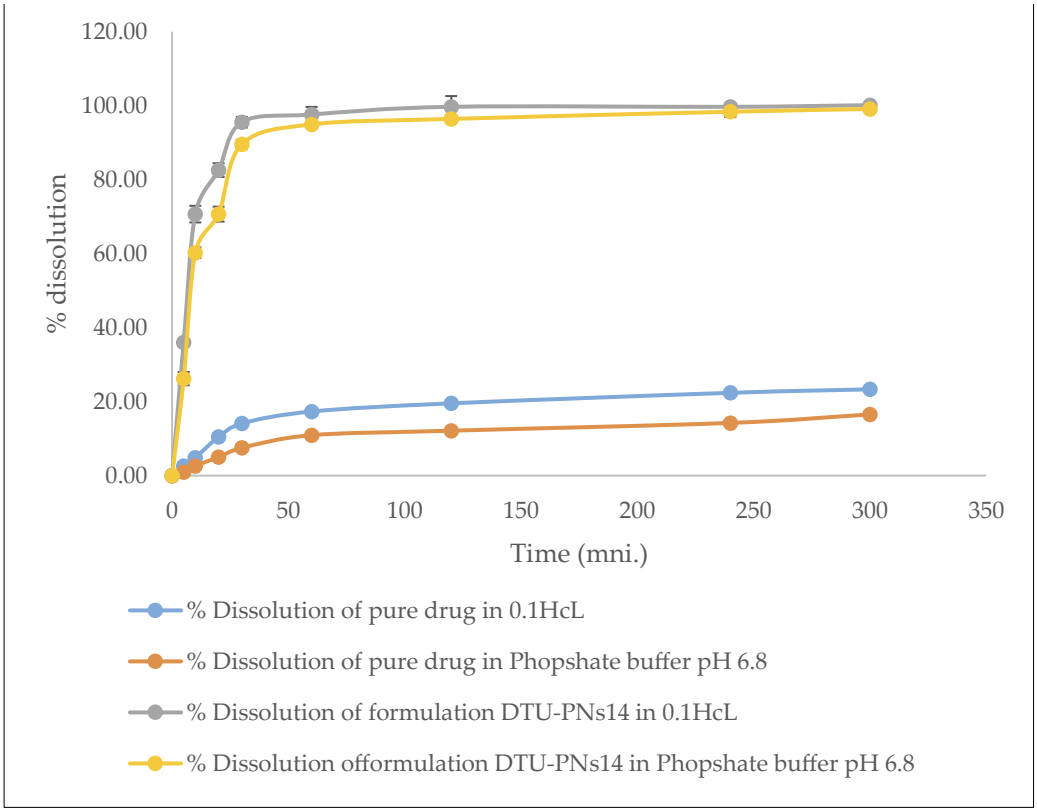

Figure 9. Comparison of the *in-vitro* dissolution profile of the pure drug and TU-loaded proniosome powder in different media

It was evident that testosterone undecanoate dissolved much more quickly in HCl (pH 1.2) than in phosphate buffer solution (pH 6.8). In contrast to the 7–14% of testosterone undecanoate from the pure drug, after 30 min., the dissolving amount of testosterone undecanoate from proniosome was above 89–95% in both buffer HCl (pH 1.2) and phosphate buffer solution (pH 6.8). This might be because of the increased solubility of testosterone undecanoate in proniosomes. This was presumably caused by the fact that testosterone undecanoate was distributed in the proniosome powder in a molecular or amorphous state and that the large surface area of the proniosome powder boosted the drug's drug dissolution rate, causing faster dissolution.

3.5.5 In vitro drug release study

Figure 10 illustrates testosterone undecanoate releases from proniosome formulations and testosterone undecanoate pure drug suspension.

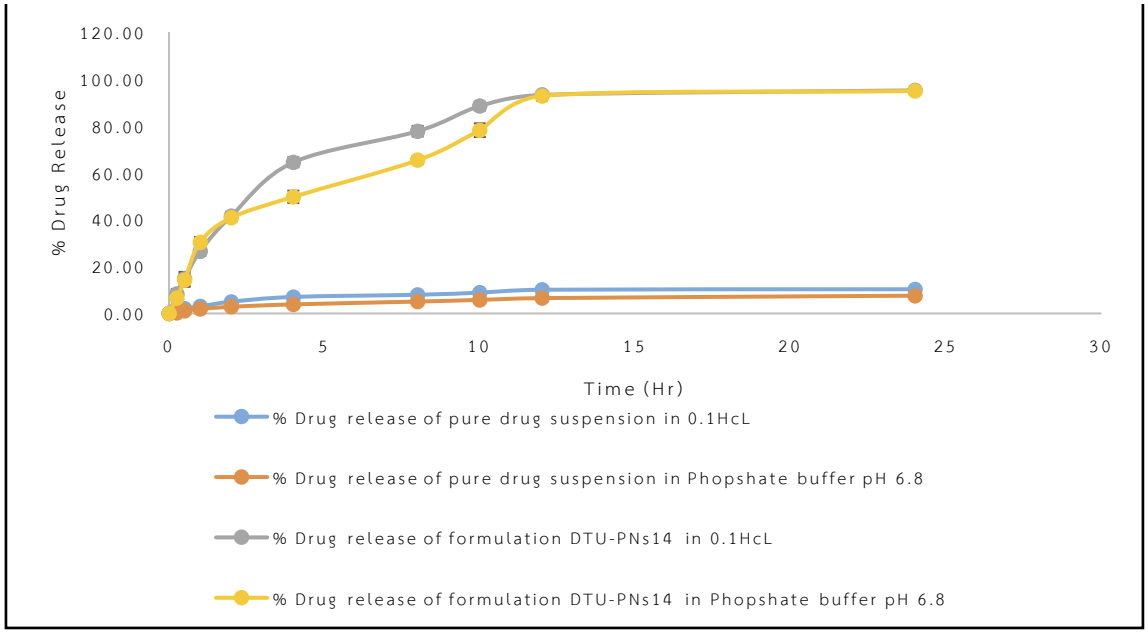

Figure 10. Comparison of the in vitro drug release profile of the testosterone undecanoate from pure drug suspension and TU-loaded proniosome powder in different media

Proniosome formulation had a much higher release rate in phosphate buffer solution (pH 0.1 or 6.8) than testosterone undecanoate pure drug suspension. In contrast to the testosterone undecanoate 26.50 ± 2.01% and 30.37 ± 2.25% from the proniosome formulation, only 3.01 ± 0.25% and 1.91 ± 0.09% of the drug from the testosterone undecanoate pure drug suspension was released in pH 1.2 and 6.8pH, respectively. A clear concentration gradient between the niosomes and the medium was thought to form as the non-trapped drug was released, causing a more rapid release than pure drug suspension. Additionally, after 24 hours, testosterone undecanoate pure drug suspension released 10.31 ± 0.18% and 7.56 ± 0.22% of the drug, whereas proniosome formulation released 95.10 ± 0.86% and 94.81 ± 1.57% of the drug. This was probably because testosterone undecanoate was incorporated into Niosomes, which protected the drug from environmental conditions. From these results, we can conclude that niosomes contributed to the differences between the release of testosterone undecanoate from the proniosome formulations and testosterone undecanoate pure drug suspension.

3.5.6 Percentage drug release kinetic study

Percentage drug release kinetics parameters of the release of the testosterone undecanoate from the optimized proniosome formulations DTU-PNs14 in 0.1N Hcl and pH 6.8 phosphate buffer are as follows:

Table 11. Drug release kinetic model of the optimized formulation DTU-PNs14 in 0.1NHcl and pH 6.8 phosphate buffer

S. No.	Name of media	Regression coefficient			
		Zero-order	First order	Higuchi order	Korsmeyer peppas
1	0.1NHcl	0.698	0.881	0.912	0.541
2	pH 6.8 phosphate buffer	0.765	0.901	0.942	0.553

Table 11 confirms that the testosterone undecanoate release from the proniosomes formulations was best explained by the Higuchi model because it has a higher regression coefficient value than the other models.

3.5.7 Stability study

At predetermined intervals of 1 month, three months, and six months, the proniosomal formulations were assessed for their physical appearance, percentage of drug entrapment, and percentage of drug loading. The stability study of the optimized testosterone undecanoate loaded proniosome formulations was carried out at three different storage conditions, namely 5℃, 30℃/65%RH, and 40℃/75%RH for 6 months. The results

revealed that no changes were noticed under various storage conditions over different time intervals (Table 12). It was observed that there was no change in the color of the proniosomes up to 6 months of storage. The results of the percentage drug entrapment indicated no leakage of the drug.

Table 12. Stability study of DTU-PNs14 indicating physical appearance, percentage drug entrapment, and percentage drug loading

Month	Physical appearance	Percentage drug entrapment			Percentage drug loading		
		Storage condition			Storage condition		
		5°C	30°C/65%RH	40°C/75%RH	5°C	30°C/65%RH	40°C/75%RH
0	White free flowing powder	98.12 ± 0.03	98.12 ± 0.030	98.12 ± 0.030	10.06 ± 0.01	10.05 ± 0.01	10.05 ± 0.01
1	White, free-flowing powder	98.04 ± 0.05	97.97 ± 0.04	97.89 ± 0.02	10.05 ± 0.01	10.05 ± 0.01	10.04 ± 0.02
3	White, free-flowing powder	97.94 ± 0.01	97.96 ± 0.03	97.84 ± 0.02	10.05 ± 0.02	10.05 ± 0.01	10.03 ± 0.01
6	White, free-flowing powder	97.93 ± 0.03	97.94 ± 0.02	97.71 ± 0.16	10.04 ± 0.02	10.04 ± 0.01	10.02 ± 0.02

3.6 *In-vivo* pharmacokinetic study

A bioavailability study was conducted on rats. The established method calculated the testosterone undecanoate concentration after a single oral dosage (10 mg/kg). The test displayed adequate accuracy and precision for application in bioavailability studies using a one-step extraction and a brief run time. Figure 11 depicts the mean plasma concentration-time profiles of testosterone undecanoate after oral administration of the drug suspension and the optimal testosterone undecanoate-loaded proniosomal formulation. PK Solver was used to determine non-compartmental pharmacokinetic parameters, as displayed in Table 13.

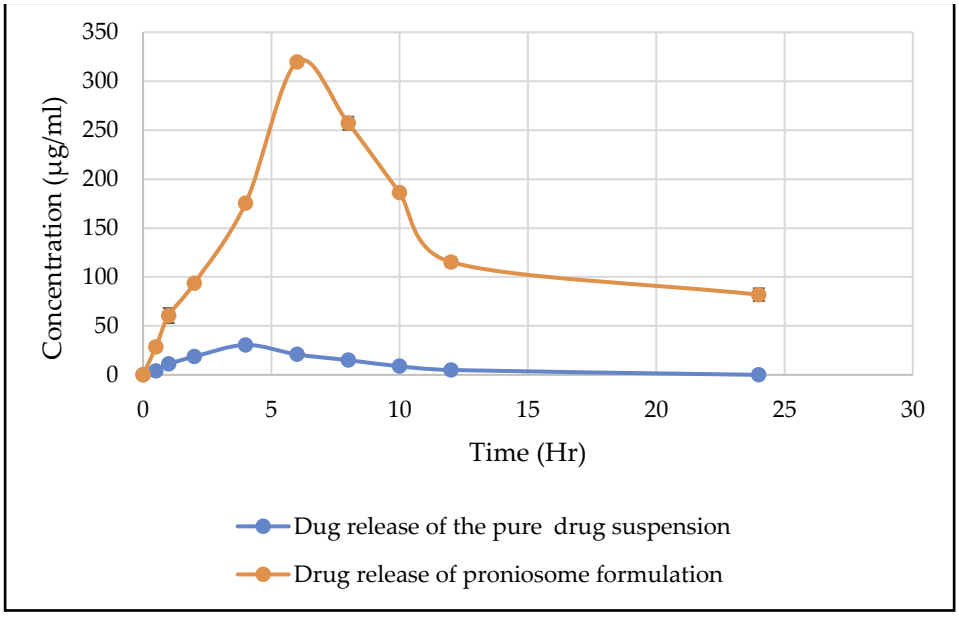

Figure 11. Mean plasma concentration-time curves of testosterone undecanoate after oral administration of its optimized proniosome formulation (equivalent to 10 mg/kg) and testosterone undecanoate drug suspension (10mg/kg) (mean ± SD, n = 3).

Table 13. Pharmacokinetic parameters

Parameter	Pharmacokinetic parameters	
	Pure drug suspension	Optimized proniosome formulations
$t_{1/2}$ (h)	3.279 ± 0.786	9.648 ± 0.591
Tmax (h)	4.000 ± 0.001	6.000 ± 0.001
Cmax (μg/ml)	31.378 ± 1.568	319.608 ± 3.441
AUC $_{0\text{-}24}$ (μg/ml*h)	192.551 ± 2.181	3374.956 ± 70.656
AUC $_{0\text{–}\infty}$.μg/ml*h)	219.259 ± 8.812	4518.856 ± 221.846
AUMC $_{0\text{–}\infty}$ (μg/ml*h^2)	1490.273 ± 199.331	78354.149 ± 8163.846
MRT (h)	6.794 ± 0.675	17.310 ± 0.948
Vz/F ((mg/kg)/(μg/ml)	0.216 ± 0.046	0.031 ± 0.001
Cl/F ((mg/kg)/(μg/ml)/h)	0.046 ± 0.002	0.002 ± 0.001

The Cmax values of testosterone undecanoate from the pure drug suspension and its optimized proniosome formulations were found to be 31.378 ± 1.568 μg/ml and 319.608 ± 3.441μg/ml, respectively. Tmax for testosterone undecanoate in its optimized proniosome formulations and pure drug suspension was 4.0 hours and 6.0 hours, respectively. In the event of an optimized proniosomal formulation, other indices, such as $AUC_{0\text{-}24}$, $AUMC_{0\text{-}24}$, $t_{1/2}$, and MRT, were higher than in the case of pure drug suspension. However, the pharmacokinetic parameters of the testosterone undecanoate proniosome showed that the proniosome enhanced the concentrations of testosterone undecanoate in blood, delayed clearance, and displayed sustained release properties. All of these findings suggested that testosterone undecanoate proniosome formulations drugs might remain for a much more extended period than pure drugs *in vivo*.

4. Conclusions

Using different ratios of span 60 and cholesterol, testosterone undecanoate-loaded proniosomal formulations were successfully fabricated using a slurry technique and optimized employing the central composite design. Based on percentage drug entrapment (%), Vesicle size (nm), and PDI, the proniosomal formulation DTU-PNs14 containing a DoE-optimized cholesterol and span 60 ratio was chosen as the optimal formulation. The formulation DTU-PNs14 was deemed to be the most optimal formulation since it had the optimum particle size and PDI (282.33 ± 1.52 nm and 0.181 ± 0.003) and the significantly high & optimum entrapment efficiency (98.12 ± 1.03%). The Higuchi model best explained the release of testosterone undecanoate from the formulations of proniosomes. It was observed that there was no change of any kind, including the color of the proniosomes, up to 6 months of storage. The results of the percentage drug entrapment indicated no leakage of the drug during the stability study. The *in vivo* pharmacokinetic study also revealed favorable results indicating that testosterone undecanoate proniosome formulations drug might remain longer than a pure drug *in vivo*.

5. Acknowledgements

The authors thank and acknowledge the School of Pharmacy, Abhilashi University, Chail-Chowk, Mandi (H.P.) – 175028, India, for providing the research environment and laboratory support throughout the work.

Author Contributions: Conceptualization, A.S. and D.A.S.; methodology, C.K.; software, A.S.; validation, A.S., D.A.S. and C.K..; formal analysis, A.S.; investigation, A.S..; resources, A.S..; data curation, A.S..; writing—original draft preparation, A.S..; writing—review and editing, D.A.S.; visualization, D.A.S.; supervision, D.A.S.; project administration. All authors have read and agreed to the published version of the manuscript.

Funding: This research received no external funding.

Conflicts of Interest: The authors declare no conflict of interest.

References

[1] Saxena, A.; Apurvi, P.; Aslam, R. A Review on Proniosomes: A Propitious Outlook to the Provesicular Drug Delivery System. *Current drug delivery.* **2023,** *20*(8), 1115-1126. 10.2174/1567201820666221019093921.

[2] Mittal, S.; Chaudhary, A.; Chaudhary, A.; Kumar, A. Proniosomes: the effective and efficient drug-carrier system. *Therapeutic delivery.* **2020,** *11* (2), 125-137. 10.4155/tde-2019-0065.

[3] Sabale, V.; Charde, M.; Dumore, N.; Mahajan, U. Recent Developments in Proniosomal Transdermal Drug Delivery: An Overview. *Current drug delivery.* **2023,** *20*(6), 683-693. 10.2174/1567201819666220422153059.

[4] Adki, K. M.; Kulkarni, Y. A. Chemistry, pharmacokinetics, pharmacology and recent novel drug delivery systems of paeonol. *Life sciences.* **2020,** *250*, 117544. 10.1016/j.lfs.2020.117544.

[5] Limongi, T.; Susa, F.; Marini, M.; Allione, M.; Torre, B.; Pisano, R.; di Fabrizio, E. Lipid-Based Nanovesicular Drug Delivery Systems. *Nanomaterials (Basel, Switzerland).* **2021,** *11*(12). 10.3390/nano11123391.

[6] Zhu, Y.; Cao, S.; Huo, M.; van Hest, J. C. M.; Che, H. Recent advances in permeable polymersomes: fabrication, responsiveness, and applications. *Chemical science.* **2023,** *14*(27), 7411-7437. 10.1039/d3sc01707a.

[7] Abildgaard, J.; Petersen, J. H.; Bang, A. K.; Aksglaede, L.; Christiansen, P.; Juul, A.; Jørgensen, N. Long-term testosterone undecanoate treatment in the elderly testosterone deficient male: An observational cohort study. *Andrology.* **2022,** *10*(2), 322-332. 10.1111/andr.13124.

[8] An, J.; Kong, H. Comparative application of testosterone undecanoate and/or testosterone propionate in induction of benign prostatic hyperplasia in Wistar rats. *PloS one.* **2022,** *17*(5), e0268695. 10.1371/journal.pone.0268695.

[9] Chillarón, J. J.; Fernández-Miró, M.; Albareda, M.; Fontserè, S.; Colom, C.; Vila, L.; Pedro-Botet, J.; Flores Le-Roux, J. A. Testosterone undecanoate improves lipid profile in patients with type 1 diabetes and hypogonadotrophic hypogonadism. *Endocrine journal.* **2016,** *63*(9), 849-855. 10.1507/endocrj.EJ16-0195.

[10] Nieschlag, E.; Nieschlag, S. Testosterone deficiency: a historical perspective. *Asian journal of andrology.* **2014,** *16*(2), 161-8. 10.4103/1008-682x.122358.

[11] Saenger, P.; Steiner, M. Oral testosterone undecanoate is an effective treatment for micropenis therapy. *Pediatric investigation.* **2021,** *5*(4), 323-324. 10.1002/ped4.12304.

[12] Miller, J. A.; Nguyen, T. T.; Loeb, C.; Khera, M.; Yafi, F. A. Oral testosterone therapy: past, present, and future. *Sexual medicine reviews.* **2023,** *11*(2), 124-138. 10.1093/sxmrev/qead003.

[13] Swerdloff, R. S.; Dudley, R. E. A new oral testosterone undecanoate therapy comes of age for the treatment of hypogonadal men. *Therapeutic advances in urology.* **2020,** *12*, 1756287220937232. 10.1177/1756287220937232.

[14] Schlich, M.; Lai, F.; Maria Fadda, A.; Sinico, C.; Pini, E. Drug-Excipients Compatibility Studies in Proniosomal Formulation: A Case Study with Resveratrol. *Journal of nanoscience and nanotechnology.* **2021,** *21*(5), 2917-2921. 10.1166/jnn.2021.19056.

[15] Pankaj, S.; Rini, T.; Dandagi, P. Formulation and Evaluation of Proniosome Based Drug Delivery System of the Antifungal Drug Clotrimazole. *International Journal of Pharmaceutical Sciences and Nanotechnology.* **2013,** *6*, 1945-1951. 10.37285/ijpsn.2013.6.1.4.

[16] Radha, G. V.; Rani, T. S.; Sarvani, B. A review on proniosomal drug delivery system for targeted drug action. *Journal of basic and clinical pharmacy.* **2013,** *4*(2), 42-8. 10.4103/0976-0105.113609.

[17] Sudhamani, T.; Ganesan, V.; Priyadarsini, N.; Radhakrishnan, M. In *FORMULATION AND EVALUATION OF IBUPROFEN LOADED MALTODEXTRIN BASED PRONIOSOME*, **2010**.

[18] Cheriyan, P.; George, B. J.; Thomas, N.; Raj, P.; Samuel, J.; Carla, S. B. Formulation and characterization of maltodextrin based proniosomes of cephalosporins. *World Journal of Pharmaceutical Sciences.* **2015**, 62-74.

[19] Hsieh, C. M.; Yang, T. L.; Putri, A. D.; Chen, C. T. Application of Design of Experiments in the Development of Self-Microemulsifying Drug Delivery Systems. *Pharmaceuticals (Basel, Switzerland).* **2023,** *16*(2). 10.3390/ph16020283.

[20] Rampado, R.; Peer, D. Design of experiments in the optimization of nanoparticle-based drug delivery systems. *Journal of controlled release : official journal of the Controlled Release Society.* **2023,** *358*, 398-419. 10.1016/j.jconrel.2023.05.001.

[21] Mukerjee, A.; Vishwanatha, J. K. Formulation, characterization and evaluation of curcumin-loaded PLGA nanospheres for cancer therapy. *Anticancer research.* **2009,** *29*(10), 3867-3875.

[22] Maji, R.; Dey, N. S.; Satapathy, B. S.; Mukherjee, B.; Mondal, S. Preparation and characterization of Tamoxifen citrate loaded nanoparticles for breast cancer therapy. *International journal of nanomedicine.* **2014,** *9*, 3107.

[23] Cetin, M.; Atila, A.; Kadioglu, Y. Formulation and in vitro characterization of Eudragit® L100 and Eudragit® L100-PLGA nanoparticles containing diclofenac sodium. *AAPS PharmSciTech.* **2010,** *11*(3), 1250-6. 10.1208/s12249-010-9489-6.

[24] Jain, S. K.; Awasthi, A. M.; Jain, N. K.; Agrawal, G. P. Calcium silicate based microspheres of repaglinide for gastroretentive floating drug delivery: preparation and in vitro characterization. *Journal of controlled release : official journal of the Controlled Release Society.* **2005,** *107*(2), 300-9. 10.1016/j.jconrel.2005.06.007.

[25] Averineni, R. K.; Shavi, G. V.; Gurram, A. K.; Deshpande, P. B.; Arumugam, K.; Maliyakkal, N.; Meka, S. R. J. B. o. M. S. PLGA 50: 50 nanoparticles of paclitaxel: development, in vitro anti-tumor activity in BT-549 cells and in vivo evaluation. *Bull. Mater. Sci.* **2012,** *35*(3), 319-326.

[26] Dora, C. P.; Singh, S. K.; Kumar, S.; Datusalia, A. K.; Deep, A. Development and characterization of nanoparticles of glibenclamide by solvent displacement method. *Acta pol pharm.* **2010,** *67*(3), 283-290.

[27] Rasul, A.; Imran Khan, M.; Ur Rehman, M.; Abbas, G.; Aslam, N.; Ahmad, S.; Abbas, K.; Akhtar Shah, P.; Iqbal, M.; Ahmed Al Subari, A. M.; Shaheer, T.; Shah, S. In vitro Characterization and Release Studies of Combined Nonionic Surfactant-Based Vesicles for the Prolonged Delivery of an Immunosuppressant Model Drug. *International journal of nanomedicine.* **2020,** *15*, 7937-7949. 10.2147/ijn.S268846.

[28] Kumar, A.; Gulati, M.; Singh, S. K.; Gowthamarajan, K.; Prashar, R.; Mankotia, D.; Gupta, J. P.; Banerjee, M.; Sinha, S.; Awasthi, A.; Corrie, L.; Kumar, R.; Patni, P.; Kumar, B.; Pandey, N. K.; Sadotra, M.; Kumar, P.; Kumar, R.; Wadhwa, S.; Khursheed, R. Effect of co-administration of probiotics with guar gum, pectin and eudragit S100 based colon targeted mini tablets containing 5-Fluorouracil for site specific release. *Journal of Drug Delivery Science and Technology.* **2020,** *60*, 102004. 10.1016/j.jddst.2020.102004.

[29] Liu, H.; Tu, L.; Zhou, Y.; Dang, Z.; Wang, L.; Du, J.; Feng, J.; Hu, K. Improved Bioavailability and Antitumor Effect of Docetaxel by TPGS Modified Proniosomes: In Vitro and In Vivo Evaluations. *Scientific reports.* **2017,** *7*, 43372. 10.1038/srep43372.

[30] Nasr, M. In vitro and in vivo evaluation of proniosomes containing celecoxib for oral administration. *AAPS PharmSciTech.* **2010,** *11*(1), 85-9. 10.1208/s12249-009-9364-5.

ASEAN
Journal of Scientific and Technological Reports
Online ISSN:2773-8752

Research article

Rubber Management Systems: A Progression from Extractive to Regenerative Production

Robbe Verhofste[1], Lauren Dunteman[2], Michael Commons[3], Oystein Kristiansen[4*] and Uraiwan Tongkaemkaew[5*]

[1] Terra Genesis International PBC, 248 Bone Plain Road, Freeville, New York 13068 USA; robbe@terra-genesis.com
[2] Terra Genesis International PBC, 248 Bone Plain Road, Freeville, New York 13068 USA; lauren@terra-genesis.com
[3] Terra Genesis International PBC, 248 Bone Plain Road, Freeville, New York 13068 USA; michael@terra-genesis.com
[4] Terra Genesis International PBC, 248 Bone Plain Road, Freeville, New York 13068 USA; oystein@terra-genesis.com
[5] Faculty of Technology and Community Development, Thaksin University, Phatthalung, 93210, Thailand; uraiwan@tsu.ac.th
* Correspondence:oystein@terra-genesis.com; uraiwan@tsu.ac.th

Citation:
Verhofste, R.; Dunteman, L.; Commons, M.; Kristiansen, O.; Tongkaemkaew, U. Rubber management systems: A progression from extractive to regenerative production. *ASEAN J. Sci. Tech. Report.* **2024**, *27*(3), e250789. https://doi.org/10.55164/ajstr.v27i3.250789.

Article history:
Received: September 2, 2023
Revised: March 13, 2024
Accepted: March 27, 2024
Available online: April 19, 2024

Abstract: Introduction: Demand for natural rubber is driving an increase in acreage under production and tonnage of rubber produced. Conventionally managed rubber monocultures have presented multiple ecological, economic, and social risks, and alternative rubber management systems must be explored. The paper outlines a gradient of rubber management systems in the provinces of Phatthalung and Songkhla in Thailand. The field observations and exchanges considering the diversity of practices of various rubber farmers were conducted from October 2020-February 2022. Rubber management systems along a gradient ranging from degenerative to regenerative, suggesting each's key principles, characteristics, and benefits were synthesized to the results. Six rubber management systems were found: monocultural, organic, simple polyculture, complex polyculture, modern jungle, and traditional jungle. Outcomes of rubber production systems include ecological health, economic stability, social well-being, farmer knowledge, and increased relationship with nature based on the rubber regeneration production of conventional systems (monocultural) to complex agroforestry systems (Wanakaset). The continuum of regenerative practices with biological monoculture became a complex polyculture; there is a high level of natural regeneration.

Keywords: Rubber; agroforestry; wanakaset; jungle rubber; natural regeneration

1. Introduction

Demand for natural rubber is driving a continuous increase in acreage under production and tonnage of rubber produced [1]. Large-scale plantations and smallholder farmers (who account for 85% of the global output, ~90% in Thailand, Indonesia, and Malaysia are forced to expand to keep up [2]. Demand mainly comes from the automotive industry for tires and non-tire applications [3], with footwear and industrial applications also driving demand [4]. Conventionally, rubber is managed as intensive monocultures, which presents many ecological, economic, and social risks [5]. Ecological degradation, biodiversity loss, global rubber price fluctuations, economic instability, clearing of natural forests, loss of natural capital, and erosion of farmer knowledge and relationship to the land are a few of many serious concerns that indicate an undeniable need to improve the way rubber production is managed [6, 7].

Rubber production systems have the potential to evolve from monocultures into regenerative and abundant complex agroforestry systems [8,9]. The shift aligns with broader sustainability goals to enhance environmental, social, and economic outcomes. This article provides an overview of management classes of rubber production on a continuum from degeneration to regeneration [10] based on lessons from working with rubber-producing farmers in southern Thailand. The progression of a rubber production system towards regeneration is not linear. Rather, each system evolves contextually, allowing farmers to design their system uniquely to suit their place [11]. The studies have reported agroforestry systems in Phatthalung, Songkhla, Satun, and Trang provinces, Thailand, with the kind of trees/shrubs and crops associated with rubber trees [12,13]. However, the study did not mention the regeneration of rubber production in complex agroforestry systems that influence ecological health, economic stability, social well-being, farmer knowledge, and relationship to the land. Songkhla and Phatthalung Provinces represent the study area in this issue. The paper describes systems observed in the field and communicated through the practice of various rubber farmers in Songkhla and Phatthalung and toward regeneration to complex agroforestry systems.

2. Methodology

Phatthalung and Songkhla provinces in southern Thailand were selected as the study sites. Rubber agroforestry has been studied extensively for its long history and is an area studied in many research reports. The population used snowball or chain-referral sampling, followed by rubber farmer purposive sampling, with those happy to share more in-depth information. The tool used in-depth interviews, group interviews, and farm survey tools. Sixty rubber farmers were involved in the sample size. First, we corresponded with knowledgeable key informants, such as the village leader and the staff of the Rubber Authority of Thailand (RAOT), about rubber agroforestry to advise key leaders and groups on this practice. They recommended rubber farmer agroforestry leaders in Rattaphum and Thepa districts, Songkhla province, Tamod and Srinakarin districts, and Phatthalung province, as all of these leaders had good successful models of practice and were either part of larger agroforestry rubber groups or recognized as places of learning for these systems. Second, visits were conducted with these local rubber agroforestry farmer leaders to interview them and visit their farms to learn about their systems, key intercrops, values, observed ecological regeneration, years of practices, and changes observed since shifting from monoculture. Then, they recommended other agroforestry farms from their groups/ networks for additional visits where we collected similar information. From this, a perspective was gained on different rubber agroforestry systems at various ages, their values, and their evolution. In subsequent interviews with key farmer leaders who had been involved in this movement for several years and had visited many other rubber agroforestry farms, supporting farmers to make this transition, they shared observations and learning as to the diversity of different rubber agroforestry systems, their evolution, benefits (and drawbacks if any). Third, we held joint discussion sessions in each community to share and exchange experiences involving several rubber farmers (10- 20) 60 different rubber farmers were involved in these sessions, including experienced rubber agroforestry farmers and about ten monoculture rubber farmers interested in learning about these methods (Figure 1). This whole process was conducted from project initiation in October 2020 through February 2022.

The data obtained were synthesized by identifying rubber production systems, sketching rubber production systems, summarizing conceptual characteristics of rubber production systems, evaluating from degenerative to regenerative rubber production systems, and focusing on the benefits of regenerative rubber production. This information was considered concerning academic papers related to this subject matter in public reference.

Figure 1. Visited rubber agroforestry farms, shared observations, and learning different rubber agroforestry systems

3. Results and Discussion

Six key classes of rubber production systems are identified in this report (Figure 2):

. Monoculture
. Organic monoculture
. Simple polyculture
. Complex polyculture
. Modern jungle rubber
. Traditional jungle rubber

The outlines several practices and options farmers have on their journey towards regeneration and associated outcomes. Traditional rubber systems, such as monoculture, have been reconstructed into biological and single polycultures. These early diversified rubber systems were developed and evolved into complex agroforestry systems.

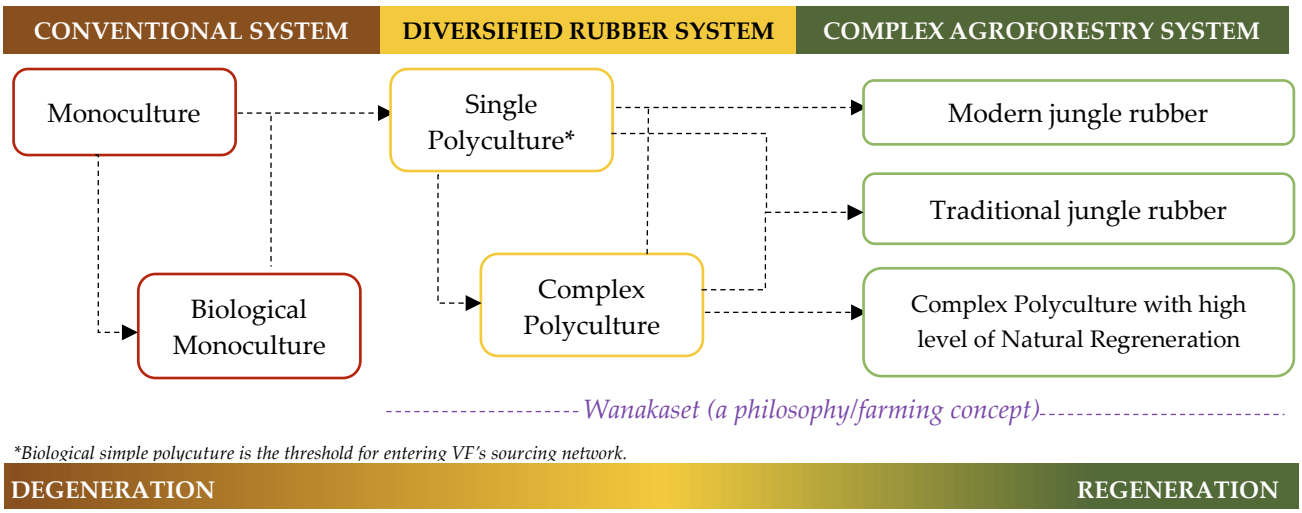

Figure 2. Evaluation from degenerative to regenerative rubber production systems

3.1 Characteristics of Rubber Production Systems

Below are brief descriptions of rubber management tiers ranging from monocultures

3.1.1 monoculture

Conventionally, rubber trees are managed as monocultures with high-yielding clonal rubber trees (Figure 3). This system requires intense management and uses synthetic inputs. Monocultures are present in

both small holdings and agro-industrial estates. Managing rubber conventionally is associated with significant ecological, economic, and social risks (Table 1).

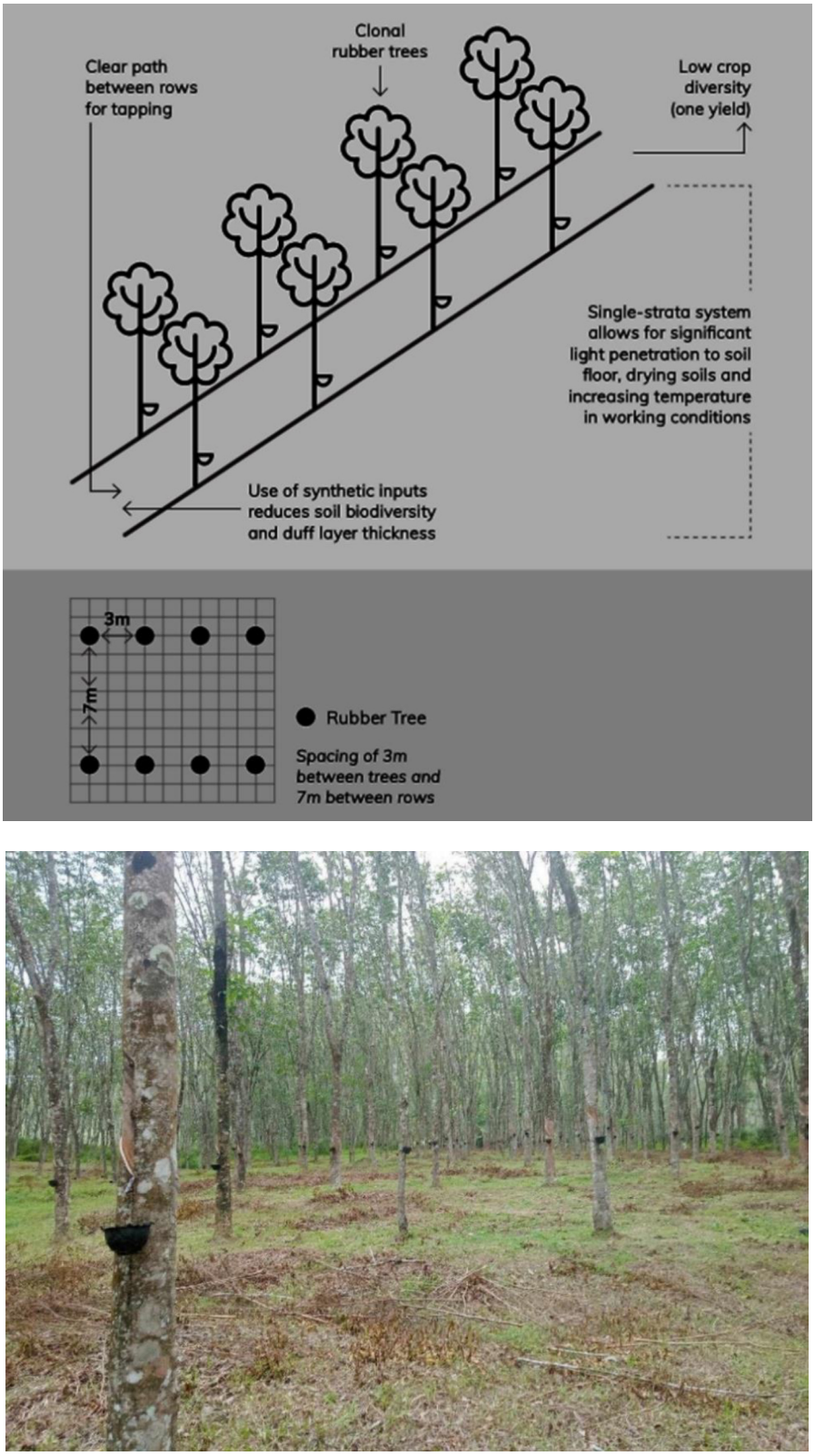

Figure 3. Monoculture rubber typology.

Table 1. Typical outcomes of monocultural rubber management systems.

Dimension	Typical outcomes
Ecological Health	. Deficient ecological health. Degraded ecosystem. . Very low biodiversity above and below ground. . There are no ground covers. No natural regrowth is allowed. . No wildlife or available habitat or fodder. . The rubber trees' low genetic diversity results in low disease resiliency.
Economic Stability	. Highly unstable. . Only one source of income is risky because global rubber prices fluctuate significantly. . Planting monocultures does not provide a yield/income for 7 years. . High input costs.
Social Well-being	. Farmers and communities are exposed to harmful chemicals - adverse health effects. . They lack a sense of culture and meaning: livelihood and economy solely for profit and export. . Farmers often feel forced into conventional production out of necessity and lack of alternatives. . Lack of agency.
Farmer Knowledge	. Farmer knowledge of land, plants, and ecosystems is mainly absent. . Lacking desire or opportunity to learn and develop knowledge.
Relationship with Nature	. Human control over the system is maximized. . Land only serves an economic purpose - farmers have no relationship to the land. . Farmers tending to monocultural, extractive plots that were only recently diversified systems, forests, or tended by a farmer's ancestors may feel emotional/psychological pain.

3.1.2 Organic Monoculture

Managing monocultures organically is an important first step away from degenerative rubber production management. In biological monocultures, synthetic inputs are reduced, phased out, and eliminated (Figure 4). Organic rubber production systems see improvements ecologically, economically, and socially (Table 2).

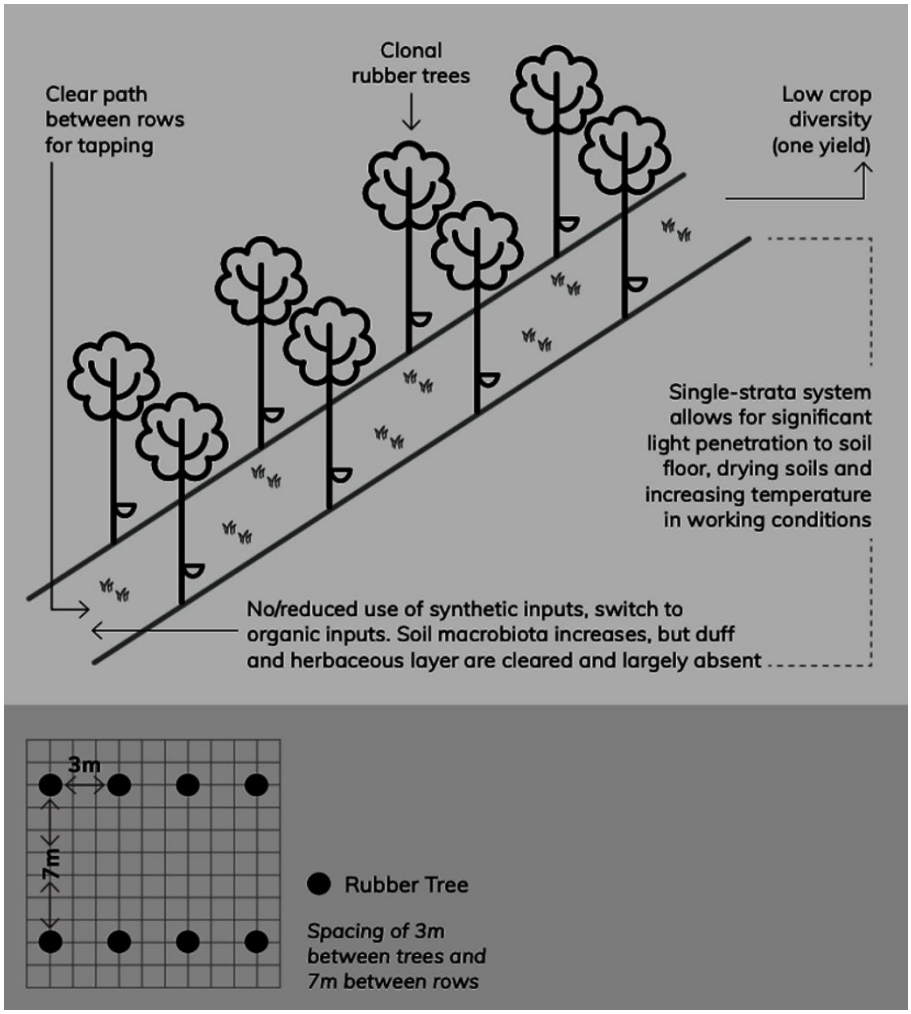

Figure 4. Organic rubber typology.

Table 2. Typical outcomes of organic rubber management systems.

Dimension	Typical outcomes
Ecological Health	. Poor ecological health. . Low but increasing biodiversity above and below ground. . Some natural regrowth may be allowed. . Minimal wildlife habitat or fodder. . The rubber trees' low genetic diversity results in low disease resiliency.
Economic Stability	. Unstable. . Only one source of income is risky because global rubber prices fluctuate significantly. . Planting monocultures does not provide a yield/income for 7 years. . Input costs can still be high.
Social Well-being	. Farmer and community exposure to chemicals decreases. . Lack of sense of culture and meaning: livelihood and economy solely for profit and export. . Lack of access to other nutritious foods. Income constraints purchase of diverse foods.
Farmer Knowledge	. Interest in doing less harm grows, but farmers likely still feel locked into conventional production. . Farmers begin to see ways in which they can work with nature.
Relationship with Nature	. High human control over the system. . Farming biologically can be the start of a deeper relationship with the land.

3.1.3 Simple Polyculture

Simple polycultures are systems that practice intercropping alongside rubber trees (Figure 5). Farmers can temporarily grow an intercrop (such as pineapple) during rubber replanting for a few years until the rubber trees mature. After this, the system is reverted to a monoculture. Alternatively, farmers can choose to intercrop permanently throughout the plantation cycle. This decision marks the starting point for evolving rubber systems towards regeneration. A farmer yields two or more food or non-food products for simple polycultures, and most natural regrowth is removed to maintain order. Ecological, economic, and social outcomes begin to see important improvements (Table 3).

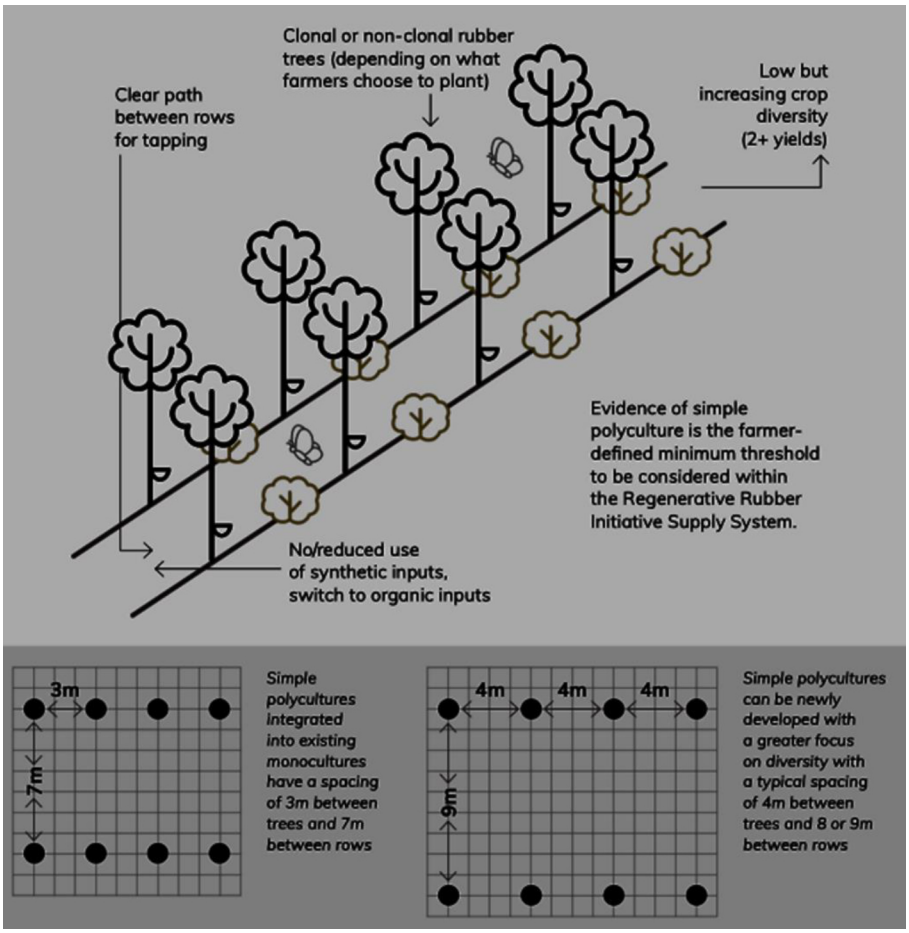

Figure 5. Simple polyculture rubber typology.

Table 3. Typical outcomes of simple polyculture rubber management systems.

Dimension	Typical outcomes
Ecological Health	. Ecological health begins to improve. . Biodiversity increases and more wildlife are attracted. . Some ground cover helps improve soil health. . Natural regrowth is limited. . Synthetic chemicals are eliminated from the system or comply with organic standards.
Economic Stability	. Stability improvements. . Additional yields may be initially used for household consumption/use but can turn into a second income. . Reduced dependence on rubber during periods of low prices. . Constraints on land and labor availability can affect profitability.
Social Well-being	. Human health improves as chemical inputs are used less and less. . Health may also improve as the diversity of local fruits, vegetables, and herbs become part of a regular diet. . It can require intensive labor.
Farmer Knowledge	. Appreciation of other life in the garden grows, but knowledge and understanding are limited.
Relationship with Nature	. Human control over the system is still high. . Farmers often desire an ordered, organized system. . Relationship to the land remains largely economic.

3.1.4 Complex Polyculture

Complex polycultures are systems with several yielding species and crops introduced intentionally or by allowing natural regrowth (Figure 6). Farmers may remove some less desirable species to leave more room and light for more desirable species; however, synthetic inputs are limited. Complex polycultures are much more diversified production systems that produce significant ecological, economic, and social benefits (Table 4).

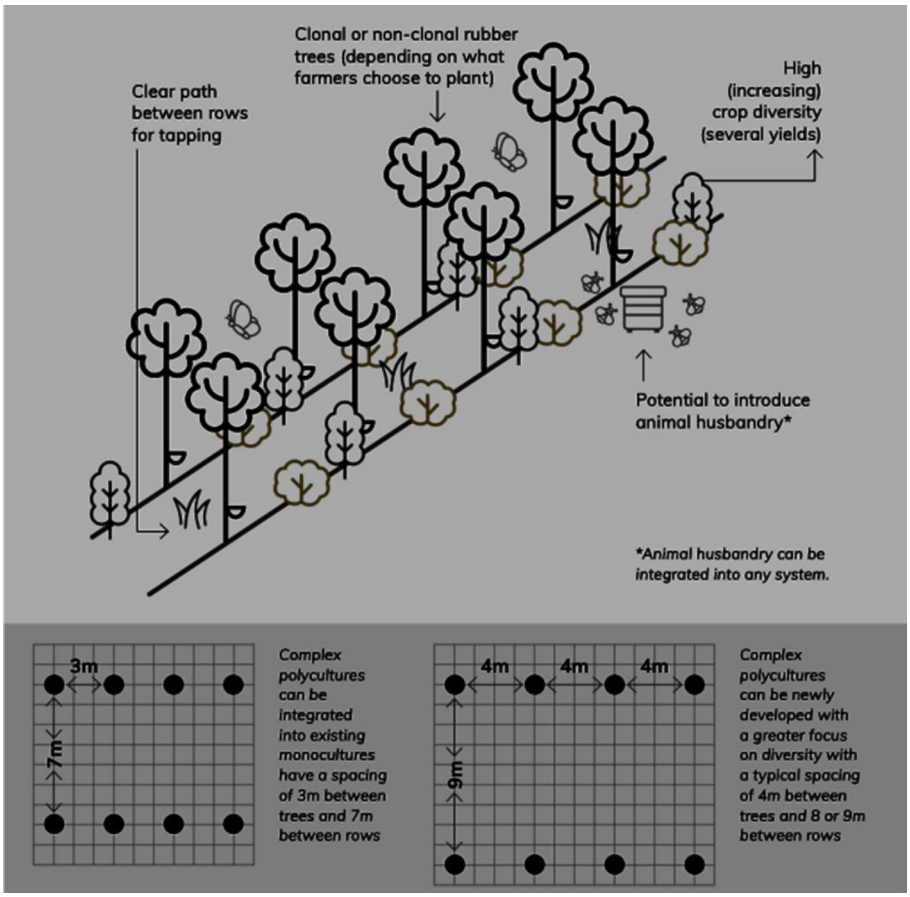

Figure 6. Complex polyculture rubber typology.

Table 4. Typical outcomes of complex polyculture rubber management systems.

Dimension	Typical outcomes
Ecological Health	. Ecological health continues to see improvements. . Biodiversity increases, more wildlife is attracted, and more habitat and fodder are available. . Natural regrowth is allowed, but farmers favor desirable species and weed less desirable species.
Economic Stability	. Increased stability due to several yields that provide for needs and offer alternative incomes. . Not only reliant on rubber.
Social Well-being	. Very limited/ eliminated use of chemical inputs - significant health risks are reduced. . Farmers and communities experience continued health benefits from the additional, nutritious yields their systems provide. . Increasing sense of culture and meaning. . Some labor requirements may be reduced (e.g., the intensity of weed removal may be reduced).
Farmer Knowledge	. Knowledge and understanding continue to increase as farmers learn more. . Beginning to learn the values of more species. . Farmers may not understand the value of certain plants in their system yet.
Relationship with Nature	. Farmers recall a more balanced relationship with nature and are more courageous and open to try something new. . Values and relationships with other plants and animals begin to be explored. . Farmers begin to feel good about their role in helping and working with nature. . Attachment to former ideals of order and organization may remain.

3.1.5 Modern Jungle Rubber

Modern jungle rubber production systems result from leaving a monoculture unmanaged or an intentional decision by farmers. This system consists of clonal rubber trees and naturally regenerating species. While evolution is primarily driven by nature, farmers often select certain species to protect or remove and choose to plant or spread specific species (Figure 7). Modern jungle rubber systems' ecological, economic, and social state are high (Table 5).

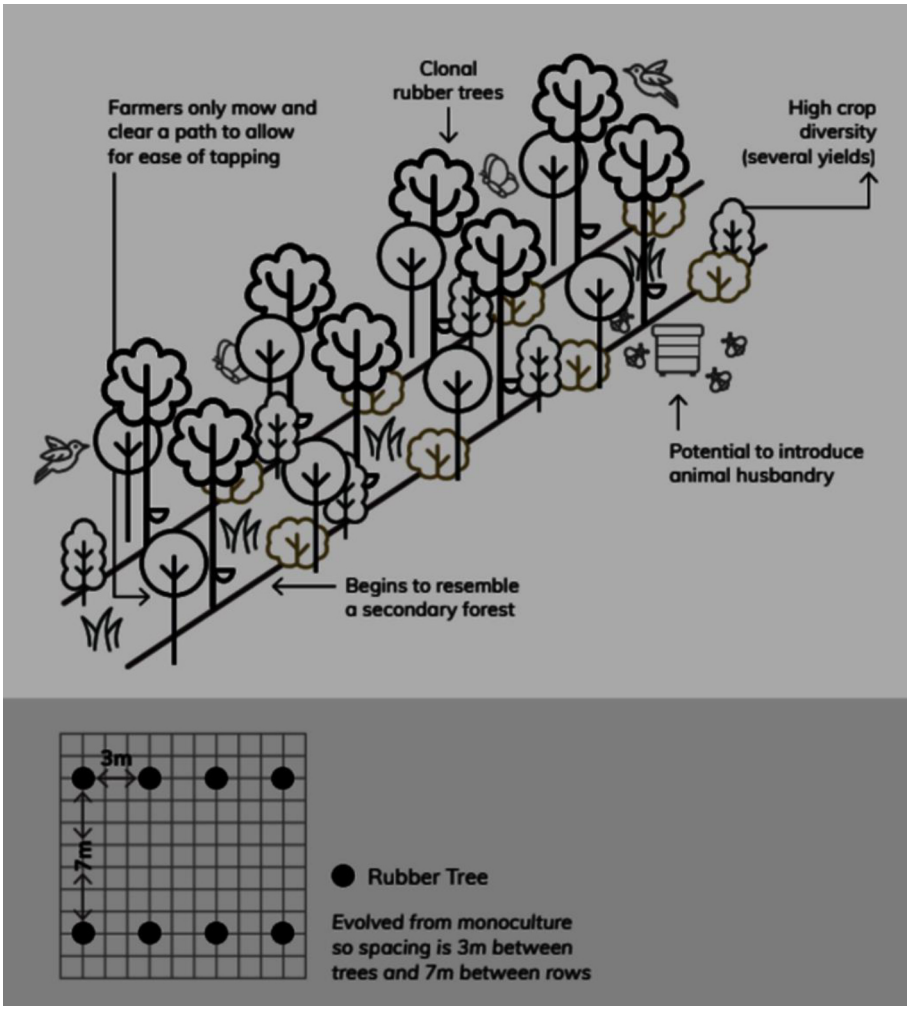

Figure 7. Modern jungle rubber typology.

Table 5. Typical outcomes of modern jungle rubber management systems.

Dimension	Typical outcomes
Ecological Health	. High ecological health. . High biodiversity, high number of wildlife are attracted, abundant habitat and fodder available. . Wildlife brings seeds from surrounding forest areas. . Ground cover and several layers of natural growth. More desirable species are supported. . Many native species are established.
Economic Stability	. Several yields mean more economically stable. . Aside from rubber, there may not be larger regular yields but rather a greater diversity of smaller yields with potential yields developing.
Social Well-being	. Years without the use of synthetic inputs result in greater overall health. . Higher sense of culture and meaning. . Health improves with the availability of medicines and nutritious foods.
Farmer Knowledge	. When part of larger Wanakaset networks that hold and develop knowledge on plant uses for food, medicine, cosmetics, natural dyes, essential oils, biopesticides, and much more, farmers build their knowledge and thus learn the value(s) of many of these species over time. . Many farmers who choose such management are happy to explore their forest gardens as vast libraries of knowledge to discover, to which new titles are always arriving.
Relationship with Nature	. Evolution is primarily driven by nature. . Increased trust and deeper relationship with the land and nature.

3.1.6 Traditional Jungle Rubber

Traditional jungle rubber describes systems using unselected, non-clonal rubber trees introduced into thinned forests or as part of swidden agriculture. These systems are extensive and resemble secondary forests (Figure 8). Management and synthetic inputs for traditional jungle rubber are very limited. Traditional jungle rubber systems operate in a more stable ecological, economic, and social state (Table 6). These systems are an inspiration for designing new regenerative rubber systems.

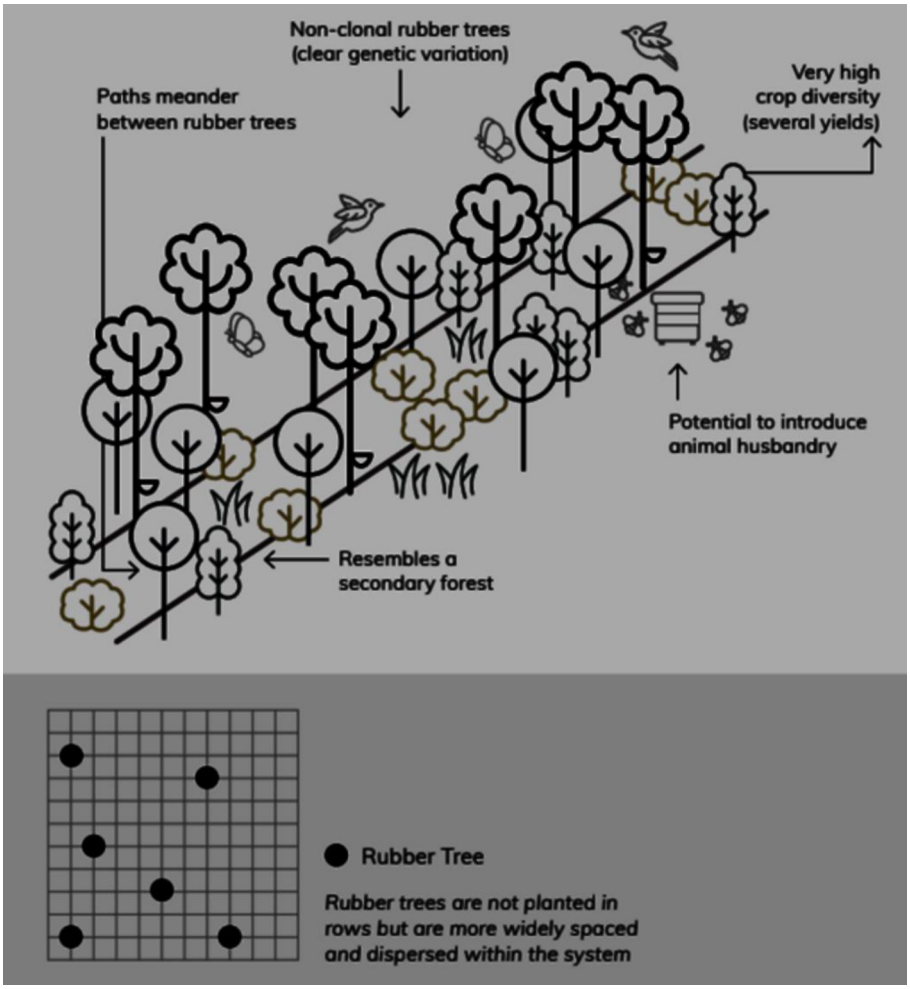

Figure 8. Traditional jungle rubber typology.

Table 6. Typical outcomes of traditional jungle rubber management systems.

Dimension	Typical outcomes
Ecological Health	. High ecological health. . Seed-grown, non-clonal rubber trees are stronger and can survive and produce for decades. . Very high biodiversity. Abundance of wildlife, habitat, and fodder.
Economic Stability	. Economically, farmers have a high level of self-reliance with many yields used for the household. However, when these production systems are found in more remote jungle regions, they will likely experience higher logistic costs. . Farmers describe that when these systems were common, they had minimal dependency on money.
Social Well-being	. Almost all of their needs are met with resources they can harvest and use. . Tapping larger trees with a higher volume of rubber requires less labor. . High level of self-reliance. . Communities, relationships, and local culture are stronger. . In remote areas, there may be fewer public services or market access. There is no electricity or cellular access in very remote areas, and transport is difficult.
Farmer Knowledge	. Farmers describe - and some still remember from previous times - a great deal of knowledge about how to use biodiversity and its products to meet their needs.
Relationship with Nature	. There is a great deal of connection with the ecology, which provides food, materials, medicine, fuel, and much more. . This sort of relationship and knowledge is what many leaders of the Wanakaset rubber movement seek to revitalize and return to their lands and communities.

The findings in this study revealed that rubber farmers have various systems for growing rubber. They are starting to adjust to increasing rubber in a more integrated way. That aligns with the government policy of changing single-crop rubber cultivation to mixed cultivation. The RAOT has promoted the creation of mixed rubber plantations by planting rubber together with other plants, namely creating rubber plantations with 1) rubber as the main crop and 2) perennial trees and trees with economic value as wood for use or 3) fruit trees, vegetables and medicinal plants for consumption or household income generation. Plants in rubber plantations are other plants that can coexist with rubber and be planted together with rubber. They are ground cover crops, rubber intercrops, rubber companion plants, and forests in rubber plantations without negative impact on rubber. The goal of creating integrated rubber plantations is to reduce costs and increase farmers' income for stability, prosperity, and sustainability while improving environmental health. RAOT has principles for selecting plant types and income-supplementing activities in rubber plantations—guidelines for planting plants to suit the rubber planting distance of 7x3 meters with recommendations for planting distance, number of plants, height, exposure to light, canopy layer, and income-generating crop. They present seven rubber systems: System 1: rubber + perennial and economically valuable trees + fruit trees + vegetables and herbs; System 2: rubber + perennial crops and economic trees + fruit trees; System 3: rubber + perennial crops and economic trees + vegetables and herbs; System 4: rubber + perennial crops and economic trees; System 5: rubber + fruit trees + vegetables and herbs; System 6: rubber + fruit trees; and System 7: rubber + vegetables and herbs. [14].

3.2 A Regenerative Approach to Rubber Production

3.2.1 Wanakaset

Rubber system: simple polyculture, complex polyculture, modern jungle rubber, and traditional jungle rubber; they are called 'Wanakaset.'

Wanakaset is a philosophy and values-driven approach to farming that can be incorporated into rubber plantations. The word "Wanakaset" directly translates to "forest agriculture" and refers to a farming

concept developed by Pooyai Viboon in Chachoengsao, Thailand [15]. Building upon traditional knowledge, Wanakaset looks at self-sufficiency and the relationship between humans and the natural environment. This philosophy focuses on developing land to provide resources for basic needs while also growing knowledge and understanding about using these resources efficiently. The greatest loss from clearing natural forests for conventional production has been farmers' and communities' knowledge and relationship with the land and its biodiversity. Without knowledge, experience, relationships, and stories, communities don't know what plants can be eaten, used as medicine, processed into suitable fibers and natural dyes, or many other uses. Leading farmers participating in the Wanakaset process are evolving their rubber gardens into more diverse and integrated systems while developing their knowledge and relationship with the land. This induces a virtuous cycle towards ecological regeneration and increasing diversity of yields and values.

In the case of rubber production in Wabajaset, the characteristics of rubber production systems are on a continuum from degenerative as a rubber monoculture to regenerative as traditional and modern jungle rubber; ecological health, economic stability, social well-being, farmer knowledge, and relationship to the land/system were increased. While clear production classes can be identified, evolving production systems to become regenerative is a highly complex process (Table 7).

Table 7. Characteristics of rubber production systems

Characteristics	**Continuum**			
	Degeneration			**Regeneration**
	Rubber monoculture	→		**Traditional/Modern jungle rubber**
Ecological Health	Low-degrades ecosystem	Increases	→	High-enhances ecosystems
Economic Stability	Low-reliance on single income	Increases	→	High reliance on multiple incomes
Social Well-being	Low-experience poor well-being	Increases	→	High-experience high well-being
Farmer Knowledge	Low-little knowledge of ecology beyond rubber trees	Increases	→	High-deep understanding of land and system
Relationship with Nature	Low-relationship is only economic	Increases	→	High-deep relationship and connection

3.2.2 Continuum of Practices

Embarking on a journey towards regenerative rubber production presents farmers with many choices. Rather than following a linear path, systems progress and evolve in a way unique to the place and to each farmer's practices. The complexity of this progression is illustrated in the continuum below (Table 8). Rubber monoculture uses very high synthetic inputs such as fertilizers and herbicides. Intentionally (re) plant-integrated rubber helps reduce the use of synthetic inputs. Then, clonal varieties and non-clonal seeds were used for genetic variations. Mature forests produce seedlings that can yield valuable yield and help others make the transition. Intentional intercropping, introducing 1-3 additional crops (simple polyculture) or introducing several (3+) different crops (more complex polyculture) increases the use of organic inputs, and synthetic inputs gradually phased out; there is a reduced need for any fertilizer application as the soil improves and more sources of organic matter, and attention to protecting key natural areas around the garden, such as riparian buffers. Allowing natural regrowth was generating natural regrowth that limited maintaining order. It favors desirable species that attract wildlife and remove other less desirable species. Intentionally fruits continue attracting wildlife; secondary unintentional yields are present in bees, wild trees, wild fruit, and herbs. Morover, farmers can collect valuable profits from several intentionally planted crops, and natural regrowth, wildlife, and seeds are protected in the garden but also spread into the surrounding areas. The mature trees can be harvested, providing space and light for other species.

Table 8. Continuum of rubber management practices.

	Use of synthetic inputs → **Use of organic inputs increase**						
	Regenerative						
	Monoculture →	**Intentionally(re)plant integrated rubber** →				**Intentional intercropping**	
Ecological Health	Clearing natural forests for monocultures has a net negative impact on carbon emissions and climate change.	Degraded soil with depleted nutrient reserves and risk of soil erosion	Very low biodiversity	Low resilience to climate change and pathogens and disease	No/very little wildlife	Low structural and functional complexity	Low water infiltration
Economic Stability	Input costs are high	Single income from a single crop-exposed to the risk of rubber price fluctuation and economically unstable				Low financial resilience	
Social Well-being	Exposure to chemicals poses negative health effects		Can experience food insecurity and malnutrition		Lack of autonomy		Reducing synthetic inputs reduces chemical exposure
Farmer Knowledge	Knowledge of plant uses and ecology has largely gone	Courage to try something new		Remembering a different and more balanced relationship with nature		Starting to explore values and relationships to plants and animals	
Relationship with Nature	Little or no sense of relationship with nature	Land serves an economic purpose		May experience spiritual, emotional/psychological pain as a result of their harmful practices		Interest in reducing harm to nature but feeling locked into system	

Table 8. Continuum of rubber management practices.

Use of organic inputs → **Larger, mature trees**

Allowing natural regrowth → **Cultivating products from wildlife**

Ecological Health	Increased		Exposure to chemicals decreases less harmful to wildlife	Water use is a concern in locations with long dry seasons, increasing the risk of climate-related drought	Some new species establish diversity begins to increase	Intercropping		Increase water infiltration	Non-clonal seeds are more resilient to disease	Increasing		
	Soil health	Ground cover				Help reduce pest and disease damage.	Help improve soil water retention.			Wildlife visits that bring seeds	Biodiversity	Above-ground biomass/carbon storage
Economic Stability	Reduces input costs - more money available for the household		Production system meets most "sustainable" rubber standards	Starting to yield plants and/or wildlife for household consumption-reduce other expenses, e.g., food and medicine		At least one significant secondary yield from the system for regular or long-term income			Yielding unintentional plants and/or wildlife that can provide a secondary income. It provides more economic stability when rubber prices are low	Initial transition to more regenerative practices can involve some financial investment and an increase in labor initially		
Social Well-being	Health may improve as diversity of local organic fruits, vegetables, and herbs become part of the regular diet			Labor requirements can be intense (varies by region)				Increasing autonomy	Increased knowledge and relationship to the agro-biodiversity means more and more value(s) from all plants in the system	If labor is scarce, additional yields must be highly profitable or require little additional labor		
Farmer Knowledge	Appreciate seeing this evolution in process, but are likely still attached to order and organization			Starting to see how every plant and animal has a place and role and multiple values		Letting go of need to organize			Excited to allow nature more space to guide the evolution	Developing healthy knowledge and understanding of plants, wildlife and ecology which both bring many values and appreciation		Exploring deeper levels of values and uses such as medicinal values, natural dyes, natural cosmetics
Relationship with Nature	Appreciate other life in the garden, but little knowledge of understanding			Feeling good about this new path and role to help bring back nature's health		Starting to fine more joy in different yields, both from intentionally planting and natural regrowth			Seeing human role and place within nature and cared for by Mother Nature	Increased inner tranquility, sense of balance, and place		

Table 8. Continuum of rubber management practices.

Manure forests → **Natural Regreneration**

Degenerative

Collecting valuable yields from several intentionally planted crops and the natural regrowth → **Traditional jungle rubber**

Ecological Health	Enhanced soil carbon, soil nutrients, and reduced water runoff, microbial biodiversity	Improved water filtration into soils	Land providers habitats for populations of different wildlife and rare native plant species	Increased resilience to effects of climate change	High water infiltration	High complexity	Healthy soil	Garden clearly functioning as a biodiversity reserve, with diverse seeds, seedlings, wildlife, mushroom spores, healthy soil microfauna	High biodiversity	Abundance of wildlife	Resembles secondary forest/traditional jungle rubber
Economic Stability	Seeds and seedlings can be sold as another source of income	Secondary yields surpass value of rubber when prices are low	Income from animal husbandry livestock reduces dependence on income from rubber	Possibility of another income from ecosystem credits	Input expenses are minimal; inputs are sourced from system itself	Income from harvesting large, mature trees can be used to pay for education, retirement or building a house	Economic reliance on rubber is reduced, secodary yields can outweigh income from rubber especially when rubber prices are low. Economic stability is much higher.				
Social Well-being	Some labor requirements can reduce e.g., less intense weeding	Taking more pride in cultural identity as rubber tappers	Contributes to improvements in food security and nutrition	Animal products help increase dietary diversity	More opportunities for female participation (this may already be strong in some regions)	Garden is a clear functional example for others of one part for regenerative rubber agroforestry	Proud and at peace with the positive impact they are having on the land				
Farmer Knowledge	Sifting from student to teacher	Looking less at present value and more at larger systemic and intergenerational values	Increasing understanding and connection with life in the soil, ecology, trees, etc.	Ability to listen and communicate with diversity of life	Deep knowledge and understanding of life, biodiversity, and uses within system/garden/forest						
Relationship with Nature	Exploring deeper levels of culture and spiritual value	Experiencing more and more natural wisdom	Understand religious/spiritual teachings (Dharma) in a vivid and lived way that is experienced in nature	Inner peace about relationship with and within nature	Deep sense of spiritual connection with life	Wildlife is not threatened or threatening at all; humans are a key part of the natural healthy ecology					

4. Conclusions

The continuum presents many practices that farmers can adopt to suit their land best. Some practices have been identified as progression barriers because they inhibit or limit the ability of the system to continue progressing toward regenerative outcomes. Along the progression from degeneration towards regeneration, the continuum identifies key ecological, economic, and social characteristics and important knowledge and relationship shifts that occur along the journey.

5. Acknowledgements

The authors would like to thank rubber farmers in Phatthalung province who have felt well enough to provide information on their experience practices in rubber agroforestry.

Author Contributions: Conceptualized and performed the experiments, R.V. and L.D; data collection and formal analysis, M.C; writing- review and editing, O.K. and U.T. review, editing, and supervision. All authors have read and agreed to the published version of the manuscript.

Funding: This research was funded by VF Corporation, USA; kindly support from 2021 to 2022.

Conflicts of Interest: The authors declare no conflict of interest.

References

[1] Warren-Thomas, E.; Dolman, P. M.; Edwards, D. P. Increasing Demand for Natural Rubber Necessitates a Robust Sustainability Initiative to Mitigate Impacts on Tropical Biodiversity. *Conservation Letters*. **2015**, *8(4)*, 230–41. https://doi.org/10.1111/conl.12170.

[2] Fox, J.; Castella, J-C. Expansion of rubber (*Hevea brasiliensis*) in Mainland Southeast Asia: What are the Prospects for Smallholders? *The Journal of Peasant Studies*. **2013**, *40*(1), 155-170. https://doi.org/10.1080/03066150.2012.750605.

[3] Laurance, W. F; Sayer, J.; Cassman, K. G. Agricultural Expansion and Its Impacts on Tropical Nature. *Trends in Ecology & Evolution*. **2014**, *29(2)*, 107–116. https://doi.org/10.1016/j.tree.2013.12.001.

[4] Rubber Market Size, Industry Share, Outlook 2020-2027. Available online: www.fortunebusinessinsights.com/industry-reports/rubber-market-101612. (Accessed 11 Apr. 2023).

[5] Stroesser, L.; Penot, E.; Isabelle, M.; Tongkaemkaew, U.; Chambon, B. Income Diversification for Rubber Farmers through Agroforestry Practices: How to Overcome Rubber Price Volatility in Phatthalung Province, Thailand. *Annual conference of the International Rubber Research and Development Board*. **2016.**

[6] Warren-Thomas, E.; Dolman, P. M.; Edwards, D. P. Increasing Demand for Natural Rubber Necessitates a Robust Sustainability Initiative to Mitigate Impacts on Tropical Biodiversity. *Conservation Letters*. **2015**, 8(4), 230–41. https://doi.org/10.1111/conl.12170.

[7] Ahrends, A.; Hollingsworth, P. M.; Ziegler, A. D.; Fox, J. M.; Chen, H.; Su, Y.; Xu, J. Current trends of rubber plantation expansion may threaten biodiversity and livelihoods. *Global Environmental Change*. **2015**, 34, *48–58*. https://doi.org/10.1016/j.gloenvcha.2015.06.002.

[8] Singh, A. K.; Liu, W.; Zakari, S.; Wu, J.; Yang, B.; Jiang, X. J.; Zhu, X.; Zou, X.; Zhang, W.; Chen, C.; Singh, R.; Nath, A. J. A Global Review of Rubber Plantations: Impacts on Ecosystem Functions, Mitigations, Future Directions, and Policies for Sustainable Cultivation. *Science of the Total Environment*. **2021**, *796*, 148948. https://doi.org/10.1016/j.scitotenv.2021.148948.

[9] Drescher, J.; Rembold, K.; Allen, K.; Beckschäfer, P.; Buchori, D.; Clough, Y.; Faust, H.; Fauzi, A. M.; Gunawan, D.; Hertel, D.; Irawan, B.; Jaya, I. N. S.; Klarner, B.; Kleinn, C.; Knohl, A.; Kotowska, M. M.; Krashevska, V.; Krishna, V.; Leuschner, C.; Lorenz, W. Ecological and Socio-Economic Functions Across Tropical Land Use Systems After Rainforest Conversion. *Philosophical Transactions of the Royal Society B: Biological Sciences*. **2016**, *371*(1694), 20150275. https://doi.org/10.1098/rstb.2015.0275.

[10] Reed, B. Shifting from "Sustainability" to Regeneration. *Building Research & Information*. **2007**, *35*(6), 674–680. https://doi.org/10.1080/09613210701475753.

[11] Mang, P.; Reed, B. Designing from Place: A Regenerative Framework and Methodology. *Building Research & Information*. **2019**, *40(1)*, 23–38. https://doi.org/10.1080/09613218.2012.621341.

[12] Tongkaemkaew, U.; Penot, E; & Chambon, B. 2020. Rubber Agroforestry Systems in Mature Plantations in Phatthalung Province, Southern Thailand. *Thaksin Journal*. **2020**, *23*(1), 78-85.

[13] Jongrungrot, V. Resilience, various benefits, and constraints of rubber agroforestry systems in southern Thailand. *International Journal of Agricultural Technology*. **2021**, *17*(2), 517-534. Available online http://www.ijat-aatsea.com. ISSN 2630-0192 (Online)

[14] Prommee, W. Guidelines for integrated rubber plantation management by planting rubber together with other plants. Rubber Research Institute Rubber Authority of Thailand, 86 pages. Available online: https://www.opsmoac.go.th/songkhla-local_wisdom-files-432891791797. (Accessed 11 Apr. 2023) **2021**. (in Thai).

[15] Commons, M. Wanakaset Network Thailand. Available online: https://ecovillage.org/ecovillage/wanakaset-network-thailand/ April 4, 2019. (Accessed 11 Apr. 2023).

ASEAN
Journal of Scientific and Technological Reports
Online ISSN:2773-8752

Research article

Noise Emission Assessment of a Utility-Scale Wind Power Plant: Case Study of a 90 MW Wind Power Plant in Mukdaharn Province, Northeastern Thailand

Sunisa Kongprasit[1], Somphol Chiwamongkhonkarn[2], Fida Ali[3], Pongsak Makhampom[4], Yves Gagnon[5], and Jompob Waewsak[6*]

[1] Faculty of Science and Digital Innovation, Thaksin University (Phatthalung Campus), Phatthalung, 93210, Thailand; sunisa@tsu.ac.th
[2] Research Center in Energy and Environment (RCEE), Division of Physics, Faculty of Science and Digital Innovation, Thaksin University (Phatthalung Campus), Phatthalung, 93210, Thailand; dungding_19@hotmail.com
[3] Research Center in Energy and Environment (RCEE), Division of Physics, Faculty of Science and Digital Innovation, Thaksin University (Phatthalung Campus), Phatthalung, 93210, Thailand; fidaali.akhss@gmail.com
[4] Faculty of Engineering, Thaksin University (Phatthalung Campus), Phatthalung, 93210, Thailand; 602995011@tsu.ac.th
[5] Université de Moncton, Edmundston (NB), Canada; yves.gagnon@umoncton.ca
[6] Research Center in Energy and Environment (RCEE), Division of Physics, Faculty of Science and Digital Innovation, Thaksin University (Phatthalung Campus), Phatthalung, 93210, Thailand; jompob@tsu.ac.th
* Correspondence: jompob@tsu.ac.th

Citation:
Kongprasit, S.; Chiwamongkhonkarn, S.; Ali, F.; Makhampom, P.; Gagnon, Y.; Waewsak, J. Noise Emission Assessment of a Utility-Scale Wind Power Plant: Case Study of a 90 MW Wind Power Plant in Mukdaharn Province, Northeastern Thailand. *ASEAN J. Sci. Tech. Report.* **2024**, *27*(3), e253184. https://doi.org/10.55164/ajstr.v27i3.253184

Article history:
Received: March 13, 2024
Revised: April 3, 2024
Accepted: April 5, 2024
Available online: April 20, 2024

Abstract: The noise impact of wind power plants is one of the major reasons for social opposition to wind energy development. The complex noise model (ISO 9613) was employed to model the noise generated by 15 GW165-6.0 MW wind turbine generator units based on the manufacturer-defined acoustic profile. The wind resource at a hub height of the wind turbine generators (144 m agl) was first predicted based on computational fluid dynamics flow modeling. The model noise levels were mapped using ArcGIS and twenty-two receptors comprising houses, temples, and other places at varying distances within the project boundary. Likewise, to compare the noise levels of the wind turbine generators with different noise levels, the ambient noise was measured at selected four receptors. The results showed that the predicted noise was less than 70 dB(A) in the vicinity of the wind turbine generators, decreased down to 40-45 dB(A) within the project boundary, and was in the range of 35-40 dB(A) in the community area. The compared results showed that the ambient noise exceeds the noise levels from the wind turbine generators at all four receptor sites. Hence, wind power plants would not cause any additional noise pollution. Such studies are vital to providing awareness to the public based on proven scientific evidence to gain the public's trust and mitigate social opposition to wind power plants.

Keywords: Onshore Wind Power Plant; Noise Disturbance; Noise Profile; Octave Band; Public Opposition.

1. Introduction

Onshore wind energy is one of the primary renewable energy sources for the transition to a net zero energy system of the future. At the COP28 climate conference, world leaders recently reiterated their commitment to global emission control, pledging to triple the installed renewable energy to 11,000 GW by 2030 [1]. Wind energy is at the forefront of this renewable energy development, with the installation of 75 GW in 2022 alone [2]. However, the net-zero energy

targets of 2050 require an unprecedented level of wind energy development, which will achieve a 35% share of electricity generation [3]. To accomplish this mammoth goal, global wind installation needs to increase significantly, with the global cumulative installed capacity of onshore wind needing to reach 1,787 GW by 2030 and 5,044 GW by 2050, a nine-fold increase from 542 GW in 2018 [3]. Achieving these targets will be a global task, with countries developing their onshore wind resources on a priority basis.

Thailand is an emerging Southeast Asian economy with relatively good onshore wind resources that can be developed to relieve its heavy reliance on fossil fuels for energy needs. Several studies have been carried out for the resource assessment of the country's onshore wind potential. Employing the wind atlas analysis and application model (WAsP), Kamdar and Taweekun [4] showed that a wind power plant in the Hat Yai region of southern Thailand could generate 2,731 MWh annually [4]. Atmospheric and computational fluid dynamics (CFD) wind flow modeling are other widely used wind resource assessment tools, with the capability to simulate wind speeds at multiple elevations above ground level (agl) [5]. The power production of a 300 MW wind power plant in southern Thailand was estimated using CFD-based wind resource assessments [5]. Similarly, another 13 to 18 GWh/year of wind power potential was estimated along the Amadan coast using CFD-based assessment at 100 and 120 m agl.

Wind energy potential was assessed for the Mekong area in the upper northeastern part of Thailand. High-resolution wind maps were developed at 100, 120, and 200 m agl [6]. This work showed that wind speeds in the 1.29 to 3.79 m/s range were presented near Laos, while the mountainous area in Mukdahan has wind speeds between 1.63 to 3.85 m/s [7].

The MC2 and Ms-Micro models were applied in the same region using mesoscale and microscale atmospheric models and 10 years of NCEP/FNL climatic database. The simulated wind resource showed that the high potential areas mainly occurred in mountainous areas. It can be concluded that the Kalasin Province would produce the largest energy output from wind power plants [8].

Given the proper regulatory and policy attention, Thailand has an onshore wind potential of 13 to 17 GW [9]. However, Thailand has installed only 1,545 MW of onshore wind energy as of 2022 [2], leaving a huge potential yet to be developed. However, in recent years, onshore wind energy development has faced another challenge in the form of public opposition due to its environmental, notably because of its acoustic footprint.

The noise produced by wind turbine generators (WTG) is a major concern for the residents living near wind power plants and has been a major cause of public opposition. Wind turbine noise and the annoyance induced can be a major cause of opposition from the communities near wind power plants [7]. Wind power plant noise has been associated with sleep disturbances in the local population, affecting their daily routines and health [10-12]. In addition to sleep deprivation, people living around wind power plants also complain of anxiety, sleepiness, fatigue, and irritability [13,14]. The low-frequency noise produced by wind turbine generators is often blamed for sleep disorders, hearing loss, and vestibular system anomalies [15].

To assess if specific public policies should be implemented to regulate wind energy development, the Government of Canada recently mandated an international panel of experts to assess the scientific literature on the impact of wind turbine noise on human health [16]. The conclusions of this exhaustive work identified that the evidence is sufficient to establish a causal relationship between exposure to wind turbine noise and annoyance. At the same time, there is limited evidence to establish a causal relationship between exposure to wind turbine noise and sleep disturbances. Further, the evidence suggested a lack of causality between exposure to wind turbine noise and hearing loss. In contrast, the evidence was inadequate to come to any conclusion about the presence or absence of a causal relationship between commonly claimed health impacts and exposure to wind turbine noise.

Nonetheless, wind turbine noise is becoming one of the major causes of public opposition to onshore wind power plants, and addressing this issue is paramount. Unfortunately, misinformation leads to public opposition due to insufficient scientific evidence. Wind power plants generate noise, but it is important to access and compare them with other sources of noise in their vicinity to know if the noise generated from the wind turbines exceeds the ambient noise.

Recently, noise emissions by a utility-scale wind power plant in Thailand were modeled based on a simple noise emission modeling (Simple - ISO9613), which requires the wind speed and the noise profile of a wind turbine generator in normal power mode at arbitrary wind speeds [17]. On the other hand, complex

noise modeling requires more information on the 1/3 octave sound power spectrum at the hub height of a wind turbine generator.

This study is aimed at assessing noise emissions of a proposed 90 MW utility-scale wind power plant and its impact on the surrounding communities in the Mukdaharn province of northeastern Thailand. The study employed complex noise modeling to map the noise levels at different locations around the proposed wind power plant, compared to the measured ambient noise within the project's boundary, to determine their impacts. The study is among a handful of studies carried out in the region to study the acoustic effect of wind power plants, which can be very important for developing wind energy and mitigating public opposition to onshore wind power plants.

2. Materials and Methods

2.1 Study Area

The study area is in Mukdaharn province, northeastern Thailand, as shown in Figure 1. This study area is the object of a proposed 90 MW utility-scale wind power plant. The 90 MW wind power plant would consist of 15 units of a 6.0 MW wind turbine generator that will be derated during the operation phase. Figure 2 shows the project boundary of the 90 MW wind power plant, the locations of each wind turbine generator, the locations of sensitive areas, and the locations of the communities around the wind power plant.

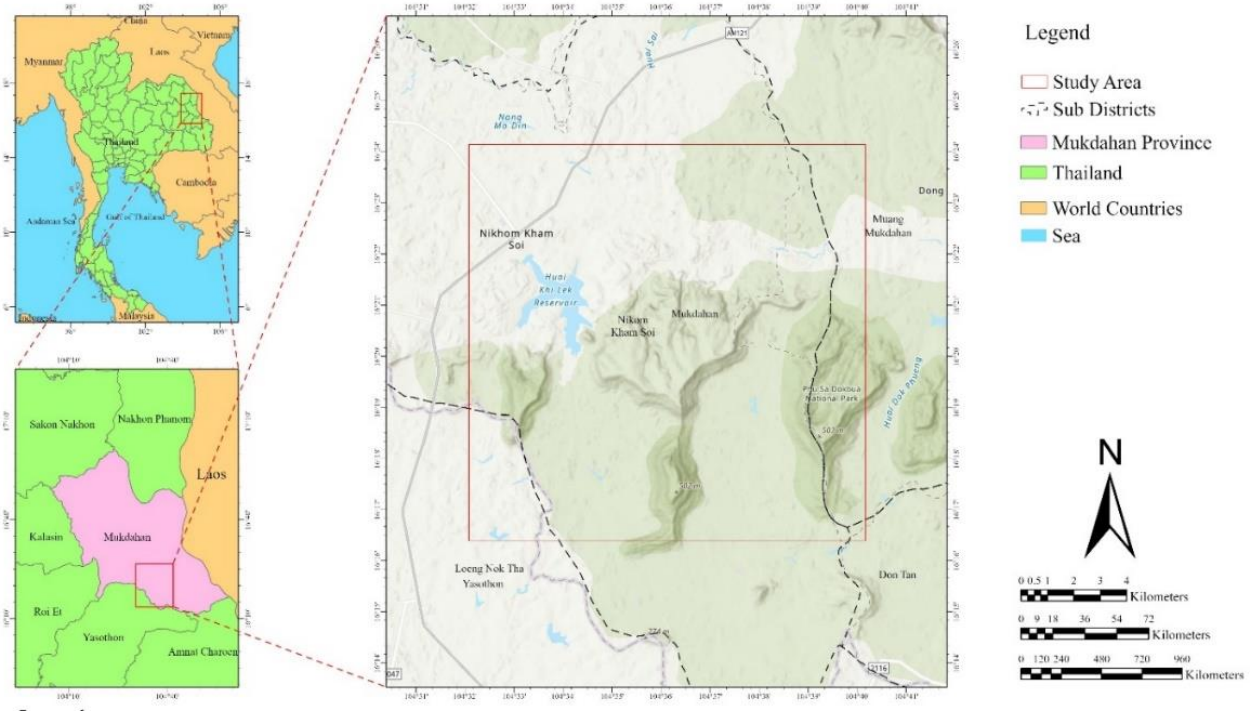

Figure 1. The study area.

2.2 Methodology

The methodology used for the study is illustrated in Figure 3. Initially, a 3 km project boundary is defined around each wind turbine generator, along with a 0.5 km buffer to comply with the Code of Practice (CoP) issued by Thailand's Office of Energy Regulatory Commission (OERC). The connection of these individual boundaries contains the locations of the 15 proposed wind turbine generators, the residences, and the receptors where the noise levels are calculated. The noise generated by the wind turbine generators in the study area is based on the wind speeds obtained from a wind resource map covering a 10 x 10 km^2 area at a resolution of 50 m.

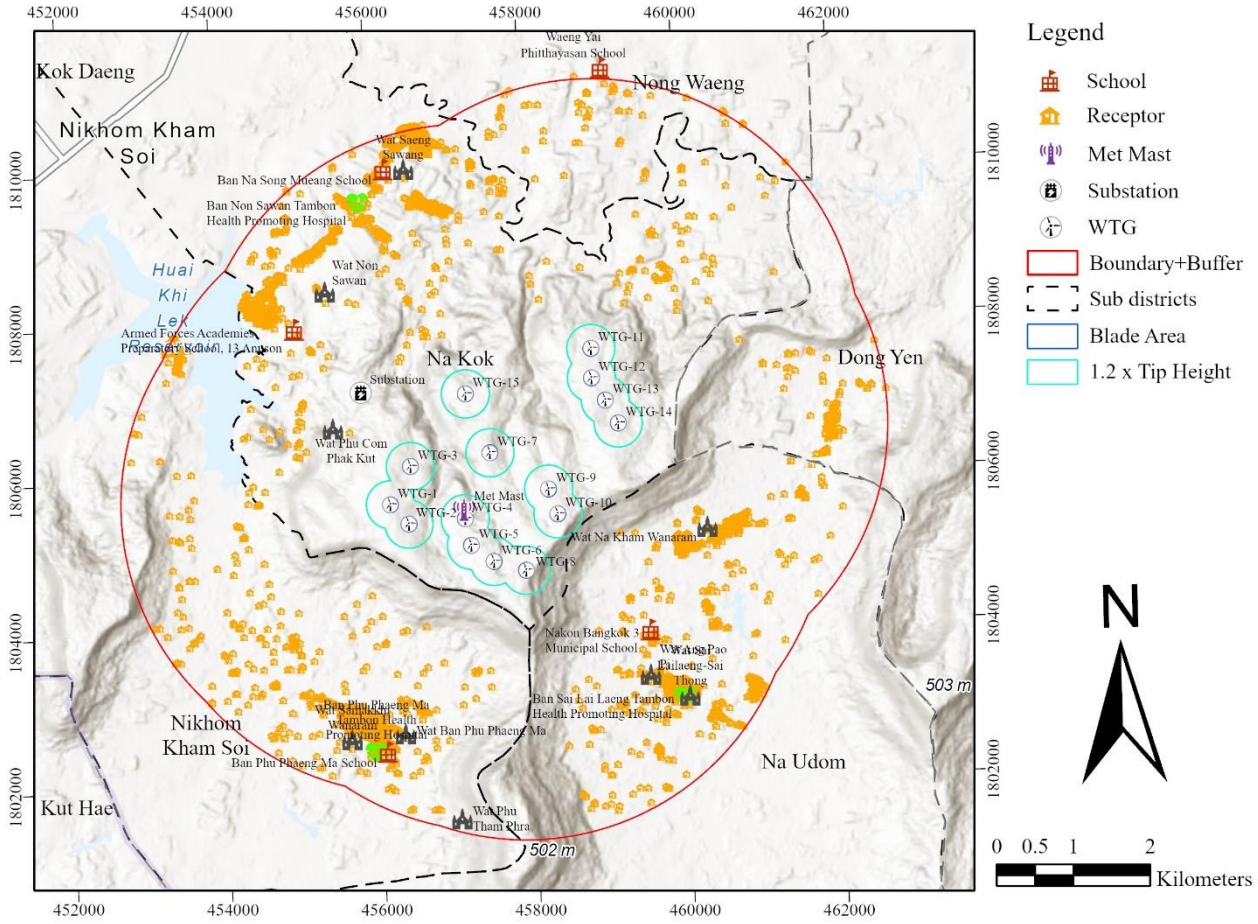

Figure 2. Project boundary of a proposed 90 MW wind power plant in the Mukdaharn province of northeastern Thailand.

The microscale wind resource map was generated from a computational fluid dynamics (CFD) wind flow modeling with the project's observed wind data, along with the input of 30 m resolution topographic data (GDEM), and the Land Cover Land Use (LCLU) from the Land Development Department data of 2021.

The noise impact assessment is simulated using complex noise modeling that complies with the ISO 9631 standards in WindFarmer modeling software. The manufacturer of the wind turbine generator provides the noise characteristics. The noise level simulation generates 24-hour average, daytime and nighttime, and maximum noise levels. Finally, the disturbance was analyzed using the Pollution Control Department (PCD) guidelines [18].

2.3 Microscale Computational Fluid Dynamics Wind Flow Modeling

Computational fluid dynamics (CFD) wind flow modeling is widely used to simulate wind flow caused by the local terrain characteristics and the topography, notably in complex terrains [19–21]. In this study, the CFD modeling was applied for the wind speed prediction over a 10 x 10 km^2 grid, with the measured wind speeds and directions from a 144 m met mast being used as the numerical modeling input. The position of the met mast is shown in Figures 2 and 5.

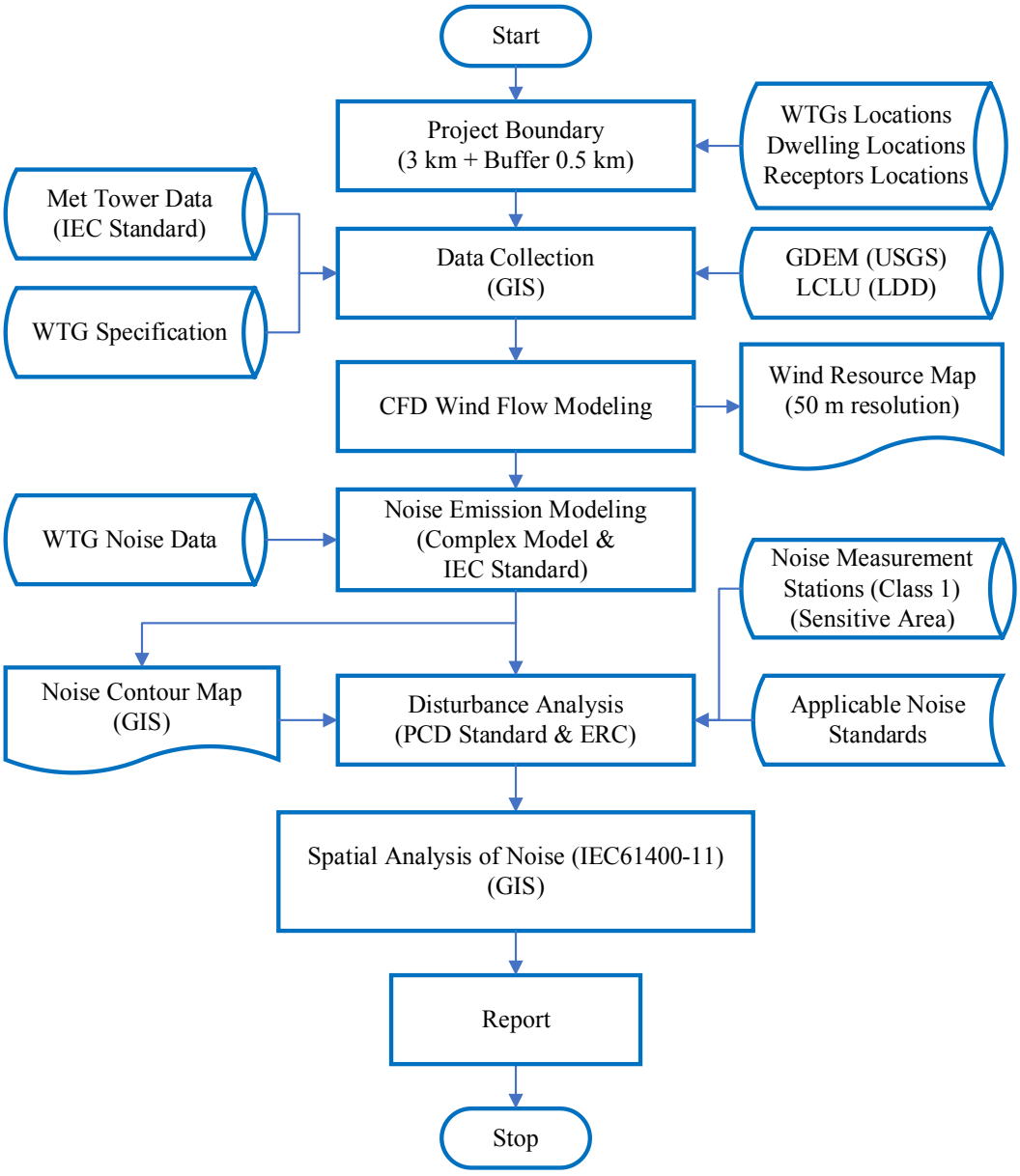

Figure 3. Methodology adopted for the study.

The main inputs required by the CFD wind flow modeling consist of the boundary conditions, i.e., the terrain features (Digital Elevation Model (DEM)), the roughness, as well as the initial conditions, i.e., the wind climatology in the form of wind speeds and directions at typical points of measurement in the study area.

The distribution of the climatic wind speeds, measured from the met mast at 144 m agl and used in the CFD simulations, is shown in Figure 4. At an elevation of 144 m agl, the wind data was collected from the met mast in the project's study area from 00:00 on October 25, 2021, to 00:00 on January 30, 2023. Using a Weibull distribution analysis, the shape parameter was determined to be 2.526 (dimensionless), the scale parameter to be 8.182 m/s, and the annual mean wind speed to be 8.79 m/s, shown in Figure 4 (left), which confirms that the study area is suitable for the development of a wind power plant. To determine the wind direction, the wind rose was partitioned into 16 sections, as shown in Figure 4 (right), indicating a clear dominant wind from the northeast direction.

In this analysis, the ASTER Global Digital Elevation Model (GDEM) V2 [22] provided by the USGS, with 30 m resolution, was used to represent the terrain features of the study area. The roughness was

interpreted using the Land Cover Land Use (LCLU) data from the Land Development Department of Thailand [23]. The DEM, the roughness, and the LCLU maps of the study area are presented in Figure 5.

The standard k-epsilon turbulent model was applied to execute the CFD wind flow modeling under neutral air stability conditions and air density of 1.225 kg/m^3 using the GCV solver in the WindSim simulation tool. The details of the conditions used for the CFD wind flow modeling are presented in Table 1.

Table 1. Wind flow simulation conditions using computational fluid dynamics.

Parameter	Condition
Model setup	3-D wind field and 16-sector run
Grid spacing (m)	50
No. of cells	1,722,840
Height of boundary layer (m)	500
Speed above boundary layer (m/s)	10.0
Boundary condition at the top	Fixed pressure
Potential temperature	No
Turbulence model	Standard k-epsilon
Solver	GCV
Air stability	Neutral
Air density (kg/m^3)	1.225

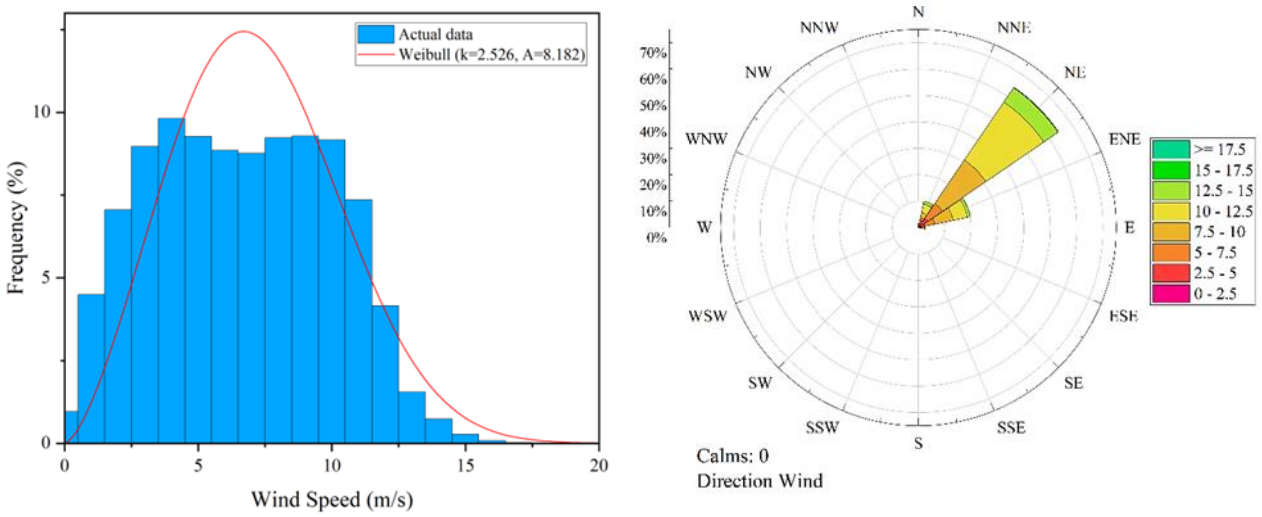

Figure 4. Weibull distribution (left) and wind rose (right) of the wind resource over the study area.

The spatial distribution of the wind speed obtained from the CFD modeling across the study area at 144 m agl is shown in Figure 6. Most of the study area has wind speeds above 8 m/s, with pockets of the area having less than 6.5 m/s and above 10 m/s, thus confirming that the study area is highly suitable for utility-scale wind power plants [24].

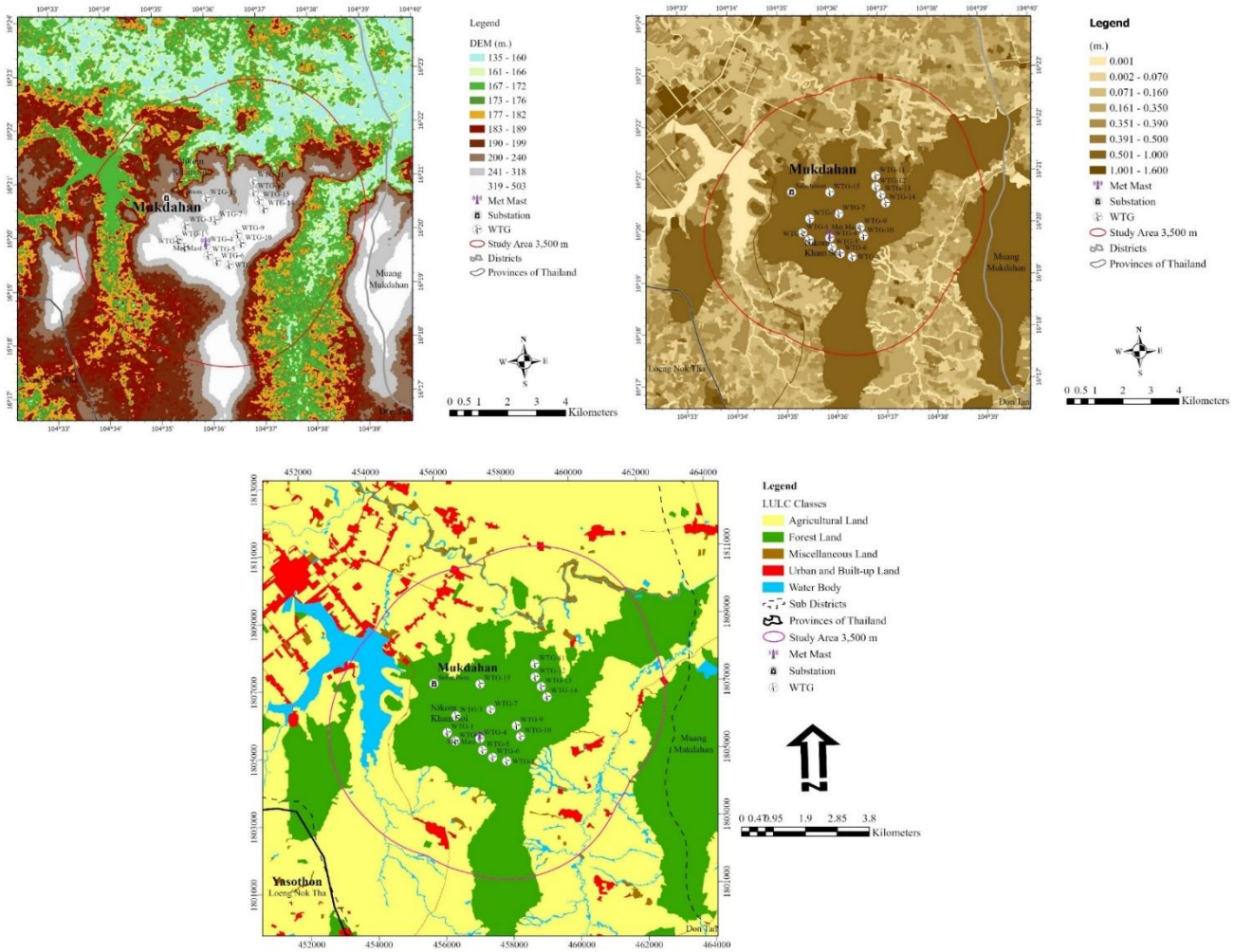

Figure 5. The topography (DEM, upper left), the roughness (upper right), and the Land Cover Land Use (LCLU, bottom) maps of the study area.

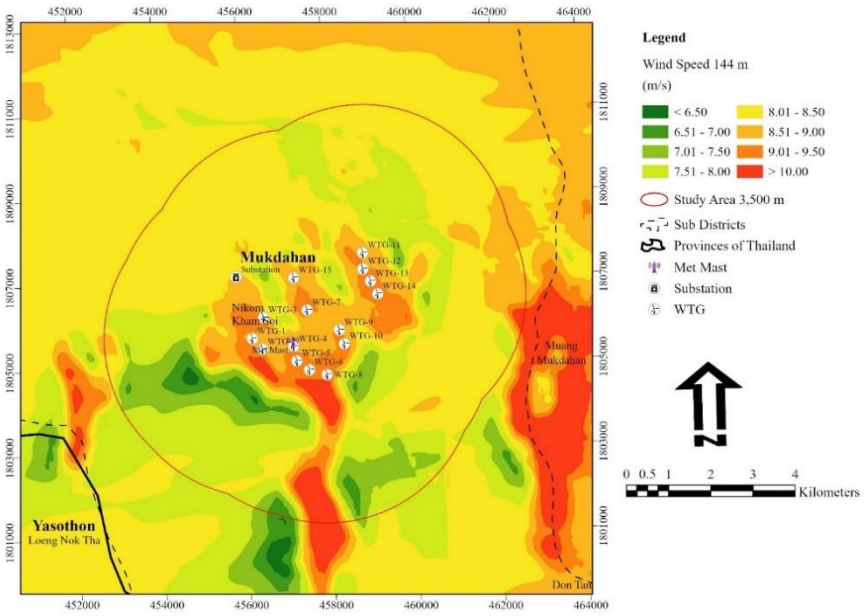

Figure 6. The spatial distribution of the wind speeds in the study area at the hub height of the wind turbine generators (144 m above ground level).

2.4 Noise Level Measurement

2.4.1 Noise Level calculation of the wind turbine generators

The noise impact assessment of the wind turbine generators installed in the wind power plant was calculated using the complex noise modeling of WindFarmer [25]. This noise model calculates the noise impact of a wind turbine generator following the ISO 9613 standard, together with the noise database of the wind turbine manufacturers. Table 2 shows the characteristics and the acoustic details of the GW165-6.0 wind turbine generator used in this study. With a hub height of 155 m agl, the acoustic footprint of the wind turbine generator at an 11.5 m/s wind speed is 110.5 dB(A). The acoustic performance of this model of wind turbine generator is in line with the IEC61400-11 edition 3.0 2012-11 standard.

Table 2. Characteristics of the GW165-6.0 MW wind turbine generator.

Parameter	Specification
Rated power (MW)	6
Hub height agl (m)	155
Rotor diameter (m)	165
Wind class	IEC IIIB
Sound level (dB(A)) at hub height and 11.5 m/s	110.5
Generator	Permanent Magnet Direct Drive (PMDD)
Tower	Steel/Hybrid
Voltage; Frequency	950 V; 50/60 Hz
Grid code	Comply
Certification	IEC IIIB
Rotational speed in operation (rpm)	5.5 – 9.5

The noise level of a wind turbine generator is directly proportional to the operational wind speed. The noise level of the wind turbine generator proportionally increases with the increased operating wind speeds. Table 3 presents the sound levels of the GW165-6.0 wind turbine generator at different operating wind speeds.

Table 3. The acoustic performance in normal power mode of the GW165-6.0 MW wind turbine generator.

Wind Speed (m/s)	Sound Level (dB(A))	Wind Speed (m/s)	Sound Level (dB(A))
6.0	102.2	9.5	110.1
6.5	104.0	10.0	110.3
7.0	105.6	10.5	110.3
7.5	106.9	11.0	110.3
8.0	108.0	11.5	110.5
8.5	108.0	12.0	110.5
9.0	109.5	-	

Humans sense sound within the frequency range of 20 to 20,000 Hz, which is notably broad. However, calculating sound levels across this broad spectrum is a significant challenge. An analysis based on octave frequency bands has been devised to address this. This method divides the frequency range from 20 to 20,000 Hz into octave bands and determines the center frequency value of each band. The approach simplifies the assessment process by quantifying the sound level exclusively at these center frequencies. The sound levels measured at individual frequencies represent their respective octave bands.

Various components of wind turbines produce sound at distinct frequencies. Usually, the manufacturers of wind turbines provide the required data for determining the center frequency of each octave band. Table 4 shows the sound level and its corresponding octave band.

Different frequencies are characteristic of various noise sources, with many employing either the 1/1 octave band or the 1/3 octave band. These bands divide frequency levels according to Equations 1 and 2, respectively:

$$1/1 \text{ octave band} = F\ x\ 2 \quad (1)$$

$$1/3 \text{ octave band} = F\ x\ 2^{1/3} \quad (2)$$

where F is the frequency.

Therefore, regarding the octave frequency values, emphasis is placed on the representative center frequency value. This value, situated between the upper and lower cutoff frequencies, is a pivotal point in the analysis. As depicted in Table 4, wind turbines, while generating electricity, emit sound waves with varying frequencies. These frequencies align with different bands, each characterized by median and corresponding sound frequencies. Following the ANSI (1966) standards, sound level measurement equipment divides the sound range into ten bands for research purposes. The specified center values for each band are 31.5, 63, 125, 250, 500, 1000, 2000, 3000, 4000, 8000, and 10000 Hz. Typically, in sound level analyses, eight wave bands are employed (Octave-Band Analysis). However, the third-octave band analysis offers more comprehensive data by recording measurements with up to three sound level values. Wind turbine manufacturers utilize the acoustic spectrum band analysis to quantify the sound level produced by the turbine operating across various frequency bands, per the IEC 61400-11 standards. This approach accounts for differences in sound levels relative to the wind speed.

Table 4. The 1/3-octave sound power spectrum value at hub height for the GW165-6.0 MW wind turbine model under normal power mode [26].

Octave Band (Hz)	Sound Level (dB(A))	Octave Band (Hz)	Sound Level (dB(A))
20.0	64.6	500.0	101.0
25.0	68.8	630.0	100.3
31.5	72.7	800.0	99.4
40.0	78.1	1,000	98.8
50.0	83.2	1,250	97.3
63.0	86.2	1,600	94.0
80.0	90.2	2,000	89.6
100.0	92.5	2,500	85.3
125.0	95.1	3,150	80.6
160.0	98.2	4,000	73.9
200.0	99.5	5,000	66.2
250.0	100.6	6,300	63.9
315.0	101.8	8,000	63.3
400.0	101.6	10,000	62.3

2.4.2 Complex Noise Model (ISO 9613)

The WindFarmer noise simulation model [25] follows the ISO 9613-2 standard to model the noise generated by wind turbine generators. The complex model (Complex - ISO 9613) used in this study considers the noise attenuation for each octave band, including the ground attenuation and directional meteorological effects.

Firstly, the continuous octave-band sound pressure level for an arbitrary receiver location (Lft) is modeled using Equation 3:

$$\text{Lft} = \text{LW} + \text{DC} - \text{A} \quad (3)$$

Where LW is the sound power level (dB(A)) that is produced by each turbine (a point source). DC is the directivity correction (dB(A)). A is the attenuation that occurs during the propagation from the point sound source to the receiver (dB(A)). For the case of an assumed omni-directional point sound source (such as a

wind turbine generator), DC will be 0 dB(A). While measuring the sound power level, the directivity of the wind turbine noise is considered.

The attenuation A is defined by Equation 4:

$$A = Adiv + Aatm + Agr + Abar + Amisc + Amet \quad (4)$$

Adiv, Aatm, Agr, Abar, Amisc, and Amet are the attenuation due to geometrical divergence, atmospheric absorption, ground effects, barriers, other effects such as foliage or buildings, and meteorological effects, respectively.

The geometric attenuation considers the spherical spreading in the free field from a point sound source over hard ground and is calculated using Equation 5:

$$Adiv = [20\log(d) + 11]\ dB = [20(d) + 11] \quad (5)$$

Where d is the 3-D distance between the source and the receiver, a hemispherical model is called for combining a hard ground plane and the spherical spreading.

The atmospheric absorption causes the sound attenuation, and it is calculated using Equation 6:

$$Aatm = \alpha\ d\ 1000 = 1000 \quad (6)$$

Where α is the atmospheric attenuation coefficient in dB(A)/km for each octave, the complex noise model uses a coefficient for each octave band. The atmospheric attenuation coefficients are the user-defined parameters and are a function of frequency, temperature, and humidity. The default attenuation coefficients are set and are valid for 10°C temperature and 70% humidity.

The sound could be reflected or absorbed by the ground surface. This is considered as an attenuation by ground (Agr). Three regions, the source, the receiver, and the middle regions, were considered in ISO 9613-2. Each region has acoustic properties depending separately on the ground factors (G), as indicated in Table 5.

Table 5. Ground factors (G) for three different ground surfaces.

Type of Ground	Example	Value of G
Hard	Low porosity surface (paving, water, ice, concrete)	0
Porous	Porous surfaces suitable for the growth of vegetation (ground covered with grass, trees, and vegetation)	1
Mixed	Both hard and porous ground	0 - 1

The sum of the individual absorption coefficients for the source region (As), the receiver region (Ar), and the middle region (Am) are calculated for the total ground attenuation for each octave band using Equation 7:

$$Agr = As + Ar + Am \quad (7)$$

As, Ar, and Am are calculated as a function of G, given in Table 5, based on the ISO 9613-2 standards.

Finally, complex noise modeling considers noise attenuation to be a function of the frequency distribution of the noise. The octave band noise emission of the wind turbines was defined. The attenuation of the noise is calculated by using the frequency-specific attenuation coefficients. In the case of wind power plants where multiple wind turbine generators operate simultaneously, the noise propagation is calculated in the complex noise modeling by summing the contributing sound pressures for each octave band of each wind turbine generator using Equation 8:

$$L_{total} = 10 \log \left[\sum_{i=1}^{n} \sum_{j=i}^{8} 10^{\frac{Lft(ij)}{10}} \right] \quad (8)$$

Where n is the number of sources i, j indicates the eight standard octave band frequencies [63 Hz to 8 kHz]. Octave band sound pressure level represented by Lft.

This work measured the noise levels over five (5) days, consisting of regular business days and holidays. The collected measured parameters were obtained following the regulations set forth by the Energy Regulatory Commission of Thailand, as follows:

- 24-hour A-weighted Equivalent Continuous Sound Level (Leq24hr), which is a common measurement used in industry to characterize noise levels in loud environments;
- Percentile Level 90 (L90), which describes the level that was exceeded 90% of the time;
- Day-night average sound level (Ldn), where the average sound level is the average noise level over 24 hours; and,
- Maximum Noise Level (Lmax) is the maximum acceptable noise level.

The noise levels calculated were then mapped using ArcGIS Pro V3.0.1 to assess the effects on the residents living inside the boundaries of the study area.

3. Results and Discussion

Using the complex noise modeling in WindFarmer, the noise of each wind turbine generator of the wind power plant was calculated and mapped according to the noise levels, the 24-hour average noise levels, the average noise levels during the day and the night, and the maximum noise levels. A comparison study of these effects was also done using the Pollution Control Board's regulations to measure the basic sound levels and analyze the disturbance. In addition, the international standard, defined by the World Health Organization (WHO) and the World Bank Group, was also considered according to the thresholds defined as follows:

- The maximum permissible noise level resulting from the power plant operations is 10 dB(A).
- The maximum permissible 24-hour average noise level resulting from the power plant operations is 70 dB(A).
- The noise level produced by the power plant operations is limited to a maximum of 115 dB(A).
- The World Health Organization (WHO) suggests the upper noise limit should not exceed 45 dB(A) when the wind speed is 10 m/s and the height is 10 m. However, the World Bank Group suggests that the LA90 be below 35 dB(A) at a wind speed of 10 m/s and 10 m from the receptor during the day and night.

Twenty-two sound receptor types, ranging from temples to houses, were selected at multiple locations and distances from the wind power plant to measure the noise levels; the individual sound receptor ID assigned to identify them and their respective details are shown in Table 6. Figure 7 shows the positions of the sound receptors, along with the positions of the wind turbine generators and their associated noise emissions within the study area.

Table 6 shows the noise at the individual sound receptors in the study area, while Table 7 shows the overall noise levels and their associated area within the study area. With 23.1 km^2, 30-35 dB(A) accounts for the highest coverage areas, while only a 2.3 km^2 area, accounting for 3.2% of the total area within the study boundary, experiences the highest noise level of 55-60 dB(A).

The ambient noise levels were also calculated and recorded in four selected spots within the study area to compare the noise produced by the wind turbine generators with other noise sources. The ambient noise level at a particular location is the overall environmental noise level caused by all noise sources in the area, both near and far. These noises can be traffic, temple rings, noise from insects, birds, and other wildlife, etc.

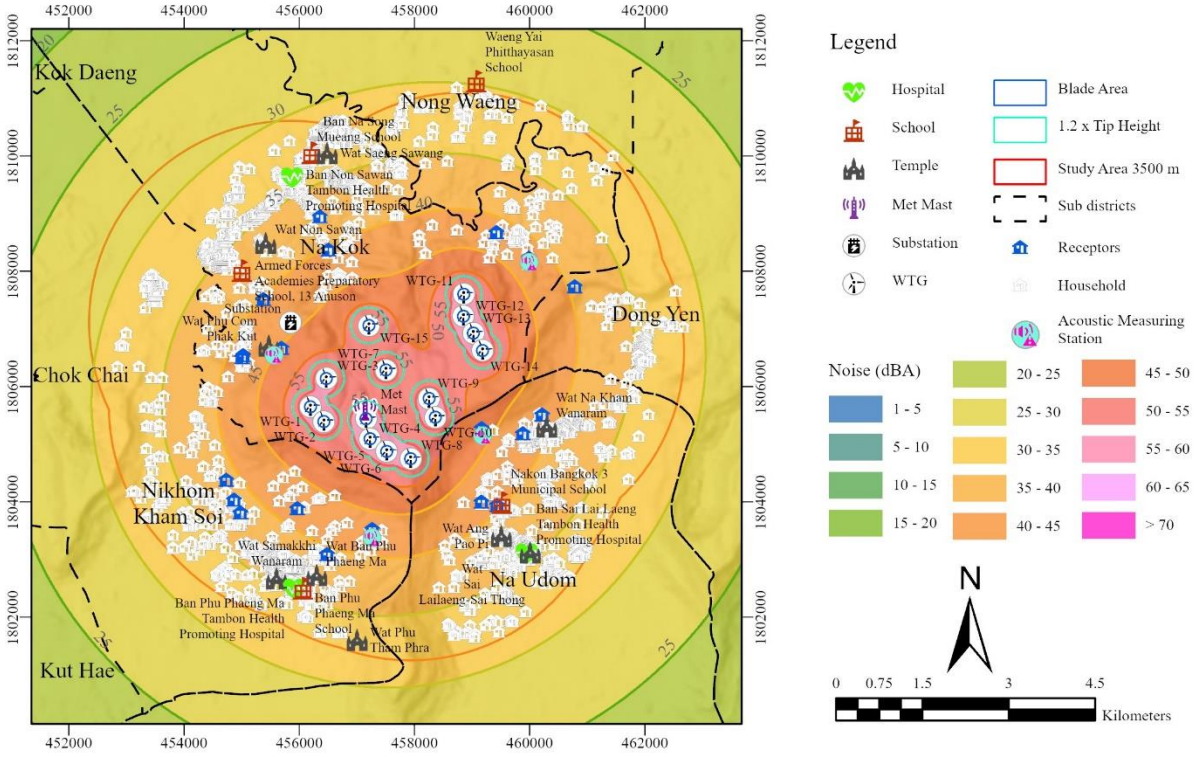

Figure 7. Noise levels and sound receptor location map.

Table 6. Sound receptor locations, detailed characteristics within the study area, and noise level at each sound receptor.

Receptor ID (KMZ)	Receptor Type	Elevation (m)	Distance to Nearest WTG (m)	Predicted Noise (dBA)
2109	House	200.0	1,403.3	33.64
2115	House	200.0	1,398.2	33.62
2517	House	200.0	2,146.9	30.09
2465	House	200.0	2,015.6	30.51
2080	Phu Com Phakkad Temple	280.2	880.6	37.37
1959	Dong Bang-i Forest Park	200.0	1,666.8	32.43
2517	House	200.0	2,146.9	30.09
2553	House	200.0	1,687.1	33.11
2568	House	200.0	2,231.7	29.81
2606	House	200.0	1,487.9	33.87
3008	House	200.0	2,166.2	30.74
2289	Huai Koh Tao Monk Residence	200.0	859.4	37.72
2338	House	200.0	1,568.1	33.80
2529	House	186.7	1,503.1	33.09
2541	Nakon Bangkok 3 Municipal School	180.1	1,761.0	31.93
1435	House	165.0	1,112.3	34.23
1602	Phuratanotham Monastery	196.7	1,242.1	34.19
1602	House	196.7	1,242.1	34.19
1855	Pa Phutthammasilakhun Temple	201.2	1,882.9	31.48
2184	House	200.0	1,606.7	33.11
1528	House	200.0	1,387.1	32.81
1327	House	200.0	1,966.1	30.10

Table 7. Percentage of the study area affected by different noise levels from the wind turbine generators.

Noise Level (dB(A))	Area within Project Boundary (km^2)	%
25 - 30	-	-
31 – 35	23.1	31.3
36 – 40	22.3	30.2
41 – 45	12.7	17.3
46 – 50	7.1	9.7
51 – 55	6.1	8.3
56 – 60	2.3	3.2
61 – 65	-	-
> 70	-	-
Total Surface Area	73.6	100

The ambient noise levels were measured using the Sound Level Meter Scarlet Tech (Model: ST-11D, Serial Number: 820965) between September 7 and 12, 2023. A magnitude of parameters was used to measure the ambient noise at four locations in the study area as follows:

- Equivalent Sound Level (Leq): average noise level value throughout the measurement period of 8 hours.
- Equivalent Sound Level (Leq24): average noise level value throughout the measurement period of 24 hours.
- Maximum Noise Level (Lmax): maximum noise level value throughout the measurement period of 8 hours; Lmax should not exceed 115 dB(A) according to international standards.
- Maximum Noise Level (Lmax24): maximum noise level value throughout the measurement period of 24 hours; its standard is also 115 dB(A).
- Percentile Level 5 (L5) for the 8-hour measurement period.
- Percentile Level 5 (L5 24) for the 24-hour measurement period.
- Percentile Level 50 (L10) for the 8-hour measurement period.
- Percentile Level 50 (L10 24) for the 24-hour measurement period.
- Percentile Level 90 (L90) for the 8-hour measurement period.
- Percentile Level 90 (L90 24) for the 24-hour measurement period.
- Day-Night Average Sound Level (Ldn): mean day-night sound level (A-weight) for the period between 10:00 p.m. and 7:00 a.m. after 10 dB(A) is added.

The ambient noise levels at four locations were measured and plotted using these parameters. Figure 8 shows the ambient noise measured at the Phu Kham Phakkad Temple in the study area. It is worth noting that the Lmax24 measurement is always above the standard 70 dB(A) threshold the Pollution Control Department set. The noise produced by the wind turbine generators is well below the ambient noise levels and lower than the standard 70 dB(A). Similarly, the Leq and L90 are also consistently higher, with occasional lower values of the wind turbine generator noise level measured at 5-minute intervals for 24 hours, as shown in Figure 8.

Likewise, the measurements at the remaining three receptors show a similar trend, with the ambient noise being higher than the noise from the wind turbine generators, as shown in Figures 9, 10, and 11.

The Leq and L90 based on 5-min measurements for all four receptors are presented in Figures 8-11. It can be observed that the Leq and L90 were occasionally lower than the noise emitted by the wind turbine generators.

The Leq and L90 are comparatively lower at Huai Koh Tao monk residence than the previous receptors, but still, much of the time, they are above the noise levels of the wind turbine generators (Figure 10). At Phuratanotham monastery, the ambient sound is much less than at the other three receptors, with Leq and

L90 going below the noise from the wind turbine generators more often than at other sites. However, it is still higher than the noise level of the wind turbine generators most of the time throughout the day, as shown in Figure 11.

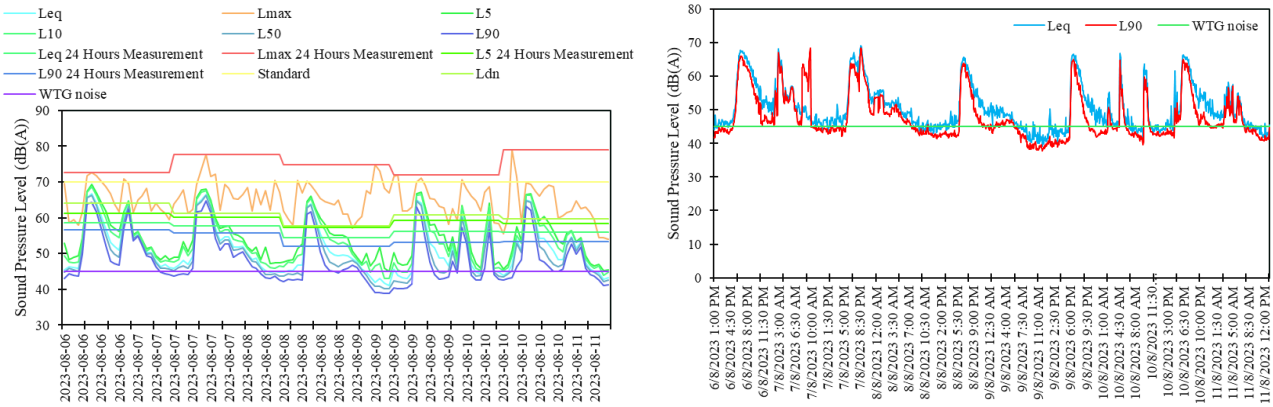

Figure 8. Ambient noise measurements (left) and sound pressure measurements every 5 minutes (right) at the Phu Kham Phakkad Temple.

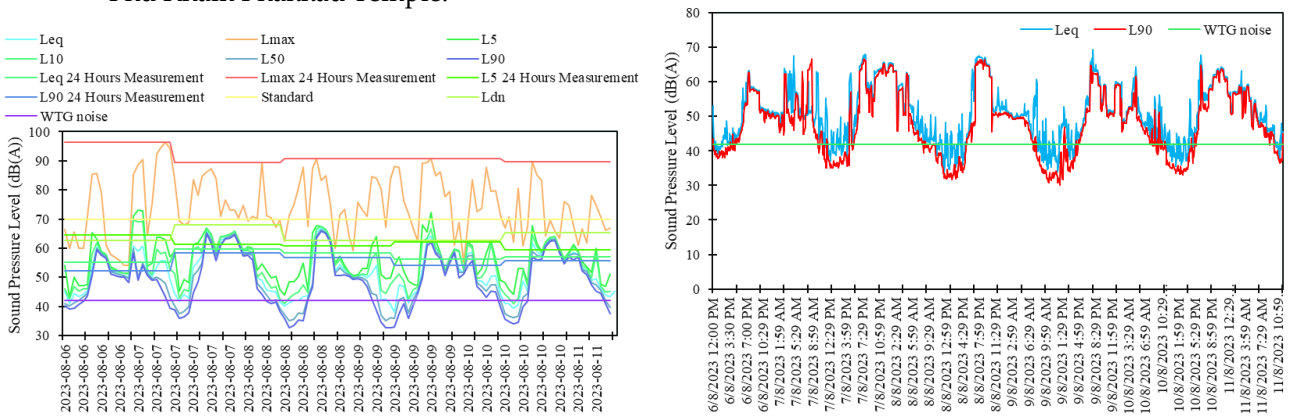

Figure 9. Sound pressures (left) and sound pressure measurements every 5 minutes (right) at the measurement site of the Phu Phaeng Ma Temple.

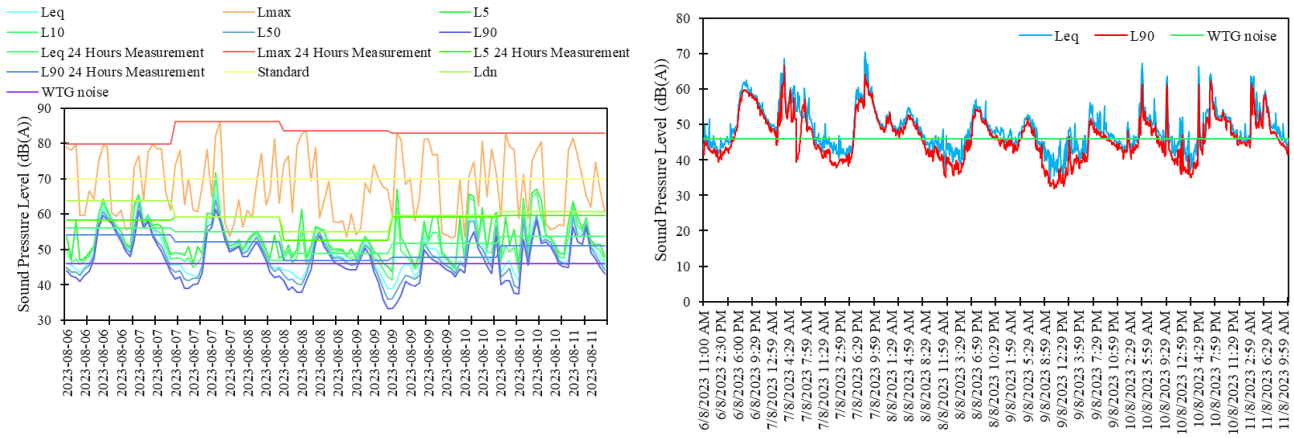

Figure 10. Sound pressures (left) and sound pressure measurements every 5 minutes (right) at the measurement site of the Huai Koh Tao monk residence.

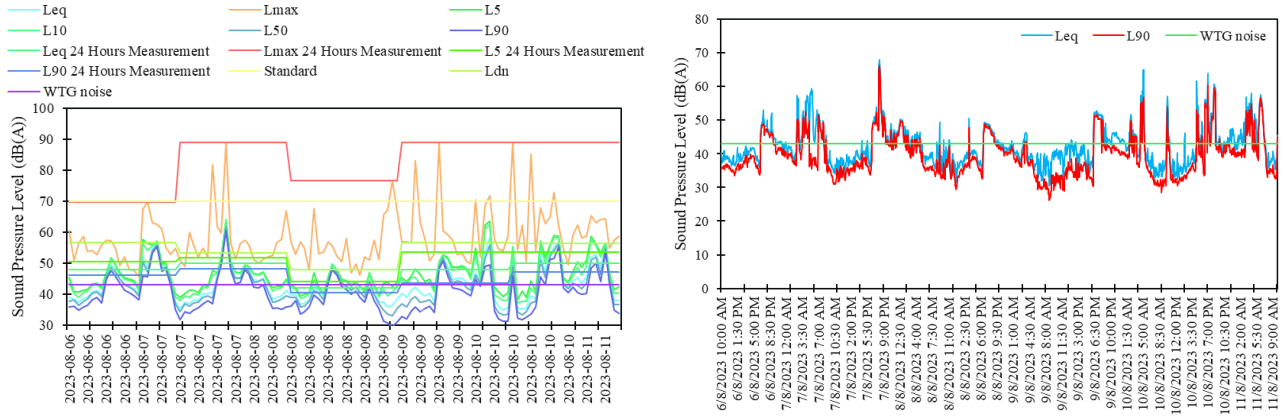

Figure 11. Sound pressures (left) and sound pressure measurements every 5 minutes (right) at the measurement site of the Phuratanotham monastery.

To compare the multiple measurement parameters of the ambient noise with the noise levels of the wind turbine generators, Table 8 shows the hours the ambient noise levels at the four acoustic measurement stations are below the noise level emitted by the wind turbine generators. The percentage of time that the Leq and the L90 are below the noise level of the wind turbine generators corresponds to less than 50%, except at Phuratanotham monastery, where they are higher than 50%. Even though it is situated closer to the wind power plant, as illustrated in Figure 7, the ambient noise at Phuratanotham monastery is quite low due to fewer activities and is far away from the community.

A further comparison of the ambient noise and the wind turbine generator noise is shown in Table 9. The ambient noises at all the receptor sites are higher than the noise from the wind turbine generators, resulting in no disturbance caused by the wind turbine generators throughout the study area. Hence, the 90 MW wind power plant in Mukdaharn province in northeastern Thailand does not cause any noise disturbance in the surrounding area as it is below the ambient noise the residents are used to hearing daily.

The results in this study were compared to a previous investigation using a simple noise emission model for a 50 MW wind power plant [18], and it was found that the predicted noise for a 50 MW wind power plant had a maximum of 50 dB(A) in the vicinity of the wind turbine generators. These results were similar to two wind power plants in Greece, where the maximum noise emission level obtained from a simple noise modeling under wind speed of 8.0 m/s was less than 45 dB(A) [27].

Table 8. Percentage of time that the ambient noise was below the noise from the wind turbine generators.

No.	Acoustic Measurement Station	Ambient Noise < WTG Noise (%)					
		L_{eq}	L_{max}	L_5	L_{10}	L_{50}	L_{90}
1	Phu Kham Phakkad Temple	11	0	0	2	21	31
2	Phu Phaeng Ma Temple	17	0	0	6	27	46
3	Huai Koh Tao Monk Residence	34	0	4	8	42	49
4	Phuratanotham Monastery	54	0	32	39	57	68

Table 9. Mean Leq, WTG noise, and disturbance.

Acoustic Measurement Station	Mean Leq	Std. Leq	WTG Noise	Residual	Disturbance (%)
Phu Com Phak Kut Temple	53.2	8.1	43	-10.2	0
Phu Phaeng Ma Temple	52.1	7.4	45	-7.1	0
Huai Koh Tao Monk Residence	50.6	6.7	46	-4.6	0
Phuratanotham Monastery	44.6	7.4	43	-1.6	0

4. Conclusions

The noise produced by wind turbine generators is often among the major causes of social opposition to wind energy development. In extreme cases, these oppositions can lead to the cancellation of planned projects, causing hurdles to achieving energy transition targets. Dedicated research to study the noise profiles and their impacts on residents near wind power plants can help mitigate social opposition. Often, misinformation can be the primary cause of the opposition to wind power plant developments. To address this important issue, this research assessed the noise emission impacts of a 90 MW utility-scale wind power plant in Mukdaharn province in northeastern Thailand.

The complex noise model (Complex - ISO 9613) of the WindFarmer simulation software was employed to model the noise profile of the GW165-6.0 MW wind turbine generator considered for the wind power plant based on the acoustic profile of the wind turbine generator provided by the manufacturer. The noise produced by the 15 wind turbine generators was mapped using ArcGIS, employing the results of the complex noise modeling to visualize the noise impacts on the surrounding areas. Twenty-two sound receptors, mainly comprised of residential buildings, temples, and other important locations, were selected throughout the study areas at varying distances to model the impacts of noise from the wind turbine generators. The 24-hour average noise levels, the average noise levels during the day and night, and the maximum noise levels were the primary parameters used to determine the noise levels, which were compared to national and international standards defined for acceptable noise levels for a healthy environment.

In addition, to compare the noise levels of the wind turbine generators with the ambient noise levels in the study area, the ambient noise levels at four selected locations within the study area were measured using a Sound Level Meter Scarlet Tech (Model: ST-11D, Serial Number: 820965) measuring tool. The equivalent sound level (Leq), the equivalent sound level (Leq24), the maximum noise level (Lmax), the maximum noise level (Lmax24), and several other parameters were measured and compared with the noise levels from the wind turbine generators. The results clearly showed that the noise levels of wind turbine generators were much lower than the ambient noise levels within the study area. Hence, the wind power plant is not the source of any additional noise for the residents living within the study area.

Studies like these are important to assess the impacts of wind power plants on residents' lives and provide evidence to confront misinformation and gain the trust of local communities to mitigate the social opposition to wind power plants.

5. Acknowledgements

The authors express their gratitude to the Research and Development Institute and the Research Center in Energy and Environment (RCEE) of Thaksin University for their financial support of this work under the framework of an International Collaborative Research Project.

Author Contributions: Conceptualization, K.S. and W.J.; methodology, K.S.; software, C.S.; validation, K.S.; formal analysis, M.P.; investigation, K.S. and W.J.; writing-original draft preparation, K.S.; writing-review and editing, A.F. and G.Y.; visualization, W.J.; supervision, W.J. and G.Y.; All authors have read and agreed to the published version of the manuscript.

Funding: The authors thank the private company for their financial support and the data used in this work. The private company was not involved in the research work or in preparing and submitting this publication.

Conflicts of Interest: There is no conflict of interest.

References

[1] Cop, T.; Charter, T.; Zero, N.; Global, U.; Action, C. COP28 Net-Zero Transition Charter : Accountability mobilization for the private sector, Retrieved from: https://www.cop28.com/en/net-zero-accountability-charter. (accessed March 6 2024).

[2] IRENA, International Renewable Energy Agency, Reneweble Energy Statistic 2023, Retrived from: https://www.irena.org/Publications/2023/Jul/Renewable-energy-statistics-2023. (accessed March, 6 2024).

[3] IRENA, International Renewable Energy Agency, Future of Wind (Deployment, investment, technology, grid integration and socio-economic aspects), 2019 Retrived from: https://www.irena.org/-/media/Files /IRENA/ Agency/ Publication/ 2019/Oct/ IRENA_Future _of_wind_2019.pdf. (accessed March, 6 2024).

[4] Kamdar, I.; Taweekun, J. Assessment of Wind Energy Potential of Hat Yai (Songkhla), Thailand, *IOP Conf. Ser. Mater. Sci. Eng.* **2021**, *1163*(1), 012001. https://doi.org/10.1088/1757-899X/1163/1/012001.

[5] Waewsak, J.; Chancham, WC.; Chiwamongkhonkarn, S.; Gagnon, Y. Wind Resource Assessment of the Southernmost Region of Thailand Using Atmospheric and Computational Fluid Dynamics Wind Flow Modeling, *Energies*. **2019** 12, 1899. https://doi.org/10.3390/en12101899.

[6] Tawinprai, S.; Polnumtiang, S.; Suksomprom, P.; Waewsak, J.; Tangchaichit, K. Modeling of Wind Energy Potential using a High-resolution Grid over Mekong Riverside Region in the Northeastern Part of Thailand, *Theoretical and Applied Climatology*. **2022**, 150, 1587 – 1604. https://doi.org/10.1007/s00704-022-04235-w.

[7] Niyomtham, L.; Lertsathittanakorn, C.; Waewsak, J.; Gagnon, Y. Mesoscale/Microscale and CFD Modeling for Wind Resource Assessment: Application to the Andaman Coast of Southern Thailand, *Energies*, **2022**. https://www.mdpi.com/1996-1073/15/9/3025.

[8] Tawinprai, S.; Polnumtiang, S.; Suksomprom, P.; Waewsak, J.; Tangchaichit, K.; Modelling, A. Approach for Evaluating the Wind Resource and Power Generation using a High-resolution Grid at Selected Regions in the Northeast of Thailand, *Modeling Earth Systems and Environment*. **2023**, https://doi.org/10.1007/s40808-022-01669-z.

[9] European Commission EU, An Industry Perspective on Strengthening Onshore Wind Development in Thailand, https://ec.europa.eu/eurostat/statistics- (accessed March 6, 2024).

[10] Rand, J.; Hoen, B. Thirty Years of North American Wind Energy Acceptance Research: What Have We Learned?, *Energy Res. Soc. Sci.* **2017**, 29. 135 – 148. https://doi.org/10.1016/j.erss.2017.05.019.

[11] Karasmanaki, E. Is It Safe to Live Near Wind Turbines? Reviewing the Impacts of Wind Turbine Noise, *Energy Sustain. Dev.* **2022**, 69, 87–102. https://doi.org/10.1016/j.esd.2022.05.012.

[12] Nissenbaum, M.A.; Aramini, J.J.; Hanning, C.D. Effects of Industrial Wind Turbine Noise on Sleep and Health, *Noise Health*. **2012**, 14, 237–243. https://doi.org/10.4103/1463-1741.102961.

[13] Jalali, L.; Bigelow, P.; Nezhad-Ahmadi, M.R.; Gohari, M.; Williams, D.; McColl, S. Before–After Field Study of Effects of Wind Turbine Noise on Polysomnographic Sleep Parameters, *Noise Health*. **2016**, 18, 194. https://doi.org/10.4103/1463-1741.189242.

[14] Smith, M.G.; Ögren, M.; Thorsson, P.; Hussain-Alkhateeb, L.; Pedersen, E.; Forssén, J.; Morsing, J.A.; Waye, K.P. A Laboratory Study on the Effects of Wind Turbine Noise on Sleep: Results of the Polysomnographic WiTNES Study, *Sleep*. **2020**, 43, 1–14. https://doi.org/10.1093/sleep/zsaa046.

[15] Leung, D.Y.C.; Yang, Y. Wind Energy Development and Its Environmental Impact : A Review, *Renew. Sustain. Energy Rev*. **2012**, 16, 1031–1039. https://doi.org/10.1016/j.rser.2011.09.024.

[16] Council of Canadian Academes, 2015. "Understanding the Evidence: Wind Turbine Noise". Ottawa (ON), Canada: The Expert Panel on Wind Turbine Noise and Human Health, Council of Canadian Academes, 180 p. (Experts Panel (alphabetical order): H.W Davies, Y. Gagnon, C. Giguère, T.L. Guidotti (Chair), S. Grace, R.V. Harrison, B. Howe, D.A. Johnson, K. Persson Waye, J.D. Roberts). https://cca-reports.ca/reports/understanding-the-evidence-wind-turbine-noise/ (accessed April 29, 2023).

[17] Kongprasit, S.; Chiwamongkhonkan, S.; Ali, F.; Makhampom, P.; Gagnon, Y.; Waewsak, J. Environmental Impact Assessment of Onshore Wind Power Plants: A Case Study of a 50 MW Wind Power Plant in Northeastern Thailand, *ASEAN J. Sci. Tech. Report*. **2024**, 27, 39-57. https://doi.org/10.55164/ajstr.v27i2.252058

[18] Pollution Control Department, Noise disturbance measurement, https://www.pcd.go.th/wp-content/uploads/2020/06/pcdnew-2023-05-16_04-09-33_776771.pdf (accessed March, 6 2024).

[19] Islam, K.D.; Theppaya, T.; Ali, F.; Waewsak, J.; Suepa, T.; Taweekun, J.; Titseesang, T.; Techato, K. Wind Energy Analysis in the Coastal Region of Bangladesh, *Energies*. **2021**, 14, 1–18. https://doi.org/10.3390/en14185628.

[20] Hu, W.; Yang, Q.; Zhang, J.; Hu, J. Coupled On-Site Measurement/CFD Based Approach for Wind Resource Assessment and Wind Farm Micro-Siting over Complex Terrain, *IOP Conf. Ser. Earth Environ. Sci.* **2020**, 455, https://doi.org/10.1088/1755-1315/455/1/012037.
[21] Tang, X.Y.; Zhao, S.; Fan, B.; Peinke, J.; Stoevesandt, B. Micro-scale Wind Resource Assessment in Complex Terrain based on CFD coupled Measurement from Multiple Masts, *Appl. Energy.* **2019**, 238, 806–815. https://doi.org/10.1016/j.apenergy.2019.01.129.
[22] https://asterweb.jpl.nasa.gov/gdem.asp (accessed March, 6 2024).
[23] https://lddcatalog.ldd.go.th/dataset/ldd_21_01 (accessed March, 6 2024).
[24] Howland, M.F.; Quesada, J.B.; Martínez, J.J.P.; Larrañaga, F.P.; Yadav, N.; Chawla, J.S.; Sivaram, V.; Dabiri, J.O. Collective Wind Farm Operation based on a Predictive Model Increases Utility-scale Energy Production, *Nat. Energy.* **2022**, 7. https://doi.org/10.1038/s41560-022-01085-8.
[25] GH and Partners. GH WindFarmer: Theory Manual. http://www.ccpo.odu.edu/~ klinck/Reprints/PDF/garradhassan2009.pdf. (accessed March 6, 2024).
[26] GoldWind International Solution Department, Description of GW165-6.0 MW, Acoustic Performance Specification.
[27] Chourpouliadis, C.; Ioannou, E.; Koras, A.; Kalfas, A. I. Comparative Study of the Power Production and Noise Emissions Impact from Two Wind Farms. *Energy Conversion and Management*. **2012**, 60, 233-242.

ASEAN
Journal of Scientific and Technological Reports
Online ISSN:2773-8752

Research article

Lactic Acid Bacteria from Fermented Asparagus and Stinky Beans Inhibit Clinical Diarrheagenic *Escherichia coli* and Clinical Methicillin-Resistant *Staphylococcus aureus*

Pattamarat Rattanachuay[1], Wilaipan Khunwilai[2], Warunee Puangsiri[3] and Pharanai Sukhumungoon[4*]

[1] Faculty of Science and Technology, Prince of Songkla University, Pattani, 94000, Thailand; pattamarat.r@gmail.com
[2] Faculty of Science, Prince of Songkla University, Songkhla, 90110, Thailand; nongjan2@hotmail.com
[3] Faculty of Science, Prince of Songkla University Songkhla, 90110, Thailand; warunee.p@psu.ac.th
[4] Faculty of Science, Prince of Songkla University, Songkhla, 90110, Thailand; pharanai82@gmail.com
* Correspondence: pharanai82@gmail.com

Citation:
Rattanachuay, P.; Khunwilai , W.; Puangsiri , W.; Sukhumungoon, P. Lactic Acid Bacteria from Fermented Asparagus and Stinky Beans Inhibits Clinical Diarrheagenic *Escherichia coli* and Clinical Methicillin-Resistant *Staphylococcus aureus*. *ASEAN J. Sci. Tech. Report*. **2024**, *27*(3), e253156. https://doi.org/10.55164/ajstr.v27i3.253156.

Article history:
Received: March 11, 2024
Revised: April 9, 2024
Accepted: April 10, 2024
Available online: April 20, 2024

Abstract: The probiotics exhibiting antagonistic activity against gastrointestinal pathogenic bacteria are essential for protecting the host from illnesses and regulating intestinal balance. In this study, we successfully isolated 7 lactic acid bacteria (LAB) from fermented asparagus and fermented stinky beans. They showed the sign of probiotic properties, especially 2 strains from fermented asparagus, PZ12 and PZ14, strongly tolerated to simulated gastric juice pH 3.0 supplemented with 0.3% pepsin. Additionally, these 2 LAB strains tolerated 0.5% bile salts for up to 3 hours. Antagonistic activity of 7 LAB strains against clinical Diarrheagenic *Escherichia coli* (DEC) and clinical MRSA in this study showed that all LAB strains were capable of inhibiting clinical DEC and clinical MRSA by providing an inhibition zone in the range between 22 and 39 mm. PZ12 and PZ14 also displayed relatively wide inhibition zones against these intestinal pathogens. Antimicrobial-resistant examination demonstrated that most LAB strains could be destroyed by most of the antimicrobial agents tested. LAB strains PZ12 and PZ14 were shown to be resistant to three antimicrobial agents. PZ12 could resist ciprofloxacin, fosfomycin, and streptomycin, and PZ14 was resistant to ciprofloxacin, cefoxitin, and streptomycin. Hence, pickles are a good source of beneficial probiotics for humans.

Keywords: Lactic acid bacteria (LAB); fermented asparagus; fermented stinky beans; Diarrheagenic *Escherichia coli* (DEC); clinical MRSA

1. Introduction

Diarrheagenic *Escherichia coli* (DEC) is an important bacterial group that plays a role in gastrointestinal tract infections, resulting in morbidities and mortalities worldwide [21]. DEC consists of 6 pathotypes, *e.g*., enteropathogenic *E. coli* (EPEC), enterotoxigenic *E. coli* (ETEC), enteroinvasive *E. coli* (EIEC), enteroaggregative *E. coli* (EAEC), diffusely adherent *E. coli* (DAEC), including the most important pathotype, enterohemorrhagic *E. coli* (EHEC). EHEC is defined by the presence of *the* coding for intimin, the protein involved with bacterial attachment, and *stx* genes encode toxins called Shiga toxins (Stx1 and Stx2), causing bloody diarrhea and kidney failure, leading to death in complicated cases. Therefore, amongst 6 DEC pathotypes, EHEC shows the most devastating impact on humans. Shiga toxin-producing *E. coli* (STEC), defined by the presence of the sole stx genes (stx1 or stx2 or both), can cause symptoms

similar to those of EHEC. In addition, another group of bacteria that can cause food poisoning is *Staphylococcus aureus*, containing staphylococcal enterotoxins (SEs), including toxic shock syndrome toxin (TSST-1), which is a member of the pyrogenic toxin superantigen (PTSAg) family [13]. Staphylococcal superantigens can stimulate the massive release of cytokines from T-lymphocytes and macrophages [20], leading to the excess of cellular immune responses causing toxic shock [33]. In addition, they can cause staphylococcal pneumonia and staphylococcal purpura fulminans [8, 14]. More importantly, methicillin-resistant *Staphylococcus aureus* (MRSA), the S. aureus strain carrying mecA, has emerged and spread worldwide [2, 4, 36]. It shows resistance to numerous antimicrobial drugs, resulting in trouble with therapeutic approaches.

Lactic acid bacteria (LAB) with probiotic potentials are considered promising solutions to regulate the balance of gut microbiota, leading to the proper work of the gastrointestinal tract. Also, they demonstrate the health-promoting effects on the hosts, for instance, lowering cholesterol and producing γ-aminobutyric acid (GABA), which plays a role as a diabetic suppressant and anti-hypertension [16]. Since LAB is generally recognized as safe (GRAS), LAB is thus widely consumed to promote health and prevent gastrointestinal tract infections. The pickles are the source of excellent probiotic strains that benefit human health. Therefore, this study aims to search for probiotic bacteria from pickled asparagus and stinky beans, which are commonly and widely consumed in southern Thailand. Their antagonistic capability is explored for the benefit of public health.

2. Materials and Methods

2.1 Indicator bacteria

Indicator bacteria used for antagonistic examination were 4 DEC strains (3 from Hat-Yai Hospital and 1 from beef) and 1 clinical MRSA strain from a patient in Songklanagarind Hospital. Characteristics of these indicator bacteria are listed in Table 1. The Ethics Committee of the Faculty of Medicine, Prince of Songkla University, Thailand (EC no. 56-225-19-2-3) approved the research protocol to collect these bacteria.

2.2 LAB isolation

To isolate LAB, 10 pickle samples (stinky beans and asparagus) were collected from fresh markets in Hat-Yai city, and all of them were processed within 2 hours. as described previously [16] with modifications. Briefly, 10 g of pickle was mixed with 90 mL of 0.85% (w/v) sodium chloride solution (normal saline solution, NSS), and 0.1 mL of the solution was spread on Lactobacilli MRS agar (Difco, USA) fortified with 400 mg/L of bromocresol purple (BCP) and incubated at 30ºC for 48 hours under microaerophilic condition. Typical yellowish Lactobacilli colonies were randomly collected to test the absence of catalase. They were also subjected to examine the characteristics of Gram-positive rod-shaped cells. For further analyses, LAB strains were stored in 20% (v/v) glycerol at -80 ºC.

2.3 Investigating the probiotic properties of LAB strains

2.3.1. Toleration of LAB to simulated gastric juice

The gastric system was simulated to examine the toleration of LAB strains in gastric juice. Phosphate buffer saline (PBS), pH 2.0 and pH 3.0, supplemented with 0.3% (w/v) pepsin (Sigma-Aldrich, USA), were prepared. The experiment was performed as described by Wang et al. [34] with slight modifications. Briefly, 1 ml of 1.5×10^9 CFU/mL bacterial culture was added into 9 ml of 0.3% (w/v) pepsin-supplemented PBS (pH 2.0 and pH 3.0) and incubated at 37ºC. The bacterial count was carried out at 0, 90, and 180 minutes by surface plate count on Lactobacilli MRS agar as described above. A 0.3% (w/v) pepsin-supplemented PBS, pH 6.2, was used as a control. The experiment was performed in triplicate.

2.3.2. Toleration of LAB to bile salt

Bile salt was used to simulate the condition of the human intestinal tract. LAB strains were tested for toleration in 2 bile salt concentrations, 0.3% and 0.5%. The experiment was performed as previously described by Tulini et al. [31] with slight modifications. In short, a working bacterial culture of 1.5×10^9 CFU/mL was prepared as described above. One milliliter of working culture was spiked into 99 ml of sterile PBS supplemented with 0.3% and 0.5% (w/v) of bile salt (Sigma-Aldrich, USA) and incubated statically at 37ºC for 3-time points, 0, 90, and 180 minutes. As described above, bacterial survival was assessed by surface plate

count on Lactobacilli MRS agar. A sterile PBS without bile salt was used as a control. The experiment was performed in triplicate.

2.4 Inhibition of DEC and MRSA by LAB strains

The antagonistic activity of the LAB strains was measured using agar spot assay as previously described by Armas et al. [1]. Briefly, overnight culture of the pathogens (DEC and MRSA) was diluted in Brain Heart Infusion (BHI) broth (Difco, USA). A 0.1 mL of each pathogen culture (approximately 1.5 x 10^6 CFU/mL) was spread onto BHI plates. The plates were left to dry for 15 minutes at room temperature. Overnight cultures of the LAB strains grown in Lactobacilli MRS broth for 48 hours were adjusted to 1.5 x 10^5 CFU/mL, and a 3 μL of the diluted culture was spotted on the agar surface containing pathogen inoculated. The experiment was performed in triplicate. Plates were left for 5 minutes for drying at ambient temperature and then incubated aerobically at 37°C for 24 hours. Vernier caliper measured the inhibition zone.

2.5 Determination of antimicrobial susceptibility of LAB strains

With slight modifications, an antimicrobial susceptibility test was performed using the disk diffusion method, as described by Duskova et al. [7]. Bacterial suspensions with turbidity equivalent to 0.5 McFarland standards were swabbed evenly onto Lactobacilli MRS agar plates. Twelve common antibiotic disks, amikacin (30 μg), chloramphenicol (30 μg), ciprofloxacin (5 μg), clindamycin (2 μg), gentamicin (10 μg), erythromycin (30 μg), fosfomycin (200 μg), cefoxitin (30 μg), imipenem (10 μg), streptomycin (10 μg), cotrimoxazole (23.75/1.25 μg), and tetracycline (30 μg) (Oxoid, Basingstoke, UK), were placed on Lactobacilli MRS agar plates. The plates were incubated at 30°C for 24 hours under microaerophilic conditions. Inhibition zone diameters, including the diameter of the disk, were measured.

2.6 Statistical analysis

Multivariate analysis of variance (ANOVA) was used to analyze the toleration of LAB to simulated gastric juice and the toleration of LAB to bile salt. A significant difference was set at p-value < 0.05.

Table 1. Characteristics of indicator bacteria (pathogens) used in this study

Bacterial strain	DEC Pathotype	Serotype	Origin (year)	Virulence trait	Reference
PSU1	STEC	O8	Beef (2012)	*stx*$_1^+$ [[a]RPLA titer = 128], *stx*$_2^+$ [RPLA titer = 16]	[29]
EDL933	EHEC	O157	Human (1982)	*stx*$_1^+$ [RPLA titer = NA], *stx*$_2^+$ [RPLA titer = 2,048], *eae*$^+$	[25]
PE-27	EPEC	O111	[b]NA	*bfp*$^+$, *eae*$^+$	[24]
PSU192	ETEC	O169	Human (2014)	*est*$^+$, *astA*$^+$	[27]
PSU263	EAEC	O127a	Human (2014)	*aggR*$^+$, *aggA*$^+$, *astA*$^+$	[28]
MRSA PSU20	NA	NA	Human (2014)	*mecA*$^+$, *spa*$^+$, *femB*$^+$, *sea*$^+$, *coa*$^+$	[30]

[a]RPLA, reverse passive latex agglutination test to quantify the amount of Stx production. [b]NA, Not applicable.

3. Results and Discussion

3.1 LAB isolation and their toleration to simulated gastric juice

In the course of LAB investigation from pickle samples, 2 LAB strains (ST4 and ST5) were successfully obtained from fermented stinky beans and 5 (GY3, PZ7, PZ9, PZ12, PZ14) from fermented asparagus. They were Gram-positive rod-shaped bacteria, presenting the typical characteristic of LAB on Lactobacilli MRS agar. Focusing on gastric juice toleration of LAB, some bacterial strains resisted simulated gastric juice. They could withstand 0.3% pepsin at pH 3 for up to 180 minutes without much reduction of bacterial population. Although at pH 2, LAB strains GY3 and PZ7 could not survive at 90 minutes, strains ST4, ST5, PZ9, and PZ12 could still survive until 180 minutes (Figure 1). Particularly, the bacterial population of PZ14 remained at the approximate amount (10^7 log CFU/mL) at 90 minutes compared to the starting time (0 minutes). At 180 minutes, LAB strain PZ14 survived at approximately 10^3 log CFU/mL (Figure 1). This demonstrates the ability of the LAB to withstand stomach acidity, suggesting their strength to survive gastric transit.

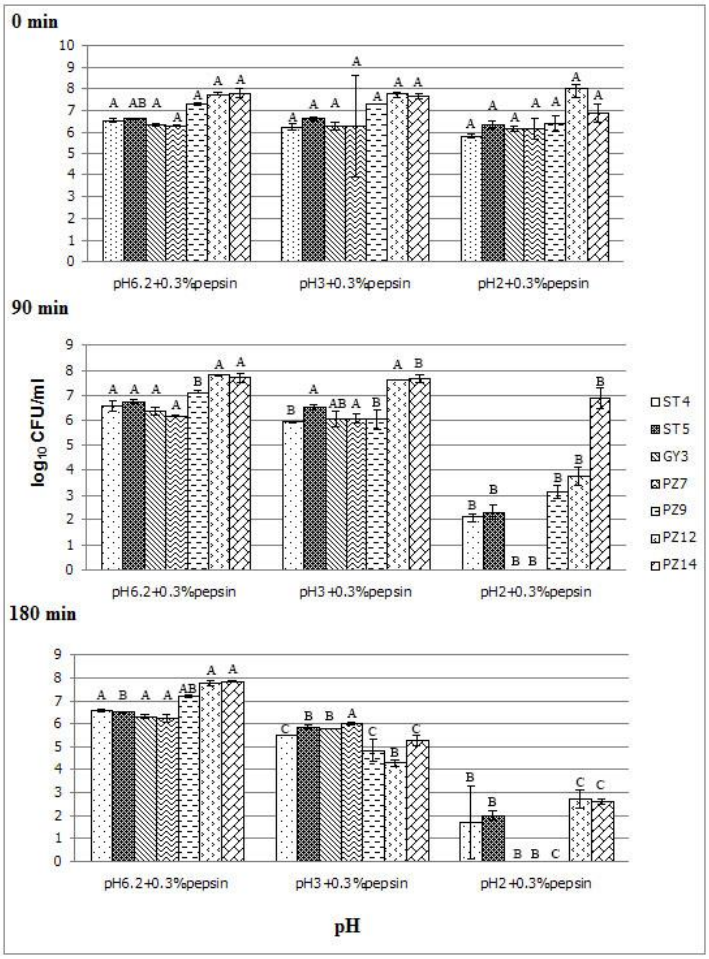

Figure 1. Toleration of LAB strains isolated from fermented asparagus and fermented stinky beans to simulated gastric juice supplemented with 0.3% pepsin, pH 3.0, and pH 2.0 for 90 minutes and 180 minutes. Uppercase letters indicate the significant difference in simulated gastric juice toleration of LAB strains among three-time points: 0 min (control), 90 min, and 180 min (p-value < 0.05).

There are several mechanisms that LAB uses for acid toleration. For example, (i) acid neutralization process by arginine dihydrolase system (ADS) by which the LAB produces alkaline substances such as urea, arginine, and ammonia to nullify acid, (ii) production of biofilm to protect the cells, and (iii) proton pump by

F1-F0- ATPase that hydrolyzes or synthesizes the ATP by F1 protein and transport proton through F0 complex [35]. In addition, stress response, such as the production of cold shock proteins (Csps) that act as RNA chaperones to prevent RNA secondary structure and promote its biological roles, may protect LAB from the destruction by acid [15].

3.2 Toleration of LAB to bile salt

Bile salt is a bio-compound secreted from the liver to help digest lipids. It also has antibacterial activity that leads to stress on bacteria through multiple mechanisms, for instance, disruption of bacterial cell membranes, denaturation of proteins, chelating the iron and calcium, and causing oxidative damage to DNA [32]. Therefore, LAB with probiotic potentials must endure the antibacterial activity of bile salts to establish itself in the human gut. Focusing on the resistance to bile salt at 0.3% and 0.5%, it was found that strains ST4, ST5, GY3, PZ7, and PZ9 had a reduction in numbers since 0 minutes, which were contrasted to the strains PZ12 and PZ14, exhibiting almost no reduction at 0 minutes. More importantly, these two strains showed a slight decrease in bacterial population at 90 minutes and 180 minutes for both bile salt concentrations (Figure 2). This result suggests LAB's ability to establish itself in the human intestine.

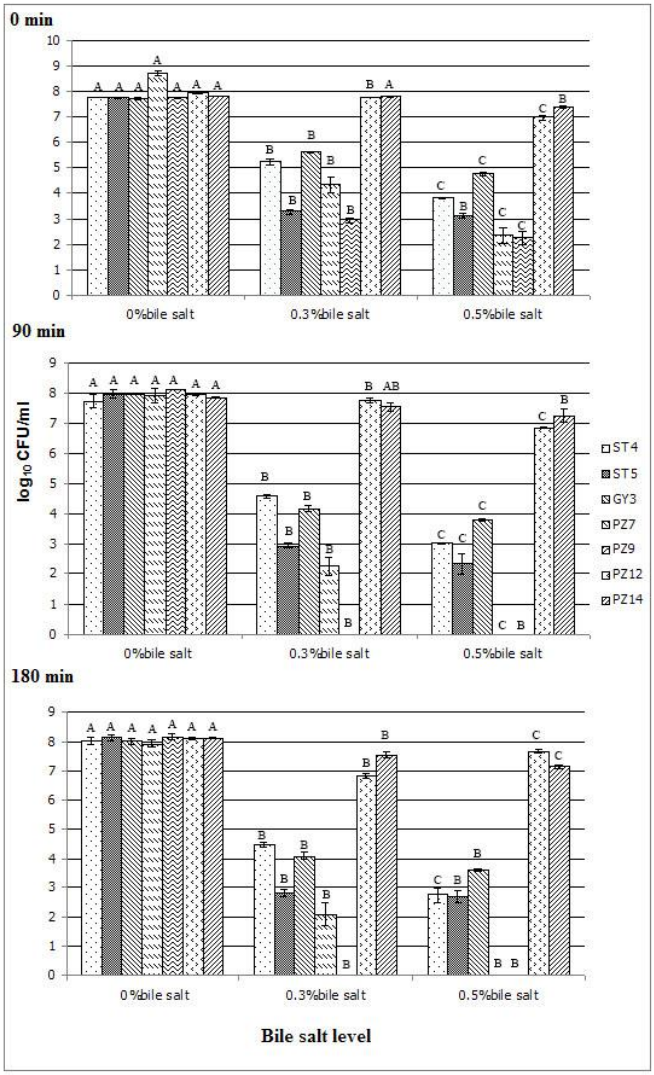

Figure 2. Toleration of LAB strains isolated from fermented asparagus and fermented stinky beans to bile salts (0.3% and 0.5%) for 90 minutes and 180 minutes. Uppercase letters indicate the significant difference in bile salt toleration of LAB strains among three bile salt concentrations: 0 % (control), 0.3%, and 0.5% (p-value < 0.05).

Bile salt is a biological compound synthesized in the liver from cholesterol. It shows a strong antimicrobial activity by destroying bacterial cell membranes and triggering DNA damage. LAB with probiotic potentials must be able to resist these mechanisms to inhabit the host's intestine [26]. The bacterial response to bile salt is a multi-factorial event. Active efflux of bile salts [23], bile salts hydrolysis [18], and the changes in cell membrane/cell wall compositions [9] are the most common bile tolerance mechanisms in *Lactobacillus* and *Bifidobacterium* [26]. Our results aligned with the Hermanns et al. [11] study. They isolated six LAB strains from artisan cheeses in Brazil and tested their toleration to 0.3% and 1.0% bile for 4 hours. It was found that there was a 1 to 2-log cycle reduction in bacterial survival compared to the control group (no bile). Hayisama-ae et al. [10] also demonstrated approximately 2 log cycle reductions in Lactobacillus plantarum strain DW12 survival after exposure to 0.3% bile salts for 6 hours. The LAB reduction of about 1 to 2 log cycles after LAB exposure to bile salts is thought to be common. A maximum of 1.5 log reduction from the initial count is a criterion defined by Charteris et al. [3]. Therefore, our LAB strains in this study demonstrate a strong toleration to bile salts and are believed to inhabit the intestine.

3.3 Inhibition of DEC and MRSA by LAB

The inhibition of pathogens is thought to be an essential weapon for the consumption of probiotics. The results of the antagonistic activity of 7 LAB strains against DEC and clinical MRSA in this study showed that all LAB strains could inhibit DEC and clinical MRSA by providing an inhibition zone between 22 and 39 mm (Table 2), focusing on LAB strains PZ12 and PZ14, which exhibited high probiotic potentials due to their ability to tolerate 0.3% pepsin and bile salt for extended time. It was found that both strains demonstrated relatively wide inhibition zones (wider than 30 mm) in all strains of DEC tested. As for the MRSA PSU20, all LAB demonstrated similar zone diameters ranging from 22 to 27 mm (Table 2). The distinct antagonistic activity of LAB against DEC and MRSA in this present study indicates that LAB produces a wide variety of compounds, e.g., organic acids, hydrogen peroxide, and bacteriocins. These compounds are documented to be capable of inhibiting spoilage and pathogens, such as Gram-positive or Gram-negative bacteria [6]. Hayisama-ae et al. [10] also investigated the antibacterial activity of Lactobacillus plantarum DW12 isolated from red seaweed against numerous pathogens and found that DW12 could inhibit all pathogens tested. A similar result was observed in the work of Makras et al. [19], who demonstrated the antibacterial activity of Lactobacilli against *Salmonella enterica* serovar Typhimurium through the production of organic acid, mainly lactic acid.

Table 2. Antagonistic activity of LAB strains isolated from pickles on diarrheagenic *E. coli* and clinical methicillin-resistant *S. aureus* by agar spot assay

LAB strain	Inhibition zone diameter (mm)					
	STEC PSU1	EHEC EDL933	EPEC PE-27	ETEC PSU192	EAEC PSU263	MRSA PSU20
ST4	31.80	30.70	27.80	26.70	25.60	23.30
ST5	30.00	28.40	34.50	26.90	32.50	24.10
GY3	35.00	27.10	30.40	25.00	29.00	21.50
PZ7	37.00	33.90	39.00	33.80	30.00	24.60
PZ9	35.20	31.70	36.40	33.60	29.60	21.50
PZ12	32.50	32.30	39.00	32.80	32.90	26.50
PZ14	36.00	34.40	34.90	34.70	34.90	23.00

3.4 Determination of antimicrobial susceptibility of LAB

Antimicrobial susceptibility assay of LAB demonstrated that all LAB strains provided an inhibition zone for most of the antimicrobial drugs tested, e.g., amikacin, chloramphenicol, gentamicin, clindamycin, erythromycin, imipenem, cotrimoxazole, and tetracycline. This suggested that these antimicrobial agents tested can destroy most LAB strains. Nevertheless, there were four drugs that most of the LAB showed resistance pattern: ciprofloxacin, fosfomycin, cefoxitin, and streptomycin (0 mm of inhibition zone) (Table 3). LAB strains PZ12 and PZ14 were resistant to three antimicrobial agents. PZ12 could withstand ciprofloxacin, fosfomycin, and streptomycin, and PZ14 was resistant to ciprofloxacin, cefoxitin, and streptomycin (Table 3).

Duskova et al. [7] examined antimicrobial resistance in lactobacilli isolated from Czech Republic foods using disk diffusion and broth microdilution methods. They found 15 strains (17%) resistant to at least one antimicrobial agent and one multi-drug resistant strain. In addition, among resistant strains, they were resistant to gentamicin at the highest frequency, 7.8%. Gentamicin resistance in these bacterial strains concords with a study by Danielsen and Wind [5] and Nawaz et al. [22] that also found high gentamicin resistance. Our present study showed that most of the LAB isolated from pickles were resistant to ciprofloxacin, fosfomycin, cefoxitin, and streptomycin. These results are concordant with the work of Karapetkov et al. [17], who investigated the drug-resistant pattern of four *Lactobacillus* spp. and one *Streptococcus thermophilus* from dairy products and fruits and found that they were suppressed by chloramphenicol, erythromycin, and tetracycline.

Table 3. Antimicrobial susceptibility of LAB strains from pickled asparagus and stinky beans

	Clear zone (mm)											
	[a]**AK**	**C**	**CIP**	**CN**	**DA**	**E**	**FOS**	**FOX**	**IPM**	**S**	**SXT**	**TE**
ST4	18.00	35.10	[b]0	17.10	17.15	37.00	0	0	51.00	0	25.40	29.50
ST5	17.20	35.60	0	19.00	12.00	38.10	0	0	40.50	8.00	25.40	31.70
GY3	10.45	34.00	0	14.50	23.30	34.50	0	0	47.20	0	21.00	29.40
PZ7	11.10	34.00	11.10	13.60	17.00	35.70	0	0	46.60	0	20.25	31.00
PZ9	19.05	34.30	10.20	16.80	9.00	38.00	0	0	48.00	9.45	29.20	29.00
PZ12	9.30	32.10	0	11.00	14.00	33.70	0	10.00	47.80	0	23.25	26.00
PZ14	8.15	32.00	0	11.80	14.00	33.00	8.30	0	47.00	0	22.20	25.50

[a]AK, amikacin; C, chloramphenicol; CIP, ciprofloxacin; CN, gentamicin; DA, clindamycin; E, erythromycin; FOS, fosfomycin; FOX, cefoxitin; IPM, imipenem; S, streptomycin; SXT; cotrimoxazole; TE, tetracyclin. [b]0, no clear zone.

The presence of antimicrobial-resistant phenotypes in LAB in this current study seems unsafe for consumers. However, the LAB isolated from probiotic products is usually reported to resist numerous antimicrobials [10], and the antimicrobial resistance in probiotics may be able to provide benefits to the host who has intestinal imbalance due to the antimicrobials used [12].

4. Conclusions

This study isolated LAB strains with good probiotic potentials from fermented asparagus and stinky beans. They exhibited antagonistic activity against clinical DEC and clinical MRSA with the capability of causing food poisoning, suggesting that they were equipped with pivotal weapons that can protect us, at least in part, from gastrointestinal pathogens. Antimicrobial resistance in LAB is common and thought to be beneficial to the host with intestinal imbalance during drug use. Therefore, pickled is an abundant source of probiotics. This study encourages the search for LAB strains from pickles with stronger probiotic properties that are useful for humans.

5. Acknowledgements

This work was partly funded by the Higher Education Research Promotion and National Research University Project of Thailand, Office of the Higher Education Commission (Grant no. SCI580528S). WK is a recipient of the scholarship as a research assistant.

Author Contributions: PR, original draft preparation, review, editing; WK, methodology, technical assistance; WP, technical assistance; PS, conceptualization, original draft preparation, editing, validation, resource. All authors have read and agreed to the published version of the manuscript.

Conflicts of Interest: The authors declare no conflict of interest.

References

[1] Armas F.; Camperio C.; Marianelli, C. In vitro assessment of the probiotic potential of *Lactococcus lactis* LMG 7930 against ruminant mastitis-causing pathogens. *PLoS One*. **2017**, *12*(1), Article e0169543.

[2] Bunnueang, N.; Kongpheng, S.; Yadrak P.; Rattanachuay, P.; Khianngam, S.; Sukhumungoon, P. Methicillin-resistant *Staphylococcus aureus*: 1-year collection and characterization from petients in two

tertiary hospitals, southern Thailand. *Southeast Asian Journal of Tropical Medicine and Public Health*. **2016**, *47*, 234-244.

[3] Charteris, W. P.; Kelly, P. M.; Morelli, L.; Collins, J. K. Selective detection, enumeration and identification of potentially probiotic Lactobacillus and Bifidobacterium species in mixed bacterial populations. *International Journal of Food Microbiology*. **1997**, *35*, 1–27.

[4] Crago, B.; Ferrato, C.; Drews, S. J.; Svenson, L. W.; Tyrrell, G.; Louie, M. Prevalence of *Staphylococcus aureus* and methicillin-resistant *S. aureus* (MRSA) in food samples associated with foodborne illness in Alberta, Canada from 2007 to 2010. *Food Microbiol.* **2012**, *32*(1), 202-5.

[5] Danielsen, M.; Wind, A. Susceptibility of *Lactobacillus* spp. to antimicrobial agents. *International Journal of Food Microbiology*. **2003**, *82*, 1–11.

[6] Duangjitcharoen, Y.; Kantachote, D.; Ongsakul, M.; Poosaran, N.; Chaiyasut, C. Potential use of probiotic *Lactobacillus plantarum* SS2 isolated from a fermented plant beverage: safety assessment and persistence in the murine gastrointestinal tract. *World Journal of Microbiology and Biotechnology*. **2009**, 25, 315-321.

[7] Dušková, M.; Karpíšková, R. Antimicrobial resistance of *Lactobacilli* isolated from food. *Czech Journal of Food Sciences*. **2013**, *31*, 27-32.

[8] Fluer, F. S. Staphylococcal toxin of toxic shock syndrome. *Zh Mikrobiol Epidemiol Immunobiol*. **2007**; Sep-Oct (5), 106-14.

[9] Gómez-Zavaglia, A.; Kociubinski, G.; Pérez, P.; DeAntoni, G. Effect of bile on the lipid composition and surface properties of bifidobacteria. *Journal of Applied Microbiology*. **2002**, 93, 794–799.

[10] Hayisama-ae, W.; Kantachote, D.; Bhongsuwan, D.; Nokkaew, U.; Chaiyasut, C. A potential synbiotic beverage from fermented red seaweed (Gracilaria fisheri) using *Lactobacillus plantarum* DE12. *International Food Research Journal*. **2014**, *21*(5): 1789-1796.

[11] Hermanns, G.; Funck, G. D.; Schmidt, J. T.; Pereira, J. Q.; Brandelli, A.; Richards, N. S. P. D. S. Evaluation of probiotic characteristics of lactic acid bacteria isolated from artisan cheese. *Journal of Food Safety*. **2014**. *34*, 380-387.

[12] Hickson, M.; Souza, A. L. D.; Muthu, N.; Rogers, T. R.; Want, S.; Rajkumar, C.; Builpitt, C. J. Use of probiotic *Lactobacillus* preparation to prevent diarrhea associated with antibiotics: randomized double blind placebo controlled trial. *British Medical Journal*. **2007**, *335* (7610), 80-83.

[13] Hwang, S. Y.; Kim, S. H.; Jang, E. J.; Kwon, N.H.; Park, Y. K.; Koo, H. C.; Jung, W. K.; Kim, J. M.; Park, Y. H. Novel multiplex PCR for the detection of the *Staphylococcus aureus* superantigen and its application to raw meat isolates in Korea. *International Journal of Food Microbiology*. **2007**, *117*(1), 99-105.

[14] Hussain, A.; Robinson, G.; Malkin, J.; Duthie, M.; Kearns, A.; Perera, N. Purpura fulminans in a child secondary to Panton-Valentine leukocidin-producing *Staphylococcus aureus*. *Journal of Medical Microbiology*. **2007**, *56* (10), 1407-1409.

[15] Jiang, W.; Hou, Y.; Inouye, M. CspA, the major cold-shock protein of *Escherichia coli*, is an RNA chaperone. *Journal of Biological Chemistry*. **1997**, *272*(1), 196-202.

[16] Jitpakdee, J.; Kantachote, D.; Kanzaki, H.; Nitoda, T. Selected probiotic lactic acid bacteria isolated from fermented foods for functional milk production: Lower cholesterol with more beneficial compounds. *LWT – Food Science and Technology*. **2021**, *135*, 110061.

[17] Karapetkov, N.; Georgieva, R.; Rumyan, N.; Karaivanova, E. Antibiotic susceptibility of different lactic acid bacteria strains. *Beneficial Microbes*. **2011**, *2*, 335-339.

[18] Kumar, R. S.; Brannigan, J. A.; Prabhune, A. A.; Pundle, A. V.; Dodson, G. G.; Dodson, E. J.; Suresh, C. G. Structural and functional analysis of a conjugated bile salt hydrolase from Bifidobacterium longum reveals an evolutionary relationship with penicillin V acylase. *Journal of Biological Chemistry*. **2006**, *281*, 32516–32525.

[19] Makras, L.; Triantafyllou, V.; Fayal-Messaoudi, D.; Adriany, T.; Zoumpopoulou, G.; Tsakalidou, E.; Servin, A; De Vuyst, L. Kinetic analysis of the antibacterial activity of probiotic lactobacilli towards Salmonella enterica serovar Typhimurium reveals a role for lactic acid and other inhibitory compounds. *Research in Microbiology*. **2005**, *157*, 241-247.

[20] Marrack, P.; Kappler, J. The staphylococcal enterotoxins and their relatives. *Science*. **1990**, *248*, 705-711.

[21] Nataro, J. P.; Kaper, J. B. Diarrheagenic *Escherichia coli*. *Clinical Microbiology Reviews.* **1998**, *11*, 142-201.

[22] Nawaz, M.; Wang, J.; Zhou, A.; Ma, C.; Wu, X.; Moore, J. E.; Millar, B. C.; Xu, J. Characterization and transfer of antibiotic resistance in lactic acid bacteria from fermented food products. *Current Microbiology*. **2011**, *62*, 1081–1089.

[23] Pfeiler, E. A.; Klaenhammer, T. R. Role of transporter proteins in bile tolerance of *Lactobacillus acidophilus*. *Applied and Environmental Microbiology*. **2009**, *75*, 6013–6016.

[24] Reid, S. D.; Betting, D. J.; Whittam, T. S. Molecular detection and identification of intimin alleles in pathogenic *Escherichia coli* by multiplex PCR. *Journal of Clinical Microbiology*. **1999**, *37*, 2719-2722.

[25] Riley, L.W.; Remis, R. S.; Helgerson, S. D.; McGee, H.B.; Wells, J. G.; Davis, B. R.; Hebert, R. J.; Olcott, E. S.; Johnson, L. M.; Hargrett, N. T.; Blake, P. A.; Cohen, M. L. Hemorrhagic colitis associated with a rare *Escherichia coli* serotype. *New England Journal of Medicine*. **1983**, *308*, 681-5.

[26] Ruiz, L.; Margolles, A.; Sanchez, B. Bile resistant mechanisms in *Lactobacillus* and *Bifidobacterium*. *Frontier in Microbiology*. **2013**, *369*(4), 1-8. https://doi.org/10.3389/fmicb.2013.00396.

[27] Sirikaew, S.; Patungkaro, W.; Rattanachuay, P.; Sukkua, K.; Sukhumungoon, P. Enterotoxigenic *Escherichia coli* O169:HUT from a diarrheal patient: Phylogenetic group and antimicrobial susceptibility. *Southeast Asian Journal of Tropical Medicine and Public Health*. **2014**, *45*, 1376-1384.

[28] Sukkua, K.; Patungkaro, W.; Sukhumungoon, P. Detection and molecular characterization of enteroaggregative *Escherichia coli* from diarrheal patients in tertiary hospitals, Southern Thailand. *Southeast Asian Journal of Tropical Medicine and Public Health*. **2015**, *46*, 901-910.

[29] Sukhumungoon, P., & Nakaguchi, Y. Shiga toxin 2-converting bacteriophages occupy *sbcB* gene as a primary integration site in bovine-origined *Escherichia coli* O157:H7 and non-O157 from Thailand. *Life Science Journal*. **2013**, *10*, 2334-2340.

[30] Sukhumungoon, P.; Hayeebilan, F.; Yadrak, P.; Kanobthammakul, S.; Nakaguchi, Y.; Saengsuwan, P.; Singkhamanan, K. Molecular characterization and relationship of methicillin-resistant *Staphylococcus aureus* among strains from healthy carriers and University hospital patients, southern Thailand. *Southeast Asian Journal of Tropical Medicine and Public Health*. **2014**, *45*, 402-412.

[31] Tulini, F.L.; Winkelströter, L. K.; De Martinis, E. C. Identification and evaluation of the probiotic potential of *Lactobacillus paraplantarum* FT259, a bacteriocinogenic strain isolated from Brazilian semi-hard artisanal cheese. *Anaerobe*. **2013**, *22*, 57-63.

[32] Urdaneta, V.; Casadesús, J. Interactions between bacteria and bile salts in the gastrointestinal and hepatobiliary tracts. *Frontiers in Medicine (Lausanne)*. **2017**, *4*, 163.

[33] Wang, S.; Li, Y.; Xiong, H.; Cao, J. A broad-spectrum inhibitory peptide against staphylococcal enterotoxin superantigen SEA, SEB and SEC. *Immunology Letters*. **2008**, *121*, 167-72.

[34] Wang, C.Y.; Lin, P.R.; Ng, C.C.; Shyu, Y. T. Probiotic properties of *Lactobacillus* strains isolated from the feces of breast-fed infants and Taiwanese pickled cabbage. *Anaerobe*. **2010**, *16*, 578-85.

[35] Wang, C.; Cui, Y.; Qu, X. Mechanism and improvement of acid resistance in lactic acid bacteria. *Archives of Microbiology*. **2018**. *200*, 195-201. https://doi.org/10.1007/s00203-017-1446-2.

[36] Witte, W.; Pasemann, B.; Cuny, C. Detection of low-level oxacillin resistance in mecA-positive *Staphylococcus aureus*. *Clinical Microbiology and Infection*. **2007**, *13*, 408-412.

ASEAN
Journal of Scientific and Technological Reports
Online ISSN:2773-8752

Research article

Evaluation and Reduction of the Carbon Footprints Associated with Steviol Glycoside Production

Jittra Duangsong[1], and Supawadee Theerathammakorn[2]*

[1] School of Science and Technology, Sukhothai Thammathirat Open University, Nonthaburi, 11120, Thailand; jittracity@gmail.com
[2] School of Science and Technology, Sukhothai Thammathirat Open University, Nonthaburi, 11120, Thailand; Supawadee.the@stou.ac.th
* Correspondence: Supawadee.the@stou.ac.th:

Citation:
Duangsong, J.; Theerathammakorn, S. Evaluation and reduction of the carbon footprints associated with steviol glycoside production. *ASEAN J. Sci. Tech. Report.* **2024**, *27*(3), e252464. https://doi.org/10.55164/ajstr.v27i3.252464.

Article history:
Received: January 19, 2024
Revised: April 27, 2024
Accepted: April 28, 2024
Available online: April 30, 2024

Abstract: This study aims to evaluate the carbon footprint generated in each step of stevia sweetener (steviol glycosides) production and to find out how to reduce the impact of the sweetener's greenhouse gas (GHG) emissions. In addition, a comparison of the carbon footprints of the sweetener and sucrose is included. A cradle-to-gate LCA was conducted on steviol glycosides (purified rebaudioside A, RA95) production in Thailand. The carbon footprint assessment method is based on the guidelines of the Food Institute, Ministry of Industry in Thailand, corresponding to ISO 14067 and PAS 2050. The study evaluates the carbon footprint by employing two sources of emission factors from the Thailand Greenhouse Gas Management Organisation database for carbon footprint and OpenLCA Version 1.10.3 with eco-invent database Version 2.2 for comparing the carbon footprint and finding out other impacts. The result from OpenLCA reveals the impact on marine aquatic ecotoxicity, followed by the Depletion of abiotic resources and human toxicity. The results showed that a kilogram of the RA95 releases 32.07 kilograms of carbon dioxide equivalent. The highest GHG emissions came from the raw material procurement process, with 53.01%, followed by production, support system, and material transportation, with 28.09%, 16.47%, and 2.43%, respectively. The three production steps with the highest GHG emissions were the second crystallization, the first crystallization, and the drying process, respectively. The RA95 releases a carbon footprint 3.55 times lower than sucrose for the same level of sweetness. The recommendations to reduce the carbon footprint in production are to reduce natural gas usage by improving boiler efficiency and reduce electricity usage by installing an automatic shutdown system for cooling machines (chiller), depending on the production volume. The findings revealed a lower carbon footprint of 0.33 kgCO2eq per kilogram of product after improvement.

Keywords: Carbon Footprint; Stevia Sweetener; Rebaudioside A; Steviol Glycosides; Life cycle assessment

1. Introduction

Nowadays, consumers are paying more attention to health care. Especially regarding sugar consumption because consuming excessive amounts of sugar causes various health problems such as obesity, diabetes, high blood pressure, heart disease, vascular disease, etc. According to the World Health Organization, in 2016, approximately 1.6 million people died directly from diabetes, and diabetes was the seventh leading cause of death worldwide [1]. Thirty-seven million children under the age of 5 years were overweight and

obese, and almost half of their deaths were linked to malnutrition, especially consuming foods and drinks containing more energy (high in sugars and fats) [2]. The rising incidence of diabetes and obesity has consumers seeking natural, calorie-free sweeteners to maintain healthy blood sugar levels. In addition, the sugar tax on beverages containing sugar, such as soft drinks, green tea, coffee, energy drinks, and fruit juices, has increased to change the consumption behavior of Thai people and help reduce the risk of overconsumption of sugar. The price of products containing sugar exceeding the standard is expected to increase, causing consumers to reduce their consumption of sugary beverages and have better health [3, 4]. There are many types of sugar substitute sweeteners. Low and No-Calorie Sweeteners (LNCS) are classified as food additives that are added to many foods and beverages. LNCS is commonly added to products as a sugar substitute because it can provide the desired sweet taste with little or no energy.

Additionally, these substances are not carcinogenic and do not trigger the same metabolic response as sugar. Because of this characteristic, products containing LNCS are often recommended for people with specific health conditions, such as sugar-free food and drinks for people with diabetes [5]. LNCS permitted many sweeteners, including steviol glycosides, in the EU [6].

Steviol glycoside is different from other sweeteners because it is safe to consume and has a very low Acceptable Daily Intake (ADI) of 4 mg/kg. of body weight. It is 200-300 times sweeter than sucrose [6]. In addition, steviol glycosides are natural extracts. At the same time, other low-calorie, no-calorie sugar substitutes are synthetic sweetener substances that have changed their chemical structure (except for thaumatin, which is commonly used to improve taste and is not allowed for use according to the United States Food and Drug Administration standards [6]. Steviol glycosides are extracted from stevia, an economic plant that can be produced in large commercial quantities. Stevia sugar substitute sweetener is an alternative product to reduce sugar consumption. It is highly safe as it is a natural extract with health benefits such as anti-obesity, anti-diabetic, and anti-oxidant [7]. In Thailand, the Food Division of the Food and Drug Administration has designated this sweetener from stevia as a food additive named steviol glycoside. The food additive standards refer to the Codex standards, JECFA Monograph INS no. 960.

Using stevia sweeteners on an industrial scale in Thailand has yet to be very popular. The international sale of stevia sweeteners continues to face commercial problems due to environmental measures that customers value and the desire to consume environmentally friendly products, especially in the European market [9]. Therefore, entrepreneurs must prepare for their business's survival and support increased competition amid changes in the global economy. The way to increase the competitiveness of entrepreneurs is by increasing production efficiency and improving the production process to reduce greenhouse gas emissions. So that consumers and trading partners can accept that this product has undergone a production process that considers environmental protection. Therefore, the carbon footprint is assessed using the principles of Life Cycle Assessment (LCA), a tool used to determine greenhouse gas emissions that occur throughout the product life cycle that leads to formulating strategies to find ways to improve and develop production to reduce greenhouse gas emissions. Resources are used efficiently and have minimal environmental impact, leading to sustainable development and increasing competitiveness in the global market. Additionally, entrepreneurs can register the product's carbon footprint label and request a global warming reduction label from the Greenhouse Gas Management Organization (Public Organization).

More research is needed into the environmental impact of stevia sweeteners. A few studies relating to stevia sweeteners are PureCircle's carbon footprints from farm to stevia sweeteners type RA95 were determined on average to be 44.57 kgCO2eq/kg using sweetness equivalence for comparison. Stevia releases an 82% and 64% lower carbon footprint compared to beet sugar and cane sugar, respectively [10]. The stevia extract type RA60 has a carbon footprint of 20.25 kgCO2eq/kg on a mass basis and 0.081 kgCO_2eq/kg on a sucrose sweetness equivalency basis for the EU's cradle-to-factory-gate life cycle [11]. Mexico's carbon footprint from farm to stevia extract is 1.81 kgCO2eq/kg, and sugar is 2.48 times greater than stevia extract [12].

Furthermore, Thailand has committed to achieving carbon neutrality by 2025 and net zero GHG emissions by 2065 through the Nationally Determined Contribution (NDC) Roadmap. Consequently, by 2030, a goal of 30 to 40% below-average greenhouse gas emissions across all economic sectors should be met [13]. The National Greenhouse Gas Reduction Action Plan, 2021–2030 [13] states that industrial entrepreneurs must develop an action plan and methods for reducing greenhouse gas emissions to support national policy. This research aims to assess the carbon footprint associated with each stage of the production of stevia sweetener

(steviol glycosides with purified rebaudioside A, RA95) and determine ways to lessen the sweetener's greenhouse gas (GHG).

2. Materials and Methods

This study covers creating carbon footprint data for the RA95 manufacturing cycle, which involves a Thai factory extracting stevia. The carbon footprint assessment method is based on the "Guideline for evaluating carbon footprint on product for the food industry" assessment method by the Food Institute, Ministry of Industry in Thailand, which details 6 main steps corresponding to ISO 14067 and PAS 2050 [11][14].

2.1 Identification of targets and boundary

This study aimed to assess RA95's carbon footprint by analyzing the greenhouse gas emissions that transpire throughout manufacturing. Every stage of the process was evaluated to ascertain the best method, leading to systematically and effectively reducing RA95's carbon footprint. A comparison of the carbon footprint between RA95 and sugar is also included.

2.2 Product selection

The selected product is RA95, which is rebaudioside A or Reb-A, purified from stevia extract. RA95 requires more energy than other products and takes a long time—roughly 150 hours per batch.

2.3 Definition of system boundary

The system boundary of carbon footprint assessment is focused on the production process by Cradle-to-Gate or Business-to-Business (B2B); that is, it covers sub-processes such as raw materials transportation and production, as shown in the picture below. The functional unit is 605 kilograms of product per production batch.

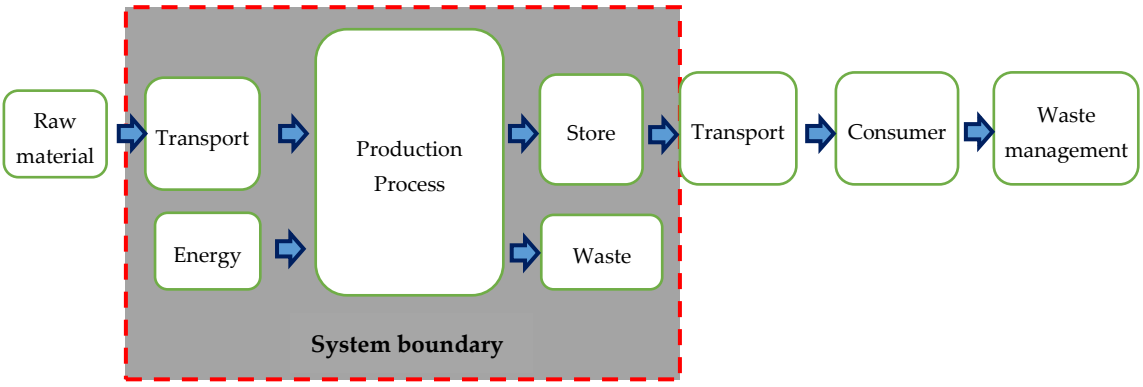

Figure 1. System boundary

2.4 Creation of life cycle diagram

The scope of this evaluation is B2B, as shown in Figure 2, considering the process of acquiring raw materials, consisting of stevia extract, ethanol, corrugated box, and aluminum laminated bag. Stevia extract is imported from China. Ethanol is imported from the United States. Both are transported by ship from the port into the production plant by truck, container, or tank car. Then, all materials enter the production, packing, and warehousing processes. In the factory, water is utilized from the industrial estate. RO (Reverse Osmosis) water is produced for use within the factory. The wastewater flows into the wastewater collection pond and is then sent to wastewater treatment by industrial estates.

2.5 Collection of life cycle data

All input and output data in the production process are collected to evaluate the product's carbon footprint. The data collection period was continuous during the six batches of stevia sweeteners RA95 production for 14 days. Data source for input and output are collected from various sources as follows:

2.5.1 Transportation information

Transportation information refers to the transportation of raw materials, resources, and production aids from suppliers to factories, and it includes detailed information on weight and distance, as shown in Table 1.

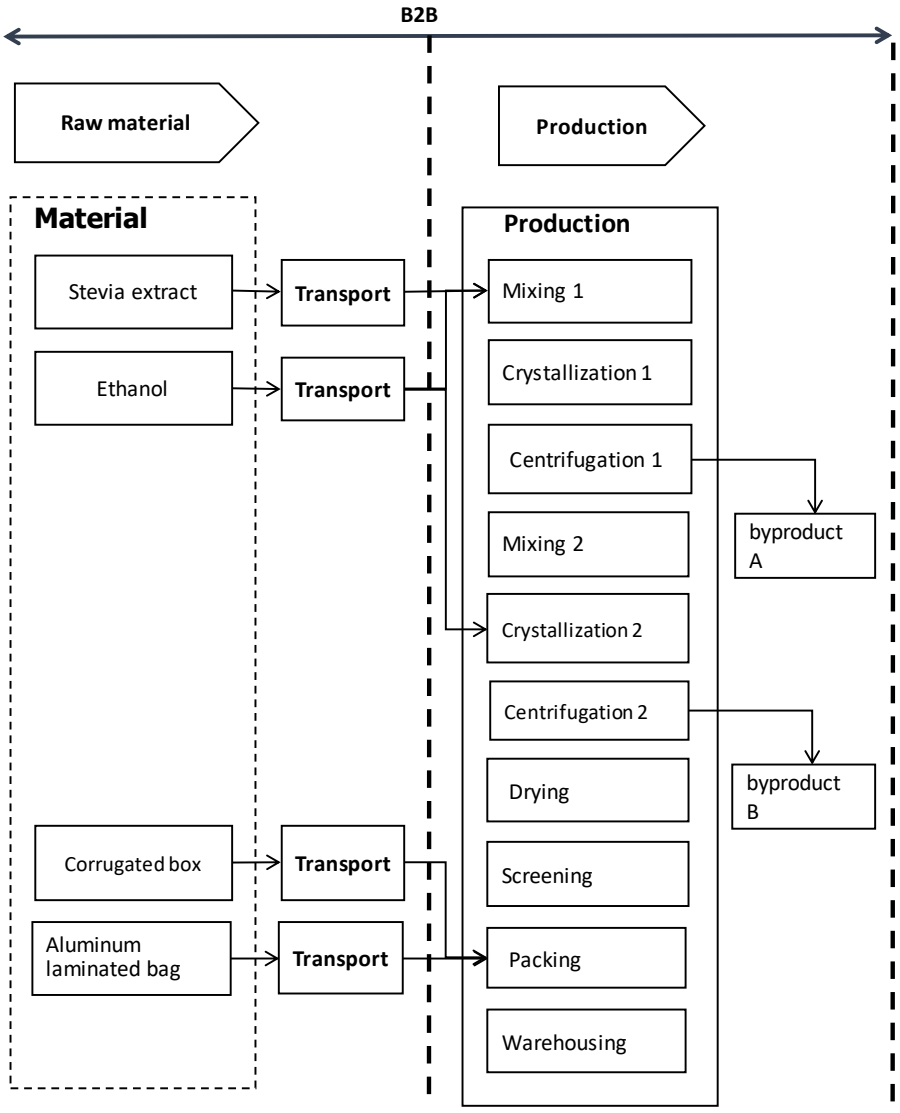

Figure 2. B2B life cycle diagram of Rebaudioside A

Table 1. Information on the transportation of raw materials, resources, and production aids from suppliers to factories

Material list	Weight (kg)	Distance (km)	Truck type
stevia extract	2,400	34	110-wheel truck container, normal running, 50% loading 16 tons
ethanol	14,516	34	Trailer, 18 wheels, 32 tons, normal running, 75% loading
corrugated box	60	16	Small pickup, 4 wheels, 7 tons, normal running, 50% loading
aluminum laminated film	36	154	Small pickup, 4 wheels, 7 tons, normal running, 50% loading

2.5.2 Daily production reports

Daily production reports can show how long each production step takes. Data collection from recording the start and end times of each step, with production data for six batches, takes the production time of each step.

2.5.3 Daily electricity usage report

Electricity meters were used at pre-arranged intervals to monitor and record the daily electrical energy consumption of the industrial process both before and after the experiment was finished. Since the data from the meter cannot show how much electricity is consumed at each stage of production, the readings were averaged to the amount of electricity used per battery. As a result, the amount of electrical energy used is computed using the machinery equipment standards. The total power used in 15 days to produce six batches is 22,934 kWh or 3,822.3 kWh per batch.

The percentage ratio of electric power to machine power, or duty factor, is obtained by dividing the total electricity usage per production batch (x) by the electricity usage from the full machinery standard per production batch (y), then multiplying the result by 100 according to equation (1).

$$\text{Duty factor} \quad = = \frac{x}{y} \times 100 \tag{1}$$

For instance, 5,205.67 kWh of power is used in every batch when calculating the whole machine standard. According to the electricity meter, 3,822.3 kWh of electricity are used overall in each batch. Subsequently, the duty element stands at 73.43%. Therefore, the electrical usage number for each process step was calculated by multiplying the duty factor by the electrical power produced by the machine's standard.

The electricity required to generate cooling water can be obtained from the meter and utilized to determine the electricity consumed step-by-step. To calculate the quantity of electrical energy consumed, Table 3 shows that cooling water was used for the first crystallization process for 26.29 hours, or 47.52%, and for the second crystallization step for 29.04 hours, or 52.48%. The first and second diluted solutions were used to create by-products A and B. Like cooling water allocation, the electrical energy used in this step is distributed. After allocating, 242.78 and 119.43 kWh of electricity were consumed for wet crystal in the first and second centrifugation processes.

2.5.4 Daily natural gas usage report

A flow meter was used to gather information on the natural gas utilized in boilers to produce steam between May 10 and 25, 2021. After the three stages of the first, second, and drying crystallization, the amount of natural gas utilized is 4,561.33 Nm^3, divided into three parts of 1550.40, 1712.32, and 1298.61 Nm^3 or 1040.32, 1,148.97, and 871.37 kg, respectively.

2.5.5 Daily water usage report

Only a minimal amount of water was used during manufacture. Most often utilized in the generation of cooling water. Water meters recorded 281 cubic meters of use between May 10 and 25, 2021, or 46.83 cubic meters per batch.

Mass and energy balance calculations were examined at every stage after inventory data was collected for the boundary study. The life cycle inventory in Table 2 shows the process step, input-output, unit, and amount per functional unit (FU) in each process unit.

2.6 Calculation of carbon footprint

The greenhouse gas emission was calculated as the carbon footprint, which is equal to multiplying the product of activity data with the emission factor (EF). The calculation is divided into three parts as follows.

(1) Greenhouse gas emissions from raw materials

(2) Greenhouse gas emissions from the transportation of materials

(3) Greenhouse gas emissions of production support systems

Production data of input and output that has been mass-balanced is used to calculate the quantity per functional unit. Then, multiply it with the EF value to get the carbon footprint value. Inputs and outputs that do not create greenhouse gas emissions were not calculated. Therefore, the carbon footprint is zero.

The study's greenhouse gas emissions data on electricity for production was obtained from the Thailand Greenhouse Gas Management Organization database. In this regard, all data's conversion of carbon dioxide equivalent (CO_2 eq) was calculated using equation (2).

$$CO_2\ eq.\ (of\ each\ production\ step) = \sum (Q(i) \times EF(i)) \quad (2)$$

Where $CO_2\ eq.$ refers to the amount of greenhouse gas emission
$\sum Q(i)$ means the sum of the data values of each activity i, $(Q(i))$ multiplied by the emission factor $(EF(i)$ in each activity i

2.7 The Carbon footprint calculated by OpenLCA Version 1.10.3

The assessment was conducted using OpenLCA program version 1.10.3 with ecoinvent database version 2.2, focusing on global warming potential.

Table 2. Life Cycle Inventory

No.	Process unit	Input-Output	Unit	Amount/FU
1	mixing 1	Electricity	kWh	41.25
		stevia extract	kg	2400
		ethanol	kg	14,516
2	crystallization 1	Electricity	kWh	42.47
		Natural gas for boiler	kg	1,040.32
		Electricity for cooling	kWh	941.73
3	centrifugation 1	Electricity	kWh	242.78
4	mixing 2	Electricity	kWh	26.36
5	crystallization 2	Electricity	kWh	46.91
		Natural gas for boiler	kg	1,148.97
		Electricity for cooling	kWh	1,040.24
6	centrifugation 2	Electricity	kWh	119.46
7	drying	Electricity	kWh	571.81
		Natural gas for boiler	kg	871
		Ethanol vapor	kg	56.58
8	screening	Electricity	kWh	71.17
9	packing	Electricity	kWh	17.76
10	Supporting	RO water	M^3	7.33
		Soft water	M^3	39.50
		Electricity	kWh	5235
11	Waste management	Waste water treatment	M^3	46.83
		Products waste	kg	4

3. Results and Discussion

In this study, carbon footprint assessment was carried out according to the "Guideline for evaluating carbon footprint on product for the food industry," corresponding to ISO 14067 and PAS 2050 [14]. The product studied is the sweetener from stevia called steviol glycosides purified Reb-A, which refers to a sweetener that purifies Reb-A from stevia extract by crystallization in an ethanol solvent. The amount of Reb-A must be at least 95%. The study's functional unit is 605 kilogram products. The factory received the stevia extract from the port. After that, it began production, packing, and storing the product to be distributed domestically and internationally. All of this was considered for the carbon footprint assessment by the Cradle-to-Gate life cycle assessment (LCA) standards. The following is a display of the results of the carbon footprint calculation.

3.1 Carbon footprint of transportation of raw materials, resources, and process aids

Raw materials, resources, and process aids are transported from suppliers to the manufacturing facility. As indicated in Table 3, it was discovered that the carbon footprint was 471.57 $kgCO_2eq$. Most of the carbon emissions came from ethanol and stevia extract, respectively.

Table 3. Carbon footprint calculation of transportation of raw materials, resources, and process aids

Material list	Load (kg)	Distance (km)	Carbon footprint ($kgCO_2eq.$)
stevia extract	2,400	34	53.85
ethanol	14,516	34	413.94
corrugated box	60	16	0.56
aluminum laminated film	36	154	3.23
Total			471.57

3.2 Carbon footprint of the raw material acquisition process

The computation results indicate that the carbon footprint of acquiring raw materials is 10,284.83 $kgCO_2eq$ per functional unit of 605 kg (Table 4). Most of the carbon emissions also came from ethanol and stevia extract.

3.3 Carbon footprint calculation results of the production process

Figure 3 illustrates the carbon footprint associated with the production process, which is 5,445.76 $kgCO_2eq$ per functional unit of 605 kg. The processes of second crystallization (crystallization 2) and first crystallization (crystallization 1) produced the highest levels of carbon emissions, respectively.

Table 4. Results of calculating the carbon footprint of the raw material acquisition process

Input-Output			Emission Factor ($kgCO_2eq$/unit)	Carbon footprint
List	unit	Amount/FU		($kgCO_2eq$)
stevia extract	kg	2,400	1.8069	4,336.52
ethanol	kg	14,516	0.3962	5,751.24
corrugated boxes	kg	60	1.6324	97.94
aluminum laminated bag	kg	36		
- nylon	kg	4	9.2691	37.62
- aluminum foil	kg	5	0.647	2.91
- LLDPE	kg	27	2.1356	58.60
			Total	**10,284.83**

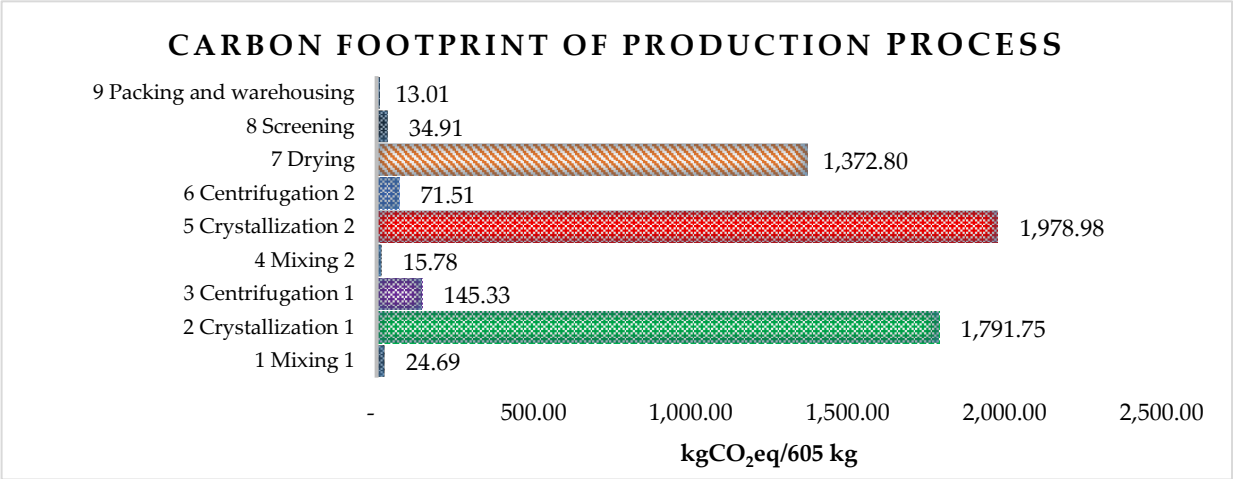

Figure 3. Greenhouse gas emissions from the production process of stevia sweetener Rebaudioside A ($kgCO_2eq$/605 kg)

3.4 Carbon footprint calculation results of production supporting

Table 5 illustrates the carbon footprint of the production support section per functional unit of 605 kg, which is 3,195.79 $kgCO_2eq$—using electricity results in the most significant carbon emissions. It is also found that the electric current used most is in the chiller section, 2526 kWh per functional unit, followed by air

compressors, electricity for steam boiler systems, lighting, and water production systems, and electricity for nitrogen tank systems, 2260, 321, 126, 2 kWh per functional unit, respectively. Reducing electricity consumption in the cooling system decreases Reb-A's carbon footprint, which was discussed later in topic 3.8.

Table 5. Carbon footprint calculation results of production supporting

Input-Output			EF, ($kgCO_2eq$/unit)	Carbon footprint ($kgCO_2eq$)
list	**unit**	**Amount/FU**		
RO water	m^3	7.33	2.1555	15.81
soft water	m^3	39.50	1.0301	40.69
electricity	kWh	5,235.00	0.5986	3,133.67
wastewater treatment	m^3	46.83	0.1201	5.62
			Total	**3,195.79**

3.5. Carbon footprint calculation results of the entire process

According to Figure 4, the results of the carbon footprint calculation for the production activity show that greenhouse gas emissions throughout the production process totaled 19,400.95 $kgCO_2eq$/605 kg or 32.07 $kgCO_2eq$/kg. The method of acquiring raw materials has the highest proportion of greenhouse gas emissions, at 10,284.83 $kgCO_2eq$ (53.01%), followed by the production process at 5,448.76 $kgCO_2eq$ (28.09%), the supporting system at 3,195.79 $kgCO_2eq$ (16.47%), and raw material transportation at 471.57 $kgCO_2eq$ (2.43%) respectively.

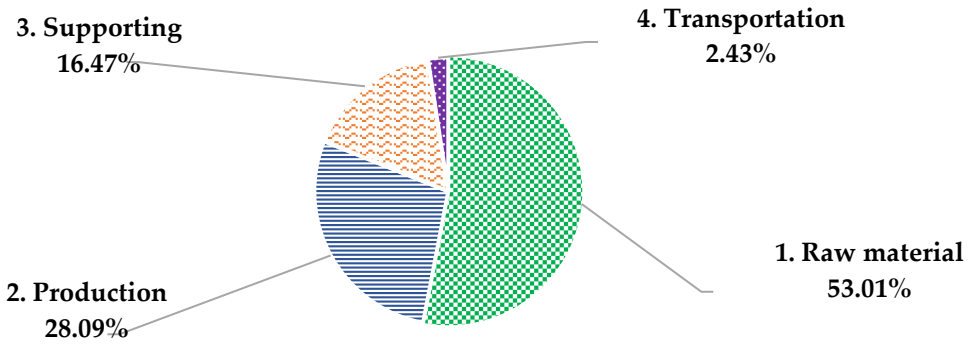

Figure 4. The carbon footprint of the entire process

When comparing the carbon footprint of Reb-A from this study (32.07 $kgCO_2eq$/kg) with the study of PureCircle Company (44.57 $kgCO_2eq$/kg) [10], which has a similar production process, it found that this study has a carbon footprint of less than PureCircle 12.5 $kgCO_2eq$/kg. The proportion of carbon footprint of each process between this study and PureCircle Company found that the highest carbon emission came from the raw material, followed by the production in the same manner.

3.6 Rebaudioside A and sucrose's carbon footprints compared at the same sweetness level

Table 6 shows that sucrose's greenhouse gas emissions value is 0.39 $kgCO_2eq$/kg, whereas the stevia sweetener Reb-A has a value of 32.07 $kgCO_2eq$/kg when used in the same amount. In this study, Reb-A is the ninety-five percent of Reb-A extracted (RA95). The greenhouse gas emissions of RA95 were found to be 89 times higher than those of sucrose. However, RA95 is sweeter than sucrose 290 times at 5% sucrose solution [10]. When used in food, it is used in tiny amounts at the same level of sweetness as sucrose. The ratio of sucrose used to RA95 was 290:1 or 5:0.017. Table 7 also reveals that RA95 reduces carbon emissions by 71.79%, or 3.55 times, compared to sucrose at the same level of sweetness. Sixty percent of Reb-A extracted or RA60 has a carbon footprint of 4.76 times less than sucrose, reducing 78.97% of carbon emission. However, RA95 has a carbon footprint of less than one $kgCO_2eq$ compared to RA60, which has the same sweetness. Reb-A (RA) has been identified as the least bitter, with a minor persistent aftertaste among stevia glycosides.

Bitterness often is significant due to the impurities in extracts [15]. Therefore, RA95 is more purified than RA60, which provides less bitterness.

Table 6. Carbon footprint comparison of Sucrose and Reb-A at the same sweetness level

Products	Usage (kg)	Carbon footprint ($kgCO_2eq/kg$)	Carbon footprint at same sweetness level ($kgCO_2eq$)	Reducing Carbon footprint
sucrose	5	0.39*	1.95	-
RA95	0.017**	32.07	0.55	-71.79% or 3.55 times
RA60	0.020***	20.25	0.41	-78.97% or 4.76 times

* calculated from the carbon footprint of 26 B2B sucrose sources. (Source: Thailand Greenhouse Gas Management Organization (Public Organization))

** calculated at 5% sweetness equivalence by RA95 is 290 times sweeter than sucrose.

***calculated at 5% sweetness equivalence by RA60 is 250 times sweeter than sucrose[11].

3.7 The Carbon footprint calculated by OpenLCA Version 1.10.3

The carbon footprint obtained by the OpenLCA program version 1.10.3 with eco-invent database version 2.2 is 21,901.34 $kgCO_2eq$/ 605 kg, or 2,500.39 $kgCO_2eq$ higher than the calculation in this study (19,400.95 $kgCO_2eq$), and because of the different sources of emission factor (EF), according to the results when using the program to determine other environmental impact. Table 7 illustrates the environmental impact analyzed using the Open LCA method. The most significant impact is attributed to marine aquatic ecotoxicity, followed by the Depletion of abiotic resources and human toxicity.

Table 7. The environmental impact calculated by OpenLCA Version 1.10.3 ecoinvent database version 2.2

Impact category	Reference unit	Result
Acidification potential - average Europe	kg SO_2 eq.	437.09
Climate change - GWP100	**kg CO_2 eq.**	**21,901.34**
Depletion of abiotic resources - elements, ultimate reserves	kg antimony eq.	0.06
Depletion of abiotic resources - fossil fuels	MJ	570,190.83
Eutrophication - generic	kg PO_4- eq.	219.33
Freshwater aquatic ecotoxicity	kg 1,4-dichlorobenzene eq.	13,228.89
Human toxicity	kg 1,4-dichlorobenzene eq.	16,232.51
Marine aquatic ecotoxicity	kg 1,4-dichlorobenzene eq.	30,330,609.46
Ozone layer depletion - ODP steady state	kg CFC-11 eq.	0.00
Photochemical oxidation	kg ethylene eq.	37.71
Terrestrial ecotoxicity	kg 1,4-dichlorobenzene eq.	409.19

Figure 5 shows the comparison results of the carbon footprint determined using this study's Thailand Greenhouse Gas Management Organisation (TGO) database with OpenLCA Version 1.10.3 with eco-invent Database Version 2.2. Based on OpenLCA's calculations, electricity has been shown to have the most significant influence, followed by natural gas and raw materials (consisting of stevia extract and ethanol). According to the study's calculations, natural gas and electricity are the most influential factors after raw materials. As Table 8 illustrates, there are differences in the carbon footprint values computed by OpenLCA and this study due to different sources of emission factors except stevia extract.

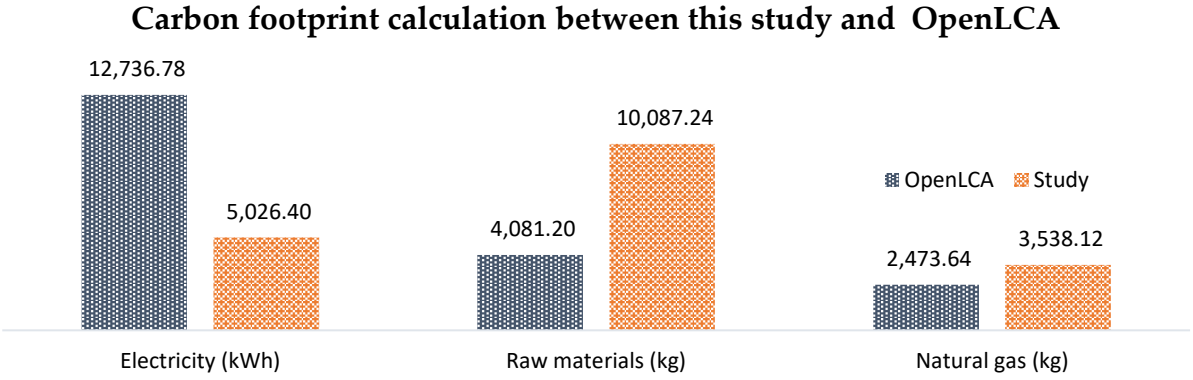

Figure 5. The source of impact of carbon footprint calculated between this study and OpenLCA

Table 8. Emission factor used comparison between this study and OpenLCA

Items	Emission factor ($kgCO_2eq$/unit)			
	OpenLCA ecoinvent 2.2		TGO (Mar, 2021)	
electricity (kWh)	1.1539	electricity, high voltage, at grid-CN	0.5986	electricity, grid mix (2016-2018; LCIA method IPCC 2013 GWP 100a V1.03)
natural gas (kg)	0.01401	natural gas, at consumer-RNA (kg)	1.156	natural gas liquid (LCIA method IPCC 2013 GWP 100a V1.03)
Raw materials				
stevia extract (kg)	1.8069	an emission factor referred to by Salinas et al. (2015)	1.8069	an emission factor referred to by Salinas et al. (2015)
ethanol, 95% in H_2O (kg)	-0.01756	ethanol, 95% in H_2O, from corn, at distillery-US (kg)	0.3962	ethanol, 95% in H_2O, from sugarcane molasses, at sugar refinery

3.8 Reduction of the carbon footprint from the stevia sweetener RA95

As mentioned, using electricity results in the most significant carbon emissions in RA95 production support, which is relatively high supplied to the chiller systems. One way to reduce the amount of electricity consumed is to use an automatic chiller. Setting the start and shutdown time according to the specified period was established. The chiller stops working automatically at the end of the tank's reaction process; do not leave it open for nothing. As seen in Table 9, the amount of electrical energy used in this phase is decreased by 200.19 $kgCO_2eq$ per functional unit or 0.33 $kgCO_2eq$ /kg product.

Table 9. Reducing carbon footprint during the RA95 production process by improving the chiller's automated start-shutdown system

Electricity	kWh/FU	EF ($kgCO_2eq$/kWh)	CFP ($kgCO_2eq$)
before improvement	2,526.00	0.5986	1,512.06
after improvement	2,191.56	0.5986	1,311.87
saving	334.44	-	200.19

Therefore, after improving the automatic start-shutdown system of the chiller project, the carbon footprint of the study factory is reduced by 20,019 $kgCO_2eq$ per year by reducing electrical energy use by 33,444 kWh or **114,387 Baht per year**.

4. Conclusions

The carbon footprint of 605 kilograms of the stevia sweetener RA95 throughout the production process is 19,400.95 kgCO_2eq or 32.07 kgCO_2eq per kilogram of product. The raw materials acquisition process has the highest proportion of greenhouse gas emissions, followed by production, production support, and raw material transportation. The second and first crystallization steps and drying are the top 3 production processes with the highest greenhouse gas emissions. The environmental impact analyzed using the Open LCA method revealed that the most significant impact is attributed to marine aquatic ecotoxicity, followed by the Depletion of abiotic resources and human toxicity. Those significant impacts are derived from packaging consisting of the lamination of three layers of nylon, aluminum foil, and LLDPE. The decrease in the impact could be considered and discussed with the packaging supplier. When comparing the result of the study's carbon footprint with that of OpenLCA, electricity from the OpenLCA revealed the most significant influence, followed by natural gas and raw materials, which are different from the study due to varying sources of emission factors. Improving the chiller system with an automated start-stop system to save electricity in production support can help reduce the carbon footprint during RA95 production. By utilizing the automatic start-shutdown system of the chiller project, power is saved, which can lower the annual release of carbon dioxide equivalent (20,019 kgCO2eq) due to a decrease in electrical energy use of 33,444 kWh, or roughly 114,387 baht, or about $3,300 US dollars. The carbon footprint of the stevia sweetener RA95 compared to the same sweetness level of sucrose presented a carbon footprint 3.55 times less than sucrose and can reduce 71.79% of the carbon footprint. Therefore, stevia RA95 as a substitute for sucrose can mitigate environmental impacts.

5. Acknowledgements

The authors sincerely thank the case study factory for the information source and colleagues for their excellent cooperation and assistance in collecting the necessary information.

Author Contributions: Conceptualization, S.T.; methodology, S.T. and J.D.; formal analysis, J.D.; experimental investigation, S.T. and J.D.; resources, J.D.; data curation, S.T. and J.D.; writing—original draft preparation, S.T. and J.D., writing—review and editing, S.T. and J.D.; Supervision, S.T.

Funding: This study received no external funding.

Conflicts of Interest: The authors declare no conflict of interest.

References

[1] World Health Organization. (2016, April 21). Global report on diabetes. *Technical document*. https://www.who.int/publications/i/item/9789241565257

[2] World Health Organization. (2023, December 23). Malnutrition. *Fact sheet*. https://www.who.int/news-room/fact-sheets/detail/malnutrition

[3] Ministerial regulations: determine the excise tax tariff. (2020, September 16). *Royal Gazette*, 134(95A), 111 (in Thai).

[4] Ministry of Finance. (2021). *Ministerial regulations: determine the excise tax tariff* (No. 16) (in Thai).

[5] Warshaw, H.; Edelman, S.V. Practical Strategies to Help Reduce Added Sugars Consumption to Support Glycemic and Weight Management Goals. *Clinical Diabetes*. **2021**, *39*(1), 45-56.

[6] International Sweeteners Association. (n.d.) *Safety&regulation*. https://www.sweeteners.org/safety-regulation.

[7] Khilar, S.; Singh, A.P.; Biagi, M.; Sharma, A. An Insight into attributes of *Stevia rebaudiana* Bertoni: Recent advanced in extraction techniques, phytochemistry, food applications and headlth benefits. *Journal of Agriculture and Food Research*. **2022**, (10).

[8] FAO and WHO. *Compendium of Food Additive Specifications. Joint FAO/WHO Expert Committee on Food Additives (JECFA), 91st Meeting – Virtual meeting, 1–12 February 2021*. FAO JECFA Monographs No. 26. Rome. https://doi.org/10.4060/cb4737en

[9] CBI Ministry of Foreign Affiars. Entering the European market for stevia. *Market information*. **2022**. https://www.cbi.eu/market-information/natural-food-additives/stevia/market-potential

[10] PureCircle. PureCircle White Paper Series Carbon and Water: Understanding and Reducing Impacts. **2015**. https://purecircle.com/app/uploads/purecircle-carbon-and-water-footprint1.pdf

[11] Suckling, J.; Morse, S.; Murphy, R.; Astley, S.; Halford, J.C.G.; Harrold, J.A.; Le-Bail, A.; Koukouna, E.; Musinovic, H.; Perret, J.; Raben, A.; Roe, M.; Scholten, J.; Scott, C.; Stamatis, C.; Westbroek, C. (2023). Environmental life cycle assessment of production of the high intensity sweetener steviol glycosides from Stevia rebaudiana leaf grown in Europe: The SWEET project. *The International Journal of Life Cycle Assessment*. **2023**, *28*, 221-233.

[12] Rodolfo, S.; Leonor, G. *Life Cycle Assessment comparing Sugar Cane vs. Stevia Rebaudiana Sweetener, for Mexico City Market*. Instituto Tecnológico de Estudios Superiores de Monterrey-CEM; and 2 Instituto de Ingeniería, UNAM, Mexio. **2011**.

[13] Ministry of Natural Resources and Environment. *Thailand's long-term low greenhouse gas emission development strategy (revised version)*. **2022**. https://unfccc.int/sites/default/files/resource/Thailand%20LT-LEDS%20%28Revised%20Version%29_08Nov2022.pdf

[14] Food Institute. *Guideline for evaluating carbon footprint on product for food industry*. Ministry of Industry, Bangkok. **2013**. (in Thai).

[15] Prakash, I.; DuBois, G.E.; King, G.A.; Upreti, M. Rebaudioside A composition and method for purifying rebaudioside A. *United States Patent Application Publication*, US2007/0292582 A1, December 20. **2007**.

ASEAN
Journal of Scientific and Technological Reports
Online ISSN:2773-8752

Research article

Long-Term Seasonal Rainfall Forecasting Using Regression Analysis and Artificial Neural Network with Larg-Scale Circulation Indices

Ketvara Sittichok[1*], Napatsorn Rattanapan[2], and Rittisak Sakulkaew[3]

[1] Research Center for Sustainable Development, Faculty of Engineering at Kamphaengsaen Campus, Kasetsart University, Nakhon Pathom, 73140, Thailand; fengkrs@ku.ac.th
[2] Faculty of Engineering at Kamphaengsaen Campus, Kasetsart University, Nakhon Pathom, 73140, Thailand; napatsorn.rtnp@gmail.com
[3] Faculty of Engineering at Kamphaengsaen Campus, Kasetsart Univers, Nakhon Pathom, 73140, Thailand; rittisak.vpz@gmail.com
* Correspondence: E-mail: fengkrs@ku.ac.th

Citation:
Sittichok, K.; Rattanapan, N.; Sakulkaew, R. Long-term seasonal rainfall forecasting using regression analysis and artificial neural network with large-scale circulation indices. *ASEAN J. Sci. Tech. Report.* **2024**, *27*(3), e252507. https://doi.org/10.55164/ajstr.v27i3.252507.

Article history:
Received: April 2, 2024
Revised: April 26, 2024
Accepted: April 27, 2024
Available online: April 30, 2024

Abstract: Several months in advance, long-term rainfall prediction plays an important role in water management, especially for countries dependent on agriculture. The objective of this study is to forecast the long-term rainfall of eight rain gauge stations in the Phetchaburi River Basin, Thailand, 12–18 months in advance using linear regression (simple linear regression (SLR)/multiple linear regression (MLR)) and non-linear relations (polynomial regression (PR)/artificial neural network (ANN)). Seven atmospheric circulation indices, ONI, DMI, MEI V. 2, NINO4, NINO3.4, NINO3, and NINO1+2, and historical rainfall data were used as predictors in the models. To avoid bias in empirical equation construction, one-year cross-validation was also applied together with a one-month moving window average approach from January to July of the preceding year (12–18 months lead time) to seek suitable periods of predictors for predicting rainfall. The results reveal that the surface temperature indices of the Indian Ocean (DMI) and Pacific Ocean (NINO) are the most essential for forecasting rainfall. MEIV2 and ONI were only positively correlated with local rainfall when non-linear regression was used. Non-linearity models showed better forecasting skills compared to linear regression. The suitability of periods varied according to the statistical models and selected predictors.

Keywords: Rainfall forecasting; Teleconnection; Statistical forecasting; Atmospheric Circulation Indices

1. Introduction

The impacts of climate change on various issues can now be seen in many regions of the globe, especially rainfall variability. Changes in increasing and decreasing rainfall, including alterations in the rainfall pattern, significantly affect people in different areas [1]. Rainfall also plays an important role in the hydrological cycle since streamflow and groundwater affect many activities, such as agriculture, livestock, and the water supply. Changes in pattern and the amount of rainfall lead to challenges in effective water management. Therefore, the ability to predict rainfall is important to government agencies in planning water allocation and management strategies to avoid water scarcity and flood damage.

Several months in advance, long-term rainfall prediction is essential for effective water management, especially in countries heavily dependent on

agricultural activities. In addition, rainfall prediction is crucial for mitigating the effects of extreme flood and drought events. Therefore, an effective rainfall forecasting method should be developed to protect and improve human lives and the environment. As part of a complex atmospheric phenomenon, rainfall varies from one region to another. Several large-scale circulation indices are proven to be significantly related to rainfall [2, 3]. El Nino Southern Oscillation (ENSO), commonly used for rainfall forecasting, significantly influences seasonal precipitation across the globe [4]. [5] investigated the relationship between ENSO signals and rainfall, finding that they showed statistical significance and were suitable for predicting rainfall in Sri Lanka. ENSO and the Indian Ocean Dipole (IOD) were also applied for long-term seasonal rainfall forecasting in Australia in the research work conducted by [6]. Various research works have also proven that El Nino and La Nina signals strongly influence local precipitation [7]. Other climate indices applied to seek a relationship with local rainfall for effective rainfall forecasting consist of the Oceanic Nino Index (ONI), Multivariate ENSO Index (MEI), Dipole Mode Index (DMI), Nino1+2, Nino3, Nino 4, and Nino 3.4. These climatic indices have been widely used in different regions to forecast precipitation [8, 9]. Nino 3.4 also performed well as a statistical method for forecasting rainfall in Bandung, Indonesia [10].

Forecasting models can be divided into dynamical and statistical. Various equations relating to the individual characteristics of the atmosphere, ocean, and land and their relations are employed in dynamical models. These models can generate weekly, monthly, or seasonal rainfall forecasts. Still, long-term forecasting carried out more than several months in advance exhibits high uncertainty since the initial conditions and a temporal framework must be determined. On the other hand, statistical models are widely used because of their capability to provide a longer forecasting lead time [11]. Various statistical techniques for rainfall forecasting have been proposed in large regions all over the world. Linear and non-linear regression are commonly employed where long-term rainfall forecasting is required. Kim C. G. et al. [11] used multiple linear regression (MLR) with lagged correlation to forecast monthly precipitation 12 months in advance with acceptable results over long periods. Six statistical methods: MLR, Multi-layer Perceptron, Pace regression, Radial Basis Function, K-star Algorithm, and Bootstrap Aggregating (bagging) were employed by Gnanasankaran, N., et al. [12] to generate rainfall forecasts, and the results showed MLR to be the most effective method for forecasting rainfall in this area. [13] forecasted rainfall in tropical regions in a seasonal time scale using MR and polynomial regression (PR), revealing that the model provided moderate to good forecasting results for long-term rainfall over 5–12 months.

Regression analysis and the Artificial Neural Network (ANN) have attracted the attention of researchers developing statistical forecasting models with long lead times. The ANN is a machine learning method that can predict non-linear relationships between various large-scale climate indices and rainfall. [14] attempted to predict rainfall for 3–12 months using the ANN in Eastern Australia, revealing that better performance was achieved with more extended historical data and single-month optimization. Monthly rainfall forecasts were also studied by Lee, J. et al. [15] using the ANN with climate indices in Korea. They concluded that the ANN and Monte-Carlo cross-validation could provide acceptable medium-term rainfall forecasting. Works on rainfall forecasting on a monthly and seasonal time scale over the medium and long term can be found in [16-18].

This study uses statistical methods, large-scale climate indices, and suitable periods for rainfall forecasting 12–18 months ahead in the Phetchaburi River Basin, Thailand. Seven circulation indices and the individual historical rain for each station were forced into statistical models with a moving average window of a one-month lag time. Statistical models comprising regression analysis (SLR, MLR, and PR) and the ANN were employed to search for a suitable method at each station. However, the model bias from using the same dataset for constructing empirical equations and the validation process needed to be considered, especially for the statistical model. The one-year cross-validation method was subsequently applied in this research. Three objective functions were used to evaluate the model, namely the correlation coefficient (R), root mean square error (RMSE), and percent bias (PBIAS).

2. Materials and Methods

2.1 Study area

The Phetchaburi River Basin is a 6,255 km^2 watershed in the middle of the Kingdom of Thailand (**Figure 1**). Three major tributaries (the Bangkloy, Maepradone Maeprchan, and Huaypak Rivers) drain into the main river (the Phetchaburi River) and play a vital role in people's livelihoods by providing water for

agriculture, mostly rice cultivation. There are 224 water resource development projects in the river basin, the most important being the Kaeng Krachan and Mae Prachan reservoirs, which deliver water for agricultural, domestic, and other uses. The mean annual precipitation in the watershed is around 1,110 mm, concentrated in the primary rainy season, which spans from May to October, with minimum, average, and maximum around 200, 500, and 900 mm, respectively. The discharge of the basin follows the same pattern as the rainfall and is around 300–600 mcm during the rainy season. The average temperature is around 28 ^{0}C, peaking in April and a low in December. Both floods and droughts tend to occur at regular intervals in the basin. The lower sub-basin was the primary location where around 197 houses were impacted by the severe floods reported in 2016, 2017, and 2018.

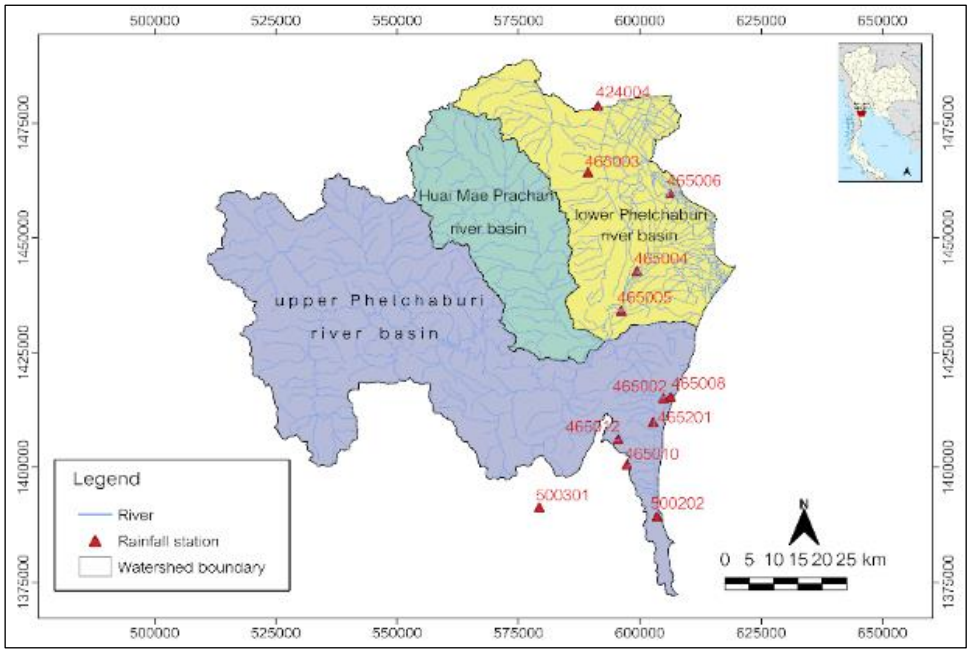

Figure 1. Phetchaburi River Basin and rainfall stations.

2.2 Data

This study uses two types of datasets: large-scale circulation indices and the observed rainfall in the basin. Details of both datasets are presented as follows.

2.2.1 Atmospheric Circulation Index

Seven atmospheric circulation indices, ONI, DMI, MEI V.2, NINO 1+2, NINO 3, NINO 3.4, and NINO 4 over 36 years (1985–2020) are used as predictors. The variability of these predictors is shown in **Figure 2**

- **Oceanic Nino Index (ONI):** The ONI is calculated from the change in sea surface temperature, its value defining an El Nino event as being equal to or higher than +0.5 ^{0}C, whereas an event equal to or less than -0.5 ^{0}C indicates the occurrence of the La Niña phenomenon. The National Oceanic and Atmospheric Administration (NOAA) uses the ONI to predict the occurrence of ENSO and analyze its severity. It is considered weak, moderate, or strong within the plus or minus 0.5–0.9, plus or minus 1.0–1.4, and greater than or equal to 1.5, respectively (The Meteorological Department of the Marine Meteorological Center, 2012). The monthly average ONI from 1985–2020 is presented in **Figure 2**.
- **Dipole Mode Index (DMI):** This is used to measure the condition of the Indian Ocean Dipole (IOD), a phenomenon occurring around the equator in the Indian Ocean. The difference in sea surface temperature (SST) between the west and east coasts of the Indian Ocean is considered. A positive IOD is determined when the west coast SST of the Indian Ocean is noticeably cooler and the east coast SST is noticeably warmer and vice versa. A positive/negative IOD leads to less/more rainfall in Thailand. **Figure 2** shows the average monthly data according to the DMI from 1985–2020 (Marine Meteorological Center Meteorological Department, 2012).

- **Multivariate ENSO Index Version 2 (MEI V.2)**: This combines five large circulation factors: sea level pressure, SST, zonal wind component, meridional wind component, and outgoing longwave radiation. A negative MEI portrays the chance of the La Niña phenomenon occurring. Meanwhile, if the MEI value is positive, it shows the chance of the El Niño phenomenon occurring (National Oceanic and Atmospheric Administration, 2021). **Figure 2** shows the average monthly data for the DMI from 1985–2020.
- **NINO SST Indices:** NINO estimates the SST change in the central Pacific Ocean. The measurement of the change in SST is divided into four levels: NINO 1+2 (0–10S, 90W - 80W), NINO 3 (5N–5S, 150W–90W), NINO 3.4 (5N–5S, 170W–120W), and NINO 4 (5N–5S, 160E–150W) (National Center for Atmospheric Research, 2018) (Figure 2). All these indices measure the severity of La Niña and El Niño phenomena. **Figure 2** presents the average monthly data for NINO 1+2, NINO 3, NINO 3.4, and NINO 4 from 1985–2020.

2.2.2 Rainfall

8 Daily rainfall measurements showing completed data prepared by the Meteorological Department are used as both predictor and predictor for the statistical models in this study. The amount of seasonal rainfall during the rainy season from August to October during the chosen period of the year is used as the predictor. Meanwhile, the forecasted amount of rainfall before the rainy season (12−18 months lead time) is used together with the atmospheric circulation index as the predictor. **Table 1** shows the details and locations of the rainfall measurement stations.

2.3 Statistical methods

2.3.1 Regression analysis

Various statistical methods have been applied in this study. Three regression methods, SLR, MLR, and PR, were used to construct the linear and non-linear equations (Equations 1–3) and obtain the rainfall forecasts. SLR and MLR were used for linear regression analysis with one and more than one predictor, respectively. PR was employed as a non-linear regression method at a power level of 2–5. The moving average method was used to predict rainfall 12–18 months in advance for all predictors. Monthly data on each predictor were collected, starting from January, one year earlier than the forecasted year ($x_{jan(Y-1)}$) to July of the same year ($x_{jul(Y-1)}$), to calculate the moving average and develop a specific period for the predictor. The starting month was also changed from January to July. The example predictor for each lead time is indicated in Table 2. Therefore, 28 periods were tested in each statistical model.

$$y = a + bx \tag{1}$$

$$y = a + b_1x_1 + b_2x_2 + \ldots + b_nx_i \tag{2}$$

$$y = a + b_1x_1 + b_2x_2^2 + b_2x_3^3 + \cdots + b_nx_i^n \tag{3}$$

Model bias should be considered when employing statistical forecasting models to avoid overestimating the results. Since the training data used to construct the relationship between predictors and predictand should not be applied for testing, one-year cross-validation was performed in this study, and the hindcast between 1986 and 2020 was investigated. Each forecasted year was left out of the model construction step, and all rainfall forecasts were then compared to the observations.

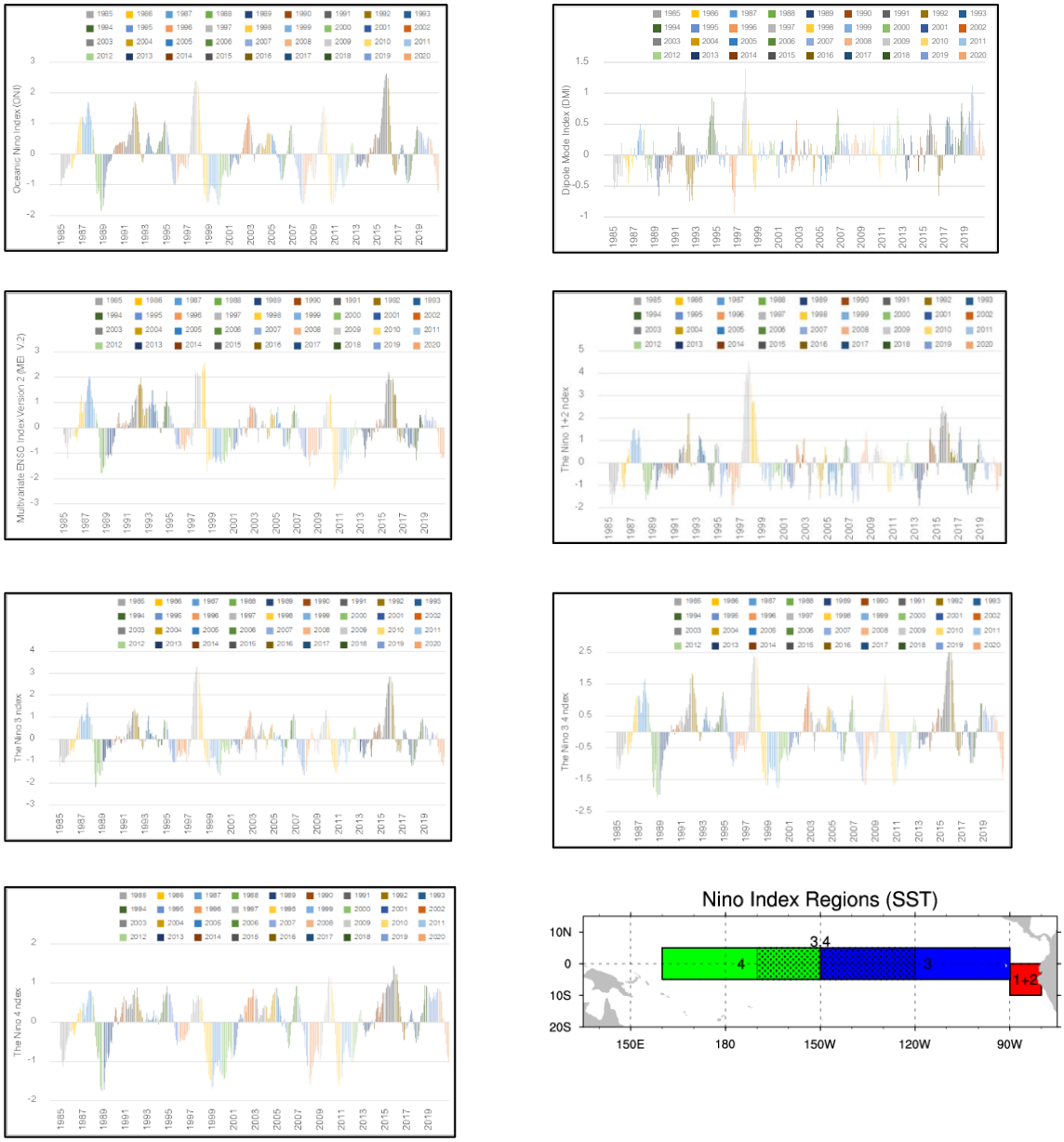

Figure 2. Average monthly data from the atmospheric circulation indices from 1985 to 2020

Table 1. Details of rain gauge stations

Station number	Station name	Latitude/ Longitude
465002	Cha-am Agricultural Office	12°47'59.6"N / 99°58'00.1"E
465004	Ban lad Agricultural Office	13°02'56.7"N /99°56'10.3"E
465008	Cha-am Forest Training Center	12°48'03.6"N/99°58'56.3"E
465010	Forest Development Project	12°41'52.4"N/99°54'09.1"E
465012	Somdet Phrasrinagarindra Park	12°43'24.2"N/99°53'36.0"E
465201	Phetchaburi Weather Station	12°59'58.8"N/100°03'39.7"E
500202	Hua-Hin Weather Station	12°34'42.6"N/99°57'17.1"E
500301	Nong-Pub Weather Station	12°35'21.0"N/99°44'04.3"E

2.3.2 Artificial neural networks

The artificial neural network (ANN) comprises a parallel distributed processor with many processing units inside the structure, initially inspired by the human brain, which contains neurons to process information. Many inputs can be received through this process, and relevant outputs can be generated. The main ANN process comprises a set of connecting links, an activation function, and bias [19]. Liu, Q. et al. [20] outlined the strengths of ANNs for rainfall forecasting. They mentioned that the ANN is a parallel process, effectively working on a large amount of data. It is also a data-driven model that is not subject to modeling restrictions. It can collect many experiences to learn how to predict rainfall patterns with complicated non-linear relationships between datasets. Equations 4–5 present the mathematical expression of ANN comprising neuron pre-activation or input activation (Equation 4) and neuron (output) activation (Equation 5), whereas x_i is the input data i, W the connection weights, and b and g the neuron bias and activation function, respectively.

$$\mathrm{a(x)} = b + \sum_i w_i x_i = b + W^T x \tag{4}$$

$$h(x) = g\big(a(x)\big) = g(b + \textstyle\sum_i w_i x_i) \tag{5}$$

ANN was also applied for rainfall forecasting using a similar process to regression, consisting of the cross-validation step and a one-month moving average. Since high efficiency is essential when dealing with many input variables, all predictors were forced into the models.

Table 2. Examples of predictor calculations with a one-month window

Start month	End month	Forecasted lead time	Predictor calculation
Jan	Jan	18	$x = x_{jan(Y-1)}$
Jan	Feb	17	$x = \frac{(x_{jan(Y-1)} + x_{feb(Y-1)})}{n}$
Jan	…		
Jan	July	12	$x = \frac{(x_{jan(Y-1)} + x_{feb(Y-1)} + x_{\ldots(Y-1)} + x_{jul(Y-1)})}{n}$
Feb	Feb	17	$x = x_{feb(Y-1)}$
Feb	Mar	16	$= \frac{(x_{feb(Y-1)} + x_{mar(Y-1)})}{n}$
Feb	…		
Feb	July	12	$x = \frac{(x_{feb(Y-1)} + x_{mar(Y-1)} + x_{\ldots(Y-1)} + x_{jul(Y-1)})}{n}$
…	…		
July	July	12	$x = x_{jul(Y-1)}$

2.3.3 Model estimation

Three objective functions were used to estimate the forecasted results in this study: the correlation coefficient (R), root mean square error (RMSE), and percentage of bias (PBIAS), as presented in Equations 6–8, respectively. y_i and p_i are the measured and predicted values of the forecasted rainfall in a year i. The r value ranges from -1 to 1, and only positive values should be considered when estimating the results. The RMSE ranges from 0 - ∞ and the predicted rainfall is correlated with the measured rainfall if the RMSE value is close to 0. Finally, a PBIAS of 0 represents the best performance of the model, whereas a higher PBIAS indicates an inferior performance. Unfortunately, no explicit criteria explain the acceptable outcomes of long-lead-time rainfall forecasting. Most research studies reported model estimates with a range of R values from 0.3-0.8, which varied based on factors such as the methodology used, the study area, and the predictors considered, as shown in Hossain, Kim, Singaroodi, et al. [2, 6, 11, 21].

$$R = \frac{\sum_{i=1}^{n}(y_i - \bar{y})(p_i - \bar{p})}{(\sqrt{\sum_{i=1}^{n}(y_i - \bar{y})^2})\,(\sqrt{\sum_{i=1}^{n}(p_i - \bar{p})^2})} \quad (6)$$

$$RMSE = \sqrt{\frac{1}{n} \times \sum (y_i - p_i)^2} \quad (7)$$

$$PBIAS = [\frac{\sum_{i=1}^{n}(p_i - y_i)}{\sum_{i=1}^{n}(y_i)}] \times 100 \quad (8)$$

2.4 Research methodology

Statistical models strongly rely on the quality of predictors and predictors; therefore, all input data require initial verification. All missing values were completed using the inverse distance weight method. The 28 independent variables of each predictor calculated from each period with the moving average method were then prepared and tested to seek the best period for forecasting using SLR. The most effective predictor of a suitable period using the SLR at each station was then reported. However, using a combination of predictors may lead to better forecasts, and MLR was then performed in this step. Only predictors demonstrating a relationship with rainfall at each station in the SLR model were selected for this second process. The number of models at each station depends on the selected predictors. Finally, PLR was employed for a non-linear regression test at 2–5 degrees. Cross-validation and moving averages were still used in these steps. All forecasting results were investigated to ascertain their relationship with observed rainfall using the three objective functions mentioned in the previous section. The effective predictors of high performance for forecasting rainfall in this area were then reported. An overview of this research is presented in **Figure 3**.

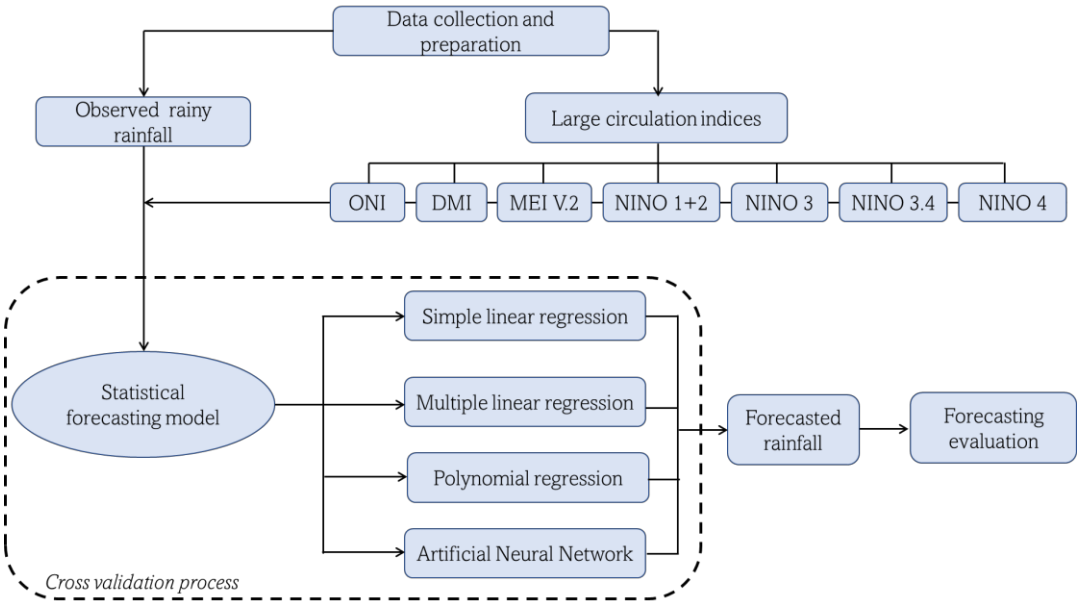

Figure 3. Methodological process

3. Results and Discussion

Teleconnection between each large circulation index and the observed rainfall for 12 stations was analyzed using SLR. Autocorrelation with a moving average window of one-month lag time was applied to search for the best period. A combination of large circulation indices and previous rainfall predictors was then used to MLR, PR, and ANN. Suitable predictors and periods are finally informed.

3.1 Forecasted rainfall using regression analysis

3.1.1 Simple linear regression

The relationship between each predictor and local rainfall was initially examined. Climate indices and historical rainfall were used as predictors in SLR, and rainfall forecasts for the rainy season in the basin for the period from 1985 to 2020 were generated. **Table 3** indicates the predictors showing a positive relationship with observed rainfall. The results revealed that the phenomenon around the Indian Ocean (DMI) effectively predicted most (seven) stations. Historical rainfall at the individual stations and NINO 1+2 were also considered effective in forecasting long lead times in this area. MEI V2 and NINO 3.4 variables could not capture changes in local rainfall, whereas NINO 3 and NINO 4 were suitable to be applied as input variables for SLR only at one station.

Table 3. Effective predictors used in SLR for each station

Station	ONI	DMI	MEI V.2	NINO 1+2	NINO 3	NINO 3.4	NINO 4	Historical rainfall	Range of R
465002		×		×					0.30–0.32
465004		×							0.37
465008		×						×	0.28–0.37
465010		×		×				×	0.21–0.34
465012		×							0.27
465201					×				0.26
500202		×						×	0.33–0.48
500301		×							0.34

Table 4 presents the best period and rainfall predictor using SLR 12–18 months in advance. Forecasting estimations using R, RMSE, and PE to obtain the best period and predictor for each station are shown in the table. All predictors start from January–July of the previous year (Y-1) with a one-month lag time and moving average window forced into the model. The results revealed that DMI was the most influential predictor for seven stations, demonstrating R values between 0.27 and 0.51, while the RMSE and PBIAS ranged from 132.2 to 179.0 mm and 13.9 to 30.4%, respectively. Only one station (465201) showed NINO 3 as the best predictor, giving an R, RMSE, and PBIAS of 0.25, 139.0 mm, and 18.8%, respectively. The most suitable prediction periods for forecasting were different at each station. The best rainfall forecast could be observed at ST-50020 with an R of 0.51, RMSE of 139.4, and PE of 20.0%. **Figure 4** indicates the rainfall in the wet season from 1992–2020. As can be observed from the SLR forecasting results, it could not capture extreme events for all stations. For example, the observed rainfall in 1999 and 2003 at ST-465002 increased to 752 and 835 mm, while forecasted rainfall amounts of 400 and 458 mm were generated using SLR. This was similar to the SLR rainfall forecasts at ST-500202, which could not reach these extreme events with observed/forecasted rainfall amounts of 725/429 and 768/443 mm. However, the models could generate reliable forecasting results during average rainfall circumstances.

3.1.2 Multiple linear regression

All predictors were combined to investigate the model efficiency using MLR. 255 models were tested for each station, each examined to find the most suitable prediction period 12–18 months in advance. These models used a combination of large circulation indices and historical rainfall, providing better rainfall forecasting skills at most stations. **Table 5** presents details of the most efficient predictors and the number of models providing R values higher than 0.3. The most significant combination was ST-465004, with 98 models using all predictors. Like the SLR model, DMI and historical rainfall remained the most effective predictors of long-lead time rainfall. NINO3.4 was the second-best predictor, showing good results when employed with other predictors (four stations). This result differed significantly from the SLR forecasting process. It is also worth considering that some variables presented higher prediction efficiency when used with others, such as NINO 3, NINO 1+2, and NINO 4.

The R, RMSE, and PBIAS ranges for all stations were 0.32–0.57, 132.6–176.9 mm, and 13.7–31.0%, respectively (**Table 4**). The best forecasting results could be found at ST-465004, which has the most significant number of predictors (six). A few extreme events in historical periods were captured by MLR forecasting (**Figure 4**). The number of rainfalls in 1993 at ST-465002 was 776 mm, differing slightly from the MLR forecast of 725 mm. In 1999, the rainy season and MLR forecasting results for ST-465010 were 682 and 706, respectively.

Table 4. Statistical forecasting results for the rainy season

Station	Method	Predictor	Period	R	RMSE (mm)	PBIAS (%)
465002	SLR	DMI	Apr-May	0.41	155.5	25.9
	MLR	DMI, NINO1+2	Apr–May	0.52	147.5	24.4
	PR	ONI	Feb	0.53	153.4	26.5
	ANN	(all)	Apr	0.42	162.9	28.9
465004	SLR	DMI	May	0.35	149.3	25.8
	MLR	ONI, DMI, MEI V.2, NINO 4, NINO 3.4, NINO 3	Apr–May	0.57	137.1	21.6
	PR	MEI V.2	Mar–Apr	0.49	142.6	24.7
	ANN	(all)	April–May	0.52	144.2	22.5
465008	SLR	DMI	Jan–Jun	0.40	145.6	30.4
	MLR	DMI, Rainfall	May–Jun	0.37	150.4	31.0
	PR	DMI	May–Jul	0.41	148.2	32.7
	ANN	(all)	Mar–Jul	0.41	146.9	28.8
465010	SLR	DMI	May–Jul	0.34	142.5	25.6
	MLR	NINO 1+2, Rainfall	Jan–Apr	0.35	142.9	27.1
	PR	MEI V2	Apr–Jul	0.43	148.1	28.3
	ANN	(all)	Jan–Jul	0.50	131.0	24.6
465012	SLR	DMI	May	0.27	179.0	26.8
	MLR	ONI, NINO 3.4	Apr	0.32	176.9	30.6
	PR	NINO 4	Jun	0.37	178.4	29.8
	ANN	(all)	Feb	0.59	150.4	25.8
465201	SLR	NINO 3	Jun	0.25	139.0	18.8
	MLR	DMI, NINO 3.4, NINO 3, Rainfall	Jun	0.38	135.1	19.6
	PR	NINO3	Jul	0.38	136.1	20.8
	ANN	(all)	May–Jul	0.40	131.8	17.8
500202	SLR	DMI	May	0.51	139.4	20.0
	MLR	DMI, NINO 4	May	0.49	142.1	20.5
	PR	DMI	May	0.42	183.8	29.7
	ANN	(all)	May–Jul	0.46	144.9	23.1
500301	SLR	DMI	May	0.37	132.2	13.9
	MLR	ONI, DMI, NINO 4, NINO 3.4, NINO 1+2	Apr–May	0.37	132.6	13.7
	PR	NINO 3.4	Jan–Feb	0.33	136.0	15.6
	ANN	(all)	May	0.58	116.7	13.2

Table 5. Effective predictors used in MLR for each station

Station	Models	ONI	DMI	MEI V.2	NINO 1+2	NINO 3	NINO 3.4	NINO 4	Historical rainfall	R Range
465002	7		x		x	x			x	0.32–0.52
465004	98	x	x	x	x	x	x	x	x	0.30–0.57
465008	7		x						x	0.30–0.37
465010	4		x		x				x	0.30–0.35
465012	3	x	x				x		x	0.30–0.32
465201	5		x			x	x		x	0.30–0.38
500202	4		x					x	x	0.30–0.49
500301	33	x	x		x		x	x	x	0.30–0.37

3.1.3 Polynomial linear regression

Another method used to forecast rainfall in this study is polynomial regression analysis (PR). Degrees of power ranging from 2–5 were applied to examine the association between all predictors and local rainfall in a non-linear regression area. Highly skilled predictors showing a positive correlation between observed and forecasted rainfall are presented in **Table 6**. Observed rainfall was used to predict long-lead time seasonal rainfall at each station, followed by DMI and ONI, respectively. The first two predictors (historical rainfall and DMI) showed similar results to when MLR was used for forecasting. However, the use of ONI and MEI V.2 showed a noticeable difference between these two methods. MEI V.2 only generated corresponding trend patterns for one station using MLR, whereas positive trends could be seen at four stations using PR. A similar situation arose with ONI at three stations using the MLR method, increasing to six stations for PR.

Tabled 6. Effective predictors used in PR for each station

Station	ONI	DMI	MEI V.2	NINO 1+2	NINO 3	NINO 3.4	NINO 4	Historical rainfall	R Range
465002	x	x				x		x	0.32–0.53
465004			x		x	x	x	x	0.32–0.49
465008	x	x						x	0.31–0.41
465010	x	x	x	x	x	x	x	x	0.33–0.43
465012	x	x		x	x		x	x	0.30–0.37
465201		x			x		x	x	0.34–0.38
500202	x	x	x		x	x		x	0.40–0.42
500301	x	x	x			x		x	0.31–0.33

3.2. Forecasted rainfall using ANN

The ANN is another statistical forecasting method employed to identify non-linear relationships between predictors and predictands. In similarity to regression analysis, all eight predictors with different one-month moving average periods were forced into the ANN application. The rainfall forecast for all stations showed R values equal to or higher than 0.40. The largest R value of 0.59 occurred at ST-465012. Minimum/maximum values of RMSE and PBIAS were 116.7 mm and 15.6%/162.9 mm and 32.7%, respectively. Five out of eight stations presented better performance using the ANN compared to all regression methods. The best overall statistical index could be found at ST-500301 with an R, RMSE, and PE of 0.58, 116.7, and 13.2%, respectively. However, when extreme rainfall events were considered, the ANN produced an inferior performance for rainfall forecasting compared to polynomial regression. The ANN showed good prediction ability for seasonal rainfall occurrence in 1992 at ST-465004, with observed and forecasted rainfall being 737 and 791 mm, respectively (**Figure 5**).

Figure 4. Observed and forecasted amounts of rainfall in the rainy season

3.3 Comparison between statistical methods for seasonal rainfall forecasting

Three regression approaches and the ANN were employed to forecast rainfall for eight stations 12–18 months in advance using large-scale circulation indices as predictors. The differences in sea surface temperatures between the west and east coasts of the Indian Ocean influenced rainfall in the study area. Seven SLR and PR stations and eight MLR stations demonstrated the most effective prediction skills, followed by the historical rainfall at each station. Even though only three stations (ST-465008, ST-465010, and ST-500202) presented that historical rainfall was an effective predictor in SLR, it indicated a better performance used with other predictors in MLR and increased with PR. The NINO Index for measuring temperature changes in the Central Pacific Ocean also impacted rainfall in the Phetchaburi Basin. Using SLR, NINO1+2 and NINO3 were effective predictors for two and one station, respectively. However, NINO1+2, when combined with other predictors, exhibited better rainfall forecasting for five stations using MLR and PR, similar to NINO 3. In addition, using NINO3.4 and ONI alone in SLR obtained less reliable forecasting results at all stations than the observations. Significant improvements can be seen with the PR method at five and six stations.

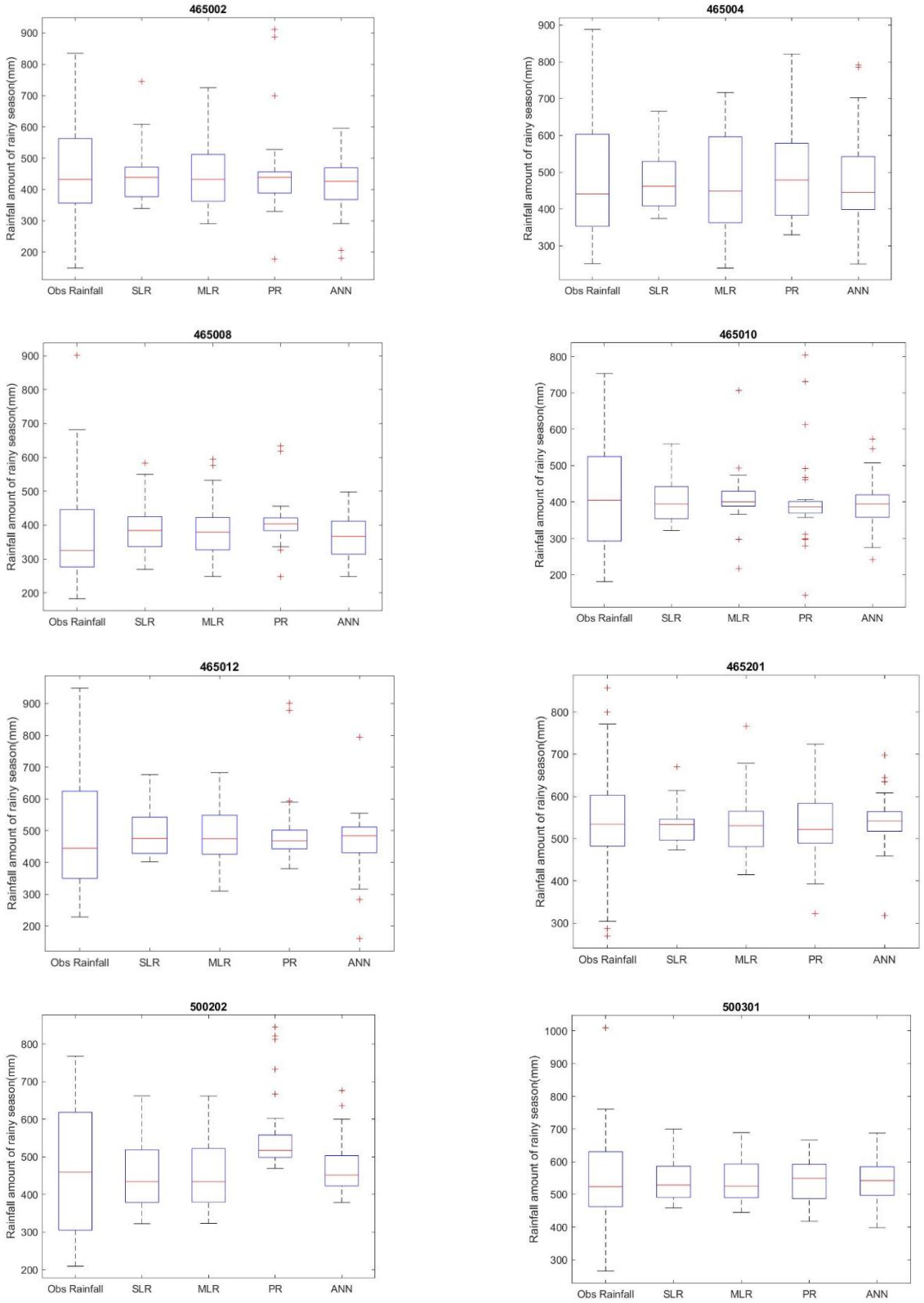

Figure 5. Statistical characteristics of rainfall forecasts and observation

The model performance of all four statistical methods showed that the ANN presented significantly better results than the others at three stations (ST-465010, ST-465012, and ST-500301). The most significant performance of the ANN could be seen at ST-465012 with R and RMSE of 0.59 and 150.4 mm, respectively, whereas the results of the other three models ranged from 0.27–0.37 and 176.9–179.0, respectively. A better regression performance than the ANN was indicated at only two stations, namely ST-465002 and ST-465004. Slightly insignificant differences between MLR and PR were exhibited at ST-465002, with R ranging from 0.52–0.53 and RMSE ranging from 147.5–153.4 mm, whereas rainfall forecasts for ST-465004 using MLR gave outstanding results with the most significant number of predictors (six indices). The statistical characteristics for rainfall during the rainy season at all stations are presented in **Figure 5**. The boxplots show that measures of central tendency between observed and forecasted rainfall in the rainy season at most stations were notably close, except ST-465008 and ST-500202, which showed significant differences with the PR method. Outliers of the forecasted results were also generated when the PR method was applied.

4. Discussion

Rainfall variability in recent years has led to effective water resource management difficulties. The ability to forecast rainfall in the long term at any time step has become vitally important for decision-makers. In this study, various statistical models have been employed along with large-scale climate indices to develop suitable methods for forecasting rainfall in the rainy season with a lead time of 12 to 18 months in advance. Robust evidence supports that DMI is the most effective predictor of rainy season rainfall in the area under study and the selected predictor for all three regressions at most stations. The impact of DMI on the Indochina Peninsula has also been investigated by [22], who revealed that Thailand is one of many countries in their study area to be DMI-sensitive. A linkage between Thailand and DMI was also found in the research work of [23, 24, 25]. Applying DMI with the historical rainfall at each station and the NINO variable significantly increased the ability of linear forecasting models compared to using DMI only. Additionally, the selective predictors applicable to each station could be distinct. Statistical models focus solely on the predictor and predictand data without considering the links between physical attributes. As a result, the selection of predictors for each station or time period may vary due to the high sensitivity of data variance, as seen in [2, 9, 21].

The selection of statistical models in rainfall forecasting is strongly related to large-scale circulation variables. In this study, MEI V.2 and ONI were correlated to local rainfall with non-linearity with PR application. Therefore, large-scale atmospheric indices should be carefully considered for use as predictors in long-lead time rainfall forecasting. The ANN's ability to capture non-linear influences in relationships between large-scale predictors and local rainfall has been widely mentioned in various research works [26,27] and is also presented in this study. However, the forecasting skills exhibited by MLR, PR, and the ANN were insignificantly different at some stations. Therefore, carefully selecting the model and variables to seek the most appropriate methods and predictors is strongly recommended before finalizing the forecasting results. In addition, bias is one of the issues of concern when using statistical models. Statistical models strongly rely on empirical equations to generate forecasting results. Bias can be avoided by removing the dataset used to construct the model before calculation.

5. Conclusion

The objective of this study is to forecast long-term seasonal rainfalls in the Phetchaburi River Basin 12–18 months in advance, using statistical methods with seven atmospheric circulation indices: ONI, DMI, MEI V. 2, NINO4, NINO3.4, NINO3, and NINO1+2, together with historical rainfall. Three statistical methods were used: simple linear regression analysis, multiple linear regression analysis, and polynomial linear regression in combination with k-cross-validation to prevent forecasting bias. In addition, the most suitable period for forecasting was analyzed using the moving window average approach from January to July of the preceding year (12–18 months lead time) to seek the best periods for rainfall forecasting.

In the study area of the Phetchaburi Basin, the Indian Ocean (DMI), and the Pacific Ocean (NINO), sea surface temperature indices were revealed to be the most crucial for forecasting rainfall. The MEI V.2 and ONI, which also reflect climate variability in the Pacific Ocean region, were positively correlated with local rainfall only using non-linear regression. At most stations, non-linear regression indicated better prediction

ability than linear regression. However, the initial selection of suitable variables and statistical models is strongly recommended before undertaking long-lead time rainfall forecasting due to the complexity of the relationship between local rainfall and large-scale circulation indices. In addition, the specific selection of predictor periods for rainfall forecasting should be avoided due to the variability involved, as the results show.

6. Acknowledgements

The authors thank the Thai Meteorological Department for providing valuable data.

Author Contributions: Conceptualization, K.S.; methodology, K.S. and N.R.; validation, N.R. and R.T; formal analysis, K.S., N.R. and R.T.; writing—original draft preparation, N.R. and R.T.; writing—review and editing, K.S.; visualization, K.S.; supervision, K.S.

Funding: This research was partially supported by the Faculty of Engineering at Kamphaengsaen Campus, Kasetsart University.

Conflicts of Interest: The authors declare no conflict of interest.

References

[1] Yumagulova, L.; Vertinsky, I. Climate Change Adaptation and Flood Management in Metro Vancouver Regional Area: Can an Exercise in Herding Cats be successful. *J. Sustain. Dev. Energy Water Environ. Syst.* **2017**, *5*(3), 273-288.

[2] Hossain, L.; Rasel, H. M.; Lmteaz, M. A.; Mekanik, F. Long-Term Seasonal Rainfall Forecasting using Linear and Non-Linear Modelling Approaches: A Case Study for Western Australia. *Meteoro. Atmos. Phys*. **2020**, *132*, 131-141.

[3] Singh, S.; Xiaosheng, Q. Study of Rainfall Variabilities in Southeast Asia using Long-Term Gridded Rainfall and Its Substantiation through Global Climate Indices. *J. Hydrol*. **2020**, *585*, 124320.

[4] Chen, L.; Dool, H.; Becker, E.; Zhang, Q. ENSO Precipitation and Temperature Forecasts in the North American Multimodel Ensemble: Composite Analysis and Validation. *Am. Meteorol. Soc*. **2017**, 1103-1125 .

[5] Adhikari, S.; Liyanaarachchi, S.; Chandimala, J.; Nawarathna, B. K.; Bandara, R.; Yahiya, Z.; Zubair, L. Rainfall Prediction based on the Relationship between Rainfall and El Nino Southern Oscillation (ENSO), *J. Natl. Sci. Found. Sri.* **2010**, *38*(4), 249-255.

[6] Hossain, L.; Rasel, H. M.; Lmteaz, M.A.; Mekanik, F.; Long-Term Seasonal Rainfall Forecasting: Efficiency of Linear Modelling Technique. *Environ. Earth Sci*. **2018**, *77*(280), 1-10.

[7] Jung, J.; Kim, H. S. Predicting Temperature and Precipitation during the Flood Season based on Teleconnection. *Geosci. Lett*. **2022**, *9*(4), 1-37.

[8] De Silva, M.; Hornberge,r G. M. Identifying El Nino-Southern Oscillation Influences of Rainfall with Classification Models: Implications for Water Resource Management of Sri Lanka. *Hydrol. Earth Syst. Sci*. **2019**, *23*, 1905-1929.

[9] Khastagir, A.; Hossain, I.; Anwar, A. H. M. F. Efficacy of Linear Multiple Regression and Artificial Neural Network for Long-Term Rainfall Forecasting in Western Australia. *Meteorol. Atmos. Phys*. **2022**, *134*, 69.

[10] Pontoh, R. S.; Toharudin, T.; Ruchjana, B. N.; Sijabat, N.; Puspita, M. D. Bandung Rainfall Forecast and Its Relationship with Nino 3.4 using Nonlinear Autoregressive Exogenous Neural Network. *Atmosphere*. **2022**, *13*, 302.

[11] Kim, C. G.; Lee, J.; Lee, J. E.; Kim, N. W.; Kim, H. Monthly Precipitation Forecasting in the Han River Basin, South Korea, using Large Scale Teleconnection and Multiple Regression Models. *Water*. **2020**, 12, 1590.

[12] Gnanasankaran, N.; Ramaraj, E. A. Multiple Linear Regression Model to Predict Rainfall using Indian Meteorological Data. *Int. J. Adv. Sci. Technol*. **2020**, *29*(8), 746-758.

[13] Sittichok, K. Seasonal Rainfall Forecasting in Tropical Region Using Statistical Models and Sea Surface Temperatures. *Science and Technology Journal*. **2016**, *5*(3), 33-50.

[14] Abbot, J.; Marohasy, J. Forecasting of Medium-Term Rainfall using Artificial Neural Networks: Case Studies from Eastern Australia. *Engineering and Mathematical Topics in rainfall Intech*. **2017**, https://doi.org/10.5772/intechopen.72619.

[15] Lee, J.; Kim, C. G.; Lee, J. E.; Kim, N. W.; Kim, H. Medium-Term Rainfall Forecasts using Artificial Neural Networks with Monte-Carlo Cross-Validation and Aggregation for the Han River Basin, Korea. *Water*. **2020**, *12*, 1743.
[16] Afshin, S.; Fahmi, H.; Alizadeh, A.; Sedghi, H.; Kaveh, F. Long Term Rainfall Forecasting by Integrated Artificial Neural Network-Fuzzy Logic-Wavelet Model in Karoon Basin. *J. Sci. Res. Essay*. **2011**, *6*, 1200-1208.
[17] Mekanik, F.; Imteaz, M. A.; Gato-Trinidad, S.; Elmahdi, A. Multiple Regression and Artificial Neural Network for Long-Term Rainfall Forecasting using Large Scale Climate Modes. *J. Hydrol*. **2013**, *503*, 11-21.
[18] Acharya, R.; Pal, J., Das, D.; Chaudhuri, S. Long-Range Forecast of Indian Summer Monsoon Rainfall using an Artificial Neural Network Model. *Meteorol. Appl.* **2017**, *26*, 347-361.
[19] Darji, M. P.; Dabhi, V. K.; Prajapati, H. B. Rainfall Forecasting using Neural Network: a Survey. Proceeding of International Conference on Advances in Computer Engineering and Applications (ICACEA), IMS Engineering College, Ghaziabad, India. **2015**.
[20] Liu, Q.; Zou, Y.; Liu, X.; Linge, N. A Survey on Rainfall Forecasting using Artificial Neural Network, Internat. *J. Embed. Syst.* **2019**, *11*(2), 240-249.
[21] Sigaroodi, S.K.; Chen, Q.; Ebrahimi, S.; Nazari, A.; Choobin, B. Long-Term Precipitation forecast for Drought Relief using Atmospheric Circulation Factors: A Study on the Maharloo Basin in Iran. *Hydrol.Earth Syst. Sci*. **2014**, https://doi.org/10.5194/hess-18-1995-2014.
[22] Gao, Q. G.; Sombutmounvong, V.; Xiong, L.; Lee, J. H.; Kim, J. S. Analysis of Drought-Sensitive Areas and Evolution Patterns through Statistical Simulations of the Indian Ocean Diploe mode. *Water*. **2019**, 11, 1302 .
[23] Muangsong, C.; Cai B.; Pumijumnong N.; Hu C.; Cheng H. An Annual Laminated Stalagmite Record of the Changes in Thailand Monsoon Rainfall over the Past 387 Years and Its Relationship to IOD and ENSO. Quat. Int. **2014**, *349*, 91-97.
[24] Ha, K. J.; Seo, Y. W.; Lee, J. Y.; Kripalani, R. H., Yun, K. S., Linkages between the South and East Asians Summer Monsoons: A Review and Revisit. *Clim. Dyn*. **2017**. DOI 10.1007/s00382-017-3773-z.
[25] Hoell, A.; Harrison, L.; Indian Ocean Dipole and Precipitation. *Agroclimatology Fact Sheet Series (Famine Early Warning Systems Network)*. **2021**, *3*, 1-2.
[26] Badr, H. S.; Zaitchik, B. F.; Guikema, S. Application of Statistical Models to the Prediction of Seasonal Rainfall Anomalies over the Sahel. *J. Appl. Meteorol. Climatol.* **2014,** *53*, 614-636.
[27] Golian, S.; Murphy, C.; Wilby, R. L.; Matthews, T.; Donegan, S.; Quinn, D. F.; Harrigan, S. Dynamical – Statistical Seasonal Forecasts of Winter and Summer Precipitation for the Island of Ireland. *Int. J. Climatol.* **2022**, https://doi.org/10.1002/joc.7557.

ASEAN
Journal of Scientific and Technological Reports
Online ISSN:2773-8752

Research article

Heat Retention Properties of Male and Female Salt in Thai Traditional Medicine

Noppadol Hongsuwan[1*], and Kanitta Isarankura[2]

[1] Faculty of Natural Resources, Rajamangala University of Technology Isan Sakon Nakhon Campus, 47160, Thailand; noppadol.ho@rmuti.ac.th
[2] Faculty of Natural Resources, Rajamangala University of Technology Isan Sakon Nakhon Campus, 47160, Thailand; kanthuma22@gmail.com
* Correspondence: noppadol.ho@rmuti.ac.th

Citation:
Hongsuwan, N.; Isarankura, K. Heat retention properties of male and female salt in Thai traditional medicine. *ASEAN J. Sci. Tech. Report.* **2024**, *27*(3), e252413. https://doi.org/10.55164/ajstr.v27i3.252413

Article history:
Received: January 16, 2024
Revised: April 26, 2024
Accepted: April 29, 2024
Available online: April 30, 2024

Abstract: The salt pot compress method in postpartum women involves putting male salt in a clay pot, known as a cooking pot, for heat retention. According to Thai traditional medicine textbooks, there are two types for the nature of salt: male and female. Nonetheless, no report has specified why it needs to be only the male salt and whether it must be sea or rock salt. Some textbooks have not explicitly stated that it must be the male salt. Thus, the objectives of this study are as follows: 1) To determine the heat retention properties of both male and female sea salt; 2) To compare the heat retention properties of both male and female sea salt. The results showed that the size and volume of both types of salt decreased after heating. Meanwhile, higher temperature and a longer time in the pot enhanced the salt's heat. However, the heat retention time of those types of salt decreased with increasing experimental cycles. Moreover, the male sea salt maintained better heat retention properties than the female sea salt. Thai traditional medicine practitioners suggest using male sea salt as an intervention for the salt pot compress method. If male sea salt is not found, large grains of salt will work in its place. The heated salt can also be reused due to no loss in its heat retention properties for up to 2-3 uses. Nevertheless, increasing the time and energy required to heat the salt depends on the number of cycles.

Keywords: Salt; sea salt; male sea salt; female sea salt.

1. Introduction

Thai traditional medicine has played an important role in the lives of Thai people for ages, usually in the forms of medical treatment, pharmaceuticals, and massage, including midwifery. [1-3] The rehabilitation of postpartum women, or "Yoo-Fire," comprises several steps. [4-5] One of them is the salt pot compress method [6], which uses the heat from the salt pot to help improve the blood and lymphatic circulation system. [7-11]

Textbooks and research studies on the salt pot compress method in postpartum women state that male salt can retain heat better. [12-13] According to Thai traditional medicine textbooks, there are two types of natural salt: male and female. Nonetheless, no reports identify why it has to be only the male salt. Besides, some texts do not specify the use of male salt. They only state that salt or salt grains are used for heat retention in the clay pot. For these reasons, the researcher is interested in building further knowledge on the salt pot compress method, including salt types and heat retention properties. Moreover, the heat retention properties of the male and female salts in this study are also compared.

2. Materials and Methods

Part 1: Measure the size and weight of the clay pot

Prepare the clay pots with a similar size of about 7 centimeters in diameter according to the standard size for the salt pot compress method. Measure the diameter at the bottom and the mouth (both inside and outside), including around the neck, the bottom of the widest part, the depth, the thickness, and the weight of the pot.

Part 2: Measure the size (volume) and weight of salt grains

Randomly select 10 male and female sea salt grains in the pot. Measure the size of salt grains using a Digital Vernier Caliper for each salt grain's width, length, and thickness. Then, weigh and calculate the mean value.

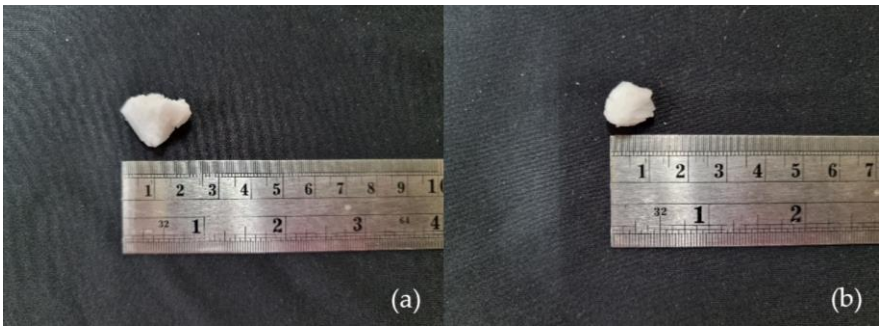

Figure 1. (a) Male sea salt, (b) Female sea salt

Part 3: The Experimental Process

1. Put the male and female salt into 3 clay pots for each type of salt, with the salt density in each pot of 0.8 g/cm^3. Then, calculate by using the formula D=m/v, where D = the density of salt, m = the mass of salt (grams), and v = the volume of the clay pot (cubic cm). The volume of the clay pot is obtained by putting water into the pot and pouring the water into a measuring cylinder to find the volume.

Figure 2. Preparation salt in pot (Mor-ta-non)

2. Set the timer to 5 minutes after setting the electric stove to 300 degrees Celsius. Then, put the pot of salt on the electric stove. Observe the timer until the salt is heated. Record the temperature and the length of time that the salt took to be heated on the form.

Figure 3. Heating the salt pot

3. Lift the pot out to place onto the Spider lily leaves with the roughly pounded fresh herbs at the bottom. The fresh herbs include. *Curcuma xanthorrhiza* Roxb, *Curcuma aromatica* Salisb, *Curcuma aeruginosa* Roxb, *Zingiber cassumunar* Roxb, and *Cinnamomum camphora* (L.) J. Presl, Equal [14-17], wrapped in the calico cloth for the prepared salt pot compress method. Then, record the salt temperature in the clay pot by wrapping it with the calico cloth until it has dropped to room temperature (34 degrees Celsius). Next, reheat the salt pot. Repeat this step for 5 rounds and record the results on the form.

Figure 4. (a) Herbal preparations, (b) Wrapping the Pot, (c) Measuring the temperature inside and outside the pot

Please refer to Memorandum No. RMUTI.5106030.HEC/141. Date: November 8, 2023
Subject: Notification of research project outcomes for consideration. According to the paper, the Human Research Ethics Subcommittee of the Rajamangala University of Technology, Isan Sakon Nakhon Campus, has reviewed the above research project documents. It was determined that "this research does not qualify as human research." As a result, it is not considered human subjects research and does not require ethical review by the Human Research Ethics Subcommittee.

3. Results and Discussion

The heat-retaining properties of male and female sea salt

Part 1: Information about the pots (Mor-ta-non)

Table 1. Size and weight information for male sea salt pots (Mor-ta-non)

Data of pots (Mor-ta-non)	Pot 1	Pot 2	Pot 3	average
Pot depth (cm)	8.50	8.50	8.50	8.50 ± 0.00
External pot mouth diameter (cm)	10.20	10.70	10.60	10.50 ± 0.26
Internal pot mouth diameter (cm)	7.00	7.50	7.40	7.30 ± 0.26
Around the neck of the pot (cm)	29.00	31.70	29.20	29.97 ± 1.50
Around the bottom of the pot (cm)	37.20	37.80	37.30	37.43 ± 0.32
Pot bottom diameter (cm)	11.70	11.90	11.80	11.80 ± 0.10
The thickness of the pot (cm)	0.70	0.70	0.70	0.70 ± 0.00
Pot weight (g)	350.00	350.00	340.00	346.67 ± 5.77

The pots of male sea salt had the sizes above for depth, outer and inner diameter of pot mouth, around the pot neck and bottom, and thickness. The mean values were 8.50 ± 0.00, 10.50 ± 0.26, 7.30 ± 0.26, 29.97 ± 1.50, 37.43 ± 0.32, 11.80 ± 0.10, and 0.70 ± 0.00 centimeters, respectively. The mean weight of the clay pots was 346.67 ± 5.77 grams (Table 1).

Table 2. Size and Weight of Female Sea Salt Pots (Mor-ta-non)

Data of pots (Mor-ta-non)	Pot 1	Pot 2	Pot 3	average
Pot depth (cm)	8.70	8.50	8.50	8.57 ± 0.12
External pot mouth diameter (cm)	10.20	10.20	10.70	10.37 ± 0.29
Internal pot mouth diameter (cm)	7.20	7.00	7.50	7.23 ± 0.25
Around the neck of the pot (cm)	29.50	29.00	31.70	30.07 ± 1.44
Around the bottom of the pot (cm)	37.00	37.20	37.80	37.33 ± 0.42
Pot bottom diameter (cm)	11.70	11.70	11.90	11.77 ± 0.12
Thickness of the pot (cm)	0.70	0.70	0.70	0.70 ± 0.00
Pot weight (g)	350.00	350.00	350.00	350.0 ± 0.00

The pots of female sea salt had the sizes mentioned above for depth, the outer and inner diameter of the pot mouth, around the pot neck and bottom, the diameter of the pot bottom, and thickness. The mean values were 8.57 ± 0.12, 10.37 ± 0.29, 7.23 ± 0.25, 30.07 ± 1.44, 37.33 ± 0.42, 11.77 ± 0.12, and 0.70 ± 0.00 centimeters, respectively. The mean weight of the clay pot was 350.0 ± 0.00 grams (Table 2).

Part 2: Data of male and female sea salt grains before and after the experiment

Before and after the experiment on heat retention of male and female sea salt, this study randomly selected the salt from the experimental pots to measure size and weight as follows:

Table 3. Volume and weight of male sea salt before and after the experiment.

	Pot 1	Pot 2	Pot 3	average
summary volume of salt grains				
Before the experiment (cm^3)	2.47	2.51	2.50	2.49 ± 0.02[a]
After the experiment (cm^3)	2.18	2.24	2.16	2.19 ± 0.04[b]
Weight of salt grains				
Before the experiment (g)	1.49	1.49	1.44	1.47 ± 0.03[a]
After the experiment (g)	1.23	1.17	1.25	1.22 ± 0.04[b]

Annotation: Different letters of a and b in each row represent a statistically significant difference at the 95% confidence interval.

The volume (width x length x thickness) and weight of male sea salt grains before and after the experiment were different ($p<0.05$). The mean volumes before and after the experiment were 2.49 ± 0.02 and 2.19 ± 0.04 cubic cm. The mean weights were 1.47 ± 0.03 and 1.22 ± 0.04 grams, respectively.

Therefore, the mean volume and weight of male sea salt after the experiment were statistically decreased compared to before the experiment (Table 3).

Table 4. Volume and weight of female sea salt before and after the experiment.

	Pot 1	Pot 2	Pot 3	average
summary volume of salt grains				
Before the experiment (cm^3)	1.45	1.12	1.26	1.28 ± 0.17[a]
After the experiment (cm^3)	0.86	0.89	1.08	0.94 ± 0.12[a]
Weight of salt grains				
Before the experiment (g)	0.84	0.93	0.79	0.85 ± 0.07[a]
After the experiment (g)	0.80	0.74	0.74	0.76 ± 0.03[a]

The volume (width x length x thickness) and weight of female sea salt grains before and after the experiment were not different ($p<0.05$). The mean volume before and after the experiment was 1.28 ± 0.17 and 0.94 ± 0.12 cubic cm. The mean weights were 0.85 ± 0.07 and 0.76 ± 0.03 grams, respectively.

Therefore, the mean volume and weight of female sea salt before and after the experiment were not different ($p\geq0.05$) (Table 4).

Part 3: Results of the heat retention experiment of male and female sea salt

Table 5. Time and temperature of heating and time of heat retention of male sea salt

	Pot 1	Pot 2	Pot 3	average
Salt ripening time				
Round 1 (minutes)	12.18	12.33	13.00	12.50 ± 0.44^{a}
Round 2 (minutes)	15.05	16.32	16.55	15.97 ± 0.81^{b}
Round 3 (minutes)	19.12	17.14	17.55	17.93 ± 1.05^{c}
Round 4 (minutes)	19.45	19.13	19.07	19.22 ± 0.20^{d}
Round 5 (minutes)	22.30	22.08	22.17	22.18 ± 0.11^{e}
Salt ripening Temperature				
Round 1 (°C)	62.40	63.90	64.20	63.50 ± 0.96^{a}
Round 2 (°C)	83.90	83.10	82.60	83.20 ± 0.66^{b}
Round 3 (°C)	88.80	91.50	88.10	89.47 ± 1.80^{c}
Round 4 (°C)	95.10	99.40	91.60	95.37 ± 3.91^{d}
Round 5 (°C)	102.60	103.50	105.70	103.93 ± 1.59^{e}
Heat retention time				
Round 1 (minutes)	175	180	170	175.00 ± 5.00^{a}
Round 2 (minutes)	170	175	165	170.00 ± 5.00^{ab}
Round 3 (minutes)	160	170	160	163.33 ± 5.77^{bc}
Round 4 (minutes)	160	165	155	160.00 ± 5.00^{bc}
Round 5 (minutes)	155	165	150	156.67 ± 7.64^{c}

Annotation: 1. Different letters of a, b, c, d, and e in each row of the experimental results represent a statistically significant difference at the 95% confidence interval.

2. Heat retention time from the temperature in heating the salt until the temperature has decreased to room temperature during the experiment (34 degrees Celsius)

The mean times for heating the male sea salt in rounds 1-5 were 12.50 ± 0.44, 15.97 ± 0.81, 17.93 ± 1.05, 19.22 ± 0.20, and 22.18 ± 0.11 minutes, respectively. The mean temperatures for heating the male sea salt in rounds 1 -5 were 63.50 ± 0.96, 83.20 ± 0.66, 89.47 ± 1.80, 95.37 ± 3.91, and 103.93 ± 1.59 degrees Celsius, respectively (Table 5). The times and temperatures at which male sea salt was heated in each cycle differed ($p<0.05$). Meanwhile, the heat retention time of male sea salt from the temperature in heating the salt until the room temperature during the experiment (34 degrees Celsius) in rounds 1-2 was not different ($p\geq0.05$). The difference in heat retention time of male sea salt was observed from round 3 onwards when compared to round 1, with the mean heat retention times in rounds 1-5 being 175.00 ± 5.00, 170.00 ± 5.00, 163.33 ± 5.77, 160.00 ± 5.00, and 156.67 ± 7.64 minutes, respectively (Table 5).

Thus, the male sea salt was heated in each round. Also, more time was required according to the number of rounds. In contrast, the heat retention time of male sea salt was less when the number of rounds for heating the salt increased.

Table 6. Time and temperature of heating and time of heat retention of female sea salt

	Pot 1	Pot 2	Pot 3	average
Salt ripening time				
Round 1 (minutes)	12.17	12.07	10.57	11.60 ± 0.90^{a}
Round 2 (minutes)	15.38	14.44	12.55	14.12 ± 1.44^{ab}
Round 3 (minutes)	18.37	18.57	18.39	18.44 ± 0.11^{b}
Round 4 (minutes)	20.15	28.36	29.43	25.98 ± 5.08^{c}
Round 5 (minutes)	29.37	29.25	29.44	29.35 ± 0.10^{c}
Salt ripening Temperature				
Round 1 **(℃)**	71.20	74.00	69.30	71.50 ± 2.36^{a}
Round 2 **(℃)**	70.30	69.60	74.00	71.30 ± 2.36^{a}
Round 3 **(℃)**	79.80	91.80	80.20	83.93 ± 6.82^{ab}
Round 4 **(℃)**	88.10	119.00	93.70	100.27 ± 16.46^{bc}
Round 5 **(℃)**	123.00	106.10	109.50	112.87 ± 8.94^{c}
Heat retention time				
Round 1 (minutes)	160	165	160	161.67 ± 2.89^{a}
Round 2 (minutes)	145	160	150	151.67 ± 7.64^{a}
Round 3 (minutes)	130	140	130	133.33 ± 5.77^{b}
Round 4 (minutes)	130	135	130	131.67 ± 2.89^{b}
Round 5 (minutes)	125	110	110	115.00 ± 8.66^{c}

Annotation: 1. Different letters of a, b, c, d, and e in each row of the experimental results represent a statistically significant difference at the 95% confidence interval.

2. Heat retention time from the heated temperature of the salt until room temperature during the experiment (34 degrees Celsius)

The time and temperature for heating the salt, including the time of heat retention of female sea salt in rounds 1-2, were not different ($p \geq 0.05$). However, the differences in the time and temperature in heating the female sea salt began from round 3 onwards compared to round 1 ($p < 0.05$). The mean times in heating the female sea salt in rounds 1-5 were 11.60 ± 0.90, 14.12 ± 1.44, 18.44 ± 0.11, 25.98 ± 5.08, and 29.35 ± 0.10 minutes, respectively. The mean temperatures in heating the female sea salt in rounds 1-5 were 71.50 ± 2.36, 71.30 ± 2.36, 83.93 ± 6.82, 100.27 ± 16.46, and 112.87 ± 8.94 degrees Celsius, respectively. The mean times for heat retention were 161.67 ± 2.89, 151.67 ± 7.64, 133.33 ± 5.77, 131.67 ± 2.89, and 115.00 ± 8.66 minutes, respectively (Table 6).

Therefore, the female sea salt was heated in each round. There was a tendency to require more time according to the number of rounds. Heat retention time was likely to decrease as the number of rounds increased.

Table 7. Comparison of time/temperature for salt heating and heat retention of male and female sea salt

Round	Male sea salt			Female sea salt		
	Salt ripening time (minutes)	**Salt ripening Temperature (℃)**	**Heat retention time (minutes)**	**Salt ripening time (minutes)**	**Salt ripening Temperature (℃)**	**Heat retention time (minutes)**
1	12.50 ± 0.44^{Aa}	62.80 ± 1.80^{Aa}	175.00 ± 5.00^{Aa}	11.60 ± 0.90^{Aa}	71.50 ± 2.36^{Ab}	161.67 ± 2.89^{Ab}
2	15.97 ± 0.81^{Ba}	83.20 ± 0.66^{Ba}	170.00 ± 5.00^{ABa}	$14.12 \pm 1.44A^{Ba}$	71.30 ± 2.36^{Ab}	151.67 ± 7.64^{Ad}
3	17.92 ± 1.05^{Ca}	89.47 ± 1.80^{Ca}	163.33 ± 5.77^{BCa}	18.44 ± 0.11^{Ba}	83.93 ± 6.82^{ABa}	133.33 ± 5.77^{Bb}
4	19.22 ± 0.20^{Da}	95.37 ± 3.91^{Da}	160.00 ± 5.00^{BCa}	25.98 ± 5.08^{Cb}	97.90 ± 11.44^{BCa}	131.67 ± 2.89^{Bb}
5	22.18 ± 0.11^{Ea}	103.93 ± 1.59^{Ea}	156.67 ± 7.64^{Ca}	29.35 ± 0.10^{Cb}	112.87 ± 8.94^{Ca}	115.00 ± 8.66^{Cb}

Annotation: 1. Different letters of A, B, C, D, and E in each column represent a statistically significant difference at the 95% confidence interval.

2. Different letters of a and b in each row represent a statistically significant difference at the 95% confidence interval.

The study results for male sea salt's time and temperature heating in rounds 1-5 were different ($p<0.05$). The time for heat retention of male sea salt began to differ ($p<0.05$) from round 3 onwards when compared to round 1.

For female sea salt, the time and temperature for heating and the time of heat retention for female sea salt in rounds 1-2 were not different ($p\geq0.05$). The difference in the time and temperature for heating female sea salt began from round 3 onwards compared to round 1 ($p<0.05$).

When comparing the results of times and temperatures for heating male and female sea salt in rounds 1-5, there was no difference in the time for heating male and female sea salt in rounds 1-3 ($p\geq0.05$). In contrast, the temperature for heating male and female sea salt differed ($p<0.05$) in rounds 1-2. The heat retention time of male and female sea salt differed ($p<0.05$) in every experiment round. Moreover, the size of male sea salt grains was more significant than that of female sea salt grains. When both types of salt were heated following the salt pot compress method in Thai traditional medicine, the size of salt grains became smaller. Therefore, the heat retention time of salt could decrease with the number of cycles used to heat the salt.

4. Conclusions

Larger matter has a higher heat storage capacity than smaller stuff. This experiment involves transporting heat, heat energy, and salt grains by heat conduction, which transfers heat through a solid material-areas of high temperatures: Electric stove in a low-temperature environment. The solid medium consists of salt granules. The size of the salt grains before receiving heat and heat energy transfer in round 1 is larger than the size of the salt grains that received heat transfer and heat energy in round 1. 2-5, which is consistent with the experimental results that the temperature in the salt can be maintained better in the first cycle of transferring heat and heat energy to the salt granules. According to rumors, as the number of cycles increases, the size of the salt grains reduces due to heat energy transfer [18]. The heat absorption theory predicts that the size of the salt granules reduces. An endothermic process absorbs energy to break bonds. Salt crystals form a crystal lattice held together by ionic connections. It takes energy to break bonds. If it is particularly huge, breaking the bonds will need significant energy. As a result, the salt particles vibrate faster when providing thermal energy to a salt pot. The heat energy destroys the bonds that hold the salt granules together. This makes huge salt granules smaller [19]. And, while the size of the salt grains decreases with the number of cycles, the density of the salt grains inside the pot grows. According to Pascal's hypothesis, the time and temperature required to cook the salt increase with each cycle. (Pascal's Principle) states that when pressure changes in one part, the change is transferred to all other parts with the same value. The time required for energy transfer varies according to the pressure change.[20]

In conclusion, the ripening periods and temperatures of male and female sea salt were comparable in each study. However, the heat retention times of male and female sea salts retained heat for a longer period than that of female sea salts in all rounds of the experiment. As a result, male sea salt outperforms female sea salt in heat retention.

5. Acknowledgements

The Science Research and Innovation Fund is supporting this research endeavor. Contract Number: FF66-P3-003.

Author Contributions: N.H. K.I.

Funding: The Science Research and Innovation Fund is supporting this research endeavor. Contract Number: FF66-P3-003.

Conflicts of Interest:

References

[1] Office of Academic Affairs, *Department of Thai Traditional and Alternative Medicine, Ministry of Public Health. Thai public health report in Thai traditional medicine, folk medicine and alternative medicine 1*. Bangkok: The Veterans Welfare Organization's printing house activities office, **2010**. pp. 451.

[2] Saowaros, C. Carrying on Thai wisdom for the new generation: Integrating Thai wisdom in caring for maternal health after giving birth. *Journal of the Center for Clinical Medicine Education Phrapokklao Hospital*, **2019**, *36*(3), 251-257.

[3] Bunyopasadham, H. Synthesis of research on local wisdom regarding women's health care. *Srinakharinwirot Research and Development Journal*, **2019**, *11*(21), 161-73.

[4] Department of Thai Traditional and Alternative Medicine. *Guidelines for providing integrated Thai traditional medicine services in primary health care units*. Bangkok: Ministry of Public Health, **2019**. pp.11.

[5] World Health Organization (WHO).*Recommendations on intrapartum care for a positive childbirth experience*. Geneva: World Health Organization, **2018**.

[6] Chompoonut, S.; Inkaew, W. Integration of academic services with teaching and learning of selected nursing practice subjects in the field of community health nursing. *Police Nursing Journal*, **2017**, *9*(1), 24-36.

[7] Kaewsarn, P.; Moyle, W.; Creedy, D. Traditional postpartum practices among Thai women. *J Adv Nurs*, **2003**, *41*(4), 358-66.

[8] Taoprasert, Y. Rajabhat Science Community Network Local wisdom in Chiang Rai. Folk Medicine Research and Development Center Chiang Rai Rajabhat Institute. **2003**.

[9] Pumtong, S.; Wirasathien, L.; Sitthithaworn, W.; Rungmekarat, A.; Paeratakul, O. Postpartum care through traditional Thai medicine in Amnat Charoen province. *Journal of Health Systems Research*, **2010**, 4(2), 81-95.

[10] Jamjan, L.; Khantarakwong, S.; Hongthong, S.; Jampates, N. Thai traditional medicine for postnatal motherin the community of Central region. *Journal of The Royal Thai Army Nurses*, **2014**, *15*(2), 195-202.

[11] Pumtong, S.; Wirasathien, L.; Sitthithaworn, W.; Rungmekarat, A.; Paeratakul, O. Postpartum care through traditional Thai medicine in Amnat Charoen province. *Journal of Health Systems Research*, **2010**, *4*(2), 281-95.

[12] Namanee, A. The enhancement of the mother and children's health care: the perspectives from the Thai medication and the modern medication. *Thammasat Medical Journal*, **2013**, *13*(1), 79-88.

[13] Laokhomprutthachan, J.; Laokhomprutthachan, T.;, Kanchanasit, W.; Wongwai, N.; Local wisdom for health: integrated into learning management In caring for mothers after giving birth. *Regional Health Promotion Center 9 Journal*, **2023**, *17*(2), 618-630.

[14] Navadach, N.; Inman, W.; Singkhamphong, N.; Boonrasri, S.; Noipha, K. Postnatal mothers' satisfaction toward postpartum care project using Thai traditional medicine of Ranod Hospital. *Songkhla province. RMUTSV Research Journal*, **2020**, *12*(3), 483-94.

[15] Talib, KA.; Khalid, Mohamed, N. Midwives and herbal remedies: The sustainable ethoscience. *Kajian Malaysia*, **2020**, *38*(1), 109-131.

[16] Ward EA, Iron Cloud-Two Dogs E, Gier EE, Littlefield L, Tandon SD. Cultural adaptation ofthe mothers and babies intervention for use in Tribal communities. *Front Psychiatry*, **2022**, *17*(13), 807432.

[17] Srithupthai, K.; Moonlao, S.; Satue, K. Effect of salt over pot (tub mor gleur) on reducing hip and waist circumference and body weight in postpartum women. *Isan Journal of Pharmaceutical Sciences*, **2015**, *11*(Suppl 1), 203-205.

[18] Ngamrungroj. T.; Wasandilok, A. Study of flow through the surface of dimples and ridges. Numbers. Bachelor of Engineering Thesis Department of Mechanical Engineering Department of Mechanical Engineering Faculty of Cast Engineering Naresuan University. **2006**.

[19] Suwannapruek, R. *General chemistry volume 1*.3. Bangkok: Wittayapat, **2016**. pp. 584.

[20] Chuaybamrung, J. *Pascal's principle (Pascal'principle) fluid mechanics (Fluid mechanic) General physics 1, mechanics section, for industrial technology students*. Faculty of Industrial Science and Technology Prince of Songkla University Surat Thani Campus. **2008**, pp. 214-215.

ASEAN
Journal of Scientific and Technological Reports
Online ISSN:2773-8752

Research article

Continuous Monitoring of Radon Contamination Levels in Lower Nam Phong River, Khon Kaen Province, Thailand

Vitsanusat Atyotha[1*], Khanuengnij Prakhammin[2], Benjawan Rattanawong[3], Rachan Udomkham[4], and Junthara Somtua[5]

[1] Faculty of Engineering, Rajamangala University of Technology Isan, Khon Kaen, 40000, Thailand; vitsanusat.at@rmuti.ac.th
[2] Faculty of Engineering, Rajamangala University of Technology Isan, Khon Kaen, 40000, Thailand; khanuengnij.pr@rmuti.ac.th
[3] Faculty of Engineering, Rajamangala University of Technology Isan, Khon Kaen, 40000, Thailand; benjawan.ca@rmuti.ac.th
[4] Department of Industrial Technology Program in Automotive Parts Manufacturing Technology, Rajamangala University of Technology Isan, Khon Kaen, 40000, Thailand; Rachan.ud@rmuti.ac.th
[5] Health Promotion Center Region 7 Khonkaen, Department of Health, Khon Kaen, 40000, Thailand; Junthara_2526@hotmail.com
* Correspondence: vitsanusat.at@rmuti.ac.th

Citation:
Atyotha, V.; Prakhammin, K., Rattanawong, B., Udomkham, R., Somtua, J. Continuous Monitoring of radon contamination levels in lower Nam Phong River, Khon Kaen Province, Thailand. *ASEAN J. Sci. Tech. Report.* **2024**, *27*(3), e252757. https://doi.org/10.55164/ajstr.v27i3.252757

Article history:
Received: February 10, 2024
Revised: April 30, 2024
Accepted: May 1, 2024
Available online: May 1, 2024

Abstract: In this research, radon concentrations in surface water samples were measured at 8 stations and along 8 boat survey routes in the lower Nam Phong River, Khon Kaen Province, Thailand, using the RAD 7 Radon Detector and RAD AQUA accessories. The results of radon concentration at the 8 stations along the Nam Phong River ranged from 0.16 to 4.87 Bq/L, with an average of 1.17 Bq/L. For the boat survey routes along the Nam Phong River, radon concentrations ranged from 0.04247 to 0.12342 Bq/L, with an average of 0.07422 Bq/L. These results were lower than the maximum contaminant level of radon in water (MCL), 11.1 Bq/L, as the United States Environmental Protection Agency recommended. Finally, the results were used to assess various health risks to people in this research area, contributing to determining the public safety of radon exposure in the lower Nam Phong River.

Keywords: Radon; RAD 7; The lower Nam Phong River Basin

1. Introduction

Radon (^{222}Rn) is a radioactive gas with a half-life of 3.82 days, colorless, odorless, and tasteless. It is a noble gas not combined with any element or another like a compound, which is one of the natural atomic radiation generated from the decay of Radium (^{226}Ra) located in the decay chain of Uranium (^{238}U) is the only metal source which is found in a gaseous state, there are almost in all places, at all times, it dissolves in water. It can readily diffuse with gases and water vapor. It is impossible to find pure surface water in the natural environment [1, 2]. One of the major pollutants that can constantly contaminate surface water is radon. Radon radiation pollutes surface water and affects human health through the use of surface water for drinking and daily use. For example, showering, washing dishes, and watering plants are other dangers of radon exposure, and radon inhalation spreads from surface water [3]. Although the amount of radon contamination in surface waters is relatively small compared to the areas where radon is dissolved. However, if radon-contaminated surface water is used regularly, it can accumulate sufficient amounts of radon that can harm the body [4, 5]. The health effects from radon-contaminated surface waters are essential factors that can cause cancer in the body: 1. Lung cancer from inhalation and 2. Stomach cancer from ingestion. One

of the significant factors that need to be determined regarding water usability is the radon concentration level and annual effective dose due to the ingestion of radon and the inhalation of radon released from surface water. [6, 7]. For this reason, radon concentrations in surface water should be measured, and health risks in different forms should be assessed to verify the safety of drinking and household water following the established standards of various agencies. The Nam Phong River is one of the most important rivers in the Northeast. It originates from Phu Kradueng and the Pa Sak River and Chi River flows through Phu Kradueng, Loei Province, Ubon Rat District, Nam Phong District, and Mueang District, Khon Kae Province before flowing into the Chi River at Kuichaug village, Kosum Phisai District, Maha Sarakham Province, then flows into the Mun River and the Mekong River respectively, all these are the lower Lam Nam Phong [8]. Geologic characteristics of the lower Nam Phong River in Khon Kaen Province is an area in the Khorat Plateau. It is in the Maha Sarakham Formation and is considered a rock salt category. From the radioactive measurement of salt, K−Ar is about 93 million years old and consists of terrace deposits and Alluvial deposits covering most areas. These two sediments consist of gravel, sand, silt, and laterite [9]. Most areas of the lower Nam Phong River together with large amounts of gravel, sand, and silt. These gravel, sand, and silt contain Uranium 238 and Radium 226, which can decay to radon. While decaying to produce radon, the lower Nam Phong River washes away radon from the gravel, sand, and silt. Although the amount of radon contamination in water bodies is small, a large amount of accumulation in the body from regular water use will result in a health hazard [4, 10]. Most of the tap water used by people in Khon Kaen in daily life is produced from the raw water pumping station of the lower Nam Phong River [10]. In the past ten years, Khon Kaen Province has experienced rapid economic expansion, expanding communities, houses, agricultural buildings, and various industrial factories, resulting in increased demand for water [11, 12]. At the same time, the Lower Nam Phong River has become the support area of waste all the time, which is causing it to exceed the ability to purify itself naturally, affecting water quality and utilization of water in the Lower Nam Phong River, which will affect damage the environment and quality of life [10, 13, 14]. In a study published in 2013 on cancer-causing factors due to radium-226 concentration in the Nam Phong River, Khon Kaen Province, it was found that the river was contaminated with radium-226 (the radium-226 is radon's parent nuclide), ranged from 0 to 77.27 Bq/L, averaging 47.61 Bq/L. This contamination resulted in an annual effective dose ranging from 7.04 to 15.45 μSv/y, averaging 10.988 μSv/y. Although the concentration of radium-226 in the Nam Phong River is below the USEPA standard of 111 mBq/L for radium-226 contamination, it is still considered high, necessitating continuous monitoring. Areas of concern include Ban Huai Bong in Thung Chomphu Subdistrict, Phu Wiang District; Ban Huai Sai in Ban Dong Subdistrict, Ubonrat District; and Ban Nong Tao in Khok Si Subdistrict, Mueang District [10]. There is a possibility that contamination levels could exceed the standard in the future. Additionally, radium-226 leads to increased radon decay, which poses direct health risks to those who consume water from the Nam Phong River. This research aimed to randomly measure radon concentrations and assess health risks in the lower Phong River, Khon Kaen Province, ensuring safety from exposure to radon-contaminated water.

2. Materials and Methods

2.1 The survey and selection of study areas

The study focused on the lower Phong River in Khon Kaen Province, northeastern Thailand. The Nam Phong River spans approximately 2,386 square kilometers, with a length of around 136 kilometers and an average elevation of 150-500 meters above mean sea level [14]. The researcher randomly selected 8 study areas and 8 boat survey routes along the Phong River for the research. These selections were based on data measuring the radium content in the Phong River from V.Atyotha's 2013 research [10] and data from the raw water pumping station used for tap water production in Khon Kaen Province [15], as illustrated in Figure 1.

2.2 RAD 7 Radon Detector

The RAD 7 is a radon detector, and most of its semiconductor probes are made of silicon. One advantage of the RAD 7 is its durability and ability to detect alpha particles' energy levels accurately. It can differentiate between energy levels of isotopes such as ^{218}Po and ^{214}Po, which are radon decay products. Another important advantage of the RAD 7 is its ability to measure radon gas quickly and in real-time. The

RAD 7 can measure radon concentration in various samples, including air, water, soil, rock, and building materials. However, to measure the radon concentration of each sample, a specific device must be used in conjunction with the RAD 7, tailored to the application for measuring radon concentration in that particular sample. For example, to measure radon concentration in a water sample, the RAD H_2O must be used. Similarly, the RAD Aqua is necessary for radon concentration measurement in rivers, canals, seas, and oceans. Likewise, for measuring radon concentration in soil samples, the RAD in soils is required [16]. This study measures radon concentration in rivers. Therefore, we chose accessories for the experiment, such as RAD 7 and RAD Aqua.

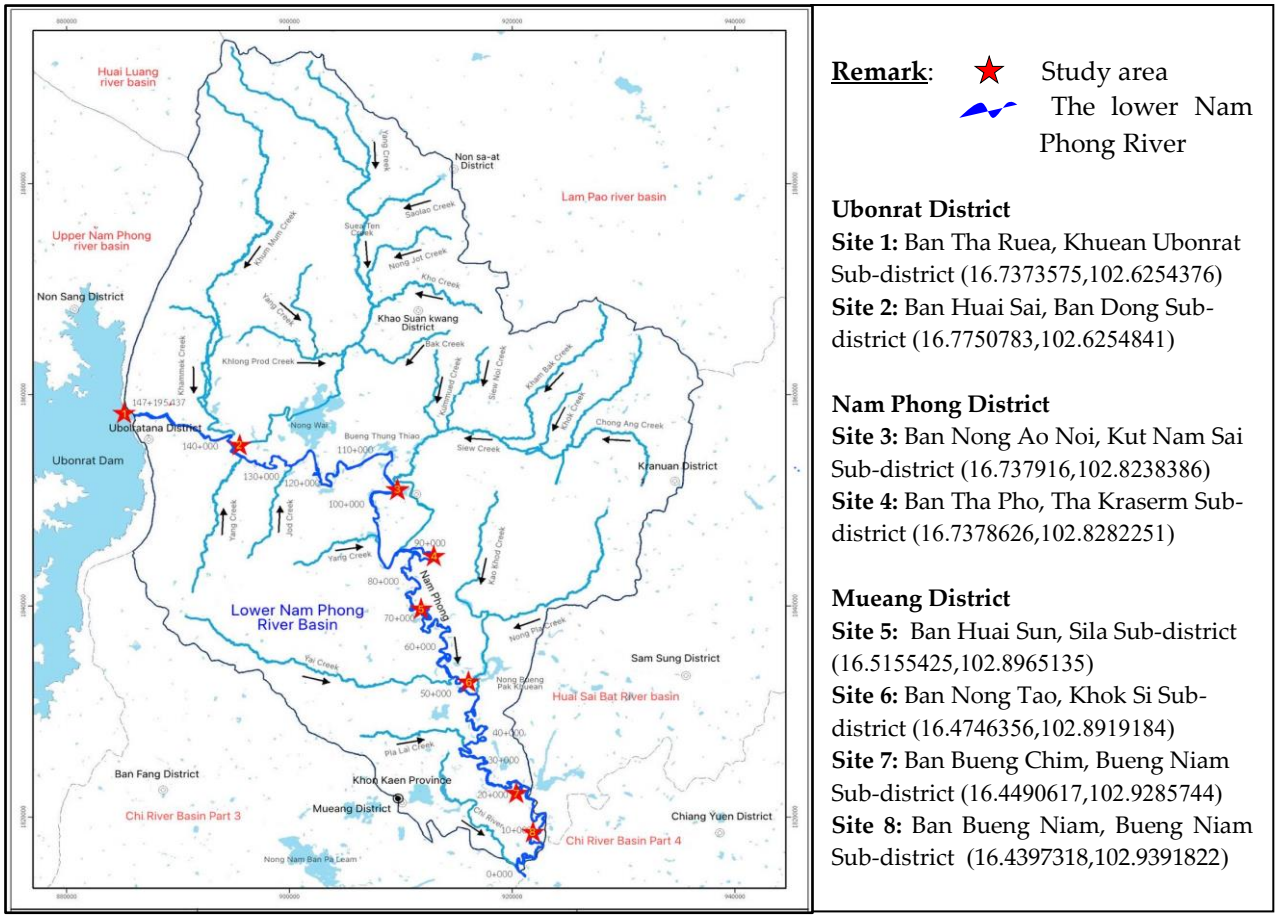

Figure 1. The study areas in Lower Nam Phong River, Khon Kaen Province, Thailand

2.3 RAD Aqua accessories

This system measures radon concentrations in water samples taken from the Nam Phong River. The samples are collected using a pump connected to a hose approximately 1 meter from the water surface. Subsequently, the Nam Phong River water passes through an air-water exchanger equipped with a water spray nozzle. This nozzle diffuses the water into tiny droplets, facilitating the continuous release of radon gas from the incoming water. The radon gas is drawn into the RAD 7's internal pump, passing through a desiccant before entering a probe to measure radon concentration. This measurement is based on the energy of alpha particles emitted by ^{218}Po and ^{214}Po. Subsequently, the measured values are converted to radon concentration units, expressed in Bq/L. A calibrated electronic radon detector (RAD7 Serial No. 4167) by DURRIDGE Company, Inc., United States [16] was used to measure radon in air, soil gas, water, and river setup of this measurement system is illustrated in Figure 2.

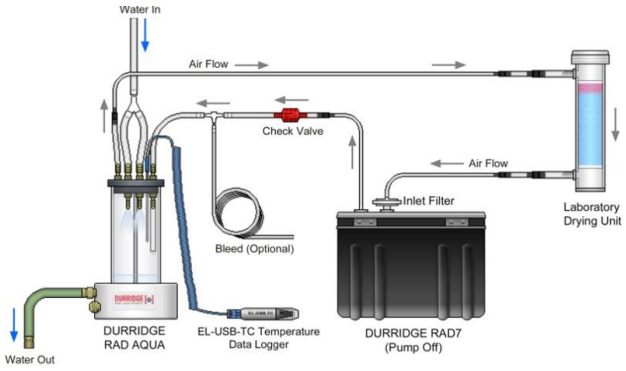

Figure 2. The continuous measurement of radon concentration in Nam Phong River [15].

2.4 The stations for continuous measurement of radon concentration

A continuous radon measuring station was established, utilizing a RAD-Aqua device that received a continuous water flow from a submersible pump fixed at a depth of 1 meter from the river level for 24 hours. The installation process of the device is illustrated in Figure 3, with measurements scheduled every 20 minutes until the 24 hours have elapsed.

Figure 3. The stations continuously measurement of radon concentration in Site 1 Ban Tha Ruea, Khuean Ubonrat Sub-district along the lower Nam Phong River.

2.5 The boat survey routes are used for continuous measurement of radon concentration.

Continuous radon measurement during boat surveys was conducted using a RAD-Aqua device, which received a continuous flow of water from a submersible pump fixed at a depth of 1 meter from the river's surface for 4-6 hours. The installation process of the device is illustrated in Figure 4

Figure 4. The route boat survey will be conducted to measure radon concentration in Site 1 Ban Tha Ruea continuously, Khuean Ubonrat Sub-district along the lower Nam Phong River.

2.6 Health Risk Calculation

The annual effective dose from the ingestion of radon concentration in surface water (D_{ing}) was calculated using Eq. 1 [17-18]:

$$D_{ing} = C_{RnW} \times F \times C_W \quad (1)$$

where C_{RnW} = the average radon concentration in surface water (Bq/L), F = dose conversion factor = 3.5 × 10^{-9} Sv/Bq, and C_w = water consumption throughout the year = 730 L/y [18].

The annual effective dose from the inhalation of radon concentration in surface water (D_{inh}) was calculated using Eq. 2 [18-19]:

$$D_{inh} = C_{RnW} \times R_{AW} \times F \times E \times T \quad (2)$$

where C_{RnW} = the average radon concentration in surface water (Bq/m^3), R_{AW} = the ratio of radon in air/water (10^{-4}), F = the dose conversion factor of radon exposure (9×10^{-9} $Sv \cdot h^{-1} \cdot Bq^{-1}m^3$), E = indoor balance factor between radon and its progeny (0.4), and T = the time indoors (7000 $h \cdot y^{-1}$) [17-18].

The excess lifetime cancer risk (ELCR) was calculated using Eq. 3 [20-21]:

$$ELCR = D_{total} \times A \times f \quad (3)$$

Where D_{total} = the sum of the annual effective dose from the ingestion and inhalation of radon concentration in surface water ($D_{ing} + D_{inh}$), A is the average duration of life estimated to be 77.74 years for Thai people [22], and f = the fatal cancer risk per Sievert (5.5×10^{-2} Sv^{-1}) suggest by ICRP [23].

Lung cancer cases per year per million people (LCC) were calculated using Eq. 4 [20-21]:

$$LCC = D_{total} \times 18 \times 10^{-6} \quad (4)$$

the risk factor for lung cancer induction is 18×10^{-6} $mSv^{-1} \cdot y$ [21].

3. Results and Discussion

3.1 The results of radon concentrations in 8 stations

This research measured radon concentrations in surface water samples at 8 stations along the Nam Phong River using the RAD 7 Radon Detector and RAD Aqua accessories. The results of the radon concentrations, D_{ing}, D_{inh}, ELCR, and LCC are shown in Table 1.

Table1 . The results of 8 stations along Nam Phong River.

Site	Location	Radon		D_{ing}	D_{inh}	D_{total}	ELCR	LCC
		Bq/L	Bq/m^3		μSv/y		%	$\times 10^{-6}$
1	16.7373575,102.6254376	0.17	170	0.43	0.43	0.86	0.037	15.53
2	16.7750783,102.6254841	4.87	4870	12.44	12.27	24.72	1.057	444.88
3	16.737916,102.8238386	0.19	190	0.49	0.48	0.96	0.041	17.36
4	16.7378626,102.8282251	0.16	160	0.41	0.40	0.81	0.035	14.62
5	16.5155425,102.8965135	0.24	240	0.61	0.61	1.22	0.053	21.92
6	16.4746356,102.8919184	1.02	1020	2.61	2.57	5.18	0.221	93.18
7	16.4490617,102.9285744	0.18	180	0.46	0.45	0.91	0.039	16.44
8	16.4397318,102.9391822	2.50	2500	6.39	6.30	12.69	0.542	228.38
	Min	0.16	160	0.41	0.40	0.81	0.035	14.62
	Max	4.87	4,870	12.44	12.27	24.72	1.057	444.88
	Mean	1.17	1,166.25	2.98	2.94	5.92	0.253	106.54
	S.D.	1.70	1,703.22	4.35	4.29	8.64	0.370	155.59

Table 1 shows that radon concentrations ranged from 0.16 to 4.87 Bq/L, with an average concentration of 1.17 Bq/L. The highest radon concentration was observed at Site 2 in Ban Huai Sai, Ban Dong Sub-district,

Ubonrat District, reaching 4.87 Bq/L. In contrast, the lowest concentration was recorded at Site 4 in Ban Huai Sun, Sila Sub-district, Mueang Khon Kaen District, with a 0.16 Bq/L concentration. The results of radon concentration in the Nam Phong River were calculated based on the annual ingestion dose (D_{ing}), the annual inhalation dose (D_{inh}), the excess lifetime cancer risk (ELCR), and the evaluation of the number of lung cancer cases per year per million people (LCC). The findings revealed that the D_{ing} ranged from 0.41 to 12.44 μSv/y (mean = 2.98 μSv/y), the D_{inh} ranged from 0.40 to 12.27 μSv/y (mean = 2.94 μSv/y), the ELCR ranged from 0.035 to 1.057 % (mean = 0.253 %), and the LCC × 10^{-6} ranged from 14.62 to 444.88 (mean = 106.54).

These results were compared with safety limit values, which WHO and USEPA recommend to the dangerous action level of radon concentration is 100 Bq/L for public or commercial drinking water supplies [1, 4-7] and the proposed regulation provides two options for the maximum level of radon that is allowable in community water supplies: 1. the proposed maximum Contaminant Level (MCL) is 11.1 Bq/L and 2. the proposed Alternative Maximum Contaminant Level (AMCL) is 148 Bq/L, respectively [1, 5] and the action level of the D_{ing} and the D_{inh} have a maximum permissible limit of 200 μSv/y if consumed by children and a maximum limit of 100 μSv/y if consumed by adults that are recommended by the WHO and the European Union Commission [1]. The comparison results show that the surface water radon concentration, the Ding, and the Dinh were lower than the action level. The mean Excess Lifetime Cancer Risk (ELCR) for radon exposure in the study area was 0.25 %, which is relatively low compared to the action level set by the US EPA. The estimated risk of 1.3 % corresponds to radon exposure of 148 Bq/m^3 for the entire population [21]. The results of LCC ranged between 14.62 and 444.80 per million persons per year with a mean value of 106.54 per million persons per year, which is lower than the limit range of 170-230 per million persons recommended by ICRP [21].

3.2 The results of radon concentrations by 8 boat survey

This research measured radon concentrations in surface water samples during 8 boat survey routes along the Nam Phong River using the RAD 7 Radon Detector and RAD AQUA accessories. The results of the radon concentrations and the Ding, Dinh, ECLR, and LCC values are shown in Table 2.

Table 2. The results of 8 boat surveys along Nam Phong River.

The boat survey	No. of routes	Distance of routes (m)	Radon		D_{ing}	D_{inh}	D_{total}	ELCR	LCC
			Bq/L	Bq/m^3		μSv/y		%	× 10^{-6}
1	4	5,308.44	0.05749	57.49	0.434	0.428	0.862	0.0369	15.53
2	2	925.45	0.05023	50.23	0.128	0.127	0.255	0.0109	4.59
3	2	1,258.30	0.09460	94.60	0.242	0.238	0.480	0.0205	8.64
4	2	1,344.13	0.12342	123.42	0.315	0.311	0.626	0.0268	11.27
5	1	635.53	0.04247	42.47	0.109	0.107	0.216	0.0092	3.88
6	1	469.01	0.08008	80.08	0.205	0.202	0.407	0.0174	7.32
7	1	498.56	0.05404	54.04	0.138	0.136	0.274	0.0117	4.94
8	1	833.43	0.09144	91.44	0.234	0.230	0.464	0.0198	8.35
		Min	0.04247	42.47	0.109	0.107	0.216	0.0092	3.88
		Max	0.12342	123.42	0.434	0.428	0.862	0.0369	15.53
		Mean	0.07422	74.22	0.226	0.222	0.448	0.0192	8.07
		S.D.	0.02787	27.87	0.109	0.108	0.216	0.0093	3.90

According to Table 2, the radon concentrations in surface water samples were measured during 8 boat survey routes along the Nam Phong River, ranging from 0.04247 to 0.12342 Bq/L, with an average concentration of 0.07422 Bq/L. The highest radon concentration was observed at Site 4: Ban Tha Pho, Tha Kraserm Sub-district, reaching 0.12342 Bq/L, while the lowest concentration was recorded at Site 5: Ban Huai Sun, Sila Sub-district, with a concentration of 0.04247 Bq/L. The results of radon concentration in the Nam Phong River were calculated based on the annual ingestion dose (D_{ing}), the annual inhalation dose (D_{inh}), the

excess lifetime cancer risk (ELCR), and the evaluation of the number of lung cancer cases per year per million people (LCC). The findings revealed that the D_{ing} ranged from 0.109 to 0.434 μSv/y (mean = 0.226 μSv/y), the D_{inh} ranged from 0.107 to 0.428 μSv/y (mean = 0.222 μSv/y), the ELCR ranged from 0.0092 to 0.0369 (mean = 0.0192), and the LCC ranged from 3.88 to 15.53 (mean = 8.07).

These results were compared with safety limit values, which WHO and USEPA recommend to find that the radon concentration, the D_{ing}, and the D_{inh} in surface water were lower than the action level. The mean Excess Lifetime Cancer Risk (ELCR) for radon exposure in the study area was 0.0192 %, which is relatively low compared to the action level set by the US EPA. The estimated risk of 1.3% corresponds to radon exposure of 148 Bq/m^3 for the entire population [21]. The results of LCC ranged between 3.88 and 15.53 per million persons per year with a mean value of 8.07 per million persons per year, which is lower than the limit range of 170 - 230 per million persons recommended by ICRP [21].

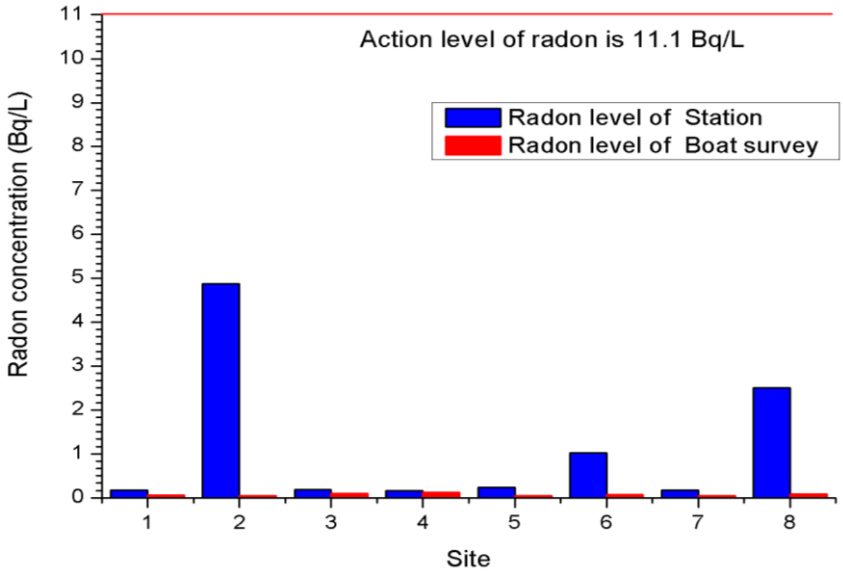

Figure 5. The relationship between radon concentration levels measured at the station and those measured during boat surveys and the action level of radon is 11.1 Bq/L, as advised by US EPA and WHO.

Figure 5 shows the levels of radon contamination in Nam Phong River obtained from measurements at stations installed along the river and measurements made on boats surveying the river. Both values were compared with the action level of the maximum contamination level of radon in the water, which is 11.1 Bq/L, recommended by the US EPA and WHO [1, 4-7]. All results from the measurements were lower than the action level. The data analysis in Figure 5 revealed that the radon concentration in the water measured at Stations 2, 6, and 8 had abnormally high values compared to the radon concentration in the water measured during the boat survey in the river. This difference is likely due to radon infiltration from shallow groundwater near the measuring station. Geological variations in different formations can influence radon content in groundwater, which is approximately 1,000 times greater than surface water. Stations in nearby areas with higher radon-producing rocks or soil may have higher concentrations, and areas with more standing water. Considering the dynamics within the river, water flow and mixing can significantly impact radon concentrations. Faster-moving water tends to have lower radon concentrations because the radon is more quickly diluted. In contrast, slower-moving or stagnant water can accumulate radon gas, leading to higher concentrations. The boat survey might have covered areas with more dilution from other water sources, resulting in lower readings [24-25].

Take data from Tables 1 and 2 and plot the graph to study the relationship between the radon concentration levels measured at stations and those measured during the boat survey, as shown in Figure 6.

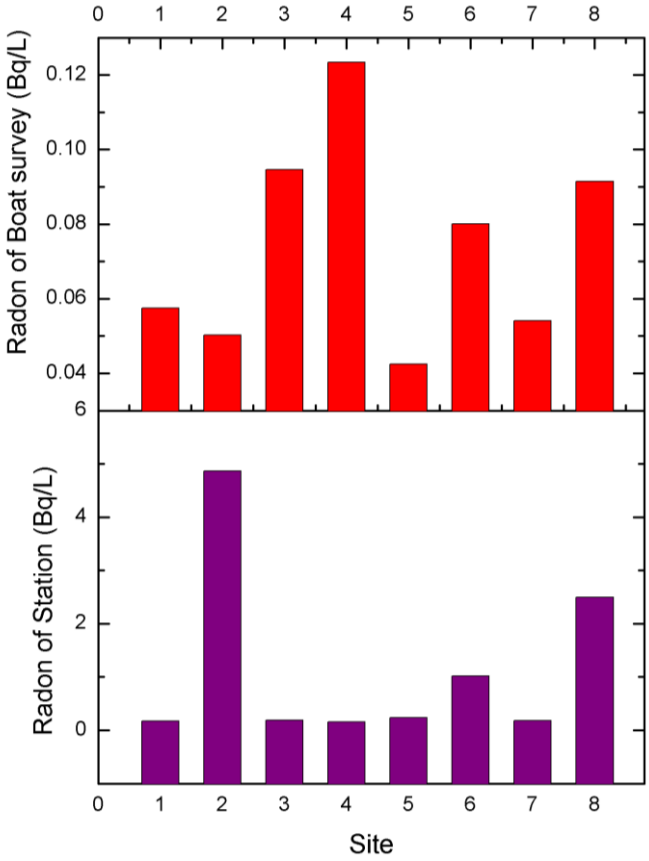

Figure 6. The relationship between radon concentration levels measured at the station and those measured during boat surveys.

Analysis of the results in Figure 6 suggests that radon may have been transferred into the Nam Phong River, particularly at stations 6 and 8, as indicated by the high radon concentration levels measured at these locations. However, at Station 2, there may have been no radon transfer into the Nam Phong River, as the radon concentration measured during the boat survey was low. Furthermore, the higher radon values measured from boat tours in Areas 3 and 4, compared to other areas, may be attributed to rocks, soil, or sediment at the bottom of the river. The high concentration of radium-rich rivers decaying into radon could contribute to the elevated radon levels in these areas. It is important to note that this is solely an analysis of the results obtained from this research. Additional factors must be studied to gain a more comprehensive understanding of the transfer of radon in groundwater flowing into rivers. These include further measurements of radium and radon in groundwater, sediment, or rivers; assessment of water velocity; analysis of water quality parameters such as temperature, pH, conductivity, and nutrient levels; and consideration of seasonal and time (day-night). The complexity of these factors may necessitate additional research in the future.

4. Conclusions

The radon contamination level in surface water from 8 stations and 8 boat surveys along the lower Nam Phong River Basin in all 3 Districts (Ubonrat District, Nam Phong District, and Mueang District), results measured radon contamination level in all samples were lower than action level by the US EPA and WHO. The total annual effective dose for inhalation and ingestion of radon in surface water samples was below 100 μSv/y suggested by the WHO. The mean excess lifetime cancer risk (ELCR) was below the permissible limit of 1.3 % indicated by the US EPA, and the mean of LCC is lower than the limit range of 170-230 per million persons recommended by ICRP. This project demonstrates that surface water in the study area is safe for public consumption. It also provides preliminary data to study the transfer of radon content from shallow groundwater flowing into rivers, which indicates locations where water pollution has occurred. If you want

to learn more about this work, the researcher suggests additional studies on several factors. These include additional measurements of radium and radon in groundwater, sediment, or rivers; water velocity; and various water quality parameters such as temperature, pH, conductivity, and nutrient levels. The study should also consider seasonal variations and the time of day (day and night). Given the complexity of the matter, further research is needed to explore these factors, which may lead to additional studies soon.

5. Acknowledge

The author would like to thank the Faculty of Engineering, Rajamangala University of Technology Isan, Khon Kaen Campus, for supporting research funds in the 2022 annual budget, as per capital contract ENG09/65.

Author Contributions: Conceptualization, V.A.; methodology, V.A., K.P., B.R., R.U. and J.S.; validation, V.A. and J.S; formal analysis, K.P. and B.R.; writing—original draft preparation, V.A. and J.S.; writing-review and editing, V.A.; visualization, R.U.; supervision, V.A.

Funding: This research was supported by research funds in the 2022 annual budget, as per capital contract number ENG09/65 of the Faculty of Engineering, Rajamangala University of Technology Isan, Khon Kaen Campus.

Conflicts of Interest: The authors declare no conflict of interest.

References

[1] Ismail, N. F.; Hashim, S.; Sanusi, M. S. M.; Abdul Rahman, A. T.; Bradley, D. A. Radon Levels of Water Sources in the Southwest Coastal Region of Peninsular Malaysia. *Appl. Sci.* **2021**, *11*, 1-12.

[2] Atyotha, V.; Thopan, P.; Fungdet, S.; Somtua, J. Radon Exhalation Rates of Soil Samples from Khon Kaen Province, Thailand. *Mindanao Journal of Science and Technology*. **2022**, *20*(S1), 223-235.

[3] Nayak, T.; De, D.; Karmakar, P.; Deb, A.; Dhal, PK. Microbial Communities of the Drinking Water with Gradient Radon Concentration Are Primarily Contributed by Radon and Heavy Metal Content. *Front. Environ. Sci.* **2021**, *9*, 1-13.

[4] Al Hilal, M. Radon as a Natural Radiotracer to Investigate Infiltration from Surface water to nearby Aquifers: A Case Study from The Barada Riverbank, Syria. *Geofísica Internacional*. **2020**, 59-3, 208-223.

[5] Titipornpun, K.; Komsan, P.; Tohsuemae, S.; Sukgree, N. Risk Assessment of Radon Concentrations in Water of the Tapi River Nearby the Tapi Estuary of Bandon Bay, Muang District, Surat Thani Province. *SWU Sci. J*. **2021**, *37*, 12-28.

[6] Mallick, J.; Singh, C. K.; AlMesfer, M. K.; Singh, V.P.; Alsubih, M. Groundwater Quality Studies in the Kingdom of Saudi Arabia: Prevalent Research and Management Dimensions. *Water.* **2021**, *13*, 1-16.

[7] Kumar, M.; Kumara, P.; Agrawalb, A.; Sahooc, B. K. Radon concentration measurement and effective dose assessment in drinking groundwater for the adult population in the surrounding area of a thermal power plant. *Journal of Water and Health* **2022**, 20.

[8] Kuntiyawichai, K.; Dau, Q. V.; Sri-Amporn, S.; Suryadi, F. X. An Assessment of Flood Hazard and Risk Zoning in the Lower Nam Phong River Basin, Thailnd. *International Journal of Technology*. **2016**, 7, 1147-1154.

[9] Department of Mineral Resources. *Classification for geological and mineral resources management in Khon Kaen Province*. Ministry of Natural Resources and Environment: Thailand, Bangkok, **2009**.

[10] Atyotha, V. The Study of Factors that Cause Cancer of the Concentration of Radium 226 in Nam Pong River at Khon Kaen Province. *Journal of Nurses' association of thailand, north-eastern division.* **2013**, *31*, 136-143.

[11] Prakongsri, P.; Santiboon, T. Effective Water Resources Management for Communities in the Chi River Basin in Thailand. *Environmental Claims Journal*. **2020**, *32*, 323-348.

[12] Phatchaney, K.; Chamaratana, T. Urbanization Impact Toward Capital Assets Accession and Holding of Labor Households in Khon Kaen Peri – Urban. *Suratthani Rajabhat Journal*. **2018**, *5*, 101-126.

[13] Jaitae, S. River Deterioration and Health. Lanna Public Health Journal. **2012**, *8*, 57-68.

[14] Duangmontri, P.; Janjarean, W.; Samart, W. Final Report: model community development monitoring health and environmental health impacts. in the eco-industrial city area, Nam Phong District, Khon Kaen Province. *Regional Health Promotion Center 7 Khonkaen*. **2019**, 1-59
[15] The raw water pumping station of the Nam Phong River [Online]; Provincial Waterworks Authority Region 6 Khon Kaen. https://reg6.pwa.co.th/ita/ (accessed Feb 7, 2024).
[16] RAD 7 electronic radon detector user manual [Online]; DURRIDGE Company, Inc. https://durridge.com/documentation/RAD7%20Manual.pdf (accessed Feb 7, 2024).
[17] Mostafa, M.; Olaoye, M. A.; Ademola, A. K.; Jegede, O. A.; Saka, A. A.; Khalaf, H. Measurement of Radon Concentration in Water within Ojo Axis of Lagos State, Nigeria. *Analytica*. **2022**, *3*, 325-334.
[18] UNSCEAR. *Exposures from Natural Radiation Sources (Annex B) Sources and Effects of Ionizing Radiation*: United Nations, USA, New York, **2000**, 84-141.
[19] Suresh, S.; Rangaswamy, D.R.; Srinivasa, E.; Sannappa, J. Measurement of radon concentration in drinking water and natural radioactivity in soil and their radiological hazards. *J. Radiat. Res. Appl. Sci* **2020**, *13*, 12-26.
[20] Pervin, S.; Yeasmin, S.; Khandaker M.U.; Begum. A. Radon Concentrations in Indoor and Outdoor Environments of Atomic Energy Centre Dhaka, Bangladesh, and Concomitant Health Hazards. Front. Nucl. Eng **2022**, 1, 1-10.
[21] Sherafat, S.; Mansour, S. N.; Mosaferi, M.; Aminisani, N.; Yousefi, Z.; Maleki, S. First Indoor Radon Mapping and Assessment Excess Lifetime Cancer Risk in Iran. MethodsX **2019**, 6, 2205-2216.
[22] Thailand Life Expectancy 1950-2024 [Online]; Macrotrends. https://www.macrotrends.net/countries/THA/thailand/life-expectancy (accessed Feb 7, 2024).
[23] ICRP, "The 2007 recommendations of the international commission on radiological protection. ICRP Publication 103", Ann. ICRP, **2007**, 37, https://doi:10.1016/j.icrp.2007.10.003.
[24] Selvam, S.; Muthukumar, P.; Sruthy Sajeev.; Venkatramanan, S.; Chung, S.Y.; Brindha, K.; Suresh Babu, D.S.; Murugan R.;. Quantification of submarine groundwater discharge (SGD) using radon, radium tracers and nutrient inputs in Punnakayal, south coast of India. *Geoscience Frontiers*. **2021**, *12*, 29-38.
[25] Du, S.; Deng, Z.; Liu, Y.; Zhang, L.; Xu, H.; Yang, H.;. Evaluation of surface water–groundwater interaction using environmental isotopes (D, 18O and 222Rn) in Chongli Area, China. *Journal of Radioanalytical and Nuclear Chemistry*. **2019**, *321*, 303-311.

ASEAN
Journal of Scientific and Technological Reports
Online ISSN:2773-8752

Research article

Enhancing Biogas Production from Empty Fruit Bunch by Weak Acid Pretreatment: Process Optimization and Synergistic Effects

Sukonlarat Chanthong[1*] and Prawit Kongjan[2]

[1] Faculty of Engineering, Prince of Songkla University, Songkhla, 90110, Thailand; sukonlarat052@gmail.com
[2] Faculty of Science and Technology, Prince of Songkla University, Pattani, 94000, Thailand; kprawit.kongjan@gmail.com
[*]Corresponding author: sukonlarat052@gmail.com

Citation:
Chanthong, S.; Kongjan, P. Enhancing biogas production from empty fruit bunch through acetic acid pretreatment: process optimization and synergistic effects. *ASEAN J. Sci. Tech. Report.* **2024**, *27*(3), 253623. https://doi.org/10.55164/ajstr.v27i3.253623.

Article history:
Received: April 11, 2024
Revised: April 29, 2024
Accepted: April 30, 2024
Available online: May 1, 2024

Abstract: Empty fruit bunch (EFB), a lignocellulosic waste generated from the palm oil industry, has emerged as a promising feedstock for biogas production. The recalcitrant nature of EFB hinders its efficient biodegradation, necessitating effective pretreatment methods to enhance biogas yield. This study investigated the effect of weak acid pretreatment using acetic acid on the composition and structure of EFB and subsequent anaerobic digestion performance. EFB was pretreated with varying concentrations of acetic acid (0-10%) at room temperature for 7 days. The pretreated EFB was characterized using compositional analysis. Anaerobic digestion experiments were conducted in batch mode for 45 days at 37°C. Pretreatment with 4% acetic acid resulted in the highest methane yield of 265.77 mL-CH_4/g-VS, representing a 55.21% improvement compared to untreated EFB. The synergistic effect of acetic acid and EFB co-fermentation was observed at 4% acetic acid, with a synergistic CH_4 value of 60.26 mL. Compositional analysis revealed that acetic acid pretreatment led to a 12.5% reduction in lignin content and a 9.3% increase in cellulose content, enhancing cellulose accessibility for microbial degradation. The energy balance analysis indicated a positive net energy gain of 879.62 kWh per ton of EFB, while the economic analysis suggested a net profit of 60.00 USD per ton of EFB. This study demonstrates weak acid pretreatment effectiveness in enhancing biogas production from EFB and its potential for large-scale application in the palm oil industry.

Keywords: Volatile fatty acids, Weak acid pretreatment, Empty fruit bunch, Biogas production, Lignocellulosic biomass

1. Introduction

Empty fruit bunch (EFB) is a lignocellulosic waste from the palm oil industry. In 2020, global palm oil production reached 72.27 million metric tons, with Indonesia and Malaysia being the largest producers, accounting for 84% of the world's palm oil supply [1]. For every ton of palm oil produced, approximately 1.1 tons of EFB are generated [2]. EFB comprises 38-40% cellulose, 21-34% hemicellulose, and 20-21% lignin [3]. The high cellulose and hemicellulose content of EFB makes it a suitable feedstock for biogas production through anaerobic digestion. The energy potential of EFB is estimated to be 2.6-2.8 GJ/ton [4]. If all the EFB generated from palm oil mills in Indonesia, Malaysia, and Thailand were used for biogas production, it could potentially generate 38-41 million m^3 of biogas per year, equivalent to 22-24 million GJ of energy (calculated based on a biogas yield of 500 m^3/ton EFB and an energy content of 22 MJ/m^3). This energy could displace 1.8-2.0 million metric tons of coal annually (assuming

a coal energy content of 29.3 GJ/ton). Moreover, the utilization of EFB for biogas production can contribute to greenhouse gas emission reductions, estimated at 0.32 metric tons of CO_2-equivalent per metric ton of EFB [5].

Despite the significant potential of EFB for biogas production, its recalcitrant structure poses challenges for efficient biodegradation. The complex arrangement of cellulose, hemicellulose, and lignin in EFB limits the accessibility of cellulose and hemicellulose to microbial enzymes during anaerobic digestion [6]. Lignin acts as a physical barrier and reduces the hydrolysis rate of cellulose and hemicellulose, leading to slow and incomplete biodegradation [7]. Consequently, the methane yield from untreated EFB is relatively low, ranging from 100-200 mL-CH_4-g$^{/}$VS [8]. Pretreatment of lignocellulosic biomass is crucial for enhancing biogas yield by overcoming the recalcitrance of the biomass structure. Pretreatment methods aim to disrupt the lignin barrier, reduce cellulose crystallinity, and increase the porosity of the biomass, thereby improving the accessibility of cellulose and hemicellulose to microbial enzymes [9]. Various pretreatment methods have been investigated for EFB, including physical (e.g., milling, irradiation), chemical (e.g., alkali, acid, ionic liquids), and biological (e.g., fungal, enzymatic) methods [6]. Among these, chemical pretreatment methods have shown promising results in enhancing biogas yield from EFB [8]. Weak acid pretreatment has emerged as an effective method for enhancing biogas production from lignocellulosic biomass. Weak acids, such as acetic acid, can solubilize hemicellulose and lignin, thereby increasing the accessibility of cellulose for microbial degradation [10]. Compared to strong acid pretreatment, weak acid pretreatment offers several advantages, including lower corrosivity, toxicity, and formation of inhibitory compounds such as furfural and 5-hydroxymethylfurfural (HMF) [11]. Moreover, weak acids are often produced as volatile fatty acids (VFAs) during anaerobic digestion, which can be utilized as in-situ pretreatment agents, reducing the need for external chemicals [12].

The objectives of this study were to investigate the effect of weak acid pretreatment using acetic acid on the composition and structure of EFB and optimize the acetic acid pretreatment conditions (concentration, duration) for maximizing biogas production from EFB. Evaluate the synergistic effects of acetic acid and EFB co-fermentation on biogas yield and production rate. Compare the performance of acetic acid pretreatment with other pretreatment methods regarding biogas yield enhancement. Assess biogas production's energy balance and economic viability from EFB pretreated with acetic acid.

2. Materials and Methods

2.1 Characterization of EFB composition

EFB was obtained from Larp Tavee Industries Co., Ltd., a palm oil mill in Satun Province, southern Thailand (6°51'42.0"N 99°52'15.3"E). EFBs were air-dried and ground to an average particle size of 15.0-50.0 mm for pretreatment. Cellulose, hemicellulose, and lignin content were determined using the methods described by [13, 14]. Cellulose content was determined by the acetic acid-nitric acid method [13]. Hemicellulose content was calculated by subtracting the cellulose and lignin content from the total carbohydrate content [14]. Lignin content was determined using the Klason lignin method [13]. Moisture content was determined using the oven-drying method described by NREL (2005) [15]. EFB samples were dried in an oven at 105°C until a constant weight was achieved. Ash content was determined using the dry ashing method, as outlined by NREL [15]. EFB samples were incinerated in a muffle furnace at 575 ± 25°C for 4 hours, and the remaining ash was weighed.

2.2 Weak acid pretreatment process

Acetic acid was selected as the representative volatile fatty acid for the pretreatment process due to its similar pKa (4.82 ± 0.05) to other volatile fatty acids in the anaerobic digestion process (Table 1) [16]. The concentration range of acetic acid solutions was 0-10%, based on preliminary studies indicating optimal lignin removal and cellulose preservation within this range [17]. 500 grams of prepared EFB was used for each pretreatment experiment. EFB was infused with 1.5 liters of acetic acid solutions at varying concentrations, prepared by diluting commercial acetic acid (95% purity) with distilled water. The EFB-acetic acid mixture was soaked for 7 days at room temperature in sealed containers to prevent evaporation and contamination, as per the protocol described by Chia et al. [17]. After the soaking period, the EFB was filtered and washed

thoroughly with distilled water to remove residual acid. The optimal pretreatment parameters were determined based on the lignin removal and cellulose preservation.

Table 1. pKa values of volatile fatty acids in the anaerobic digestion process

Volatile Fatty Acid	pKa
Acetic acid	4.82 ± 0.05
Propionic acid	4.87 ± 0.05
Butyric acid	4.82 ± 0.05
Valeric acid	4.84 ± 0.05
Caproic acid	4.85 ± 0.05

2.3 Experimental setup for biogas production

The inoculum for anaerobic digestion was obtained from a mesophilic anaerobic digester treating palm oil mill effluent. The inoculum was pre-incubated at 37°C for 7 days to ensure the reduction of endogenous methane production. Batch anaerobic digestion experiments were conducted in 0.5-liter glass bottles with a working volume of 200 mL. Anaerobic methane production was measured by batch BMP assay under mesophilic conditions, using 80% inoculum and 20% substrate [18] in a glass bottle containing 160 ml of inoculum, 40 ml of EFBs soaked with weak acid (2-10%), that substrate was mixed particulate and soluble. The bottles were sealed with rubber stoppers and aluminum crimps and flushed with nitrogen gas to ensure anaerobic conditions [19]. The bottles were incubated at 37°C for 45 days in a temperature-controlled incubator. The negative control uses only the substrate, and the positive control uses avicel (cellulose microcrystalline particle size 50 μm).

2.4 Analytical Methods

Biogas production was measured daily using the water displacement method. Biogas composition (H_2, CH_4, and CO_2) was determined using a gas chromatograph (Agilent 7890B, Agilent Technologies, USA) equipped with a thermal conductivity detector (TCD) and a Carboxen 1010 PLOT capillary column (30 m × 0.53 mm). The carrier gas was argon, and the temperature program was set as follows: initial temperature of 35°C, held for 5 min, increased to 225°C at a rate of 20°C/min and then held for 5 min. [20]. Total solids (TS) and volatile solids (VS) were determined according to the standard methods described by APHA [21]. pH was measured using a digital pH meter. All experiments were conducted in triplicate, and the results were expressed as mean ± standard deviation. Tukey's post hoc test was used for multiple comparisons, with a significance level of $p < 0.05$. The cumulative methane production achieved from this batch could be further used to evaluate the hydrolysis constant (k_h) using the first-order kinetic reaction, as shown in Equation 1.

$$ln = \frac{B_\infty - B}{B} \quad (1)$$

The kinetics of methane formation under batch fermentation fitting with a modified Gompertz model, as shown in Equation 2.

$$B_t = B_\infty \times exp\left\{-exp\left[\frac{R_{max} \times e}{B_\infty}(\lambda - t) + 1\right]\right\} \quad (2)$$

Bt is methane cumulated at time t, B(is the ultimate methane cumulating at the end of an experimental period, and t is time (day). R_{max} is the maximum methane production rate (mL-CH_4/gVS-day); e = exp (1) = 2.7183; and λ is the lag phase period (day).

3. Results and Discussion

3.1 EFB composition

The composition of raw and pretreated empty fruit bunch (EFB) is presented in Table 2. The raw EFB consisted of 38.0% cellulose, 43.0% hemicellulose, and 18.0% lignin, with a total solids content of 27.82 g/L and volatile solids of 94.35% of the total solids. These values are consistent with the findings of Díez et al. [22], who

reported similar compositions for EFB. Pretreatment with acetic acid (AC) at various concentrations resulted in changes to the EFB composition. Soaking the EFB in water alone (0% AC) led to a slight decrease in cellulose and hemicellulose content, while the lignin content increased to 20.0%. This change can be attributed to the solubilization of some easily accessible carbohydrates during the soaking process [23]. As the concentration of acetic acid increased from 2% to 6%, the lignin content increased from 20.0% to 22.0%, while the cellulose content decreased from 33.0% to 30.0%. This trend suggests that acetic acid pretreatment is more effective in removing hemicellulose and cellulose than lignin [24]. The relative decrease in the other components can explain the increase in lignin content. Interestingly, at higher acetic acid concentrations (8% and 10%), the lignin content decreased to 20.0% and 18.0%, respectively. This reduction in lignin content at higher acid concentrations has also been observed by Sun et al. [25], who suggested that stronger acidic conditions might lead to the partial degradation of lignin. The total solids content increased with increasing acetic acid concentration up to 6%, indicating the solubilization of EFB components into the liquid phase during pretreatment [23]. However, at higher concentrations (8% and 10%), the total solids content decreased slightly, possibly due to the degradation of some solubilized components [26]. The pretreatment of EFB with acetic acid led to changes in its composition, with a general trend of decreasing cellulose and hemicellulose content and increasing lignin content at lower acid concentrations. Higher acid concentrations slightly reduced lignin content, suggesting partial degradation under stronger acidic conditions.

Table 2. Composition of raw and pretreated empty fruit bunch (EFB)

Methods	Cellulose (%TS)	Hemicellulose (%TS)	lignin (%TS)	TS (g/L)	VS (g/L)
Raw-EFB	0.38 ± 0.02	0.43 ± 0.02	0.18 ± 0.01	27.82 ± 1.39	94.3 ± 4.725
Soaked with H_2O	0.34 ± 0.02	0.39 ± 0.02	0.2 ± 0.01	71.85 ± 3.59	67.88 ± 3.39
Soaked with 2%AC	0.33 ± 0.02	0.41 ± 0.02	0.2 ± 0.01	83.54 ± 4.18	82.33 ± 4.12
Soaked with 4%AC	0.34 ± 0.02	0.39 ± 0.02	0.21 ± 0.01	104.8 ± 5.24	100.23 ± 5.01
Soaked with 6%AC	0.30 ± 0.02	0.39 ± 0.02	0.22 ± 0.01	109.2 ± 5.46	93.73 ± 4.69
Soaked with 8%AC	0.35 ± 0.02	0.39 ± 0.02	0.2 ± 0.01	91.2 ± 4.56	85.79 ± 4.29
Soaked with 10%AC	0.35 ± 0.02	0.4 ± 0.02	0.18 ± 0.01	102.5 ± 5.13	97.6 ± 4.88

Remark: AC: Acetic acid

3.2 Effect of weak acid pretreatment on EFB structure and composition

Acid pretreatment is commonly used to hydrolyze lignocellulosic materials into reducing sugars. However, strong acids can generate toxic compounds such as furfural and hydroxymethyl furfural [27]. In this experiment, we focused on using volatile fatty acids (VFAs) to pretreat EFB, taking advantage of the biogas system failure caused by VFA accumulation, which inhibits methanogens and causes an adverse shift in the microbial population. The system's buffering capacity is crucial to withstand VFA accumulation without a significant drop in pH. VFAs are produced during the acidogenesis phase of anaerobic digestion when complex organic compounds are broken down into simpler molecules. Concentrations of VFAs accumulated between 10,034 and 13,381 mg/L have been shown to effectively inhibit methanogens ([28, 29, 30]. The effect of acetic acid pretreatment on the structure and composition of EFB was investigated using various analytical techniques. Table 3 presents the changes in the crystallinity index, specific surface area, and pore volume of EFB after pretreatment. The crystallinity index of raw EFB was 45.2 ± 1.8%, which increased to 55.1 ± 1.9% after pretreatment with 6% acetic acid. This increase in crystallinity can be attributed to the removal of amorphous hemicellulose and lignin during pretreatment, which leads to a higher proportion of crystalline cellulose in the pretreated EFB [25]. The specific surface area and pore volume of EFB also increased by up to 6% with the increase in acetic acid concentration. The specific surface area increased from 1.5 ± 0.2 m^2/g for raw EFB to 2.8 ± 0.5 m^2/g for EFB pretreated with 6% acetic acid, while the pore volume increased from 0.005 ± 0.001 cm^3/g to 0.013 ± 0.002 cm^3/g. These changes in the physical structure of EFB can be attributed to the partial removal of hemicellulose and lignin, which creates more pores and exposes more surface area [31]. The acetic acid

pretreatment of EFB led to significant changes in its structure and composition. Table 4 shows that on day 7, all conditions resulted in a pH of approximately 3.0-3.7, less than the pKa of acetic acid, indicating complete dissociation in water. The increase in crystallinity index, specific surface area, pore volume, and partial removal of hemicellulose and lignin demonstrate the effectiveness of acetic acid pretreatment in modifying the physical and chemical properties of EFB. These changes in the structure and composition of EFB can enhance its biodegradability and improve its potential for biogas production.

Table 3. Structural changes in EFB after acetic acid pretreatment

Pretreatment Condition	Crystallinity Index (%)	Specific Surface Area (m^2/g)	Pore Volume (cm^3/g)
Raw EFB	45.2 ± 1.8	1.5 ± 0.2	0.005 ± 0.001
Soaked with H2O	47.1 ± 2.1	1.8 ± 0.3	0.007 ± 0.002
Soaked with 2% AC	50.3 ± 1.5	2.2 ± 0.4	0.009 ± 0.002
Soaked with 4% AC	52.8 ± 2.3	2.5 ± 0.3	0.011 ± 0.003
Soaked with 6% AC	55.1 ± 1.9	2.8 ± 0.5	0.013 ± 0.002
Soaked with 8% AC	53.6 ± 2.2	2.6 ± 0.4	0.012 ± 0.003
Soaked with 10% AC	51.9 ± 1.7	2.4 ± 0.3	0.010 ± 0.002

AC: Acetic acid

The effect of weak acid pretreatment on the structure and composition of empty fruit bunch (EFB) was investigated by soaking EFB in various concentrations of acetic acid (AC) and monitoring the pH changes for 7 days (Table 4). The pH profile provides insights into the extent of acidification and the potential impact on the lignocellulosic structure of EFB. When EFB was soaked in water (control), the pH decreased from 7.50 ± 0.06 on day 0 to 4.73 ± 0.21 on day 7. This decrease in pH can be attributed to the natural release of organic acids from the EFB during the soaking process [32]. However, the pH remained above 4.5 throughout the experiment, indicating a limited effect on the lignocellulosic structure of EFB. In contrast, soaking EFB in acetic acid solutions resulted in a rapid decrease in pH within the first day, followed by a gradual stabilization over the remaining period. The extent of pH reduction was proportional to the concentration of acetic acid used. For instance, soaking EFB in 2% AC resulted in a pH of 3.22 ± 0.20 on day 0, which decreased to 3.73 ± 0.07 by day 7. Similarly, the pH of EFB soaked in 4% AC and 6% AC decreased to 3.37±0.05 and 3.29±0.46, respectively, by the end of the experiment. The lower pH values achieved by acetic acid pretreatment can be attributed to the dissociation of acetic acid in water, releasing hydrogen ions (H^+) and acetate ions (CH_3COO^-). The increased concentration of H^+ ions in the soaking solution promotes the hydrolysis of hemicellulose and the disruption of lignin-carbohydrate complexes, thereby enhancing cellulose accessibility for subsequent enzymatic hydrolysis [33]. However, it is important to note that excessive acidification can lead to the formation of inhibitory compounds, such as furfural and 5-hydroxymethylfurfural (HMF), which can negatively impact the downstream processes [34]. In this study, the pH of EFB soaked in 8% AC and 10% AC remained below 3.0 throughout the experiment, indicating a potential risk of inhibitor formation. The structural changes induced by weak acid pretreatment can be further evaluated through compositional analysis and imaging techniques, such as scanning electron microscopy (SEM) and Fourier-transform infrared spectroscopy (FTIR) [25]. These analyses provide information on the removal of hemicellulose and lignin, the increase in cellulose accessibility, and the overall changes in the surface morphology of the pretreated biomass. Weak acid pretreatment using acetic acid effectively reduced the pH of EFB, with the extent of acidification proportional to the acetic acid concentration used. The lower pH achieved by acetic acid pretreatment can enhance the hydrolysis of hemicellulose and the disruption of lignin-carbohydrate complexes, potentially improving cellulose accessibility for subsequent enzymatic hydrolysis. However, excessive acidification may lead to the formation of inhibitory compounds, necessitating the optimization of pretreatment conditions to maximize the beneficial effects while minimizing the formation of inhibitors.

3.3 Biogas production from pretreated and untreated EFB

The cumulative methane production from empty fruit bunch (EFB) soaked with water (EFB-H_2O) and pretreated with weak acid (EFB-%AC) is shown in Figure 1. The highest cumulative methane production was observed for EFB pretreated with 4% acetic acid (EFB-4%AC), reaching 666.09 mL-CH_4 (Table 5). This corresponds to a methane yield of 265.77 mL-CH_4/g-VS, 55.21% higher than the yield obtained from EFB soaked with water (171.24 mL-CH_4/g-VS). The improved methane yield can be attributed to the enhanced accessibility of cellulose and hemicellulose for microbial degradation after pretreatment with acetic acid [24]. The methane production rate for EFB-4%AC was 8.37 mL-CH_4 /L/d, which is higher than the rates observed for EFB-H_2O (7.37 mL-CH_4/L/d) and other pretreated conditions (Table 5). This higher production rate can be attributed to the increased hydrolysis rate of the pretreated EFB, which provides more readily available substrates for methanogenic archaea [25]. The methane content in the biogas produced from pretreated and untreated EFB is an important parameter for evaluating the quality of the biogas.

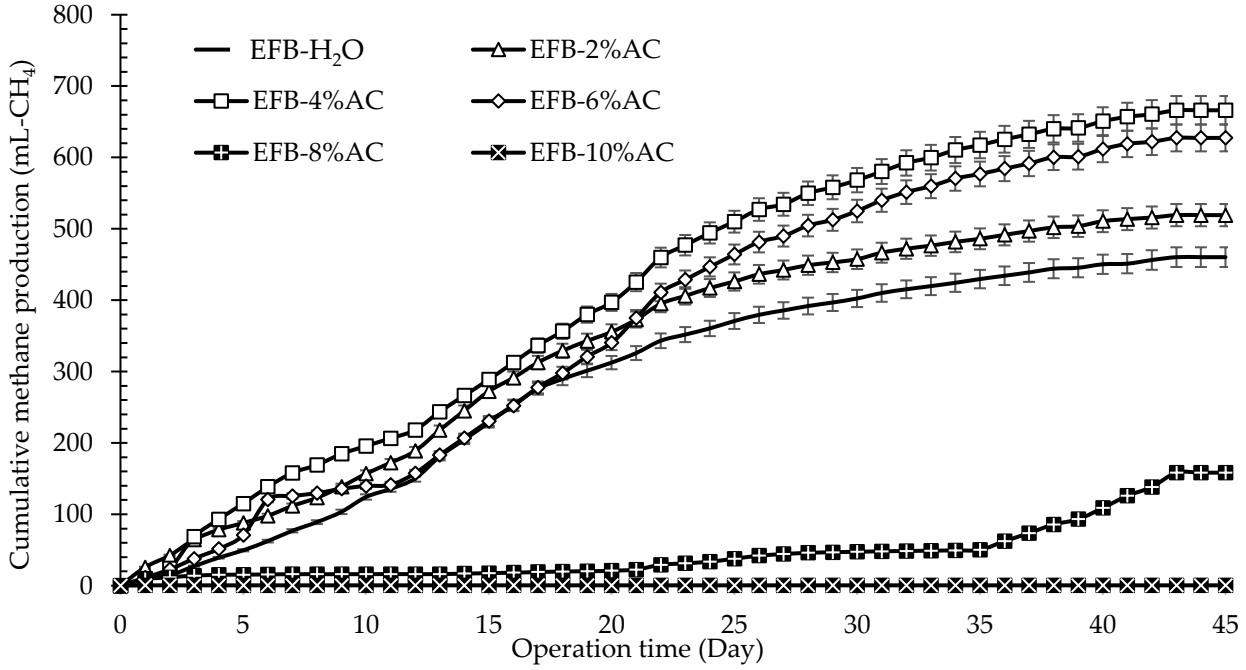

Figure 1. Cumulative methane production from empty fruity bunch soaked with water (EFB-H_2O) and weak acid pretreatment (EFB-%AC)

The cumulative methane production, methane yield, and other key parameters of biogas production from pretreated and untreated empty fruit bunch (EFB) are presented in Table 5. The EFB soaked with water (untreated) produced a cumulative methane volume of 460.30 mL-CH_4, with a methane yield of 171.24 mL-CH_4/g-VS. The untreated EFB served as a control to evaluate the effectiveness of weak acid pretreatment on biogas production. Among the pretreated EFB samples, the highest cumulative methane production (666.09 mL-CH_4) and methane yield (265.77 mL-CH_4/g-VS) were observed for EFB soaked with 4% acetic acid (AC). This represents a 54.62% improvement in methane yield compared to the untreated EFB. The enhanced biogas production can be attributed to the ability of weak acid pretreatment to disrupt the lignocellulosic structure of EFB, making it more accessible to microbial degradation during anaerobic digestion[32, 33]. The methane production rate for EFB soaked with 4% AC was 8.37 mL-CH_4/L/d, higher than that of untreated EFB (7.37 mL-CH_4/L/d) and other pretreated samples. The lag phase for EFB soaked with 4% AC was also shorter (1.66 d) compared to untreated EFB (3.70 d), indicating faster initiation of the anaerobic digestion process. These findings suggest that weak acid pretreatment not only enhances the overall biogas yield but also improves the kinetics of the anaerobic digestion process [33, 35]. However, it is important to note that increasing the acetic acid concentration beyond 4% had a detrimental effect on biogas production. EFB soaked with 6% AC showed

a lower methane yield (209.53 mL-CH_4/g-VS) and a longer lag phase (3.82 d) than EFB with 4% AC. Further increasing the acetic acid concentration to 8% and 10% resulted in a significant reduction in methane yield and an extended lag phase. This can be attributed to the inhibitory effects of high concentrations of volatile fatty acids on the anaerobic digestion process, particularly on the methanogenic archaea [28, 36]. The hydrolysis rate constant (Kh) for EFB soaked with 4% AC (0.0960 d^{-1}) was similar to that of untreated EFB (0.0986 d^{-1}), suggesting that weak acid pretreatment at this concentration did not significantly impact the hydrolysis step of anaerobic digestion. However, the Kh value for EFB soaked with 2% AC was notably higher (1.0240 d^{-1}), indicating faster hydrolysis of the pretreated biomass [37]. Weak acid pretreatment using 4% acetic acid significantly enhanced biogas production from EFB, with a 54.62% improvement in methane yield compared to untreated EFB. The pretreatment also improved the kinetics of the anaerobic digestion process, resulting in a shorter lag phase and a higher methane production rate. However, the effectiveness of weak acid pretreatment was found to be concentration-dependent, with higher acetic acid concentrations (6%, 8%, and 10%) exhibiting inhibitory effects on biogas production.

3.4 Synergistic effects in co-fermentation of acetic acid and empty fruit bunch

The synergistic effects of co-fermentation of acetic acid and empty fruit bunch (EFB) were investigated by comparing the theoretical and experimental methane production (MP) values (Figure 2). The theoretical MP values for EFB (Theoretical-EFB) and acetic acid (Theoretical-Acetic) were calculated based on their methane production potentials. The anaerobic digestion experiments obtained the experimental MP values for EFB (EFB-MP) and acetic acid (Acetic-MP). The synergistic effect on methane production (Syn-CH_4) was calculated as the difference between the theoretical MP (Theoretical-MP) and the sum of the experimental MP values for EFB and acetic acid (EFB-MP + Acetic-MP). A positive value of Syn-CH_4 indicates a synergistic effect, while a negative value suggests an antagonistic effect [38]. The results showed that the co-fermentation of EFB with 4% acetic acid (Soaked with 4%AC) resulted in the highest synergistic effect, with a Syn-CH_4 value of 60.26 mL. This indicates that the combination of EFB and 4% acetic acid produced more methane than the sum of their contributions. This synergistic effect can be attributed to the enhanced hydrolysis of EFB by acetic acid, which increases the availability of easily degradable substrates for methane production [24]. However, at higher concentrations of acetic acid (6%, 8%, and 10%), the Syn-CH_4 values were negative, suggesting an antagonistic effect. This can be attributed to the inhibitory effects of high concentrations of acetic acid on the anaerobic microbial community, particularly the methanogens. The inhibition of methanogenic activity leads to decreased methane production despite the increased availability of substrates from the enhanced hydrolysis of EFB. The theoretical MP values for EFB (Theoretical-EFB) remained constant at 169.53 for all conditions, representing the maximum methane production potential of EFB under ideal conditions. The experimental MP values for EFB (EFB-MP) increased with increasing acetic acid concentration, indicating the positive effect of acetic acid pretreatment on EFB hydrolysis and methane production [25]. The co-fermentation of EFB with acetic acid showed a synergistic effect on methane production at a 4% acetic acid concentration. This synergistic effect can be attributed to the enhanced hydrolysis of EFB by acetic acid, which increases the availability of easily degradable substrates for methane production. However, at higher concentrations of acetic acid, an antagonistic effect was observed due to the inhibition of methanogenic activity. These findings highlight the importance of optimizing the concentration of acetic acid in the co-fermentation process to maximize methane production while minimizing inhibitory effects on the anaerobic microbial community.

Table 4. Profile of pH change on variable concentrations of weak acid soaking empty fruit bunch.

Parameters	Operation (day)							
	0	1	2	3	4	5	6	7
Soaked with H_2O	7.50 ± 0.06	6.06 ± 0.07	5.45 ± 0.18	4.97 ± 0.15	4.65 ± 0.15	4.66 ± 0.17	4.58 ± 0.18	4.73 ± 0.21
Soaked with 2%AC	3.22 ± 0.20	3.37± 0.05	3.47 ± 0.09	3.54 ± 1.16	4.18 ± 1.16	3.64 ± 0.06	3.56 ± 0.05	3.73 ± 0.07
Soaked with 4%AC	2.91 ± 0.05	3.16 ± 0.02	3.15 ± 1.72	4.24 ± 0.06	3.19 ± 0.06	3.29 ± 0.08	3.20 ± 0.06	3.37 ± 0.05
Soaked with 6%AC	2.85 ± 0.05	3.11 ± 0.09	2.99 ± 0.04	3.04 ± 0.05	2.96 ± 0.05	3.02 ± 0.00	2.97 ± 0.05	3.29 ± 0.46
Soaked with 8%AC	2.85 ± 0.09	2.98 ± 0.06	2.95 ± 0.02	3.08 ± 0.09	2.93 ± 0.09	3.04 ± 0.09	2.95 ± 0.10	3.07 ± 0.12
Soaked with 10%AC	2.83 ± 0.03	2.89 ± 0.06	2.85 ± 0.11	2.92 ± 0.11	2.82 ± 0.11	2.91 ± 0.11	2.81 ± 0.11	3.00 ± 0.04

Table 5. Methane production of pretreated empty fruit bunch with weak acid pretreatment

Conditions	Cumulative methane ($mL\text{-}CH_4$)	Methane yield ($mL\text{-}CH_4/g\text{-}VS$)	Kh (d^{-1})	Methane production rate ($mL\text{-}CH_4/L/d$)	Lag phase (d)	Digestion time (d)	Improvement efficiency (%)
Soaked with H_2O	460.30	171.24	0.0986	7.37	3.70	40	0
Soaked with 2%AC	519.19	162.37	1.0240	6.27	1.91	39	-5.18
Soaked with 4%AC	666.09	265.77	0.0960	8.37	1.66	40	54.62
Soaked with 6%AC	627.38	209.53	0.0953	6.71	3.82	> 45	22.36
Soaked with 8%AC	158.34	58.32	0.0247	0.00	202.71	> 45	-65.9
Soaked with 10%AC	0.50	0.15	0.0986	0.00	0	> 45	-100

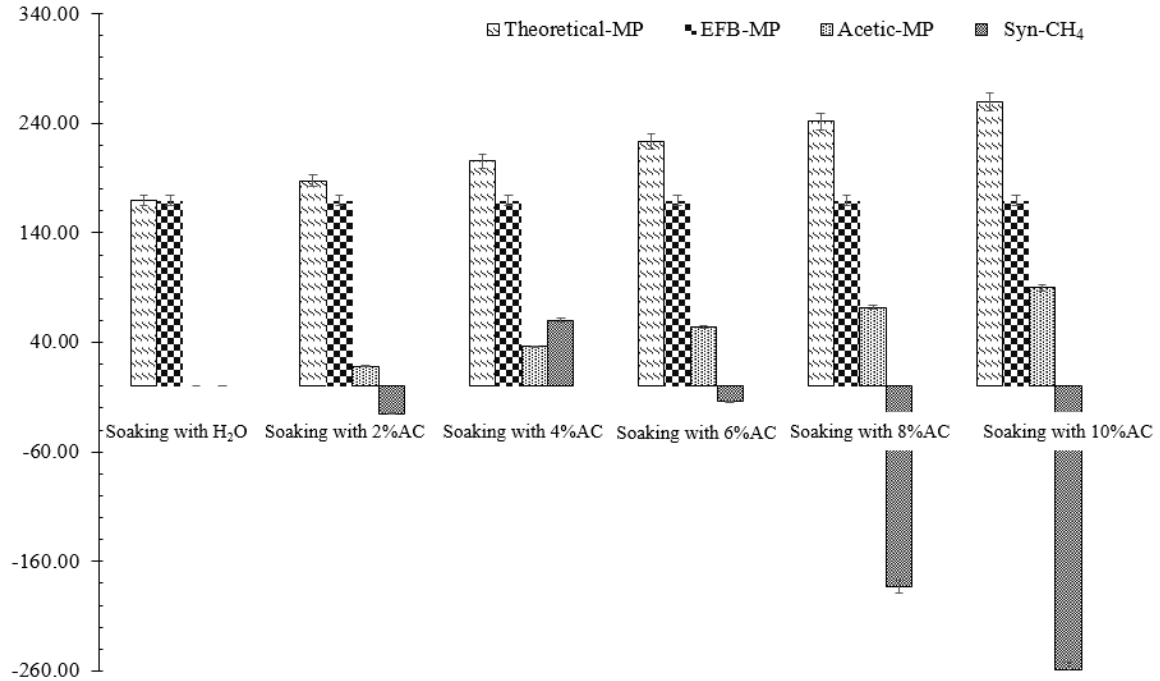

Figure 2 Synergistic effects in co-fermentation of acetic acid and empty fruit bunch

3.5 Comparison with other pretreatment methods

The methane yield obtained from EFB pretreated with 4% acetic acid (265.77 mL-CH_4/g-VS) was compared with other pretreatment methods reported in the literature (Figure 3). Alkaline pretreatment using NaOH resulted in a methane yield of 220.50 mL-CH_4/g-VS (Nieves et al., 2011), while steam explosion and enzymatic pretreatment yielded 190.00 mL-CH_4/g-VS [40]. and 240.00 mL-CH_4/g-VS [41], respectively (Table 6). The acetic acid pretreatment showed a 55.21% improvement in methane yield compared to untreated EFB, which was higher than the improvements observed for alkaline (28.77%), steam explosion (10.96%), and enzymatic (40.18%) pretreatments. This superior performance of acetic acid pretreatment can be attributed to its ability to remove hemicellulose and lignin while preserving the cellulose fraction effectively, the main substrate for methane production [25]. However, it should be noted that the effectiveness of pretreatment methods can vary depending on the specific characteristics of the lignocellulosic biomass and the operating conditions employed [34]. Therefore, further optimization of the acetic acid pretreatment process and a comprehensive techno-economic analysis are necessary to establish its feasibility for large-scale biogas production from EFB.

Table 6. Comparison of different pretreatment methods for EFB

Pretreatment Method	Methane Yield (mL-CH_4/g-VS)	Improvement (%)	Reference
Acetic Acid (4%)	265.77	55.21	This study
Alkaline (NaOH)	220.50	28.77	[8]
Steam Explosion	190.00	10.96	[40]
Enzymatic	240.00	40.18	[41]

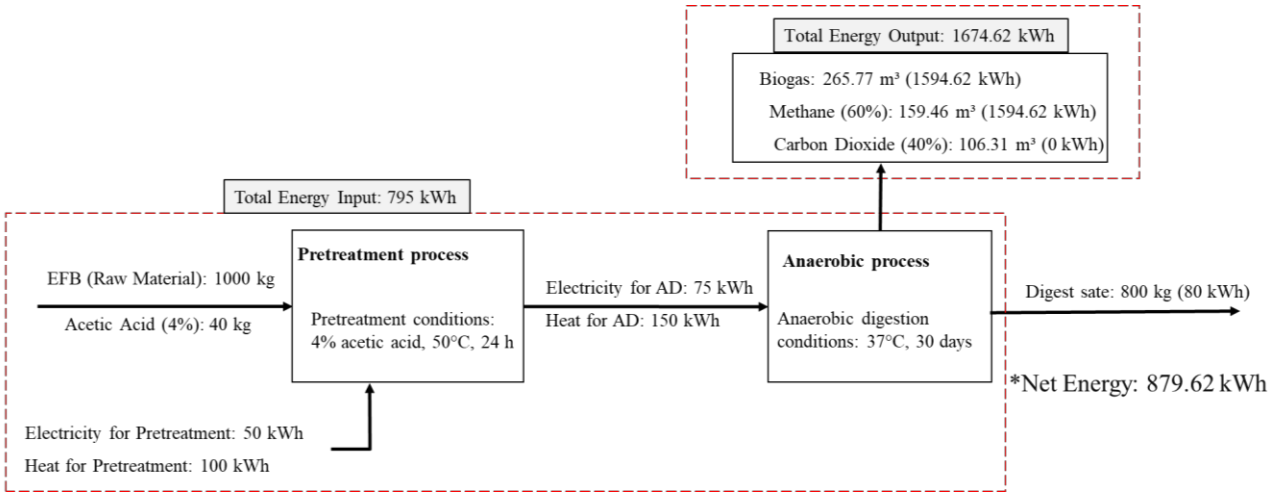

Figure 3. Energy balance of biogas production from EFB pretreated with acetic acid

3.6 Energy balance and economic analysis

The energy balance of biogas production from EFB pretreated with acetic acid was evaluated using a Sankey diagram (Figure 3). The total energy input, including the energy content of EFB (400 kWh/ton) and acetic acid (500 kWh/ton), as well as the electricity and heat requirements for pretreatment and anaerobic digestion, amounted to 795 kWh. The total energy output, comprising the energy content of biogas (1594.62 kWh) and digestate (80 kWh), was 1674.62 kWh. The net energy gain from the process was 879.62 kWh, indicating a positive energy balance. The economic analysis of biogas production from EFB pretreated with acetic acid was performed based on the estimated costs and revenues (Table 7). EFB and acetic acid costs were assumed to be 20.00 USD/ton and 0.50 USD/kg, respectively. The pretreatment and anaerobic digestion costs were estimated at 15.00 USD/ton and 25.00 USD/ton, respectively. With a biogas production of 200.00 m3/ton EFB and an electricity price of 0.10 USD/kWh, the revenue from electricity generation was calculated to be 120.00 USD/ton EFB. The net profit from the process was estimated at 60.00 USD/ton EFB, suggesting the economic viability of the proposed pretreatment method. However, it is important to consider that the energy balance and economic analysis presented here are based on hypothetical data and assumptions. Actual values may vary depending on the specific conditions and scale of the biogas production process. Additionally, factors such as the availability and cost of EFB and acetic acid and the market price of electricity can significantly influence the economic feasibility of the process [42]. Therefore, a detailed techno-economic analysis based on experimental data and local market conditions is necessary to accurately assess the viability of the proposed pretreatment method for large-scale biogas production from EFB.

Table 7. Economic analysis of biogas production from EFB pretreated with acetic acid.

Parameter	Value	Unit
EFB cost	20.00	USD/ton
Acetic acid cost	0.50	USD/kg
Pretreatment cost	15.00	USD/ton
Anaerobic digestion cost	25.00	USD/ton
Biogas production	200.00	m3/ton EFB
Biogas energy content	6.00	kWh/m3
Electricity price	0.10	USD/kWh
Revenue from electricity	120.00	USD/ton EFB
Net profit	60.00	USD/ton EFB

4. Conclusions

This study investigated the effect of weak acid pretreatment on the composition and structure of empty fruit bunch (EFB) and its subsequent anaerobic digestion for biogas production. Pretreatment of EFB with 4% acetic acid resulted in the highest methane yield (265.77 mL-CH_4/g-VS) and improvement in biogas production (55.21%) compared to untreated EFB. Acetic acid pretreatment partially removed hemicellulose and lignin, increasing cellulose accessibility for microbial degradation during anaerobic digestion. The synergistic effect of co-fermentation of acetic acid and EFB was observed at 4% acetic acid concentration, with a positive synergistic-CH_4 value of 60.26 mL. Comparative analysis showed that acetic acid pretreatment outperformed other methods regarding methane yield improvement, such as alkaline, steam explosion, and enzymatic pretreatments. The energy balance analysis indicated a positive net energy gain of 879.62 kWh per ton of EFB, while the economic analysis suggested a net profit of 60.00 USD per ton of EFB. The findings of this study have significant implications for the utilization of EFB as a feedstock for biogas production. Weak acid pretreatment using acetic acid can be an effective method to enhance the biodegradability of EFB and increase biogas production. The optimization of pretreatment conditions, particularly the acetic acid concentration, is crucial to maximize methane yield while minimizing inhibitory effects on the anaerobic digestion process. The co-fermentation of acetic acid and EFB can synergistically affect biogas production, offering a potential strategy for process intensification. The proposed pretreatment method's positive energy balance and economic viability suggest its potential for large-scale biogas production from EFB. Further optimization of the acetic acid pretreatment process, considering factors such as temperature, reaction time, and solid-to-liquid ratio, enhances the efficiency of EFB delignification and saccharification. Investigating the long-term effects of acetic acid pretreatment on the stability and performance of anaerobic digestion systems using EFB as a feedstock. Evaluation of the scalability and techno-economic feasibility of the proposed pretreatment method through pilot-scale studies and comprehensive lifecycle assessment.

5. Acknowledgements

The authors would like to thank the National Research Council of Thailand (NRCT) for the grant under the Research and Researcher for PhD Industry (RRi) program (grant.NO. NRCT5-RRI 63017-P20).

Author Contributions: S.C.; methodology, conducted the research, analyzed the data, and wrote the paper; P.K., methodology, proofread, funded, validating the results, and reviewed a manuscript.

Funding: The National Research Council of Thailand (NRCT) to the grant under the Research and Researcher for funding this research.

Conflicts of Interest: The authors declare no conflict of interest.

References

[1] Statista. Production volume of palm oil worldwide from 2012/13 to 2020/21 (in million metric tons). **2021**. https://www.statista.com/statistics/613471/palm-oil-production-volume-worldwide/

[2] Dolah, R.; Karnik, R.; Hamdan, H. A Comprehensive Review on Biofuels from Oil Palm Empty Bunch (EFB): Current Status, Potential, Barriers and Way Forward. *Sustainability*. **2021**, *13*, 10210. https://doi.org/10.3390/su131810210

[3] Nieves, D. C.; Karimi, K.; Horváth, I. S. Improvement of biogas production from oil palm empty fruit bunches (OPEFB). *Industrial Crops and Products*. **2011**, *34*(1), 1097-1101.

[4] Liu, J.; Zuo, X.; Peng, K. et al. Biogas and Volatile Fatty Acid Production During Anaerobic Digestion of Straw, Cellulose, and Hemicellulose with Analysis of Microbial Communities and Functions. Applied *Biochemistry and Biotechnology*. **2022**, *194*, 762–782. https://doi.org/10.1007/s12010-021-03675-w

[5] Brown, Craig.; Tao, Ling. Biofuel Production and Greenhouse Gas Reduction Potential. *United States*: N. p., **2023**. https://doi.org/10.2172/2202642

[6] Chaudhary, I.; Verma, S.R. Ligninolysis: Roles of Microbes and Their Extracellular Enzymes. In: Shah, M. (eds) *Microbial Bioremediation & Biodegradation. Springer, Singapore*. **2020**. https://doi.org/10.1007/978-981-15-1812-6_14

[7] Mukherjee, P.; Pal, S.; Sivaprakasam, S. Process Parameter Controls for Efficient Enzymatic Hydrolysis of Cellulosic Biomass. In: Bisaria, V. (eds) *Handbook of Biorefinery Research and Technology*. Springer, Dordrecht. **2024**. https://doi.org/10.1007/978-94-007-6724-9_77-1

[8] Lahboubi, N.; Kerrou, O.; Karouach, F. et al. Methane production from mesophilic fed-batch anaerobic digestion of empty fruit bunch of palm tree. *Biomass conversion and biorefinery*. **2022**, *12*, 3751–3760. https://doi.org/10.1007/s13399-020-00864-1

[9] Olatunji, K.O.; Ahmed, N.A.; Ogunkunle, O. Optimization of biogas yield from lignocellulosic materials with different pretreatment methods: a review. *Biotechnology for biofuels*. **2021**, *14*, 159. https://doi.org/10.1186/s13068-021-02012-x

[10] Poddar, B.J.; Nakhate, S.P.; Gupta, R.K. et al. A comprehensive review on the pretreatment of lignocellulosic wastes for improved biogas production by anaerobic digestion. *International journal of environmental science and technology*. **2022**, *19*, 3429–3456 https://doi.org/10.1007/s13762-021-03248-8

[11] Baksi, S.; Saha, D.; Saha, S. et al. Pre-treatment of lignocellulosic biomass: review of various physico-chemical and biological methods influencing the extent of biomass depolymerization. *International journal of environmental science and technology*. **2023**. *20*, 13895–13922 https://doi.org/10.1007/s13762-023-04838-4

[12] Yin, D.M.; Uwineza, C.; Sapmaz, T.; Mahboubi, A.; De Wever, H.; Qiao, W.; Taherzadeh, M.J. Volatile Fatty Acids (VFA) Production and Recovery from Chicken Manure Using a High-Solid Anaerobic Membrane Bioreactor (AnMBR). *Membranes* **2022**, *12*, 1133. https://doi.org/10.3390/membranes12111133

[13] Sluiter, A.; Hames, B, Ruiz.; R, Scarlata, C.; Sluiter, J.; Templeton, D.; Crocker D. Determination of Structural Carbohydrates and Lignin in Biomass. *National Renewable Energy Laboratory*, Golden, Colorado. **2012**.

[14] Goering, H.; Soest, P.J. Forage fiber analyses (apparatus, reagents, prcedures, and some applications) **1970**.

[15] Sluiter, A.; Hames, B.; Ruiz, R.; Scarlata, C.; Sluiter, J.; Templeton, D. Determination of total solids in biomass. *NREL Biomass Analysis Technology Team Laboratory Analytical Procedure*. **2005**, 1.

[16] Agnihotri, S.; Yin, D. M.; Mahboubi, A.; Sapmaz, T.; Varjani, S.; Qiao, W.; et al. A Glimpse of the World of Volatile Fatty Acids Production and Application: *A review. Bioengineered*. **2022**, 13(1), 1249–1275. https://doi.org/10.1080/21655979.2021.1996044

[17] Chia, S.M.; Chiong, M.C.; Panpranot, J. et al. Process optimization on co-production of lignin and cellulose in deep eutectic solvent pretreatment of oil palm empty fruit bunch. *Biomass conversion and biorefinery*. **2023**. https://doi.org/10.1007/s13399-023-05025-8

[18] Wadchasit P.; Siripattana C.; Seengenyoung J.; Thaweesaksakul S.; Nuithitikul K. *Lecture Notes in Applied Mathematics and Applied Science in Engineering*. **2019** (pp.94-102) Publisher: Malaysia Technical Scientist Association.

[19] Angelidaki, I.; Alves, M.; Bolzonella, D.; Borzacconi, L.; Campos, J. L.; Guwy, A. J.; Kalyuzhnyi, S. V.; Jenicek, P.; van Lier, J. B. Defining the biomethane potential (BMP) of solid organic wastes and energy crops: a proposed protocol for batch assays. *Water science and technology*. **2009,** *59*(5), 927-934. https://doi.org/10.2166/wst.2009.040

[20] Mamimin, C.; Prasertsan, P.; Kongjan, P.; O-Thong, S. Effects of volatile fatty acids in biohydrogen effluent on biohythane production from palm oil mill effluent under thermophilic condition. *Electronic journal of biotechnology*, **2017**, *29*, 78–85. https://doi.org/10.1016/j.ejbt.2017.07.006.

[21] APHA, Standard methods for the examination of water and waste water, 22nd edn. *American Public Health Association*, Washington, DC. **2012**.

[22] Díez, D.; Urueña, A.; Piñero, R.; Barrio, A.; Tamminen, T. Determination of Hemicellulose, Cellulose, and Lignin Content in Different Types of Biomasses by Thermogravimetric Analysis and

Pseudocomponent Kinetic Model (TGA-PKM Method). *Processes,* **2020**, *8*, 1048. https://doi.org/10.3390/pr8091048

[23] Nugraha, W.; Syafrudin, S.; Pradita, L.; Matin, H.; Yono, B. Biogas Production from Water Hyacinth (Eichhornia Crassipes): The Effect of F/M Ratio. IOP Conference Series: *Earth and Environmental Science*. **2018**, *150*. 012019. https://doi.org/10.1088/1755-1315/150/1/012019.

[24] Zhao, R.; Zhang, Z.; Zhang, R.; Li, M.; Lei, Z.; Utsumi, M.; Sugiura, N. Methane production from rice straw pretreated by a mixture of acetic-propionic acid. *Bioresource Technology*, **2020**, *101*(3), 990-994. https://doi.org/10.1016/j.biortech.2009.09.020

[25] Sun, S.; Sun, S.; Cao, X.; Sun, R. The role of pretreatment in improving the enzymatic hydrolysis of lignocellulosic materials. *Bioresource Technology*. **2016**, *199*, 49-58. https://doi.org/10.1016/j.biortech.2015.08.061

[26] Yadav, M.; Balan, V.; Varjani, S. et al. Multidisciplinary Pretreatment Approaches to Improve the Bio-methane Production from Lignocellulosic Biomass. *Bioenergy Research.* **2023**, *16*, 228–247. https://doi.org/10.1007/s12155-022-10489-z

[27] Dasgupta, A.; Chandel, M.K. Enhancement of biogas production from organic fraction of municipal solid waste using acid pretreatment. *Applied Sciences*. **2020**, *2*, 1437. https://doi.org/10.1007/s42452-020-03213-z

[28] Wang, Y.; Zhang, Y.; Wang, J.; Meng, L. Effects of volatile fatty acid concentrations on methane yield and methanogenic bacteria. *Biomass and Bioenergy*, **2009**, *33*(5), 848-853. https://doi.org/10.1016/j.biombioe.2009.01.007

[29] Li, X.; Peng, Y.; Yaqian, Z.; Zhang, L.; Han, B. Volatile Fatty Acid Accumulation by Alkaline Control Strategy in Anaerobic Fermentation of Primary Sludge. *Environmental Engineering Science*. **2017,** *34*. http://doi.org/10.1089/ees.2016.0399.

[30] Cheah, YK.; Vidal-Antich, C.; Dosta, J. et al. Volatile fatty acid production from mesophilic acidogenic fermentation of organic fraction of municipal solid waste and food waste under acidic and alkaline pH. *Environmental Science and Pollution Research*. **2019**, *26*, 35509–35522. https://doi.org/10.1007/s11356-019-05394-6

[31] Mohammad, I.N.; Ongkudon, C.M.; Misson, M. Physicochemical Properties and Lignin Degradation of Thermal-Pretreated Oil Palm Empty Fruit Bunch. Energies. **2020**, 13, 5966. https://doi.org/10.3390/en13225966

[32] Li, Y.; Jin, Y.; Li, J.; Chen, Y.; Gong, Y.; Li, Y.; Zhang, J. Current state and perspectives of anaerobic digestion for agricultural straw and lignocellulosic biomass in China. *Renewable and Sustainable Energy Reviews.* **2020**, *127*, 109880.

[33] Bah, H.; Zhang, W.; Wu, S. Methane production from different biomass materials: The effect of biomass characteristics. *Bioresource Technology*. **2014**, *158*, 257-266.

[34] Jönsson, L.J.; Martín, C. Pretreatment of lignocellulose: Formation of inhibitory by-products and strategies for minimizing their effects. *Bioresource Technology*. **2016**, *199*, 103-112. http://doi.org/10.1016/j.biortech.2015.10.009.

[35] Janke, L.; Leite, A.; Batista, K.; Weinrich, S.; Sträuber, H.; Nikolausz, M.; Nelles, M.; Stinner, W. Optimization of hydrolysis and volatile fatty acids production from sugarcane filter cake: Effects of urea supplementation and sodium hydroxide pretreatment. *Bioresource Technology*, **2015**, *199*, 235-244. https://doi.org/10.1016/j.biortech.2015.07.117

[36] Chen, Y.; Cheng, J. J.; Creamer, K. S. Inhibition of anaerobic digestion process: A review. *Bioresource Technology*. **2014**, *99*(10), 4044-4064. https://doi.org/10.1016/j.biortech.2007.01.057

[37] Yan, Z.; Song, Z.; Li, D.; Yuan, Y.; Liu, X.; Zheng, T. The effects of initial substrate concentration, C/N ratio, and temperature on solid-state anaerobic digestion from composting rice straw. *Bioresource Technology*. **2015**, *177*, 266-273. https://doi.org/10.1016/j.biortech.2014.11.089

[38] Astals, S.; Batstone, D.J.; Tait, S.; Jensen, P.D. Development and validation of a rapid test for anaerobic inhibition and toxicity. *Water Research*. **2015**, *81*. 208-215. https://doi.org/10.1016/j.watres.2015.05.063.

[39] Franke-Whittle, I. H.; Walter, A.; Ebner, C.; Insam, H. Investigation into the effect of high concentrations of volatile fatty acids in anaerobic digestion on methanogenic communities. *Waste management (New York*, N.Y.), **2014**, *34*(11), 2080–2089. https://doi.org/10.1016/j.wasman.2014.07.020

[40] Chandra, R.; Takeuchi, H.; Hasegawa, T. Methane production from lignocellulosic agricultural crop wastes: A review in context to second generation of biofuel production. *Renewable and Sustainable Energy Reviews*, **2012**, *16*(3), 1462-1476. https://doi.org/10.1016/j.rser.2011.11.035

[41] Baba, Y.; Tanabe, T.; Shirai, N.; Watanabe, T.; Honda, Y.; Watanabe, T. Pretreatment of Japanese cedar wood by white rot fungi and ethanolysis for bioethanol production. *Biomass and Bioenergy*, **2013**, *52*, 316-324.

[42] Carrere, H.; Antonopoulou, G.; Affes, R.; Passos, F.; Battimelli, A.; Lyberatos, G.; Ferrer, I. Review of feedstock pretreatment strategies for improved anaerobic digestion: From lab-scale research to full-scale application. *Bioresource Technology*, **2016**, *199*, 386-397. https://doi.org/10.1016/j.biortech.2015.09.007

ASEAN
Journal of Scientific and Technological Reports
Online ISSN:2773-8752

ASEAN
Journal of Scientific and Technological Reports
Online ISSN: 2773-8752

Article type

Type of the Paper (Article, Review, Communication, etc.) *about 8,000 words maximum*

Title (Palatino Linotype 18 pt, bold)

Firstname Lastname[1], Firstname Lastname[2] and Firstname Lastname[2*]

[1] Affiliation 1; e-mail@e-mail.com
[2] Affiliation 2; e-mail@e-mail.com
* Correspondence: e-mail@e-mail.com; (one corresponding authors, add author initials)

Citation:
Lastname, F.; Lastname, F.; Lastname, F. Title. *ASEAN J. Sci. Tech. Report.* **2023**, *26*(X), xx-xx. https://doi.org/10.55164/ajstr.vxxix.xxxxxx

Article history:
Received: date
Revised: date
Accepted: date
Available online: date

Abstract: A single paragraph of about 400 words maximum. Self-contained and concisely describe the reason for the work, methodology, results, and conclusions. Uncommon abbreviations should be spelled out at first use. We strongly encourage authors to use the following style of structured abstracts, but without headings: (1) Background: Place the question addressed in a broad context and highlight the purpose of the study; (2) Methods: briefly describe the main methods or treatments applied; (3) Results: summarize the article's main findings; (4) Conclusions: indicate the main conclusions or interpretations.

Keywords: keyword 1; keyword 2; keyword 3 (List three to ten pertinent keywords specific to the article yet reasonably common within the subject discipline.)

1. Introduction

The introduction should briefly place the study in a broad context and highlight why it is crucial. It should define the purpose of the work and its significance. The current state of the research field should be carefully reviewed and critical publications cited. Please highlight controversial and diverging hypotheses when necessary. Finally, briefly mention the main aim of the work. References should be numbered in order of appearance and indicated by a numeral or numerals in square brackets—e.g., [1] or [2, 3], or [4–6]. See the end of the document for further details on references.

2. Materials and Methods

The materials and methods should be described with sufficient details to allow others to replicate and build on the published results. Please note that your manuscript's publication implicates that you must make all materials, data, computer code, and protocols associated with the publication available to readers. Please disclose at the submission stage any restrictions on the availability of materials or information. New methods and protocols should be described in detail, while well-established methods can be briefly described and appropriately cited.

Interventional studies involving animals or humans, and other studies that require ethical approval, must list the authority that provided approval and the corresponding ethical approval code.

2.1 Subsection

2.1.1. Subsubsection

3. Results and Discussion

This section may be divided by subheadings. It should provide a concise and precise description of the experimental results, their interpretation, as well as the experimental conclusions that can be drawn.Authors should discuss the results and how they can be interpreted from previous studies and the working hypotheses. The findings and their implications should be discussed in the broadest context possible. Future research directions may also be highlighted.

3.1. Subsection

3.1.1. Subsubsection

3.2. Figures, Tables, and Schemes

All figures and tables should be cited in the main text as Figure 1, Table 1, etc.

Figure 1. This is a figure. Schemes follow the same formatting.

Table 1. This is a table. Tables should be placed in the main text near the first time they are cited.

Title 1	Title 2	Title 3
entry 1	data	data
entry 2	data	data [1]

[1] Table may have a footer.

3.3. Formatting of Mathematical Components

This is example 1 of an equation:

$$a = 1, \tag{1}$$

The text following an equation need not be a new paragraph. Please punctuate equations as regular text. This is example 2 of an equation:

$$a = b + c + d + e + f + g + h + i + j + k + l + m + n + o + p + q + r + s + t + u \tag{2}$$

The text following an equation need not be a new paragraph. Please punctuate equations as regular text. The text continues here.

4. Conclusions

Concisely restate the hypothesis and most important findings. Summarize the significant findings, contributions to existing knowledge, and limitations. What are the future directions? Conclusions MUST be well stated, linked to original research question & limited to supporting results.

5. Acknowledgements

Should not be used to acknowledge funders – funding will be entered as a separate. As a matter of courtesy, we suggest you inform anyone whom you acknowledge.

Author Contributions: For research articles with several authors, a short paragraph specifying their individual contributions must be provided. The following statements should be used "Conceptualization, X.X. and Y.Y.; methodology, X.X.; software, X.X.; validation, X.X., Y.Y. and Z.Z.; formal analysis, X.X.; investigation, X.X.; resources, X.X.; data curation, X.X.; writing—original draft preparation, X.X.; writing—review and editing, X.X.; visualization, X.X.; supervision, X.X.; project administration, X.X.; funding acquisition, Y.Y. All authors have read and agreed to the published version of the manuscript." Please turn to the CRediT taxonomy for the term explanation. Authorship must be limited to those who have contributed substantially to the work reported.

Funding: Please add: "This research received no external funding" or "This research was funded by NAME OF FUNDER, grant number XXX" and "The APC was funded by XXX". Check carefully that the details given are accurate and use the standard spelling of funding agency names at https://search.crossref.org/funding. Any errors may affect your future funding.

Conflicts of Interest: Declare conflicts of interest or state "The authors declare no conflict of interest." Authors must identify and declare any personal circumstances or interest that may be perceived as inappropriately influencing the representation or interpretation of reported research results. Any role of the funders in the design of the study; in the collection, analyses or interpretation of data; in the writing of the manuscript, or in the decision to publish the results must be declared in this section. If there is no role, please state "The funders had no role in the design of the study; in the collection, analyses, or interpretation of data; in the writing of the manuscript, or in the decision to publish the results".

References

References must be numbered in order of appearance in the text (including citations in tables and legends) and listed individually at the end of the manuscript. We recommend preparing the references with a bibliography software package, such as EndNote, ReferenceManager to avoid typing mistakes and duplicated references. Include the digital object identifier (DOI) for all references where available.

Citations and references in the Supplementary Materials are permitted provided that they also appear in the reference list here.

In the text, reference numbers should be placed in square brackets [ ] and placed before the punctuation; for example [1], [1–3] or [1, 3]. For embedded citations in the text with pagination, use both parentheses and brackets to indicate the reference number and page numbers; for example [5] (p. 100), or [6] (pp. 101–105).

Using the American Chemical Society (ACS) referencing style

[1] Author 1, A.B.; Author 2, C.D. Title of the article. *Abbreviated Journal Name* Year, *Volume*, page range.

[2] Author 1, A.; Author 2, B. Title of the chapter. In *Book Title*, 2nd ed.; Editor 1, A., Editor 2, B., Eds.; Publisher: Publisher Location, Country. **2007**, Volume *3*, pp. 154–196.

[3] Author 1, A.; Author 2, B. *Book Title*, 3rd ed.; Publisher: Publisher Location, Country, **2008**, pp. 154–196.
[4] Author 1, A.B.; Author 2, C. Title of Unpublished Work. *Abbreviated Journal Name* stage of publication (under review; accepted; in press).
[5] Author 1, A.B. (University, City, State, Country); Author 2, C. (Institute, City, State, Country). Personal communication, 2012.
[6] Author 1, A.B.; Author 2, C.D.; Author 3, E.F. Title of Presentation. In Title of the Collected Work (if available), Proceedings of the Name of the Conference, Location of Conference, Country, Date of Conference; Editor 1, Editor 2, Eds. (if available); Publisher: City, Country, Year (if available); Abstract Number (optional), Pagination (optional).
[7] Author 1, A.B. Title of Thesis. Level of Thesis, Degree-Granting University, Location of University, Date of Completion.
[8] Title of Site. Available online: URL (accessed on Day Month Year).

Reviewers sugestion

1. Name, Address, e-mail
2. Name, Address, e-mail
3. Name, Address, e-mail
4. Name, Address, e-mail

URL link:

Notes for Authors >>
https://drive.google.com/file/d/1r0zegnIVeQqe4iLQyT1xDEIinNggINPD/view?usp=sharing
https://drive.google.com/file/d/1r0zegnIVeQqe4iLQyT1xDEIinNggINPD/view?usp=sharing

Online Submissions >> https://ph02.tci-thaijo.org/index.php/tsujournal/user/register

Current Issue >> https://ph02.tci-thaijo.org/index.php/tsujournal/issue/view/16516

AJSTR Publication Ethics and Malpractice >> https://ph02.tci-thaijo.org/index.php/tsujournal/ethics

Journal Title Abbreviations >> http://library.caltech.edu/reference/abbreviations

ASEAN
Journal of Scientific and Technological Reports
Online ISSN:2773-8752

ASEAN
Journal of Scientific and Technological Reports
Online ISSN:2773-8752

ASEAN Journal of Scientific and Technological Reports (AJSTR)
Institute of Research and Innovation, Thaksin University, Phatthalung Campus
222 Moo. 2, Baan Prao Sub-District, Papayom District, Phatthalung, 93210, Thailand
Tel. +668 1540 7304